University of Alberta

Characterization of functional determinants of nucleoside analogs and nucleoside transporters

By

Jing Zhang

A thesis submitted to the Faculty of Graduate Studies and Research in partial fulfillment of the requirements for the degree of Doctor of Philosophy

Department of Oncology

Edmonton, Alberta
Spring 2006

Your file Votre référence
ISBN: 0-494-14070-4
Our file Notre référence
ISBN: 0-494-14070-4

To Xuejie for all your love and support

Abstract

Nucleoside transporters are responsible for the uptake of natural nucleosides and cytotoxic nucleoside analogs. The human concentrative nucleoside transporters, hCNT1, 2 and 3 exhibit different permeant selectivities. The uridine permease FUI1 of *S. cerevisiae* is a unique uridine-specific nucleoside transporter. The synthesis of uridine analogs and development of yeast-based high throughput transport assay enabled the characterization of Urd binding profiles of these transporters. hCNT1, hCNT2, hCNT3 and FUI1 recognized uridine through distinguishable binding motifs. hCNT1 interacts with C(3'), C(5') and N(3) of Urd; hCNT2 interacts with C(3'), C(5') and N(3) of uridine; hCNT3 interacts with C(3') of Urd; and FUI1 interacts with C(3'), C(2'), C(5) and N(3) of uridine. The Urd transportability profiles of hCNT1, 2 and 3 identified by two-electrode voltage clamp assay reflected well their uridine binding profiles and should prove useful in the development of anti-cancer and antiviral therapies with nucleoside drugs that are permeants of the hCNT protein family. To understand uridine binding and translocation mechanisms, cysteine-accessibility and permeant-protection assays were used to probe a series of cysteine-substitution mutants spanning predicted transmembrane domains (TMs) 11, 12 and 13 of cysteine-less hCNT3. Two mutants in putative TM 11 and four mutants in putative TM 12 were sensitive to modifications by sulfhydryl reagents in a permeant-protectable manner, indicating that TM 11 and 12 may form part of the nucleoside translocation pathway. On the basis of the lack of accessibility of methanethiosulfonate reagents to the thiol groups in mutants of TM 13, it appears that TM 13 is not exposed to the nucleoside translocation pathway. Functional characterization and mutagenesis analysis revealed that FUI1 is a proton-dependent

symporter and only one of the three charged amino acids in the putative TM regions is required for maintaining high transport efficiency of FUI1. Finally, to better understand nucleoside transport processes and intracellular fates of nucleosides, fluorescent nucleoside analogs, FuPmR [3-(β-D-ribofuranosyl)furo[2,3-*d*]pyrimidin-2(3*H*)-one] and dFuPmR [3-(2-deoxy-β-D-*erythro*-pentofuranosyl)furo[2,3-*d*]pyrimidin-2(3*H*)-one] were developed for real-time analysis of nucleoside transport by confocal microscopy. Quantitative analysis of fluorescence signals revealed two stages of FuPmR uptake and demonstrated for the first time the intracellular distribution of nucleosides and/or nucleoside metabolites in living cells.

Acknowledgements

I wish to thank Dr. Carol Cass sincerely for mentoring me throughout my graduate education. Carol has been a wonderful supervisor for me. Her devotion, encouragement, wisdom and guidance have been of great help in the completion of this research project. The very high standards Carol holds in both scholarship and research are an invaluable inspiration that certainly shaped my academic pursuits and will continually encourage me all my life. I would like to thank Carol's collaborators, Dr. Morris Robins, Dr. James Young, Dr. Steve Baldwin and Dr. Xuejun Sun, for guidance with my research projects and vigorous revision of my manuscripts. I would also like to thank the members of my supervisory and candidacy examination committees, Dr. Roseline Godbout, Dr. Michael Weinfeld, Dr. John Mackey, Dr. Susan Andrew and Dr. Andrew Shaw, for their support, helpful insights and useful suggestions for the progression of my research. Special thanks go to Dr. Scott Landfear, for being the external examiner of my thesis defense. I am also very grateful to Dr. Kyla Smith for her collaborative work on electrophysiological studies of our favorite transporters throughout these years.

I would like to thank the present and past members of the Cass laboratory, Frank Visser, Mark Vickers, Adam Elwi, Karen King, Miguel Cabrita, Thack Lang, Robert Paproski, Alan Doucette, Nancy Zhang, Elizabeth Silver, Taylor Raborn, Pat Carpenter, Tracey Tackaberry, Gerry Barron, Delores Mowles, Kathryn Graham, Vijaya Damaraju, Rajam Mani, Cheryl Santos, Lily Zombor, Milada Selner, Kate Hamilton, Michelle Kuzma, Haide Razavy, Helen Steed and Michael Sawyer, for their tremendous help, warm friendship and great fun. I enjoyed working in this extraordinary laboratory so much. I would also like to thank the supporting and academic staff of the Department of Oncology at the Cross Cancer Institute for supplying a first-class research and education environment.

Last, but not least, I would like to thank my husband, Xuejie, for his tireless encouragement, support and belief that I could count on through these years in Canada. I would like to extend my gratitude to my parents, Shiqin Zhang and Shuhua Hang and my brother Yue Zhang for their unconditional love and support throughout my life and in pursuit of my Ph.D. degree.

Table of Contents

List of Tables

List of Figures

List of Abbreviations, Symbols and Nomenclature

araC	cytarabine
araU	1-(β-D-arabinofuranosyl)uracil
2'AzdUrd	2'-azido-2'-deoxyuridine
3'AzdUrd	3'-azido-3'-deoxyuridine
5'AzdUrd	5'-azido-5'-deoxyuridine
AZT	3'-azido-3'-deoxythymidine
BrdUrd	5-bromo-2'-deoxyuridine
BrUrd	5-bromouridine
Ca	*Candida albicans*
CCCP	carbonyl cyanide m-chlorophenylhydrazone
Ce	*Caenorhabditis elegans*
5'CldUrd	5'-chloro-5'-deoxyuridine
CLL	chronic lymphatic leukemia
CMM	complete minimal media
CNT,	concentrative nucleoside transporter
dCK	deoxycytidine kinase
ddC	2',3'-dideoxycytidine
ddI	2',3'-dideoxyinosine
dilazep	*N,N'-bis*-[3-(3,4,5-trimethoxybenzoyloxy)propyl]-homopiperazine
dipyridamole	2,2',2",2"'-[(4,8-Dipiperidinylpyrimido[5,4-d]pyrimidine-2,6-diyl)dinitrilo]tetraethanol
draflazine	2-aminocarbonyl-*N*-(4-amino-2,6-dichlorophenyl)-4-[5,5-*bis*(4-fluorophenyl)pentyl]-1-piperazineacetamide)
2',3'ddUrd	2',3'-dideoxyuridine
2',5'ddUrd	2',5'-dideoxyuridine
3',5'ddUrd	3',5'-dideoxyuridine
dFuPmR	3-(2-deoxy-β-D-*erythro*-pentofuranosyl)furo[2,3-*d*]pyrimidin-2(*3H*)-one

ΔG^0	Gibbs Free energy
dGK	deoxyguanosine kinase
DMSO	dimethylsulfoxide
2'dUrd	2'-deoxyuridine
3'dUrd	3'-deoxyuridine
5'dUrd	5'-deoxyuridine
ei	equilibrative insensitive
ENT	equilibrative nucleoside transporter
es	equilibrative sensitive
EtdUrd	5-ethyl-2'-deoxyuridine
FdUrd	5-fluoro-2'-deoxyuridine
FRAP	fluorescence recovery after photobleaching
FUI1	uridine permease from *Saccharomyces cerevisiae*
FUN26	function unknown now 26; an intracellular ENT isoform from *Saccharomyces cerevisiae*
FUR4	uracil/uridine permease from *Saccharomyces cerevisiae*
FuPmR	3-(β-D-ribofuranosyl)furo[2,3-*d*]pyrimidin-2(3*H*)-one
FUrd	5-fluorouridine
GFP	green fluorescent protein
GLU	glucose
h	human
hf	hagfish
IC_{50}	inhibitory concentration 50%
IdUrd	5-iodo-2'-deoxyuridine
iPUrd	2',3'-O-isopropylideneuridine
IUrd	5-iodouridine
K_i,	inhibitory constant
LdNT	*Leishmania donovani* nucleoside transporter
m	mouse
MAPK	mitogen-activated protein kinase
MDCK cells	Madin-Darby canine kidney cells

3MeUrd	3-methyluridine
MeUrd	5-methyluridine
MTS	methanethiosulfonate
MTSEA	MTS-ethylammonium
MTSES	MTS-ethylsulfonate
MTSET	MTS-ethyltrimethylammonium
MTT	3-(4,5-dimethylthiazol-2-yl)-5-(3-carboxymethoxyphenyl)-2-(4-sulfophenyl)-2H-tetrazolium
NBMPR	nitrobenzylmercaptopurine ribonucleoside
ND	not determined
NHL	non-Hodgkin's lymphoma
NT	nucleoside transporter
5'Nucl	5'-nucleotidase
2'OMeUrd	2'-O-methyluridine
3'OMeUrd	3'-O-methyluridine
5'OMeUrd	5'-O-methyluridine
ORF	open reading frame
PBS	phosphate-buffered saline, pH 7.2
PBST	PBS with 1 % Triton X-100
PCMBS	p-chloromercuribenzene sulfonate
PCR	polymerase chain reaction
pk	pig
r	rat
rb	rabbit
RR	ribonucleotide reductase
SB203580	4-(4-fluorophenyl)-2-(4-methylsulfinylphenyl)-5-(4-pyridyl)1H-imidazole
SCAM	substituted-cysteine accessibility method
S. cerevisiae	*Saccharomyces cerevisiae*
SDS	sodium dodecyl sulfate
S.E.	standard error

SLC28	solute carrier family 28
SLC29	solute carrier family 29
SNPs	single nucleotide polymorphisms
soluflazine	3-(aminocarbonyl)-4-[4, 4-(fluorophenyl-3-pyridinyl)butyl]-*N*-(2,6-dichlorophenyl)-1-piperazineacetamide
$t_{1/2}$	half-recovery time
TaraC	4'-Thio-β-D-arabinofuranosyl cytosine
TbNTs	*Trypanosoma brucei* nucleoside transporters
Thd	Thymidine
TMs	transmembrane segments
TTBS	0.2% Tween-20, Tris-buffered saline
Urd	uridine
V_h	holding potential
X. laevis	*Xenopus laevis*
xyloU	1-(β-D-xylofuranosyl)uracil

Chapter 1 : Structural and Functional Insights into Nucleoside Transporters

An overview of nucleoside and nucleoside transporters

Nucleosides

Naturally occurring nucleosides (Fig. 1-1) include purine nucleosides, such as adenosine, guanosine and inosine, and pyrimidine nucleosides, such as uridine, cytidine and thymidine. Nucleosides play multiple roles in cell physiology by acting not only as the metabolic precursors of many fundamental biological molecules including ATP, DNA and RNA, but also as signaling molecules and neuromodulators that contribute to the regulation of a broad range of cellular events. Adenosine is a ubiquitous signaling molecule that functions as a ligand for cell-surface adenosine receptors, facilitating a variety of physiological responses, including coronary vasodilation, neuromodulation and platelet aggregation (1,2). In addition, nucleosides can be used as nitrogen sources in plants and many microorganisms (3).

Although de novo biosynthesis is crucial for whole-body nucleotide/nucleoside homeostasis, nucleoside salvage is energetically favored. Salvaging nucleosides from the extracellular environment is required when the de novo synthesis pathways are either lacking or inadequate, e.g., in parasitic protozoa and certain mammalian cell types with high metabolic turnover rates, such as enterocytes and bone marrow cells. Since nucleosides are hydrophilic molecules and their passive diffusion across biological membranes is limited, specialized transporter proteins are required to mediate the movement of nucleosides across plasma membranes or between intracellular compartments. Two major families of nucleoside transporters (NTs), the equilibrative nucleoside transporters (ENTs; SLC29) and the concentrative nucleoside transporters (CNTs; SLC28), have been identified by molecular cloning and functional expression of cDNAs encoding transporter proteins from a variety of species, including mammals, protozoan parasites and bacteria (4-6).

Nucleoside transporters

Since the molecular cloning from tissues of cDNAs encoding human (h) ENT1 and hENT2 in 1996, ENTs from numerous eukaryotic organisms, including mammals, worms, plants, protozoan parasites and yeast have been identified by functional cloning

and genome analysis. The cloning from rat (r) jejunal epithelium of the cDNA encoding rCNT1 and its functional characterization in *Xenopus laevis* oocytes initiated the process of understanding sodium-dependent nucleoside transport proteins at the molecular level (7). In mammals, three CNT subtypes, CNT1, CNT2 and CNT3 have been identified by molecular cloning and functional expression, whereas four ENT subtypes, hENT1, hENT2, hENT3 and hENT4 have been identified from human tissues. The potent transport inhibitor nitrobenzylmercaptopurine ribonucleoside (NBMPR) can be used to functionally distinguish hENT1, which mediates equilibrative NBMPR-sensitive (*es*) transport activity, from hENT2, which mediates equilibrative NBMPR-insensitive (*ei*) transport activity (8-10). Vasodilator drugs, such as dilazep and dipyridamole, are non-nucleoside inhibitors of both hENT1 and 2 although hENT1 is about three orders of magnitude more sensitive to their inhibitions (11,12). hENT1 and hENT2 are well-characterized plasma-membrane transporters that transport both purine and pyrimidine nucleosides with hENT2 bearing additional selectivity for certain nucleobases (13). hENT3 and hENT4 are less well-characterized members of the SLC29 gene family (14-16). hENT3, which is broadly selective, is believed to be a transporter of intracellular membranes (16-18) and hENT4, which mediates equilibrative transport of adenosine (15,16) also transports monoamine neurotransmitters (19). No pharmacological inhibitors are known for hCNTs and unlike hENTs, which mediate nucleoside diffusion down their concentration gradients, hCNT1, 2 and 3 couple uphill nucleoside transport to downhill sodium transport and, in the case of hCNT3, also to downhill proton transport. In humans, mice and rats, although CNT1, 2 and 3 all accept uridine as a permeant, they differ functionally with respect to their selectivities for other permeants. CNT1 prefers pyrimidine nucleosides but also transports adenosine, whereas CNT2 prefers purine nucleosides but also transports uridine (20-23). CNT3 transport both pyrimidine and purine nucleosides (24).

In humans, *es* transport activity, mRNA and/or protein have been detected in many different cell types and tissues and hENT1 is believed to have a ubiquitous tissue distribution whereas the distribution of hENT2 appears to be more limited although it is particularly abundant in skeletal muscle (25-27). hCNT1 and hCNT2 are less widespread than hENT1 and hENT2 and seem to be expressed in specific tissues, such as kidney,

intestine and liver. Compared to hCNT1 and hCNT2, hCNT3 is expressed in a wider variety of tissues, suggesting that hCNT3 plays multiple roles in nucleoside homeostasis in the body (24,28). The high expression levels of hCNTs in the intestine, kidney and liver suggest their involvement in the systemic absorption and disposal of nucleosides and nucleoside analogs. In polarized cells, such as in the renal and intestinal epithelia, CNT and ENT activities and/or proteins have been detected in the apical and basolateral membrane, respectively, suggesting that they play a role in vectorial transepithelial flux of nucleosides (29-31). rCNT1 was found predominantly in the brush-border membranes of epithelial cells of rat jejunum and renal cortical tubules and in the bile canalicular membranes of liver parenchymal cells, consistent with roles in the absorption of dietary nucleosides, of reabsorption of nucleosides in the glomerular filtrate, or of nucleosides arising from the metabolite action of extracellular nucleotidases, respectively (32). Investigations of the differential localizations of hENTs or hCNTs in epithelial tissues is now possible with the recent development of transporter-specific antibodies. For example, the apical localization of endogenous hENT1 and hCNT3 in proximal renal tubule epithelial cells has recently been shown in human kidney tissues (Damaraju V. and Cass C.E., unpublished data). The mechanisms that direct these transporter proteins to apical membrane remain unknown. Appropriate model systems, such as primary cell culture and nonmetabolizable nucleoside analogs, are needed to determine the role of hCNTs and hENTs in transepithelial movements of nucleosides in intestine and kidney.

Most cells investigated so far possess more than one NT subtype with overlapping transport properties; the reason for this redundancy is unclear. Possible reasons for the presence of multiple NT subtypes in the same cell are: (i) NTs are highly regulated proteins; (ii) NT subtypes are not constitutively expressed and (iii) differential plasma and intracellular localizations of different NT proteins exist. The co-existence of hENT1 and hENT2, which exhibit similar nucleoside selectivities, may reflect the importance of hypoxanthine salvage mediated by hENT2 (15). Co-expression of concentrative and equilibrative NTs might be required in liver cells to deliver synthesized nucleosides for extrahepatic supply and to salvage nucleosides during special circumstances, such as liver injury (33),(34). Although ENT1 is found predominantly on plasma membranes, there is evidence in studies with humans and rodents that ENT1 is also present in

membrane of mitochondria, lysosome, nuclear envelop and endoplasmic reticulum (35-37). Recently, dynamic monitoring of hCNT3 protein expression in a colon cancer cell line, CaCo2 revealed the gradual accumulation of hCNT3 protein in plasma membranes upon cell differentiation (38), indicating that its sorting is strictly controlled. hCNT3 proteins have been localized in intracellular compartments of prolymphocyte cells isolated from chronic lymphatic leukemia (CLL) patients (39). The mechanism of membrane targeting and intracellular trafficking of NT proteins remains largely unknown. The regulation of expression of nucleoside transporters have recently been reviewed extensively (6,33,40).

Although there is currently no evidence implicating hENT and hCNT proteins in the pathogenesis of human disease, they play key roles in nucleoside and nucleobase uptake for salvage pathways of nucleotide synthesis and are determinants of cellular uptake of nucleoside analogs used in anticancer and antiviral therapies. In addition, by regulating the extracellular concentration of adenosine available to cell surface purinergic receptors, hENTs influence multiple physiological processes, including cardiovascular activity, neurotransmission and neuroprotection. Studies with ENT1-null mice have established an important role for ENT1 in regulating ethanol intoxication in vivo by decreasing A1 adenosine receptor function and promoting alcohol consumption (41). Although all three CNTs have been found in brain and heart and CNT activity is inhibited by some adenosine receptor ligands (42), the role of CNTs in adenosine homeostasis remains another open question for future investigation.

Nucleoside analogs and cancer chemotherapy

Anticancer pyrimidine and purine nucleoside drugs commonly used clinically are cytarabine (araC), cladribine, fludarabine, gemcitabine, clofaribine and capecitabine (structures are shown in Fig. 1-1). As nucleoside analog drugs are hydrophilic compounds and do not readily cross plasma membranes by diffusion, the presence of functional nucleoside transporters that accept nucleoside drugs as permeants is required for cellular entry at rates sufficient to achieve cytotoxic levels of intracellular metabolites. The structural differences of these nucleoside analogs are expected to lead to differences in their interactions with different NT proteins since there are differences

in permeant selectivities among different NTs. Different NT distribution patterns in various tissues may result in differences in the tissue distributions of nucleoside drugs (43), which, in turn, may influence their pharmacokinetic and toxicological properties. Altered abundance of NT proteins in malignant cells (27) may result in decreased or increased uptake of some types of nucleoside drugs. The presence of functional NT proteins in some tissues other than tumors may affect the distribution of anticancer nucleoside drugs. hENTs and hCNTs have been identified in kidney tubular cells with distinct membrane distribution (29,30,44), suggesting the possibility of renal reabsorption and secretion of nucleoside drugs.

As shown in Fig. 1-2, once transported into the cells by ENTs or CNTs, nucleoside analogs are first phosphorylated by nucleoside kinases, such as deoxycytidine kinase (dCK), deoxyguanosine kinase (dGK) and thymidine kinase. Some nucleoside analogs may be deaminated by either adenosine deaminase or cytidine deaminase and thus degraded. Various cytoplasmic 5'-nucleotidases (5'Nucl) could antagonize the nucleoside kinases by dephosphorylating monophosphorylated nucleoside derivatives. Monophosphorylated derivatives are further phosphorylated to active 5'-triphosphate derivatives by 5' nucleoside monophosphate and 5' nucleoside diphosphate kinases. The incorporation of active triphosphate derivatives (i.e., derivatives of nucleoside analogs with 3' modifications) into DNA and RNA may result in chain termination and cell death. Some cytotoxic nucleoside analogs may exert indirect cytotoxicity action by inhibiting ribonucleotide reductase (RR), which in turn inhibits transferring of normal NDPs to dNDPs. With the reduction of normal dNTPs pools, more active 5'-triphosphate derivatives could be incorporated into DNA (45). Although most anticancer nucleoside analogs share common intracellular targets, each of these compounds also exhibit specific properties of drug-target interactions which result in their differences in activity in various malignancies (43). For instance, araC cytotoxicity is due to a combination of DNA polymerase inhibition and DNA incorporation (46). Fludarabine, an analog of adenosine, is resistant to deamination by adenosine deaminase (47). Gemcitabine, a cytidine analog, is not only incorporated into DNA, but also into RNA (48). Once the active gemcitabine is incorporated into DNA, an additional natural nucleoside is added,

thus "masking" gemcitabine enabling it to escape DNA repair, leading to "masked" DNA chain termination (49,50).

For most nucleoside drugs, NT-mediated uptake is a prerequisite step to initiate cytotoxicity. One rational for use of anticancer nucleoside drugs lies in the fact that high proliferation rates observed in malignant cells have been associated with higher levels of *es* transport activity (51). hENT1 protein abundance was higher in breast cancer cells than in normal breast epithelia using immunohistochemistry with anti-hENT1 monoclonal antibodies (52). The abundance of hENT1 in plasma membranes has been correlated with sensitivity to various nucleoside anticancer drugs (51-54). A positive correlation between hENT1 expression and chemosensitivity to nucleoside drugs, azacytidine and inosine-glycodialdehyde, was shown by oligonucleotide array analysis (55). Decreased expression of hENT1 transcripts was related to an increased risk of early relapse of acute myelogenous leukemia patients treated with cytarabine (56) and low abundance of hENT1 protein was associated with reduced survival in pancreas adenocarcinoma patients treated with gemcitabine (57). Introduction of hCNT2 into a NT-deficient CEM cell line (CEM is an acute lymphoblastic leukemia cell line) by gene transfer restored sensitivity to fluoropyrimidine nucleoside drugs (58). Although it is believed that the presence of functional NTs in plasma membranes is a key determinant of nucleoside chemotherapy for most nucleoside drugs, the correlation of clinical outcome with the activity of nucleoside transporters is far from well defined. Nucleoside drug sensitivity is determined by multiple factors and it may not be possible to isolate the role of individual NT subtypes from the combined effects of other nucleoside-metabolizing proteins (6).

Deficient transporter activity may result in clinical resistance to nucleoside analogs. Although decreased activity of dCK, increased activities of 5'Nucl and/or cytidine deaminase, and defective cell-death pathways have been observed to contribute to resistance to cytotoxic nucleoside drugs (53,59,60), a recent study showed that only increased expression of 5'Nucl or hENT1 deficiency in leukemic blasts at diagnosis were correlated with shorter disease-free survival and may play a role in araC resistance mechanisms in acute leukemia patients (53). Since the targets of nucleoside drugs are intracellular, reduced inwardly mediated transport could decrease cytoplasmic

accumulation of nucleosides, thus weakening cytotoxicity and conferring resistance. Many studies with cultured cell lines have demonstrated that NT-deficient cells are highly resistant to nucleoside drugs. For example, NT deficiency was responsible for high resistance to gemcitabine cytotoxicity (61). Whether acquired resistance to nucleoside drugs is due to down-regulated NT activity, or to the selective growth of malignant cells with transport-deficient phenotypes or a combination of these requires further investigation (43). Up to now, no specific NT mutations that result in defective NT transportability have been identified in cancer patients with nucleoside drug resistance. Nevertheless, the widely distributed hENT proteins may be determinants for pharmacologic action and resistance of nucleoside anticancer drugs. For instance, hENT1 protein abundance varied in different subtypes of non-Hodgkin' lymphoma (NHL), raising the possibility that hENT1 abundance assessed by immunostaining might be used to predict resistance to nucleoside chemotherapy for NHL patients (62). In addition, since hENT1 and hENT2 are bidirectional and concentration-dependent, drug efflux is a potential resistance mechanism for nucleoside drugs. It is predicted that continuous intravenous drug delivery to maintain relatively high extracellular drug concentrations might prevent this type of resistance.

Elucidating the physiological significance of intracellular nucleoside transporters may open a new avenue to explain nucleoside drug toxicity. Mitochondrial hENT1 resulted in enhanced mitochondrial toxicity of some nucleoside analog drugs (37). CLL patients with elevated hCNT3 mRNA expression experienced a lower response rate to fludarabine therapy; it was suggested that resistance to fludarabine might be related to intracellular membrane localization of hCNT3 protein, which was observed in samples collected from CLL patients subsequent to the clinical trial (39). The recently cloned hENT3 (17), which has been detected partially located in lysosomal membranes, has raised the possibility that accumulation and degradation of nucleoside drugs in intracellular compartments of cancer cells through hENT3 may result in drug resistance. This hypothesis needs to be investigated.

Understanding of the roles of NTs in nucleoside drug toxicity and resistance will provide opportunities for potentiating antitumor efficiency and avoiding resistance. As transportability is a possible determinant of toxicity and resistance, nucleoside drug

uptake and NT abundance might be a prognostic marker to assess drug resistance. Elucidation of the structural determinants of nucleoside analogs for interaction with NT proteins as well as the structural features of NT proteins required for permeant interaction and translocation will lead to "transportability guidelines" for the rational design and application of nucleoside anticancer drugs. It should eventually be possible to develop clinical tests that predict sensitivity to nucleoside drugs and identify patient populations that will benefit from optimal nucleoside analog treatments.

Structure and function of nucleoside transporters

Molecular and functional characteristics

ENTs and CNTs are structurally unrelated protein families. hENT1 (456 amino acid residues) shares 78% sequence identity with rENT1 (457 residues) and 79% sequence identity with the mouse (m) protein, mENT1 (460 residues) (9,63,64). hENT2 contains 456 residues and shares 88% sequence identity with mENT2 and rENT2, both of which also contain 456 residues (8,10,64,65). hENT1 and hENT2 share 46% amino acid sequence identity, with the most homologous regions found in the transmembrane helixes and the least in the hydrophilic termini and loops. hENT3 is a 475-residue protein with 29% identity to hENT1. hENT4 (530 residues) is larger than hENT1 and shares only 18% sequence identity with hENT1 (15). All of the protozoan nucleoside permeases identified to date belong to the ENT family and exhibit ~30% identity at the amino acid level with mammalian ENTs (66).

hCNT1 contains 650 amino acid residues and is 83% and 65% identical to rCNT1 and mCNT1, respectively (7,20,67). hCNT2 contains 659 residues and is 81% and 77% identical to rCNT2 and mCNT2, respectively (21,22,68,69). CNT3 proteins are slightly bigger than CNT1 and CNT2 proteins. hCNT3 contains 691 amino acid residues and shares 88% sequence identity with the 705-residue rCNT3 and 78% identity with the 703-residue mCNT3(24). hCNT1 and hCNT2 share 72% amino acid identity. hCNT3 is 79% identical in amino acid sequence to hfCNT, the hagfish nucleoside transporter, and 48% and 47% identical to hCNT1 and hCNT2, respectively (24,70). mCNT3 contains

additional amino acids at its amino terminus and has higher sequence identity to hfCNT (57%) than to mCNT2 (48%). Phylogenetic analysis revealed that CNT3 cluster closer to hfCNT than to h, m and r CNT1 and CNT2 proteins, indicating that CNT3 (as well as hfCNT) and CNT1/2 comprise two distinct CNT subfamilies (71).

Because the interpretation of transport results obtained from cells and tissues of different origins is often difficult due to variations in the membrane environment and posttranslational modifications and the presence of multiple transporter types, three different expression systems (*X. laevis* oocytes, *S. cerevisie* and cultured mammalian cell lines) that lack endogenous NT activity have been commonly used to functionally characterize recombinant nucleoside transporters. Table 1-1 shows a comparison of K_m and/or K_i values of the five major human NTs produced in oocytes, yeast and cultured mammalian cells. The permeant selectivities of recombinant human NTs were initially demonstrated in *X. laevis* oocytes and this system has been used extensively to characterize kinetic properties of the CNTs. Generally speaking, recombinant hENTs and hCNTs produced in yeast tend to have lower K_m and K_i values than those obtained in oocytes or cultured cells. Recombinant hENTs generally exhibited higher K_m values than the hCNTs in these three expression systems. Recombinant hENT1 exhibits lower K_m values than recombinant hENT2 for all natural nucleosides except inosine. Although the K_m value of recombinant hENT1 produced in yeast was 20% of that of recombinant hENT2, the K_m value of hENT1 produced in cultured cells for inosine was 3-fold higher than that of hENT2 (72,73). The K_m values for hCNT3-mediated transport activity measured in oocytes were 4-15% of that of endogenous CNT3 activity detected in HL60 cells (24,25). The K_m values of hCNT3 obtained from yeast or cultured cells seemed to be closer to those of endogenous hCNT3 process than those obtained from oocytes. It is necessary to fill the gaps of K_m values for various NTs produced in different expression systems so that the functional properties of the transporters can be compared and analyzed in identical genetic and proteomic backgrounds.

Different NT subtypes possess overlapping, as well as different, permeant selectivities for not only naturally occurring nucleosides but also nucleoside analogs including nucleoside anticancer and antiviral drugs. Gemcitabine (61), cytarabine (56), 4'-thio-β-D-arabinofuranosyl cytosine (TaraC) (74), cladribine (40), fludarabine (75) and

5'-deoxy-5-fluorouridine (5'dFUrd, an intermediate metabolite of capecitabine) (52) have been proven to be permeants of hENT1. Both hENT2 and rENT2 showed higher efficiency for the transport of antiviral 3'-deoxy-nucleosides including AZT (3'-azido-3'-deoxythymidine), ddC (2',3'-dideoxycytidine) and ddI (2',3'-dideoxyinosine) than hENT1 (76). hENT2 was also able to transport gemcitabine (77), cladribine and clofarabine (40). hCNT1 was able to transport gemcitabine with high affinity (61,78). Cytarabine, lamivudine and 5'dFUrd (79,80) have also been demonstrated to be permeants of hCNT1. Although ddI and cladribine appeared to be good permeants for rCNT2, they were poorly transported by hCNT2 (81,82). hCNT2 was also able to transport cladribine, fludarabine and clofarabine into cells (40,42). hCNT3 exhibited a broader range of permeant selectivity to various therapeutic nucleoside analogs. It was able to transport both pyrimidine (5-flourouridine, 5'dFUrd, gemcitabine, zebularine) and purine (fludarabine, cladribine, clofarabine) nucleoside drugs with high efficiencies (24,40). Although poorly transported by hCNT3, AZT, ddC and ddI were permeants of recombinant hCNT3 produced in *X. laevis* oocytes (24).

In the absence of high-resolution structures for nucleoside transporter proteins, several experimental approaches have been used to define the structural requirements of nucleosides for interaction with the transporters (42,58,83,84). Inhibitory sensitivity analysis involving a series of uridine analogs indicated that hENT1 formed strong interactions with the 3'-hydroxyl group and moderate interactions with the 2'- and 5'-hydroxyl groups whereas hENT2 formed strong interactions with the 3'-hydroxyl group and only weak interactions with the 5'-hydroxyl group (85), suggesting that hENT2 was more tolerant of sugar modifications than hENT1. A study with human intestinal brush border membrane vesicles suggested that the binding sites of hCNT1 and hCNT2 differentially interacted with analogs of their common permeants, uridine and adenosine, although both transporters were sensitive to modifications at the 6 and 8 positions of the uracil and adenine rings, respectively (84). Using three-dimensional quantitative structure-activity relationships that were based on inhibition data obtained previously, this same group generated pharmacophore models in which the predominant determinants for ligand interaction were hydrogen bonding for hCNT2 and electrostatic and steric features for hCNT1 and hENT1 (83). In a study with stably transfected human

cell lines, hCNT1 and hCNT2 exhibited different capacities for binding of uridine and adenosine analogs with substituents on the ribosyl and/or base moieties (42,58). hCNT1 generally exhibited higher affinities for most uridine analogs tested than hCNT2 and the uridine analogs were transported at two-fold higher rates by hCNT1 than by hCNT2 (42,58). Enantiomeric configuration and the 3'-hydroxyl group of the ribose ring were important determinants for interaction with hCNTs, whereas the 2'-hydroxyl group was less important (42). Although hCNT1 bound several adenosine analogs relatively well, it did not transport any of them whereas hCNT2 transported many adenosine analogs, albeit with low activities (42). A common observation in all of these inhibition studies was the importance of the 3'-hydroxyl group for high affinity interaction of permeants and/or inhibitors with the transporters.

More evidence showed that human nucleoside transporters are able to interact and/or transport a large variety of compounds beyond naturally occurring D-nucleosides and their analogs. Two C-nucleosides, benzamide riboside (1-β-D-ribofuranosylbenzene-3-carboxamide) and tiazofurin riboside (2-β-D-ribofuranosylthiazole-4-carboxamide) were proved to be permeants for hENT1 and 2 and hCNT1, 2 and 3, although different human NTs exhibited different affinities towards them (86). A cyclic nucleotide, cyclic ADP-ribose, was demonstrated to be an inhibitor and probably a permeant for hENT1 and hCNT2 (87). Both hCNT1 and hCNT2 were able to bind some adenosine receptor ligands, including N^6-(p-aminobenzyl)adenosine, caffeine and nicotine, with moderate affinities, although none of them were permeants of both transporters (42). Unexpectedly, a wide variety of protein kinase inhibitors, including p38 mitogen-activated protein kinase (MAPK) inhibitors, protein kinase C inhibitors, tyrosine kinase inhibitors and cyclin-dependent kinase inhibitors, affected nucleoside uptake through selective inhibition of nucleoside transporters in the human erythroleukemia cell line K562 that was independent of kinase inhibition (88,89). We also found that SB203580 and SB203580-iodo, two p38 MAPK inhibitors, were capable of inhibiting uridine and cytidine transport mediated by recombinant hCNT1, hENT1 and hENT2 (at micromole range concentrations) but not by recombinant hCNT3 produced in yeast (Zhang J., Visser F., and Cass C.E., unpublished data). The abilities of human NTs to interact with non-nucleosides warrant further characterization and synthesis of new

analogs of these potential inhibitors with the hope of obtaining high-affinity inhibitors for nucleoside transporters, especially for hCNTs.

Membrane topology

Our present understanding of nucleoside transporter structure is restricted to topological models. Immunological approaches and computer-based sequence analysis in combination with native and engineered N-glycosylation sites have been used to experimentally define the transmembrane helical segment architecture of recombinant hENT1 produced in *Xenopus* oocytes (90). Despite limited sequence homology, family members of SLC29 are predicted to share a common topology of 11 transmembrane segments (TMs), with a cytoplasmic N terminus and extracellular C terminus, and typically contain a large cytoplasmic loop linking TM 6 and TM 7 (Fig. 1-3). A glycosylation site at Asn48 in the extracellular loop between TM 1 and TM 2 has been confirmed in hENT1 (90). hENT2 is glycosylated at Asn48 and Asn57 (91). Although glycosylation is not required for the transport activity of hENT1 and hENT2, it may slightly affect the binding affinities for some NT inhibitors such as NBMPR and dipyridamole and efficient plasma membrane targeting of hENT2 (91,92).

The architecture of the CNT proteins is quite different from that of the ENT proteins, suggesting that these two transporter families have different ancestries. rCNT1 was originally predicted to contain 14 TMs but is now believed to possess 13 putative TMs, with an intracellular N-terminus and an extracellular C-terminus (Fig. 1-3) based on rCNT1 studies using N-glycosylation and immunocytochemistry analysis (32). NupC, a proton-dependent CNT from *Escherichia coli*, shares a similar predicted topology but lacks TMs 1-3 (93). Evidence showed that the large loop located between TM 11 and 12 may form a membrane re-entrant loop, which might be an essential structural element for the permeation of the nucleosides and/or the co-transported cations (Young J., personal communication). By epitope-tagging, hCNT3 has been demonstrated to be N-glycosylated (94). Endoglycosidase treatment of recombinant rCNT1 expressed in *X. laevis* oocytes revealed that rCNT1 could be glycosylated at either or both of Asn605 and Asn643 (32). Although three unique potential glycosylation sites were predicted in hCNT2, removal of two of the three sites, Asn606 and Asn625, resulted in recombinant

proteins produced in *Xenopus* oocytes of reduced molecular mass, indicating that these sites, corresponding to Asn605 and Asn643 of rCNT1, were glycosylated (95). Furthermore, mutation of each of the three sites alone or in tandem resulted in functional proteins and unchanged apical membrane targeting in stably transfected Madin-Darby canine kidney (MDCK) cells, suggesting that N-linked glycosylation is not essential for the function and polarized sorting of hCNT2 (95). Considering that recombinant hCNTs show unchanged transport properties in different expression systems with potentially different glycosylation mechanisms, glycosylation probably does not play essential roles on the structure and function of CNT family of proteins.

Mechanisms of transport

In recent years, the resolving of three-dimensional structures at atomic resolution (96,97) has dramatically increased our knowledge of the structure and molecular mechanisms of transporters. Nucleoside transporters belong to the major facilitator superfamily, which are believed to function as monomers, transporting solute and co-ions using the "alternating access mechanism", a theory that was proposed a half-century ago by Widdas (98). This alternating access mechanism involves conformational changes that enable the solute and co-ions to bind to sites on the transporter that are exposed to the extracellular side of the cell, after which the binding site reorients and the solute and co-ions dissociate into the cytoplasm (99,100). According to this model, a transporter has two major conformations: inward-facing and outward-facing and permeant binding sites are accessible to only one side or the other at a given time. The *es* transporter (i.e, ENT1) has been shown to be capable of switching between the inward-facing and outward-facing conformations in either the permeant-bound or unbound states and the conformational alternating rate was substantially more rapid when the permeant was available (25). NBMPR sites of *es* transporters are believed to be located on the extracellular aspect of plasma membranes and site-bound NBMPR is thought to lock the hENT1 protein in the outward-facing conformation state (101,102). Because the CNTs accept two different solutes, nucleoside and cation, it has been proposed that two inward-facing and that two outward-facing conformational states (binding cation only or binding

both cation and nucleoside) exist and the addition of cation unlocks and opens the nucleoside binding sites, thereby initiating active transport (103).

Although ENTs and CNTs are thought to share the alternating access model for nucleoside transport, they differ in that most ENTs mediate facilitated diffusion and most CNTs mediate sodium- or proton-dependent permeant uptake. Sodium-dependency of a concentrative transporter can be determined simply by comparing initial transport rates in buffers containing sodium at physiological concentration with those in buffers for which sodium has been replaced by an alternative cation, e.g., choline or N-methyl-D-glucamine. In lower organisms, such as bacteria, yeast and *Caenorhabditis elegans*, CNT transport processes are performed by proton-symporters rather than sodium cotranspoters and the energy is derived from the proton motive force maintained by H^+/K^+-ATPase (93,104,105). Despite being named equilibrative transporters, the SLC29 family includes active, proton-linked members, such as those of plant and kinetoplastid protozoa (66,106,107). The transporter activity of hENT3, a transporter thought to be present in lysosomal membranes, exhibited a strong dependence on pH with optimal uptake into oocytes occurring at pH 5.5 (17). It is unclear whether such pH dependence reflects proton-coupling transport activity. However, the optimum pH value is similar to that of late endosomes/lysosomes, indicating that the likely physiological function of hENT3 is the release of nucleosides produced by nucleic acid breakdown in the lysosomal interior.

CNTs are electrogenic and utilize energy stored in the transmembrane potential and the sodium or proton concentration gradients to accumulate nucleosides in the cell, which enables the study of molecular mechanisms of transport using electrophysiological approaches. The dependence of hCNT1- or hCNT3-mediated sodium currents on uridine concentrations has been examined at several different extracellular sodium concentrations (103,108). For both transporters, the apparent affinities for uridine increased as the extracellular sodium concentration increased without significant change in maximal currents, indicating a sequential ordered binding mechanism in which sodium binds to the transporter first, resulting in a conformation state of the transporter with increased affinity for the nucleoside (109,110). Steady-state kinetic studies revealed that the affinities for uridine and sodium of both hCNT1 and hCNT3 were voltage-dependent

and the voltage dependence of uridine binding was the result of the voltage dependence of sodium binding (109,110). Therefore, membrane potential influences both ion-binding and permeant translocation. Besides studying the rate-limiting reaction step in the transport cycle under steady-state conditions, the properties of non-rate-limiting partial reaction steps of the hCNT1 produced in oocytes have been determined by a method that is based on rapidly perturbing the steady state and subsequently following the kinetics of the relaxation to a new steady state (pre-steady-state) (111). In the absence of nucleoside and in response to rapid changes of the transmembrane potential, hCNT1 exhibited presteady-state currents in the presence and absence of extracellular sodium (108). The presteady-state current-time integrals of hCNT1 obeyed a Boltzmann function and were used to quantitatively estimate the fraction of membrane field sensed by sodium (61%), the valency of the movable charge (-0.81, which is consistent with the 1:1 sodium/nucleoside coupling ratio), and the average number of transporters present in the oocyte plasma membrane yielding the turnover rate (9.6 uridine molecules/hCNT1 protein/sec at membrane potential of -50 mV) (108).

The stoichiometry of sodium-nucleoside cotransport has also been determined in CNT-producing oocytes by simultaneously measuring nucleoside-induced current and nucleoside uptake under voltage-clamp conditions. Mammalian CNT1 and CNT2 have a sodium/nucleoside coupling ratio of 1:1, whereas hfCNT and mammalian CNT3 is 2:1 (24,70,103,108). The transport of nucleosides mediated by CeCNT3 or CaCNT (from *C. elegans* and *C. albicans*, respectively) was dependent on pH, with optimal uptake at about pH 5.5 (105,112). CaCNT has a proton:nucleoside coupling ratio of 1:1 (112). Examination of the effects of a proton ionophore that disrupts the transmembrane proton gradient confirmed that CeCNT3 is proton-coupled; however, the permeant-induced proton currents were too small to be measured (105). CNT1, CNT2, NupC, CeCNT3 and CaCNT showed either sodium or proton dependence whereas hCNT3 and mCNT3 exhibited broad cation interactions with Na^+, H^+ and Li^+ (103).

Amongst the CNTs for which voltage dependence has been examined to date (hCNT1, hfCNT and CaCNT) (70,108,112), sodium/nucleoside coupling ratio of hCNT3 was demonstrated to be voltage-dependent, progressively approaching its maximum value of 2:1 as the membrane potential became more negative (103). Sodium and proton

can individually activate hCNT3-mediated nucleoside transport through mechanisms involving increased permeant binding affinities. In the presence of Na^+, addition of H^+ elicited no further increase of permeant binding affinity. Furthermore, the cation/nucleoside coupling ratio of hCNT3 was 2:1 in the presence of Na^+ and both Na^+ plus H^+ but was only 1:1 in the presence of H^+ alone, suggesting that hCNT3 possesses two sodium binding sites only one of which is shared by protons (103). hCNT3 interacted with protons and sodium with different affinities; protons bound the protein four orders of magnitude tighter than sodium. Proton-coupled hCNT3 exhibited significantly reduced transportability for thymidine, cytidine, adenosine and inosine, and no ability to transport guanosine, AZT and ddC when compared to transportability in the presence of sodium. These markedly different permeant selectivities for both physiologic nucleosides and therapeutic nucleoside analogs between proton-coupled hCNT3 and sodium-coupled hCNT3 demonstrated that the binding of sodium and protons induced different conformational changes of hCNT3 that resulted in formation of different nucleoside binding pockets and /or translocation pores (103).

Protein structure determinants of transporters

Characterization of chimeric constructs between different hENTs and rENTs has revealed regions of the proteins that are involved in permeant and inhibitor interactions. Although hENT1 and rENT1 exhibit similar binding affinities for NBMPR, hENT1 is 50-fold more sensitive to dipyridamole and dilazep inhibition than rENT1 (64,73,113). The inhibitor sensitivities of the chimeras between hENT1 and rENT1 suggested that TMs 3-6 contain the major site(s) of interaction with secondary contributions from TMs 1-2, providing the first insight into the regions of hENT1 that are important for interaction with dilazep and dipyridamole. Studies with recombinant chimeric constructs between rENT1 and rENT2 indicated that TMs 3-6 contained residues responsible for sensitivity or resistance to NBMPR interaction (114). Uptake experiments using the same chimeric constructs demonstrated that TMs 5-6 appear to be important for the ability of ENT2 to efficiently transport 3'-deoxynulcoesides (76) and TMs 5-6 of rENT2 are required for nucleobase translocation (13).

Recently, studies using site-directed mutagenesis have identified several individual amino acid residues located within TMs 3-6 that are responsible for interaction with nucleosides or inhibitors. Gly154 in TM 4 of hENT1 has been implicated in sensitivity to NBMPR: substitution of Gly154 to serine resulted in loss of NBMPR binding (18). Further characterization of the properties of the Gly154 mutant demonstrated that mutation of this residue to serine converted hENT1 to a transporter that functioned like hENT2 (115). hENT1-G154S exhibited decreased sensitivities to inhibitors NBMPR, dilazep and dipyridamole and decreased affinities for cytidine and adenosine, suggesting that Gly154 plays dual roles in permeant uptake and inhibitor interactions. The involvement of this residue in inhibitor/permeant binding is also supported by chemical modification of the corresponding Cys140 residue of rENT2. Modification of Cys140 by p-chloromercuribenzene sulfonate (PCMBS), a membrane impermeable sulfhydryl-specific reagent, inhibited nucleoside transport mediated by rENT2 and high concentrations of uridine protected against inactivation by thiol modification, indicating that Cys140 of rENT2 was located on the exofacial side of TM 4 and may form part of the permeant binding sites or translocation pore (116). Gly179 and Gly184, located in TM 5 of hENT1, are highly conserved residues across various species. Mutation of Gly179 to alanine resulted in impaired uridine transport and this residue has been implicated in playing a direct role in NBMPR binding (117). Mutation of Gly184, on the other hand, resulted in reduced plasma membrane abundance of hENT1, indicating that this residue likely plays a role in targeting of hENT1 to the plasma membrane (117). Furthermore, the altered properties of mutants of these two glycine residues may reflect their roles in helix-helix contacts.

Six amino acid residues of hENT1 (Met33, Leu442, Trp29, Phe80, Phe334 and Asn338) that were involved in inhibitor interactions have been identified by random mutagenesis of several ENT cDNAs and phenotypic complementation screening in yeast (11,12,72,102). Met33 in TM 1 of hENT1 was first identified as a determinant for dipyridamole and dilazep sensitivity. Mutation of hENT1 Met33 to the corresponding isoleucine of hENT2 decreased dipyridamole/dilazep inhibition of uridine transport and the reciprocal mutation (Ile33 to Met) in hENT2 increased sensitivity to these inhibitors (11). In-depth studies using kinetic analysis and pCMBS modification revealed that

Ile33 in hENT2 resides in an extracellular aspect of TM 1, directly interacts with dipyridamole and is a common component of both the permeant and dipyridamole binding sites (72). Despite limited amino acid sequence identity, hENT1 and CeENT1 both bound dipyridamole with high affinities. Random mutagenesis and screening of CeENT1 for mutants with reduced dipyridamole inhibition identified residue Ile429, which corresponds to Leu442 (TM 11) of hENT1, as a critical residue for high affinity interactions with dipyridamole and dilazep (12). hENT1-L442I displayed a 10-fold lower affinity for uridine transport and impaired adenosine transport compared with those of hENT1, suggesting that Leu442 may be involved in transporter function and permeant selectivity. Detailed functional analysis of single and double mutants at positions 33 and 442 of hENT1 and the corresponding mutants of CeENT1 suggested that TM 1 and TM 11 of hENT1 and CeENT1 form part of the dipyridamole binding sites and dipyridamole bound these two positions sequentially: TM 1 residue is a primary site of interaction of dipyridamole with hENT1 and this interaction resulted in close packing of TMs 1 and 11, thus bringing Met33 close to Leu442 followed by Leu442-dipyridamole interaction; and for CeENT1, the reverse sequence is the case (12).

Both Trp29 and Phe334 are highly conserved in the ENT protein family and mutation of either residue altered the sensitivity to inhibitors including NBMPR, dipyridamole, dilazep, draflazine and soluflazine (102). It was proposed that draflazine and soluflazine form hydrogen bonds with Asn338 and, like NBMPR, interact with Trp29 via aromatic stacking interaction with the fluorophenyl groups. Given the location of Asn338 on the intracellular end of TM 8, draflazine may access its binding site from either side of the membrane (102). Kinetic studies suggested that Trp29 was functionally important for adenosine transport with various mutations of this residue causing reduced transport capacity and/or permeant binding affinity. It was also observed that hENT1-W29T lacked uridine transportability whereas adenosine transportability was not severely compromised, implying that Trp29 is involved in permeant selectivity. Several protozoan ENTs, including LdNT2 (*Leishmania donovani* nucleoside transporter 2) and TbNTs1-7 (*Trypanosoma brucei* nucleoside transporters 1-7), which are purine nucleoside selective and unable to transport uridine and other pyrimidine nucleosides, contain a threonine residue at the corresponding position of Trp29 of hENT1. It would

be interesting to determine if the reciprocal mutation (substitution of the threonine residue of the protozoan ENTs with tryptophan) would allow transport of pyrimidine nucleosides. Phe80 and Phe334 were significant contributors to dipyridamole and dilazep sensitivity, although to a lesser extent than Trp29 and Met33. Phe334 mutants of hENT1 also showed reduced affinity for NBMPR. Phe80 mutations induced modest changes in transporter function whereas Phe334 markedly increased catalytic activities of hENT1 and rENT1 when mutated to tyrosine.

Three more residues of hENT1 (Met89, Leu92 and Ser160) that are important for inhibitor binding and/or nucleoside transport have been identified by random mutagenesis and yeast adenosine complementation (19,118). Met89 and Leu92, which are located in the hydrophilic side of the helical wheel and near the intracellular aspect of TM 2, are both minor determinants for permeant affinities. The Met89 mutant exhibited slightly decreased sensitivity for NBMPR whereas the Leu92 mutant exhibited decreased sensitivity for both NBMPR and dilazep. Mutation of Ser160 in TM 6 resulted in a slight decrease in permeant affinity and a slight increase in sensitivity to dipyridamole inhibition. Genetic and mutagenesis studies of LdNT1.1 and LdNT2 have identified several functionally important determinants that may play significant roles in many, if not all, ENT family members (66). Mutation of Gly183 in TM 5 of LdNT1.1, which corresponds to Gly184 of hENT1, resulted in impaired transport activity and changed permeant selectivity without affecting plasma membrane targeting (119), implying that TM 5 of LdNT1.1 interacts with permeant. The subsequent studies of TM 5 using the substituted cysteine accessibility method (SCAM) revealed that six residues that are clustered along one face of the amphipathic helix were accessible to sulfhydryl reagents, suggesting that TM 5 formed part of the nucleoside translocation pathway (120). Phe334 and Asn338 (TM 8) of hENT1 are in close proximity to the highly conserved hydrophilic residues Asp341 and Arg345, the corresponding residues of which were shown in LdNT2 to be critical for transporter function and targeting (121), further indicating that TM 8 is important for properly maintaining the function of ENT family.

According to helical wheel projections involving TMs 1, 2, 4, 5, 8 and 11 containing the important residues mentioned above, all of these TMs display amphipathic characteristics to varying degrees, and contribute to inhibitor interactions and/or

permeant transport, suggesting that they may form part of the permeant translocation channel and/or inhibitor-binding sites. Dipyridamole and dilazep were the only two inhibitors whose interactions were affected by mutation of most residues identified, suggesting that dipyridamole and dilazep, although structurally different, bind to the same site. Except Asn338, all of the identified residues that played roles in inhibitor sensitivity were functionally important and most of them appeared to be located on extracellular aspects of the TMs (Fig. 1-3). It was concluded that multiple sites of the transporter were involved in inhibitor/permeant binding and inhibitors competed with permeants for binding by the transporter.

While considerable progress has been made in elucidating the structural basis of ENT proteins, studies on the structurally and functionally important residues of CNT family are still at an early stage. Nevertheless, the first three TMs are considered to be not essential for transport function, since rCNT1 or hCNT1 with TMs 1-3 deleted retained significant sodium-dependence and transport activity (32). Phe316 and Gly476, located in putative TM 7 and TM 11 of hCNT1, respectively, are highly conversed residues across 17 CNT-type sequences from eight different species. Substitution of Gly476 with either alanine or leucine resulted in loss of plasma membrane expression of hCNT1-GFP (green fluorescence protein) in undifferentiated or differentiated MDCK cells, suggesting that Gly476 may play a role in membrane targeting, protein folding and/or intracellular trafficking (122). A conserved hCNT1 mutant, F316Y produced in MDCK cells showed significant increased sensitivity to guanosine inhibition, which partially resembled a CNT transport activity called *csg* (concentrative, sensitive to NBMPR and accepts guanosine as permeant) (123) observed in the human kidney. Genotyping of hCNT1 revealed that a natural variant, hCNT1-F316H, which also displayed an unusual sensitivity to guanosine inhibition, occurred with an extremely low allele frequency in the population, suggesting that it is more likely to be a rare mutation rather than a polymorphism (122).

Uptake experiments using a series of chimeric constructs between rCNT1 and rCNT2 demonstrated that TMs 7-8 of the 13-TMs model (Fig. 1-3) is the major structural domain for permeant recognition and selectivity (124). According to helical wheel analysis, TM 7 and TM 8 may form amphipathic alpha helices and contain abundant

hydroxyl and amide side chains that could participate in nucleoside binding or line a transmembrane pore through which the nucleoside moves. Subsequent mutagenesis studies demonstrated that Ser318/Gln319 of rCNT1 and Ser319/Gln320 of hCNT1 were essential for pyrimidine selectivity of CNT1-mediated transport (124,125). Substitution of Ser318 with glycine transformed rCNT2 to a broadly selective transporter (124). Furthermore, mutation of two adjacent pairs of residues (Ser319/Gln320 and Ser353/Leu354) in the TM 7-9 region of hCNT1 to the corresponding residues in hCNT2 (Gly313/Met314 and Thr347/Val348) converted hCNT1 into a transporter with hCNT2 functional characteristics (125). An intermediate broad specificity hCNT3-like transport activity was produced by mutation of the two TM 7 residues alone (125). The amino acid residues of hCNT3 and hfCNT at these four corresponding positions represent the intermediate state between hCNT1 and hCNT2 that allow transport of both purine and pyrimidine nucleosides. These studies demonstrate that only a limited number of amino acid changes resulte in permeant-specialized transporters. Consistent with these chimera and mutagenesis experiments, the 50:50 chimeric proteins between hCNT3 (TMs 1-6) and hCNT1 (TMs 7-13) and between hfCNT (TMs 1-6) and hCNT1 (TMs 7-13) produced in *X. laevis* oocytes exhibited hCNT1-like cation interactions, as well as hCNT1-like permeant selectivities, that transport pyrimidine nucleosides but not guanosine or inosine (70,103), indicating that the structural determinants of cation stoichiometry and binding affinity were located within the C-terminal half of the protein. The loss of proton-dependence of the hCNT3 and hCNT1 chimera indicated that the proton binding site resided in the C-terminal half of the protein (103), limiting the region for mutagenesis experiments to identify the amino acid residues involved in proton interactions.

Genetic variants of CNTs

To explore whether genetic variations may explain the heterogeneous response to nucleoside anticancer treatment and account for part of the drug resistance mechanism, comprehensive genetic and functional analysis approaches have been used to identify and characterize the genetic variants of nucleoside transporters in ethnically diverse population. Data on the variants of hENTs and hCNTs are available at two

pharmacogene websites: http://www.pharmgkb.org and http://pharmacogenetics.ucsf.edu. Relative to the other 24 human membrane transporter genes analyzed, *hENT1* exhibited exceptionally low mutability, even in non-coding regions (126). Four synonymous and two non-synonymous coding region hENT1 variants with low allele frequencies were identified from 247 individuals (127). The two non-synonymous variant transporters, ENT1-I216T and ENT1-E391K, and the reference ENT1 exhibited similar uptake of nucleosides and nucleoside analogs in a yeast expression system, indicating that coding region variants of ENT1 do not contribute to inter-individual differences in response to nucleoside analog drugs. Fifty-six single nucleotide polymorphisms (SNPs) in the exons and introns of hCNT3 were identified in a collection of 270 DNA samples from US populations (128). Of the 16 coding region variants, 10 resulted in amino acid changes (S5N, T113C, I328V, R4K, D62S, R67K, R349Q, G367R, L419I and R585H). Nucleotide diversity at nonsynonymous and synonymous sites of the *hCNT3* gene was low, suggesting that *hCNT3* is under negative selection. All non-synonymous variants maintained similar transport properties of wild-type hCNT3 protein except a rare variant, hCNT3-G367R. Gly367 is one of the four highly conserved residues in TM 8 and mutation at this position resulted in an 80% decrease in transportability, suggesting that TM 8 is a putative permeant recognition domain of hCNT3. A parallel study of the *hCNT3* gene using 96 DNA samples from Caucasians revealed sixteen variants in exons and flanking intronic regions, of which five were coding variants with three non-synonymous variants (S5N, L131F, Y513F) (86). Functional expression of these CNT3 variants and wild-type hCNT3 in yeast and *X. laevis* oocytes revealed no difference in protein abundance, transport activity and sodium/proton dependence. The observed low allele frequencies of various SNPs and lack of functional diversity of various non-synonymous coding SNPs in hENT1 and hCNT3 implied high conservation of function in these two broadly selective transporters and their critical role for human fitness.

hCNT1 is a highly variable gene. Using DNA samples from the same study of hENT1 variants (127), fifty-eight SNPs were identified in the exons and flanking introns, resulting in a high frequency of 1.5 SNPs per 100 bp (129). Of the 26 coding region SNPs, 13 were nonsynonymous. An insertion (CNT1 + 140Val) and a deletion (CNT1–1153del) mutation with high frequencies were also identified. Functional analysis of

these CNT1 variants, including the insertion and deletion mutants, in *X. laevis* oocytes revealed that all variant transporters took up thymidine with the exception of CNT1-S546P and CNT1–1153del, a bp deletion resulting in a frame-shift followed by a stop codon. Compared with wild-type CNT1, CNT1-V189I exhibited a reduced affinity for gemcitabine. These data suggested that common genetic variants of CNT1 may contribute to variation in systemic and intracellular levels of anti-cancer nucleoside analogs. *hCNT2* is less mutable than *hCNT1*. The same DNA samples that were used for the *hCNT2* analysis identified 10 coding region variants, of which six were non-synonymous (130). All six non-synonymous variants were able to transport guanosine in *X. laevis* oocytes. Although no differences were observed among the four common variants (P22L, S75R, S245T and F355S) and wild-type CNT2 in uptake of the antiviral drug, ribavirin, CNT2-F355S exhibited a change in specificity for the naturally occurring nucleosides, inosine and uridine. The existence of the hCNT2 variant that results in a specificity change among naturally occurring nucleosides could mean that individuals bearing this variant may have an alteration in nucleoside homeostasis with possible changes in the disposition of nucleoside analog drugs (130).

The intronic SNPs of nucleoside transporter genes need to be investigated for possible roles in the generation of differentially spliced transcripts. Relatively little is known about the regulation of the human nucleoside transporters and the possible influence of promoter region polymorphisms (regulatory SNPs) (86). Variations in non-coding regions that might alter mRNA stability or transcription efficiency through polymorphisms in 3'-untranslated regions or promoter regions of the hENT and hCNT genes have not been described. Continuing determination of the roles of genetic variants of nucleoside transporters in the systemic and intracellular disposition of nucleosides and nucleoside analog drugs is an important task for the future.

Nucleoside transporters of yeast *S. cerevisiae*

Yeast have been utilized as a heterogeneous expression system for functional characterization of a variety of recombinant eukaryotic transporters such as those for glucose, peptides, nucleosides, nucleobases and multidrug resistance transporters (11,72,92,131-137). In the laboratory of my supervisor (Dr. C. E. Cass), yeast *S. cerevisiae* has been successfully used to produce both recombinant hENTs and hCNTs that enabled functional analysis of transporters using a cell-harvester-based high-throughput transport assay (72,102,138,139). A phenotype complementation growth assay in which recombinant hENT1- or CeENT1-mediated thymidine uptake can be blocked by NT inhibitors was developed and NT mutants with reduced inhibitor sensitivities have been successfully identified using this assay (11,12,102). The hENT/hCNT yeast expression system also supplied large amounts of recombinant proteins for reconstitution of transporters into proteoliposomes (92) and screening of anti-hENT or anti-hCNT antibodies. Characterization of the role and functional properties of nucleoside transporters in *S. cerevisiae* (termed "permeases" in the yeast literature) is essential for the understanding of endogenous nucleoside transport process in such an important model organism and for the improvement of using yeast as the host for functional expression of human nucleoside transporters. Two nucleoside transporters, FUN26 and FUI1 have been identified in *S. cerevisiae* (140).

FUN26

Database searching of the *S. cerevisiae* genome revealed that a protein encoded by YAL022 and termed FUN26 shares no sequence similarity with other yeast proteins but limited amino acid identity (18.4%) with hENT1 and hENT2 (8,9). FUN26 contains 517 amino acid residues and topology modeling shows that it shares 11 TMs with other ENT family proteins and has a very long hydrophilic N-terminus that is characteristic of yeast permeases (141,142). No nucleoside transport activities could be detected in yeast that overexpressed the *FUN26* gene; however, FUN26 heterogeneously produced in *Xenopus laevis* oocytes was demonstrated to initiate low, but significant, uptake of a broad range of both purine and pyrimidine nucleosides (140), indicating that FUN26 may

function intracellularly. Unlike most yeast nutrient permeases, FUN26-mediated nucleoside uptake was not pH-dependent and, unlike hENTs, was not sensitive to the ENT inhibitors NBMPR, dipyridamole or dilazep (140). Immunotagged recombinant FUN26 produced in *S. cerevisiae* was localized in late endosomal membranes not in plasma membranes. Recombinant FUN26 produced in yeast, but not endogenous FUN26, was detected by immunoblottting using polyclonal anti-FUN26 antibodies raised against a peptide (RRTNGTRDDNDEGEE) located in the intracellular loop between the putative TM 1 and TM 2 (Zhang J, Vicker MF and Cass CE, unpublished data). Microarray analysis of all known genes expressed in *S. cerevisiae* during the cell cycle revealed that FUN26 mRNA was most abundant during M phase. The promoter region of FUN26 contains two *cis* elements that could potentially be activated by an M phase-specific transcription factor. These results indicated that *FUN26* is cell-cycle regulated. Further promoter analysis techniques need to be applied to identify the regulation mechanisms of FUN26 expression.

Uridine permease FUI1

Unlike FUN26, which is a homolog of human nucleoside transporters, uridine permease FUI1 shares no significant homology with any mammalian proteins. FUI1 belongs to the uracil/allantoin permease family (FUR family) of yeast, including FUR4, THI10 (thiamine permease) and DAL4 (allantoin permease). FUI1 (629 amino acids, 72 KDa) shares high amino acid identity (50-60%) with its members and is predicted to have similar topology model of FUR4 that contains 10 TMs with long intracellular N- and C-terminal tails (143). *fui1* is not an essential gene since a *fui1* knockout yeast strain remained viable; however, *fui1* disruption resulted in resistance to cytotoxic effects of 5-fluorouridine, which led to the suggestion that FUI1 may mediate uridine uptake (140).

FUI1 is the only NT identified in the plasma membrane of *S. cerevisiae* so far (140). Knockout of *fui1* enabled the creation of a yeast strain with NT-free background that has been used to heterogeneously express mammalian nucleoside transporters. FUI1 is a unique nucleoside transporter since it only accepts uridine but not any other naturally occurring nucleosides as its permeant (140). FUI1-mediated uridine uptake was not affected by ENT inhibitors such as NBMPR, dilazep and dipyridamole and it exhibited

high affinity for uridine but not for most uridine analogs tested (140). Unlike the well-studied uracil permease FUR4, little is known about the transport mechanism, structural and functional determinants and regulation of FUI1.

Summary and objectives

Nucleoside transporters recognize most nucleoside-derived drugs used in anticancer and antiviral treatments and thus are pharmacological determinants that likely influence drug bioavailability and the consequent response to therapy (2,43). Since the molecular characterization of two families of human nucleoside transporters, there has been dramatic progress in the understanding of the properties of nucleoside transporters including their role in nucleoside chemotherapy, structural and functional determinants, inhibitor interactions and transport mechanisms. Although an ultimate understanding of the molecular mechanisms of transport will depend on determination of the high-resolution structure of the transporters, detailed investigations of structure-function relationships of transporters and their permeants/inhibitors using non-crystallographic approaches are likely to continue to reveal key information that should enable the rational design of nucleoside analogs and inhibitors with enhanced target-cell selectivity and specificity to potentiate the therapeutic effects of nucleoside drugs and nucleoside transporter inhibitors.

Molecular cloning and functional expression of nucleoside transporters in heterogeneous expression systems have allowed detailed studies of permeant selectivity and kinetic and electrophysiological properties of individual nucleoside transporter subtypes. Research using chimeric constructions, site-directed mutagenesis, genetic polymorphisms, and phenotypic screening in yeast has started to define the structural domains and individual amino acids of hENTs and hCNTs involved in permeant and/or inhibitor interactions. Systematic studies using SCAM approaches on functional cysteine-less versions of nucleoside transporters would test the validity of the existing models of the nucleoside transporters and allow more detailed structural modeling of permeant/inhibitor binding sites of the transporter proteins. The high-throughput transport assay system developed using yeast as the model host system is ideal for systematic studies to define kinetic properties and transportability profiles of individual nucleoside transporter for the existing and newly developed nucleoside analog drugs, which in turn, will allow the prediction of *in vivo* disposition and targeting of therapeutic nucleoside drugs. Moreover, the yeast expression system can be applied to screen a large

number of chemicals for the discovery of high-affinity inhibitors for CNT proteins. With many ENTs and CNTs identified from different species, it would be informative to assess the species differences in permeant selectivity and inhibitor sensitivity in the yeast expression system, with the possibility of identifying critical structural elements responsible for functional difference among different nucleoside transporter subtypes from different species. With the availability and continued development of specific NT antibodies and labeled nucleosides, the tissue and cellular locations of NT subtypes as well as intracellular distributions of nucleosides and/or their metabolites can be determined. Studies using cell and animal models with particular NTs modified by gene knockout should establish the biochemical and physiological roles of a particular nucleoside transporter.

The objectives of the research of this thesis were (1) to identify uridine binding motifs of hCNTs and FUI1 as well as the uridine transportability profiles of hCNT proteins using inhibitory-sensitivity assay and voltage-clamp techniques, (2) to identify structural determinants of hCNT3 and FUI1 that are involved in permeant interactions and/or translocation using SCAM and mutagenesis approaches, and (3) to monitor nucleoside transport processes in living cells using autofluorescence nucleoside analogs and real-time confocal microscopy. The results of these studies provided the binding and transportability profiles for hCNT1, hCNT2, hCNT3 and FUI1 and new information on the structural and functional roles of the last three putative TMs of hCNT3.

Table 1-1 Affinities of recombinant nucleoside transporters produced in *Xenopus laevis* oocytes, *S. cerevisiae* and cultured cells.

		X. laevis oocytes		*S. cerevisiae*		Cultured cells	
NT	Permeant	K_m (μM)	K_i (μM)	K_m (μM)	K_i (μM)	K_m (μM)	K_i (μM)
hENT1	Uridine	240[8]		44.1[72]	51.9[72]	260[91]	
	Cytidine			234[72]	346[72]	580[91]	
	Thymidine				81.6[72]	300[91]	
	Adenosine			17.8[72]	10.3[72]	40[91]	
	Inosine			28.5[72]	34.6[72]	170[91]	
	Guanosine			47.5[72]	48.6[72]	140[91]	
hENT2	Uridine	200[9]	250[13]	195[72]	216[72]	250[91]	
	Cytidine				1380[72]	5610[91]	
	Thymidine				129[72]	710[91]	
	Adenosine			106[72]	129[72]	140[91]	
	Inosine			180[72]	192[72]	50[91]	
	Guanosine				394[72]	2700[91]	
hCNT 1	Uridine	45[20], 32[108]	50[20]	9.2[138]	3.1[138]	34[42]	
	Cytidine				16.4[74]	120[79]	
	Thymidine				2.6[138]		
	Adenosine		50[20]				39[42]
hCNT 2	Uridine	40[21], 80[22]		29[139]	28[139]	46[58], 28.1[144]	
	Cytidine				1397[138]		
	Thymidine				151[139]		>500[58]
	Adenosine	8[21]	6[22]	11.2*	8.3*		25[42]
	Inosine	4.5[22]				20.6[144] 13.7[145]	
	Guanosine						
hCNT 3	Uridine	21.6[24]		1.7[86]	2.0[138]	1.1[94]	
	Cytidine	15.4[24]		3.6[86]	4[138]	3.4[94]	
	Thymidine	21.2[24]			26.5[138]	3.7[94]	
	Adenosine	15.1[24]		2.2[86]		4.6[94]	
	Inosine	52.5[24]		2.1[86]		4.3[94]	
	Guanosine	43[24]				5.1[94]	

* Zhang J. and Cass C.E., unpublished data.

The radiolabeled permeants used in the inhibitory assays for obtaining K_i values of various nucleosides were uridine (8,13,20,42,58,74,138,139), inosine (22), or adenosine (72).

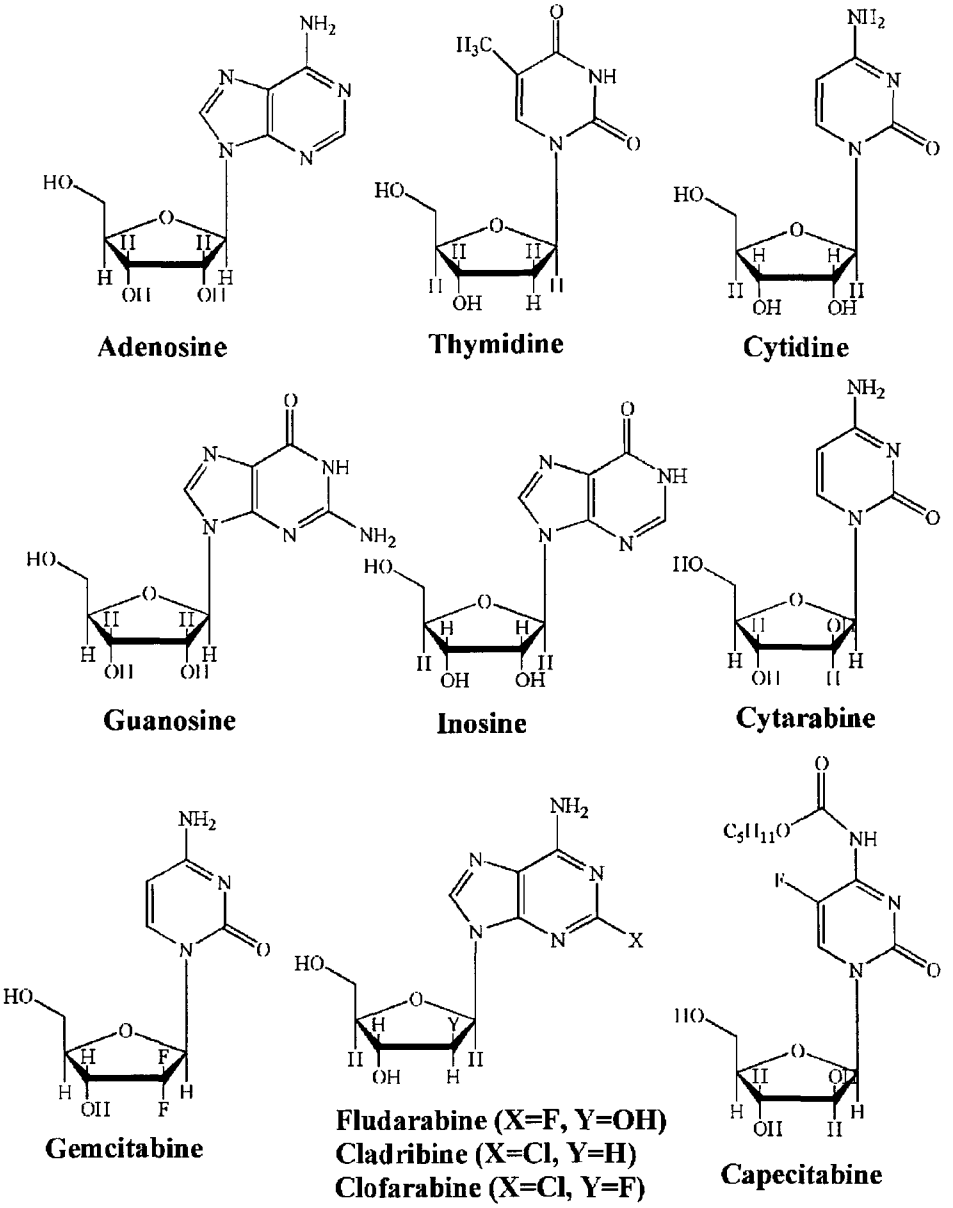

Figure 1-1 Chemical structures of nucleosides and nucleoside analogs.

The structures of adenosine, thymidine, cytidine, guanosine, inosine, gemcitabine (2',2'-difluoro-2'-deoxycytidine), cytarabine (araC, cytosine-β-D-arabinofuranoside), fludarabine (9-*β*-D-arabinofuranosyl-2-fluoroadenine), cladribine (2-chloro-2'-deoxyadenosine), clofarabine [2-chloro-9-(2'-deoxy-2'-fluoro-β-D-arabinofuranosyl) adenine] and capecitabine (5'-deoxy-5-N-[(pentoxy)carbonyl]-cytidine) were generated using ChemDraw Version 6.0 software.

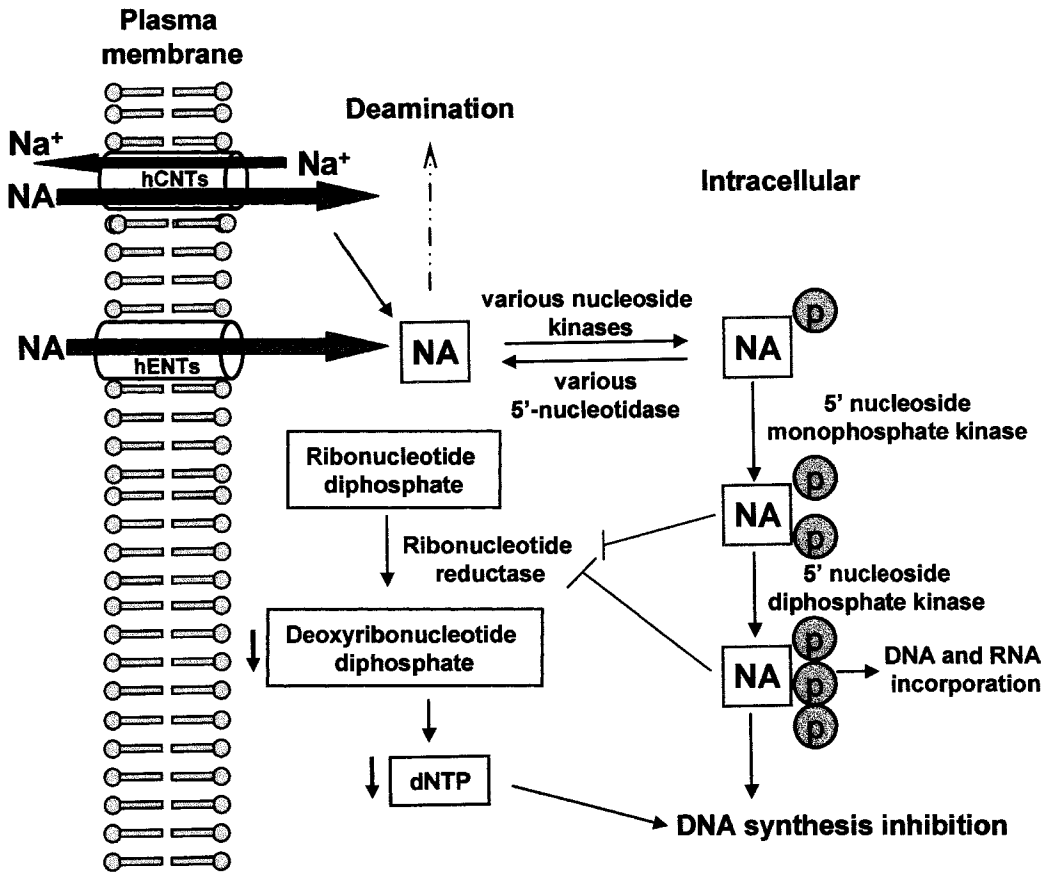

Figure 1-2 The metabolism of nucleoside analogs (NAs) in proliferating cells.

The uptake of NAs is mediated via specific nucleoside transporters. Once inside cells, NAs are phosphorylated by various nucleoside kinases (such as deoxycytidine kinase, thymidine kinase or deoxyguanosine kinase), to the 5'-monophosphate and subsequently to the 5'-diphosphate and the ultimate 5'-triphosphate derivatives. Some NAs could be rapidly degraded via deamination by either adenosine deaminase or cytidine deaminase. The 5'-monophosphate derivatives can be dephosphoralated to NAs by various 5'-nucleotidases. The incorporations of NA mononucleotides into newly synthesized DNA may result in chain termination and subsequent cell death. Some NA triphosphates can inhibit ribonucleoside reductase, resulting in decreased normal dNDPs and dNTP pools, thus indirectly inhibiting DNA synthesis.

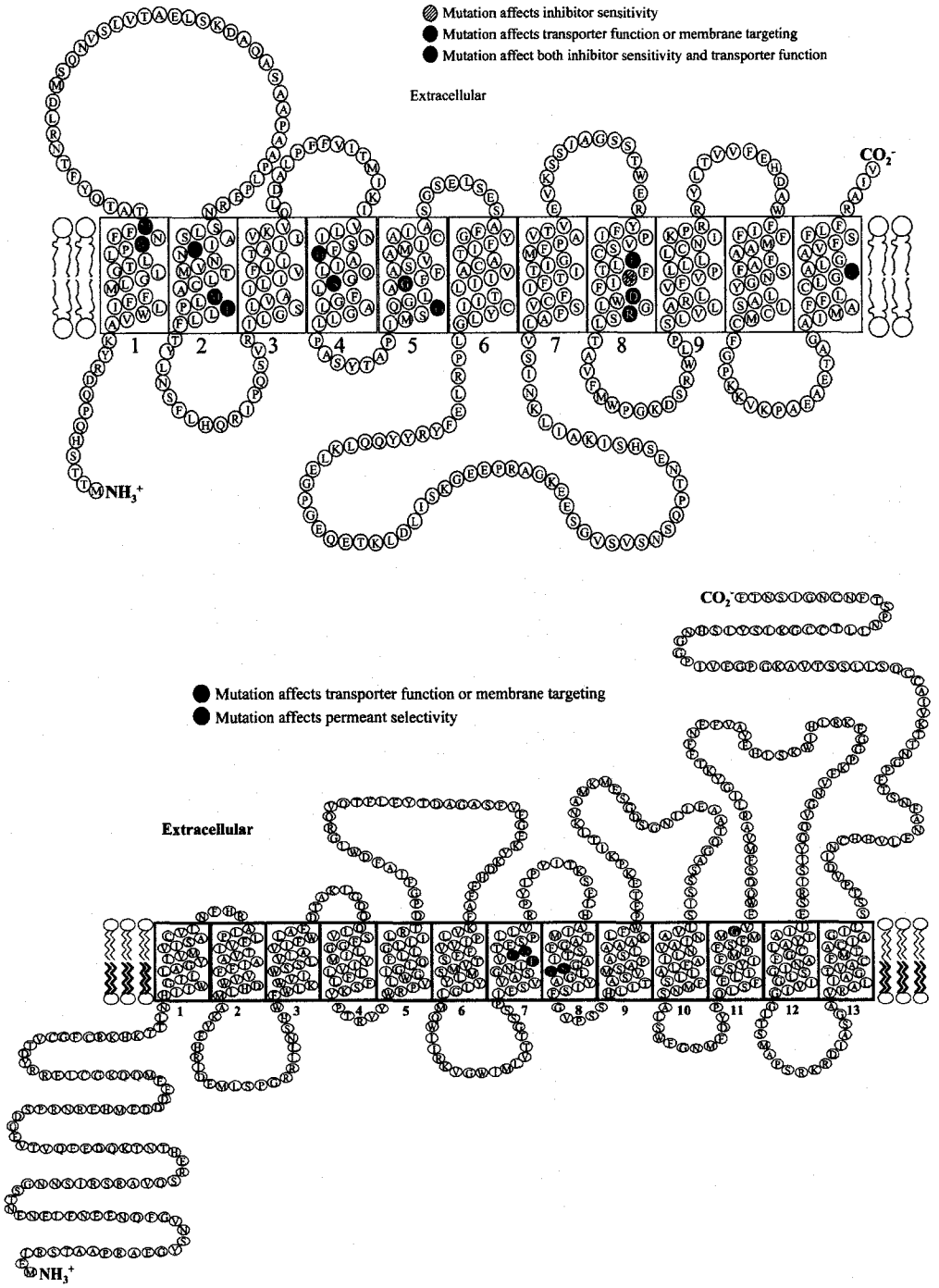

Figure 1-3 Topology models of hENT1 and hCNT3.

hENT1 (upper panel) and hCNT3 (lower panel) contain 11 and 13 transmembrane segments, respectively. Amino acid residues that have been identified as structurally or functionally important determinants in ENTs and CNTs are indicated by the filled circles.

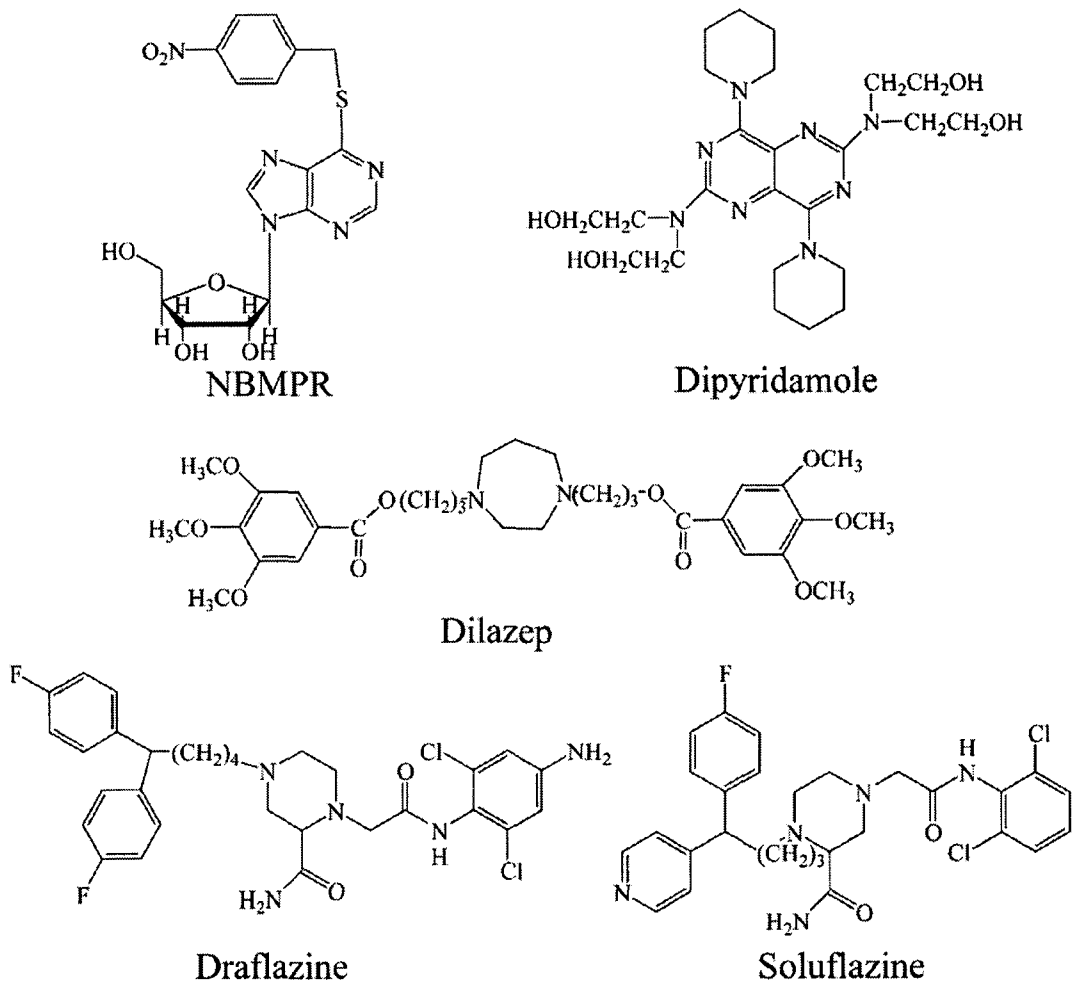

Figure 1-4 Chemical structures of some ENT inhibitors.

The structures of NBMPR (6-[(4-nitrobenzyl)thio]-9-(β-Dribofuranosyl) purine), dipyridamole (2,2',2",2'"-[(4,8-dipiperidinylpyrimido[5,4-d]pyrimidine-2,6-diyl)dinitrilo]tetraethanol), dilazep (*N,N'-bis*[3-(3,4,5-trimethoxybenzoyloxy)propyl]-homopiperazine), draflazine (2-(aminocarbonyl)-*N*-(4-amino-2,6-dichlorophenyl)-4-[5,5-*bis*-(4-fluorophenyl)pentyl]-1-piperazineacetamide), and soluflazine (3-(aminocarbonyl)-4-[4,4-(fluorophenyl-3-pyridinyl)butyl]-*N*-(2,6-dichlorophenyl)-1-piperazineacetamide) were generated using ChemDraw Ultra.

References

1. Van Belle, H. (1993) *Cardiovasc Res* **27**, 68-76
2. Baldwin, S. A., Mackey, J. R., Cass, C. E., and Young, J. D. (1999) *Mol Med Today* **5**, 216-224
3. de Koning, H., and Diallinas, G. (2000) *Mol Membr Biol* **17**, 75-94
4. Vickers, M. F., Young, J. D., Baldwin, S. A., and Cass, C. E. (2000) *Emerging Therapeutic Targets* **4**, 515-539
5. Cabrita, M. A., Baldwin, S. A., Young, J. D., and Cass, C. E. (2002) *Biochem Cell Biol* **80**, 623-638
6. Kong, W., Engel, K., and Wang, J. (2004) *Curr Drug Metab* **5**, 63-84
7. Huang, Q. Q., Yao, S. Y., Ritzel, M. W., Paterson, A. R., Cass, C. E., and Young, J. D. (1994) *J Biol Chem* **269**, 17757-17760
8. Griffiths, M., Beaumont, N., Yao, S. Y., Sundaram, M., Boumah, C. E., Davies, A., Kwong, F. Y., Coe, I., Cass, C. E., Young, J. D., and Baldwin, S. A. (1997) *Nat Med* **3**, 89-93
9. Griffiths, M., Yao, S. Y., Abidi, F., Phillips, S. E., Cass, C. E., Young, J. D., and Baldwin, S. A. (1997) *Biochem J* **328**, 739-743
10. Crawford, C. R., Patel, D. H., Naeve, C., and Belt, J. A. (1998) *J Biol Chem* **273**, 5288-5293
11. Visser, F., Vickers, M. F., Ng, A. M., Baldwin, S. A., Young, J. D., and Cass, C. E. (2002) *J Biol Chem* **277**, 395-401.
12. Visser, F., Baldwin, S. A., Isaac, R. E., Young, J. D., and Cass, C. E. (2005) *J Biol Chem* **280**, 11025-11034
13. Yao, S. Y., Ng, A. M., Vickers, M. F., Sundaram, M., Cass, C. E., Baldwin, S. A., and Young, J. D. (2002) *J Biol Chem* **277**, 24938-24948
14. Hyde, R. J., Cass, C. E., Young, J. D., and Baldwin, S. A. (2001) *Mol Membr Biol* **18**, 53-63
15. Baldwin, S. A., Beal, P. R., Yao, S. Y., King, A. E., Cass, C. E., and Young, J. D. (2004) *Pflugers Arch* **447**, 735-743
16. Acimovic, Y., and Coe, I. R. (2002) *Mol Biol Evol* **19**, 2199-2210

17. Baldwin, S. A., Yao, S. Y., Hyde, R. J., Ng, A. M., Foppolo, S., Barnes, K., Ritzel, M. W., Cass, C. E., and Young, J. D. (2005) *J Biol Chem* **280**, 15880-7
18. Hyde, R. J., Abidi, F., Griffiths, M., Yao, S. Y. M., Sundaram, M., Phillips, S. E. V., Cass, C. E., Young, J. D. (2000) *Drug Dev Res* **50**, 38
19. Engel, K., Zhou, M., and Wang, J. (2004) *J Biol Chem* **279**, 50042-50049
20. Ritzel, M. W., Yao, S. Y., Huang, M. Y., Elliott, J. F., Cass, C. E., and Young, J. D. (1997) *Am J Physiol* **272**, C707-714
21. Ritzel, M. W., Yao, S. Y., Ng, A. M., Mackey, J. R., Cass, C. E., and Young, J. D. (1998) *Mol Membr Biol* **15**, 203-211
22. Wang, J., Su, S. F., Dresser, M. J., Schaner, M. E., Washington, C. B., and Giacomini, K. M. (1997) *Am J Physiol* **273**, F1058-1065
23. Wang, J., Schaner, M. E., Thomassen, S., Su, S. F., Piquette-Miller, M., and Giacomini, K. M. (1997) *Pharm Res* **14**, 1524-1532
24. Ritzel, M. W. L., Ng, A. M., Yao, S. Y. M., Graham, K., Loewen, S. K., Smith, K. M., Ritzel, R. G., Mowles, D. A., Carpenter, P., Chen, X., Karpinski, E., Hyde, R. J., Baldwin, S. A., Cass, C. E., and Young, J. D. (2001) *J Biol Chem* **276**, 2914-2927
25. Griffith, D. A., and Jarvis, S. M. (1996) *Biochim Biophys Acta* **1286**, 153-181
26. Lu, X., Gong, S., Monks, A., Zaharevitz, D., and Moscow, J. A. (2002) *J Exp Ther Oncol* **2**, 200-212
27. Pennycooke, M., Chaudary, N., Shuralyova, I., Zhang, Y., and Coe, I. R. (2001) *Biochem Biophys Res Commun* **280**, 951-959.
28. Molina-Arcas, M., Bellosillo, B., Casado, F. J., Montserrat, E., Gil, J., Colomer, D., and Pastor-Anglada, M. (2003) *Blood* **101**, 2328-2334
29. Lai, Y., Bakken, A. H., and Unadkat, J. D. (2002) *J Biol Chem* **277**, 37711-37717
30. Mangravite, L. M., Lipshutz, J. H., Mostov, K .E., Giacomini, K. M. (2001) *Am J Phisiol Renal Physiol* **280**, F879-885
31. Mangravite, L. M., Badagnani, I., and Giacomini, K. M. (2003) *Eur J Pharmacol* **479**, 269-281
32. Hamilton, S. R., Yao, S. Y., Ingram, J. C., Hadden, D. A., Ritzel, M. W., Gallagher, M. P., Henderson, P. J., Cass, C. E., Young, J. D., and Baldwin, S. A. (2001) *J Biol Chem* **276**, 27981-27988

33. Pastor-Anglada, M., Casado, F. J., Valdes, R., Mata, J., Garcia-Manteiga, J., and Molina, M. (2001) *Mol Membr Biol* **18**, 81-85
34. Felipe, A., Valdes, R., Santo, B., Lloberas, J., Casado, J., and Pastor-Anglada, M. (1998) *Biochem J* **330**, 997-1001
35. Pisoni, R. L., and Thoene, J. G. (1991) *Biochim-Biophys-Acta* **1071**, 351-373
36. Mani, R. S., Hammond, J. R., Marjan, J. M., Graham, K. A., Young, J. D., Baldwin, S. A., and Cass, C. E. (1998) *J Biol Chem* **273**, 30818-30825
37. Lai, Y., Tse, C. M., and Unadkat, J. D. (2004) *J Biol Chem* **279**, 4490-4497
38. Lang, T. (2003) in *Department of Oncology*, pp. 405, University of Alberta, Edmonton
39. Mackey, J. R., Galmarini, C. M., Graham, K. A., Joy, A. A., Delmer, A., Dabbagh, L., Glubrecht, D., Jewell, L. D., Lai, R., Lang, T., Hanson, J., Young, J. D., Merle-Beral, H., Binet, J. L., Cass, C. E., and Dumontet, C. (2005) *Blood* **105**, 767-774
40. Damaraju, V. L., Damaraju, S., Young, J. D., Baldwin, S. A., Mackey, J., Sawyer, M. B., and Cass, C. E. (2003) *Oncogene* **22**, 7524-7536
41. Choi, D. S., Cascini, M. G., Mailliard, W., Young, H., Paredes, P., McMahon, T., Diamond, I., Bonci, A., and Messing, R. O. (2004) *Nat Neurosci* **7**, 855-861
42. Lang, T. T., Young, J. D., and Cass, C. E. (2004) *Mol Pharmacol* **65**, 925-933
43. Clarke, M. L., Mackey, J. R., Baldwin, S. A., Young, J. D., and Cass, C. E. (2002) *Cancer Treat Res* **112**, 27-47
44. Mangravite, L. M., Xiao, G., and Giacomini, K. M. (2003) *Am J Physiol Renal Physiol* **284**, F902-910
45. Galmarini, C. M., Mackey, J. R., and Dumontet, C. (2001) *Leukemia* **15**, 875-890.
46. Gourdeau, H., Clarke, M. L., Ouellet, F., Mowles, D., Selner, M., Richard, A., Lee, N., Mackey, J. R., Young, J. D., Jolivet, J., Lafreniere, R. G., and Cass, C. E. (2001) *Cancer Res* **61**, 7217-7224
47. Plunkett, W., and Cohen, S. S. (1977) *Ann N Y Acad Sci* **284**, 91-102
48. Ruiz van Haperen, V. W., Veerman, G., Vermorken, J. B., and Peters, G. J. (1993) *Biochem Pharmacol* **46**, 762-766
49. Huang, P., and Plunkett, W. (1995) *Cancer Chemother Pharmacol* **36**, 181-188
50. Huang, P., and Plunkett, W. (1995) *Semin Oncol* **22**, 19-25

51. Mackey, J. R., Baldwin, S. A., Young, J. D., and Cass, C. E. (1998) *Drug Resistance Updates* **1**, 310-324

52. Mackey, J. R., Jennings, L. L., Clarke, M. L., Santos, C. L., Dabbagh, L., Vsianska, M., Koski, S. L., Coupland, R. W., Baldwin, S. A., Young, J. D., and Cass, C. E. (2002) *Clin Cancer Res* **8**, 110-116.

53. Galmarini, C. M., Mackey, J. R., and Dumontet, C. (2002) *Lancet Oncol* **3**, 415-424

54. Stam, R. W., den Boer, M. L., Meijerink, J. P., Ebus, M. E., Peters, G. J., Noordhuis, P., Janka-Schaub, G. E., Armstrong, S. A., Korsmeyer, S. J., and Pieters, R. (2003) *Blood* **101**, 1270-1276

55. Huang, Y., Anderle, P., Bussey, K. J., Barbacioru, C., Shankavaram, U., Dai, Z., Reinhold, W. C., Papp, A., Weinstein, J. N., and Sadee, W. (2004) *Cancer Res* **64**, 4294-4301

56. Galmarini, C. M., Thomas, X., Calvo, F., Rousselot, P., Rabilloud, M., El Jaffari, A., Cros, E., and Dumontet, C. (2002) *Br J Haematol* **117**, 860-868

57. Spratlin, J., Sangha, R., Glubrecht, D., Dabbagh, L., Young, J. D., Dumontet, C., Cass, C., Lai, R., and Mackey, J. R. (2004) *Clin Cancer Res* **10**, 6956-6961

58. Lang, T. T., Selner, M., Young, J. D., and Cass, C. E. (2001) *Mol Pharmacol* **60**, 1143-1152

59. Galmarini, C. M., Clarke, M. L., Jordheim, L., Santos, C. L., Cros, E., Mackey, J. R., and Dumontet, C. (2004) *BMC Pharmacol* **4**, 8

60. Jordheim, L. P., Cros, E., Gouy, M. H., Galmarini, C. M., Peyrottes, S., Mackey, J., Perigaud, C., and Dumontet, C. (2004) *Clin Cancer Res* **10**, 5614-5621

61. Mackey, J. R., Mani, R. S., Selner, M., Mowles, D., Young, J. D., Belt, J. A., Crawford, C. R., and Cass, C. E. (1998) *Cancer Res* **58**, 4349-4357

62. Chow, L., Lai, R., Dabbagh, L., Belch, A., Young, J. D., Cass, C. E., and Mackey, J. R. (2005) *Mod Pathol* **18**, 558-564

63. Handa, M., Choi, D. S., Caldeiro, R. M., Messing, R. O., Gordon, A. S., and Diamond, I. (2001) *Gene* **262**, 301-307

64. Yao, S. Y., Ng, A. M., Muzyka, W. R., Griffiths, M., Cass, C. E., Baldwin, S. A., and Young, J. D. (1997) *J Biol Chem* **272**, 28423-28430

65. Kiss, A., Farah, K., Kim, J., Garriock, R. J., Drysdale, T. A., Hammond, J. R. (2000) *Biochem J* **352**, 363-372

66. Landfear, S. M., Ullman, B., Carter, N. S., and Sanchez, M. A. (2004) *Eukaryot Cell* **3**, 245-254

67. Strausberg, R. L., Feingold, E. A., Grouse, L. H., Derge, J. G., Klausner, R. D., Collins, F. S., Wagner, L., Shenmen, C. M., Schuler, G. D., Altschul, S. F., Zeeberg, B., Buetow, K. H., Schaefer, C. F., Bhat, N. K., Hopkins, R. F., Jordan, H., Moore, T., Max, S. I., Wang, J., Hsieh, F., Diatchenko, L., Marusina, K., Farmer, A. A., Rubin, G. M., Hong, L., Stapleton, M., Soares, M. B., Bonaldo, M. F., Casavant, T. L., Scheetz, T. E., Brownstein, M. J., Usdin, T. B., Toshiyuki, S., Carninci, P., Prange, C., Raha, S. S., Loquellano, N. A., Peters, G. J., Abramson, R. D., Mullahy, S. J., Bosak, S. A., McEwan, P. J., McKernan, K. J., Malek, J. A., Gunaratne, P. H., Richards, S., Worley, K. C., Hale, S., Garcia, A. M., Gay, L. J., Hulyk, S. W., Villalon, D. K., Muzny, D. M., Sodergren, E. J., Lu, X., Gibbs, R. A., Fahey, J., Helton, E., Ketteman, M., Madan, A., Rodrigues, S., Sanchez, A., Whiting, M., Young, A. C., Shevchenko, Y., Bouffard, G. G., Blakesley, R. W., Touchman, J. W., Green, E. D., Dickson, M. C., Rodriguez, A. C., Grimwood, J., Schmutz, J., Myers, R. M., Butterfield, Y. S., Krzywinski, M. I., Skalska, U., Smailus, D. E., Schnerch, A., Schein, J. E., Jones, S. J., and Marra, M. A. (2002) *Proc Natl Acad Sci U S A* **99**, 16899-16903

68. Patel, D. H., Crawford, C. R., Naeve, C. W., and Belt, J. A. (2000) *Gene* **242**, 51-58

69. Che, M., Ortiz, D. F., and Arias, I. M. (1995) *J Biol Chem* **270**, 13596-13599

70. Yao, S. Y., Ng, A. M., Loewen, S. K., Cass, C. E., Baldwin, S. A., and Young, J. D. (2002) *Am J Physiol Cell Physiol* **283**, C155-168

71. Ritzel, M. W., Ng, A. M., Yao, S. Y., Graham, K., Loewen, S. K., Smith, K. M., Hyde, R. J., Karpinski, E., Cass, C. E., Baldwin, S. A., and Young, J. D. (2001) *Mol Membr Biol* **18**, 65-72

72. Visser, F., Zhang, J., Raborn, R. T., Baldwin, S. A., Young, J. D., and Cass, C. E. (2005) *Mol Pharmacol* **67**, 1291-1298

73. Ward, J. L., Sherali, A., Mo, Z. P., and Tse, C. M. (2000) *J Biol Chem* **275**, 8375-8381

74. Clarke, M. L., Damaraju, V. L., Zhang, J., Mowles, D., Tackaberry, T., Lang, T., Young, D., Tomkinson, B., and Cass, C. E. (2005) for submission to *Molecular Cancer Therapeutics*

75. Gati, W. P., Paterson, A. R., Belch, A. R., Chlumecky, V., Larratt, L. M., Mant, M. J., and Turner, A. R. (1998) *Leuk Lymphoma* **32**, 45-54

76. Yao, S. Y., Ng, A. M., Sundaram, M., Cass, C. E., Baldwin, S. A., and Young, J. D. (2001) *Mol Membr Biol* **18**, 161-167.

77. Mackey, J. R., Yao, S. Y., Smith, K. M., Karpinski, E., Baldwin, S. A., Cass, C. E., and Young, J. D. (1999) *J Natl Cancer Inst* **91**, 1876-1881

78. Lostao, M. P., Mata, J. F., Larrayoz, I. M., Inzillo, S. M., Casado, F. J., and Pastor-Anglada, M. (2000) *FEBS Lett* **481**, 137-140

79. Graham, K. A., Leithoff, J., Coe, I. R., Mowles, D., Mackey, J. R., Young, J. D., and Cass, C. E. (2000) *Nucleosides Nucleotides Nucleic Acids* **19**, 415-434

80. Mata, J. F., Garcia-Manteiga, J. M., Lostao, M. P., Fernandez-Veledo, S., Guillen-Gomez, E., Larrayoz, I. M., Lloberas, J., Casado, F. J., and Pastor-Anglada, M. (2001) *Mol Pharmacol* **59**, 1542-1548

81. Li, J. Y., Boado, R. J., and Pardridge, W. M. (2001) *J Pharmacol Exp Ther* **299**, 735-740

82. Gerstin, K. M., Dresser, M. J., and Giacomini, K. M. (2002) *Am J Physiol Renal Physiol* **283**, F344-349

83. Chang, C., Swaan, P. W., Ngo, L. Y., Lum, P. Y., Patil, S. D., and Unadkat, J. D. (2004) *Mol Pharmacol* **65**, 558-570

84. Patil, S. D., Ngo, L. Y., and Unadkat, J. D. (2000) *Cancer Chemother Pharmacol* **46**, 394-402

85. Vickers, M. F., Zhang, J., Visser, F., Tackaberry, T., Robins, M. J., Nielsen, L. P., Nowak, I., Baldwin, S. A., Young, J. D., and Cass, C. E. (2004) *Nucleosides Nucleotides Nucleic Acids* **23**, 361-373

86. Damaraju, S., Zhang, J., Visser, F., Tackaberry, T., Dufour, J., Smith, K. M., Slugoski, M., Ritzel, M. W., Baldwin, S. A., Young, J. D., and Cass, C. E. (2005) *Pharmacogenet Genomics* **15**, 173-182

87. Guida, L., Bruzzone, S., Sturla, L., Franco, L., Zocchi, E., and De Flora, A. (2002) *J Biol Chem* **277**, 47097-47105

88. Huang, M., Wang, Y., Collins, M., Gu, J. J., Mitchell, B. S., and Graves, L. M. (2002) *J Biol Chem* **277**, 28364-28367

89. Huang, M., Wang, Y., Cogut, S. B., Mitchell, B. S., and Graves, L. M. (2003) *J Pharmacol Exp Ther* **304**, 753-760

90. Sundaram, M., Yao, S. Y. M., Ingram, J. C., Berry, Z. A., Abidi, F., Cass, C. E., Baldwin, S. A., Young, J. D. (2001) *J Biol Chem* **276**, 45270-45275

91. Ward, J. L., Leung, G. P., Toan, S. V., and Tse, C. M. (2003) *Arch Biochem Biophys* **411**, 19-26

92. Vickers, M. F., Mani, R. S., Sundaram, M., Hogue, D. L., Young, J. D., Baldwin, S. A., and Cass, C. E. (1999) *Biochem J* **339**, 21-32

93. Craig, J. E., Zhang, Y., and Gallagher, M. P. (1994) *Mol Microbiol* **11**, 1159-1168

94. Toan, S. V., To, K. K., Leung, G. P., de Souza, M. O., Ward, J. L., and Tse, C. M. (2003) *Pflugers Arch* **447**, 195-204

95. Mangravite, L. M., and Giacomini, K. M. (2003) *Pharm Res* **20**, 319-323

96. Huang, Y., Lemieux, M. J., Song, J., Auer, M., and Wang, D. N. (2003) *Science* **301**, 616-620

97. Abramson, J., Smirnova, I., Kasho, V., Verner, G., Kaback, H. R., and Iwata, S. (2003) *Science* **301**, 610-615

98. Widdas, W. F. (1952) *J Physiol* **118**, 23-39

99. DeFelice, L. J. (2004) *Trends Neurosci* **27**, 352-359

100. Locher, K. P., Bass, R. B., and Rees, D. C. (2003) *Science* **301**, 603-604

101. Agbanyo, F. R., Cass, C. E., and Paterson, A. R. (1988) *Mol Pharmacol* **33**, 332-337

102. Visser, F., Zhang, J., Tackaberry, T., Baldwin, S. A., Young, J. D., and Cass, C. E. (2005) *J Biol Chem*, **submitted**

103. Smith, K. M., Slugoski, M. D., Loewen, S. K., Ng, A. M., Yao, S. Y., Chen, X. Z., Karpinski, E., Cass, C. E., Baldwin, S. A., and Young, J. D. (2005) *J Biol Chem* **280**, 25436-25449

104. Mohlmann, T., Mezher, Z., Schwerdtfeger, G., and Neuhaus, H. E. (2001) *FEBS Lett* **509**, 370-374.

105. Xiao, G., Wang, J., Tangen, T., and Giacomini, K. M. (2001) *Mol Pharmacol* **59**, 339-348

106. Wormit, A., Traub, M., Florchinger, M., Neuhaus, H. E., and Mohlmann, T. (2004) *Biochem J* **383**, 19-26

107. Li, G., Liu, K., Baldwin, S. A., and Wang, D. (2003) *J Biol Chem* **278**, 35732-35742

108. Smith, K. M., Ng, A. M., Yao, S. Y., Labedz, K. A., Knaus, E. E., Wiebe, L. I., Cass, C. E., Baldwin, S. A., Chen, X. Z., Karpinski, E., and Young, J. D. (2004) *J Physiol* **558**, 807-823

109. Jauch, P., Petersen, O. H., and Lauger, P. (1986) *J Membr Biol* **94**, 99-115

110. Mackenzie, B., Loo, D. D., Panayotova-Heiermann, M., and Wright, E. M. (1996) *J Biol Chem* **271**, 32678-32683

111. Grewer, C., and Rauen, T. (2005) *J Membr Biol* **203**, 1-20

112. Loewen, S. K., Ng, A. M., Mohabir, N. N., Baldwin, S. A., Cass, C. E., and Young, J. D. (2003) *Yeast* **20**, 661-675

113. Sundaram, M., Yao, S. Y. M., Ng, A. M. L., Griffiths, M., Cass, C. E., Baldwin, S. A., and Young, J. D. (1998) *J Biol Chem* **273**, 21519-21525

114. Sundaram, M., Yao, S. Y., Ng, A. M., Cass, C. E., Baldwin, S. A., and Young, J. D. (2001) *Biochemistry* **40**, 8146-8151

115. SenGupta, D. J., and Unadkat, J. D. (2004) *Biochem Pharmacol* **67**, 453-458

116. Yao, S. M., Sundaram, M., Chomey, E. G., Cass, C. E., Baldwin, S. A., Young, J. D. (2001) *Biochem J* **353**, 387-393

117. SenGupta, D. J., Lum, P. Y., Lai, Y., Shubochkina, E., Bakken, A. H., Schneider, G., and Unadkat, J. D. (2002) *Biochemistry* **41**, 1512-1519

118. Endres, C. J., and Unadkat, J. D. (2005) *Mol Pharmacol* **67**, 837-844

119. Vasudevan, G., Ullman, B., and Landfear, S. M. (2001) *Proc Natl Acad Sci U S A* **98**, 6092-6097

120. Valdes, R., Vasudevan, G., Conklin, D., and Landfear, S. M. (2004) *Biochemistry* **43**, 6793-6802

121. Arastu-Kapur, S., Ford, E., Ullman, B., and Carter, N. S. (2003) *J Biol Chem* **278**, 33327-33333

122. Lai, Y., Lee, E. W., Ton, C. C., Vijay, S., Zhang, H., and Unadkat, J. D. (2005) *Am J Physiol Cell Physiol* **288**, C39-45

123. Flanagan, S. A., and Meckling-Gill, K. A. (1997) *J Biol Chem* **272**, 18026-18032

124. Wang, J., and Giacomini, K. M. (1997) *J Biol Chem* **272**, 28845-28848

125. Loewen, S. K., Ng, A. M., Yao, S. Y., Cass, C. E., Baldwin, S. A., and Young, J. D. (1999) *J Biol Chem* **274**, 24475-24484

126. Leabman, M. K., Huang, C. C., DeYoung, J., Carlson, E. J., Taylor, T. R., de la Cruz, M., Johns, S. J., Stryke, D., Kawamoto, M., Urban, T. J., Kroetz, D. L., Ferrin, T. E., Clark, A. G., Risch, N., Herskowitz, I., and Giacomini, K. M. (2003) *Proc Natl Acad Sci U S A* **100**, 5896-5901

127. Osato, D. H., Huang, C. C., Kawamoto, M., Johns, S. J., Stryke, D., Wang, J., Ferrin, T. E., Herskowitz, I., and Giacomini, K. M. (2003) *Pharmacogenetics* **13**, 297-301

128. Badagnani, I., Chan, W., Castro, R. A., Brett, C. M., Huang, C. C., Stryke, D., Kawamoto, M., Johns, S. J., Ferrin, T. E., Carlson, E. J., Burchard, E. G., and Giacomini, K. M. (2005) *Pharmacogenomics J* **5**, 157-65

129. Gray, J. H., Mangravite, L. M., Owen, R. P., Urban, T. J., Chan, W., Carlson, E. J., Huang, C. C., Kawamoto, M., Johns, S. J., Stryke, D., Ferrin, T. E., and Giacomini, K. M. (2004) *Mol Pharmacol* **65**, 512-519

130. Owen, R. P., Gray, J. H., Taylor, T. R., Carlson, E. J., Huang, C. C., Kawamoto, M., Johns, S. J., Stryke, D., Ferrin, T. E., and Giacomini, K. M. (2005) *Pharmacogenet Genomics* **15**, 83-90

131. Bill, R. M. (2001) *Curr Genet* **40**, 157-171

132. Doring, F., Theis, S., and Daniel, H. (1997) *Biochem Biophys Res Commun* **232**, 656-662

133. Theis, S., Doring, F., and Daniel, H. (2001) *Protein Expr Purif* **22**, 436-442

134. Wieczorke, R., Dlugai, S., Krampe, S., and Boles, E. (2003) *Cell Physiol Biochem* **13**, 123-134

135. Vickers, M. F., Young, J. D., Baldwin, S. A., Ellison, M. J., and Cass, C. E. (2001) *Mol Membr Biol* **18**, 73-79.

136. Cai, J., Daoud, R., Georges, E., and Gros, P. (2001) *Biochemistry* **40**, 8307-8316

137. Burchmore, R. J., Wallace, L. J., Candlish, D., Al-Salabi, M. I., Beal, P. R., Barrett, M. P., Baldwin, S. A., and de Koning, H. P. (2003) *J Biol Chem* **278**, 23502-23507

138. Zhang, J., Visser, F., Vickers, M. F., Lang, T., Robins, M. J., Nielsen, L. P., Nowak, I., Baldwin, S. A., Young, J. D., and Cass, C. E. (2003) *Mol Pharmacol* **64**, 1512-1520

139. Zhang, J., Smith, K. M., Tackaberry, T., Visser, F., Robins, M. J., Nielsen, L. P., Nowak, I., Baldwin, S. A., Young, J. D., and Cass, C. E. (2005) *Mol Pharmacol* **68**, 830-839

140. Vickers, M. F., Yao, S. Y., Baldwin, S. A., Young, J. D., and Cass, C. E. (2000) *J Biol Chem* **275**, 25931-25938.

141. Andre, B. (1995) *Yeast* **11**, 1575-1611

142. Horak, J. (1997) *Biochim Biophys Acta* **1331**, 41-79

143. Garnier, C., Blondel, M. O., and Haguenauer-Tsapis, R. (1996) *Mol Microbiol* **21**, 1061-1073

144. Schaner, M. E., Wang, J., Zevin, S., Gerstin, K. M., and Giacomini, K. M. (1997) *Pharm Res* **14**, 1316-1321

145. Schaner, M. E., Wang, J., Zhang, L., Su, S. F., Gerstin, K. M., and Giacomini, K. M. (1999) *J Pharmacol Exp Ther* **289**, 1487-1491

Chapter 2 Uridine Binding Motifs of Human Concentrative Nucleoside Transporters 1 and 3 Produced in *Saccharomyces cerevisiae*

A version of this chapter has been published:

Zhang, J., Visser, F., Vickers, M. F., Lang, T., Robins, M. J., Nielsen, L. P., Nowak, I., Baldwin, S. A., Young, J. D., and Cass, C. E. *Mol Pharmacol*, 64: 1512-1520, 2003

Acknowledgements

Drs. Frank Visser and Mark Vickers contributed to this project by helping the development of the cell-harvester based transport assay. Dr. Thack Lang designed the antigen for making of anti-hCNT3 antibodies. Dr. Morris Robins, Mr. Lars Nielsen and Mr. Ireneusz Nowak are the chemists who developed the series of uridine analogs. Drs. Stephen Baldwin and James Young are collaborative principle investigators who helped obtain research funding for this project and aided in manuscript preparation.

Introduction

Nucleoside transporters (NTs) are required for most natural and synthetic nucleosides to cross cell membranes (1). NT-mediated permeation is a determinant of cellular uptake of physiologic nucleosides and antineoplastic and antiviral nucleoside drugs (2). NTs also affect extracellular concentrations of adenosine, which acts as a signaling molecule to affect many physiological processes, including neurotransmission, vasodilation, platelet aggregation and lipolysis (3,4). Mammalian NTs are classified into two structurally unrelated protein families, the concentrative and equilibrative nucleoside transporters (CNTs and ENTs) (1,2), which exhibit different mechanisms of transport. In mammals, the ENTs transport a broad range of both purine and pyrimidine nucleosides and have a ubiquitous tissue and cell distribution, whereas the CNTs appear to exhibit more limited permeant selectivities and tissue distributions. Three human CNTs (hCNTs) with different permeant selectivities have been identified (5-7). hCNT1 and hCNT2 prefer pyrimidine nucleosides and purine nucleosides, respectively, although hCNT1 transports adenosine and hCNT2 transports uridine (Urd). hCNT3 transports a broad range of pyrimidine and purine nucleosides, including anticancer nucleoside drugs (7). hCNT1 and hCNT2, which contain 650 and 659 amino acid residues respectively, share 72% amino acid identity and are predicted to have 13 putative transmembrane segments with an exofacial glycosylated tail at the carboxyl terminus (8). hCNT3 is 48% and 47% identical to hCNT1 and hCNT2, respectively, and its predicted topology is similar to that predicted for other hCNT family members. The hCNTs are mainly found in specialized cells, such as intestinal and renal epithelia (6,7,9); they have also been observed in leukemic cells and a few cancer cell lines (10). Differences in tissue distribution of hCNTs suggest unique physiological roles for the hCNTs and may reflect different nucleoside-transport capacities of various tissues. Normal and tumor tissues exhibited different expression of hCNT transcripts (11). hCNT1 mRNA distributions in some cancer cell lines were found to correspond to drug cytotoxicity patterns (12), suggesting that nucleoside chemotherapy could be optimized based on differences among individuals in the abundance of hCNTs.

The differences in permeant selectivities among hCNT1, hCNT2, and hCNT3 are also reflected in their different abilities to transport anticancer and antiviral nucleoside drugs. For example, gemcitabine, which is used in therapy of metastatic solid tumors, is transported by recombinant hCNT1 and hCNT3 in oocytes (7,13), but not by recombinant hCNT2 (13). Studies in oocytes have shown that AZT (3'-azido-3'-deoxythymidine), an anti-HIV drug, is a low-affinity permeant of recombinant hCNT1 (14) and a moderate permeant of recombinant hCNT3 (7), but is not a permeant of recombinant hCNT2 (6). These differences in transportability of different nucleoside drugs by hCNT1, hCNT2, and hCNT3 imply that different hCNTs have unique binding site(s) for nucleoside drugs. We hypothesize that each hCNT will exhibit a unique binding profile for nucleoside analogs because of differences in their permeant binding and translocation sites.

Urd is a permeant of most human NTs identified so far. Urd analogs such as 5-fluoro-5'-deoxyuridine (a cytotoxic prodrug metabolite of capecitabine) are commonly used in the treatment of advanced human cancers, especially colorectal and breast cancers. Despite the common application of Urd analogs in anticancer therapy, the interactions of these drugs with hCNTs and the mechanisms of selectivity at the transporter level remain unclear. To investigate the Urd recognition motifs of individual hCNTs in a NT-free background, hCNTs were expressed in a yeast strain that lacks NT activity and the capacity of the transporter proteins to mediate uptake of radiolabeled Urd was determined. We developed a high-throughput inhibitor-sensitivity assay with the hCNT yeast expression system that was used to quantify the inhibitory effects of a series of Urd analogs with various sugar and base modifications. The resulting K_i values were used to calculate the binding energies for the interactions of various inhibitors for hCNTs, thereby identifying structural determinants of Urd for interactions with the nucleoside-binding sites of hCNT1 and hCNT3.

Material and methods

Strains and media

fui1::TRP1 (MATα, gal, ura3-52, trp1, lys2, ade2, hisd2000, Δ*fui1::TRP1*), which contains a disruption in the gene encoding the endogenous Urd permease (FUI1) (15), was the parental yeast strain used to generate the hCNT expression system (16,17). Other strains were generated by transformation of the yeast-*Escherichia coli* shuttle vector pYPGE15 (18) into *Fui1::TRP1* using a standard lithium acetate method (19). Yeast strains were maintained in complete minimal media (CMM) containing 0.67% yeast nitrogen base (Difco, Detroit MI), amino acids (as required to maintain auxotrophic selection), and 2% glucose (CMM/GLU). Agar plates contained CMM with various supplements and 2% agar (Difco). Plasmids were propagated in *E. coli* strain TOP10F' (Invitrogen, Carlsbad, CA) and maintained in Luria broth with ampicillin (100 μg/ml).

Plasmid construction

For *S. cerevisiae* expression, the hCNT1 and hCNT3 open reading frames were amplified from vectors (pCDNA3-hCNT1 and pCDNA3-hCNT3) by PCR methodology using the following primers (restriction sited underlined, c-Myc tag sequence in italic): 5'-XbaI-hCNT1 (5'-CTG TCT AGA ATG GAGA ACG ACC CCT CGA GAC G-3'), 3'-KpnI-hCNT1 (5'-CGA GGT ACC TCA CTG TGC ACA GAT CGT GTG GTT G-3'), 3'-KpnI-hCNT1-Myc (5'-CGA GGT ACC TCA *CAG ATC CTC TTC TGA GAT GAG TTT TTG TTC* CTG TGC ACA GAT CGT GTG GTT G-3'), 5'-BglII-hCNT3 (5'-CTG AGA TCT ATG GAG CTG AGG AGT ACA GCA G-3'), and 3'-XhoI-hCNT3 (5'-CGA CTC GAG TCA AAA TGT ATT AGA GAT CCC ATT G-3'). The amplified open reading frames were inserted into the yeast expression vector pYPGE15, which is a high copy-number episomal vector that expresses the inserted DNA under the transcriptional control of a constitutive promoter (phosphoglycerate kinase promoter) to generate pYPhCNT1, pYPhCNT1-Myc and pYPhCNT3. The PCR reactions were performed using *Pwo* polymerase (Roche Molecular Biochemicals) and the resulting PCR products were verified by DNA sequencing using an ABI PRISM 310 sequence detection system (PerkinElmer Life Sciences).

Preparation of yeast membranes and immunostaining

Yeast membranes were prepared by a previously described method (15). Briefly, yeast were grown to an optical density at 600 nm (A_{600}) of 0.7-1.0, collected by centrifugation (1000 × *g*, 5 min, 4 °C), washed three times with breaking buffer (10 mM Tris, 1 mM EDTA, 1 mM phenylmethylsulfonyl fluoride, 0.1% (v/v) 2-mercaptoethanol, pH 7.4) that contained additional protease inhibitors (complete protease inhibitors, Roche Molecular Biochemicals), and lysed by vortexing in the presence of glass beads (425-600 μm, Sigma-Aldrich Canada Ltd., Oakville, ON) for 15 min at 4°C. Unbroken cells and glass beads were removed from lysates by centrifugation (500 × *g*, 5 min, 4°C), and membrane fractions were obtained by centrifugation of lysates (100,000 × *g*, 60 min, 4°C). The resulting membrane pellets were resuspended in breaking buffer that contained protease inhibitors. The samples were either used immediately or frozen (−80°C) in breaking buffer.

Yeast membranes were subjected to SDS-polyacrylamide gel electrophoresis (20), after which proteins were transferred to polyvinylidene fluoride membranes (Immobilon-P, Millipore, Bedford, MA). The transfer membranes were incubated overnight at 4°C first in TTBS (0.2% Tween-20, Tris-buffered saline) containing 5% (w/v) skim milk powder and then in TTBS with the primary antibodies and 5% (w/v) skim milk powder. The membranes were then washed three times with TTBS, incubated with TTBS-containing species-specific horseradish-peroxidase secondary antibodies (Jackson ImmunoResearch Laboratories Inc., West Grove, PA) and 5% (w/v) skim milk powder, washed with TTBS, and visualized with enhanced chemiluminescence (ECL, Amersham Pharmacia Biotech) and autoradiography. The primary antibodies used were monoclonal antibodies against the c-myc epitope tag (9E10, BAbCo, Richmond, CA.) and against hCNT3. The latter were raised against an immunogenic epitope (the amino acid sequence REHTNTKQDEEQVTVEQDSPRNREH) that corresponded to residues 45-69 of hCNT3, a region predicted to be located in a large intracellular loop close to the amino terminus.

Urd uptake in yeast producing recombinant hCNTs

The uptake of [^{3}H]nucleosides (Moravek Biochemicals, Brea, CA) into logarithmically proliferating yeast was measured using a modified transport assay (16). Yeast were grown in CMM/GLU to an A_{600} of 0.8-1.5, washed twice with fresh media (pH 7.4), and resuspended in CMM/GLU (pH 7.4) to an A_{600} of 4.0. Transport reactions were initiated by rapid mixing of 100 µl of yeast suspension with 100 µl of CMM/GLU (pH 7.4) containing [^{3}H]Urd (final concentration, 1 µM) preloaded in a 96-well cell culture plate. The 96-well plates were placed on the semi-automated cell harvester (Micro96^{TM} HARVESTER, Skatron instruments, Norway) and every 24 transport reactions were terminated simultaneously at graded time intervals by harvesting yeast on glass-fiber filters (Skatron instruments, Norway) with continued washing with demineralized water. The filters were air-dried for about 5 min, and the portions of the filter that corresponded to individual assays were excised and placed in scintillation vials. The amounts of radioactivity associated with the filters were determined by liquid scintillation counting.

The inhibitory capacities of Urd and Urd analogs against the recombinant hCNTs were assessed by measuring their relative abilities to inhibit the uptake of [^{3}H]Urd in the "inhibitor-sensitivity" assay as follows. Yeast cells were incubated with graded concentrations of a particular test compound and 1 µM [^{3}H]Urd in CMM/GLU (pH 7.4) for 30 and 10 min for recombinant hCNT1 and hCNT3, respectively, and [^{3}H]Urd uptake was measured. All experiments were carried out in quadruplicate. The amount of [^{3}H]Urd associated with yeast in the presence of 10 mM Urd was also determined to quantify non-specifically associated radioactivity, which was subtracted from total radioactivity for each transport assay. Data were fitted to theoretical inhibition curves by nonlinear regression with the use of the Graphpad Prism Version 3.0 Software to obtain IC_{50} (inhibitory concentration 50%) values for compounds that inhibited uptake of [^{3}H]Urd using concentration-effect curves with at least 11 points distributed over the relevant range of concentrations. K_i (inhibitory constant) values were determined from the Cheng and Prusoff equation (21), in which $K_i = IC_{50}/[1 + (L/K_m)]$ and L = [^{3}H]Urd concentration, which was always 1 µM. Gibbs free energy (ΔG^0) was calculated from $\Delta G^0 = -RT\ln(K_i)$, in which R is the gas constant and T is the absolute temperature. The

thermodynamic stability of transporter-inhibitor complexes was quantitatively estimated from ΔG^0 as described elsewhere (22).

Urd analogs

Abbreviations of uridine and uridine analogs are given in Table 1. Uridine, 5-fluorouridine, 5-iodouridine, 3-methyluridine, 2'-deoxyuridine, 5-ethyl-2'-deoxyuridine, 5-fluoro-2'-deoxyuridine, 5-bromo-2'-deoxyuridine and thymidine were obtained from Sigma-Aldrich (Oakville, Ont.); AZT was obtained from Aldrich Chem. Co., WI); 3'-*O*-methyluridine, 2',3'-*O*-isopropylideneuridine, 2',3'-dideoxyuridine, and 2',5'-dideoxyuridine were obtained from R. I. Chemical, Inc. (Orange, CA). 1-(β-D-Arabinofuranosyl)uracil (23,24), 2'-azido-2'-deoxyuridine (25), 2'-*O*-methyluridine (26), 1-(β-D-xylofuranosyl)uracil (27), 3'-deoxyuridine (28), 3'-azido-3'-deoxyuridine (29), 5'-deoxyuridine (30), 5'-chloro-5'-deoxyuridine (31), 5'-azido-5'-deoxyuridine (32), and 5'-*O*-methyluridine (33) were prepared as described in the references noted. 3',5'-Dideoxyuridine was prepared from 3'-deoxyuridine by the following procedure: to a solution of 2'-*O*-(*tert*-butyldimethylsilyl)-3'-deoxyuridine (34) (0.60 g, 1.75 mmol) in *N,N*-dimethylformamide (DMF) (8 mL), was added a solution of methyltriphenylphosphonium iodide (1.6 g, 3.5 mmol) in DMF (4 mL). The mixture was stirred at room temperature for 25 min, and then partitioned between H_2O (50 mL) and CH_2Cl_2 (50 mL). The aqueous phase was extracted with CH_2Cl_2 (2 x 30 mL), and the combined organic phase was concentrated. The residue was purified by silica gel column chromatography [ethyl acetate (EtOAc)/hexanes, 1:3 → 1:1] to give 2'-*O*-(*tert*-butyldimethylsilyl)-5'-iodo-3',5'-dideoxyuridine (700 mg, 88%). This material (700 mg, 1.55 mmol), Bu_3SnH (1.25 mL, 1.36 g, 4.65 mmol) and α,α'-azobisisobutyronitrile (AIBN) (50 mg) were dissolved in deoxygenated toluene (15 mL), and the solution was heated at 100°C for 1 h. Volatiles were evaporated *in vacuo*, and the residue was purified by chromatography (silica gel, EtOAc/hexanes, 1:3 → 1:1) to give a colorless oil (~430 mg, 85%). This material was dissolved in acetonitrile (10 mL), and 48% aqueous hydrofluoric acid (0.5 mL) was added with stirring. After 1.5 h, the mixture was added to a column of silica gel. Elution with EtOAc gave 3',5'-dideoxyuridine (260 mg, 70%) as a colorless syrup: ^{1}H NMR (CD_3OD, 500 MHz) δ 1.42 (d, J = 6.3 Hz, 3H), 1.67–1.74

(ddd, J = 5.4, 10.7, 13.7 Hz, 1H), 1.99–2.04 (ddd, J = 1.5, 4.8, 13.2 Hz, 1H), 4.32–4.35 (m, 1H), 4.46–4.53 (m, 1H), 5.69 (d, J = 1.0 Hz, 1H), 5.70 (d, J = 7.8 Hz, 1H), 7.60 (d, J = 7.8 Hz, 1H); ^{13}C NMR (CD_3OD, 125 MHz) δ 20.4, 77.8, 78.5, 95.0, 102.4, 142.0, 152.3, 166.5; MS (EI) *m/z* 212 (M^+, 10), 194, 141, 113, 101, 72, 57 (100%); HRMS *m/z* 212.0800 (M^+ [$C_9H_{12}N_2O_4$] = 212.0797).

Stock solutions of test compounds were either prepared in water or dimethylsulfoxide (DMSO) (Sigma) and the final concentration of DMSO in transport reactions was 0.1% if DMSO was used as a solvent.

Results

Detection of recombinant hCNT1-myc and hCNT3 in yeast membranes

The production of recombinant hCNT1-myc and hCNT3 in *S. cerevisiae* was verified by immunoblotting using either anti-myc or anti-hCNT3 antibodies (Fig. 2-1). A 75-kDa and an 80-kDa immunoreactive species were detected in membranes of pYPhCNT1-myc-containing (Fig. 2-1, panel A) and pYPhCNT3-containing (Fig. 2-1, panel B) yeast, respectively, that were not present in membranes of pYPGE15-containing yeast. The electrophoretic mobilities of the detected proteins were consistent with the predicted molecular masses of hCNT1-myc and hCNT3. The apparent abundance of hCNT3 was probably much greater than that of hCNT1-myc given that the amounts of membrane loaded for electrophoresis for detection of hCNT1-myc and hCNT3 were 20 and 5 μg, respectively, and the exposure times for autoradiography for hCNT1-myc and hCNT3 were 10 min and 2 s, respectively.

Urd transport by recombinant hCNT1 and hCNT3 in yeast

The time course for Urd uptake into *fui1::TRP1* that contained pYPGE15 was reported previously to yield a rate of 0.11 ± 0.01 pmol/mg protein/min (17). To determine the initial rates of Urd uptake into *fui1::TRP1* yeast that contained either pYPhCNT1 or pYPhCNT3, time courses for influx of [^{3}H]Urd were measured in the experiments of Fig. 2-2. The Urd uptake time course for pYPhCNT1-containing yeast

was linear for up to 60 min with a mean rate (± S.E.) of 10.43 ± 0.22 pmol/mg protein/min. The uptake time course for pYPhCNT3-containing yeast was linear for about 12 min with a mean rate (± S.E.) of 282.6 ± 14.27 pmol/mg protein/min. The rate calculated from the time course for Urd uptake into pYPhCNT3-containing yeast over the first 60 s (Fig. 2-2, inset) was the same as that calculated from the 12-min time course, indicating that initial rates of Urd transport were maintained over long periods of time. The extended linear time courses were likely due to efficient intracellular metabolism of Urd by conversion of Urd to UMP by Urd kinase, thereby maintaining the concentration gradient of Urd between the extracellular medium and the intracellular compartment. Urd uptake into pYPhCNT1- and pYPhCNT3-containing yeast was greatly reduced by addition of 10 mM cold Urd to assay mixtures, with mean rates (± S.E.) of 0.46 ± 0.1 and 0.58 ± 0.18 pmol/mg protein/min, respectively, indicating that most of the observed uptake was mediated by functional transporters.

The C-terminal tag of c-myc on hCNT1 had no obvious impact on the function of hCNT1 protein since time courses of Urd uptake mediated by the *fui1::TRP1* strain transformed with pYPhCNT1-myc gave a mean rate (± S.E.) of 9.25 ± 0.36 pmol/mg protein/min, which was similar to the rate obtained from pYPhCNT1-containing yeast in the experiments of Fig. 2-2. Initial rates of ^{3}H-labeled cytidine and thymidine into pYPhCNT1-containing yeast were also measured, giving mean rates (± S.E.) of 6.21 ± 0.41 pmol/mg protein/min and 2.42 ± 0.36 pmol/mg protein/min, respectively. In contrast, rates of uptake of ^{3}H-labeled guanosine and adenosine were low, indicating that these nucleosides were not good permeants for recombinant hCNT1. Recombinant hCNT3 exhibited broad transportabilities for naturally occurring nucleosides, with mean uptake rates (± S.E.) of 312 ± 2, 283 ± 4 and 336 ± 4 pmol/mg protein/min for ^{3}H-labeled cytidine, guanosine, and adenosine, respectively. These results demonstrated that the recombinant hCNT1 and hCNT3 produced in yeast showed characteristics similar to those reported previously (5,7). Urd transport rates were determined for all subsequent experiments using incubation times of 30 and 10 min for recombinant hCNT1 and hCNT3, respectively, thereby providing large signal-to-noise ratios and initial rates of uptake.

Kinetic properties of recombinant hCNT1 and hCNT3

The experiments of Fig. 2-3 showed that recombinant hCNT3 had similar apparent affinity but higher capacity for Urd (K_m = 8.7 ± 1.1 μM, V_{max} = 1400 ± 286 pmol/mg protein/min; mean ± S.E., n = 3) than recombinant hCNT1 (K_m = 9.2 ± 3.8 μM, V_{max} = 86.9 ± 12.9 pmol/mg protein/min, mean ± S.E., n = 3). The higher capacity of hCNT3 could be explained by its likely higher abundance in yeast membranes, which was detected in the immunoblotting experiment of Fig. 2-1. The K_m values of recombinant hCNT1 and hCNT3 in yeast were slightly lower than those obtained with other expression systems, such as *X. laevis* oocytes and cultured mammalian cells (5,7,35,36), which might be due to different recombinant expression systems.

Interaction of Urd analogs with recombinant hCNT1 and hCNT3

To obtain an understanding of the structural regions of Urd that interact with the transporters, Urd analogs with modifications of the base and/or sugar moieties were tested for their ability to inhibit uptake of 1 μM [^{3}H]Urd mediated by recombinant hCNT1 or hCNT3. The structures of the analogs that were studied are shown in Fig. 2-4 and representative concentration-effect curves of some of the analogs for inhibition of hCNT1-mediated Urd transport are shown in Fig. 2-5. In all cases, the Hill coefficients were close to –1, indicating a single class of inhibitor binding sites, and apparent K_i values were therefore determined from the IC_{50} values. The mean K_i values (± S.E.) and the corresponding Gibbs free energy values are listed in Table 1.

hCNT1 The C(5) of Urd did not form part of a stringent binding motif because FUrd, IUrd, and BrdUrd were potent inhibitors with somewhat higher affinities than Urd itself for hCNT1 (t-test, $P < 0.05$). Thymidine, which is 5-methyl-2'-dUrd, was a high-affinity inhibitor of Urd uptake with a K_i value (2.6 ± 0.1 μM) close to that of Urd (3.1 ± 0.3 μM). EtdUrd exhibited a ΔG^0 value of 27.2 kJ/mol, as compared to that of Urd (31.5 KJ/mol), suggesting that the ethyl group, with a larger volume than a fluoro or a bromo group, may have sterically reduced the ability of the analog to efficiently contact the transporter protein. In contrast, the 3 position of the base moiety (N(3)-H), which is a potential hydrogen bond donor, contributed a recognition determinant for binding to hCNT1. The low affinity of 3MeUrd, with a 24-fold increase in K_i value compared to

that of Urd, demonstrated the importance of the 3 position for binding to the transporter. The difference of 8 kJ/mol binding energy of 3MeUrd might be due to the loss of a weak hydrogen bond.

hCNT1 displayed relatively high affinities for 2'dUrd, 2'AzdUrd, FdUrd and BrdUrd (Fig. 2-4), suggesting that the 2'-hydroxyl group was not an important determinant for interaction of Urd with hCNT1. However, araU (Fig. 2-4), an epimer of Urd with the 2'-hydroxyl group above the plane of the sugar ring, exhibited a pronounced reduction in its interaction with the transporter (K_i > 1 mM). The inverted orientation of the hydroxyl group evidently produced an analog that could no longer interact with the transporter protein. The 36-fold difference in potency of 2'OMeUrd to inhibit Urd uptake might result from the bulkier size of the C(2')-O-CH_3 group ($\delta(\Delta G^0)$ = 9 kJ/mol, relative to ΔG^0 of Urd).

There was an apparent interaction between hCNT1 and the 5'-hydroxyl group since its removal (5'dUrd) produced a difference of 6.9 kJ/mol in ΔG^0 with a 16-fold increase in K_i value, suggesting that hydrogen bonding could be important. The further change of 4.7 kJ/mol in ΔG^0 value upon substitution of an azido group for a hydrogen atom at the C(5') of 5'dUrd ($\delta(\Delta G^0)$ = 11.5 kJ/mol, relative to ΔG^0 of Urd) was also consistent with the loss of hydrogen bonding between Urd and hCNT1. Since 2'dUrd was a high-affinity inhibitor of hCNT1, the difference of 8.5 kJ/mol in ΔG^0 for 2',5'ddUrd relative to Urd was most likely due to the removal of the 5'-hydroxyl group.

Although hCNT1 exhibited lower apparent affinity for 5'OMeUrd (K_i = 210 ± 42 μM) with a difference in ΔG^0 of 10.5 kJ/mol relative to Urd, the substitution of a chloro group for the 5'-hydroxyl group restored high affinity binding to hCNT1 (5'CldUrd, K_i = 8.5 ± 1.1 μM). The slightly higher apparent affinity observed with 5-fluoro-5'-deoxyuridine than with 5'dUrd was evidently due to gained energy by addition of the fluoro group at the 5 position of the base.

Although removal of the 3'-hydroxyl group shifted the concentration-effect curve far to the right (Fig. 2-5), 3'dUrd inhibited Urd transport mediated by hCNT1 at high concentrations, with a K_i value of 420 ± 68 μM. The difference in binding energy for this ligand was 12.2 kJ/mol relative to that of Urd, suggesting loss of hydrogen bonding.

Removal of the hydroxyl groups from both C(3') and C(5'), which could result in additional loss of hydrogen bonding, seriously limited interaction of this ligand with the transporter, as indicated by the extremely low affinity (K_i > 2 mM) of hCNT1 for 3',5'ddUrd. Although 2'dUrd was a high-affinity inhibitor of hCNT1-mediated Urd transport, additional removal of the 3'-hydroxyl group (2',3'ddUrd) abolished its inhibitory effect. The possible involvement of the 3'-hydroxyl group in H-bonding was also apparent from the effects of substitution of an azido group or O-methyl group at C(3') since neither 3'AzdUrd or 3'OMeUrd inhibited hCNT1-mediated Urd transport. Although hCNT1 strongly bound Urd with the 3'-hydroxyl group below the sugar ring plane, xyloU (Fig. 2-4), with the 3'-hydroxyl group oriented upwards, had little effect on hCNT1-mediated Urd transport (K_i > 1 mM). Similarly, iPUrd (Fig. 2-4) failed to inhibit Urd transport, presumably because the 3' position was no longer available and the bulky isopropylidene group was a steric barrier for interaction with hCNT1.

Recombinant hCNT1 has previously been shown to accept AZT (Fig. 2-4) as a permeant (apparent K_m = 0.49 mM) (14). It appeared that any modifications at C(3') abolished the inhibitory effect of the resulting Urd analogs to interact with hCNT1, with the notable exception of AZT. Albeit a poor inhibitor (K_i = 293 ± 44 μM), AZT inhibited hCNT1-mediated Urd transport in yeast with a greater potency than that of 3'dUrd.

hCNT3 As observed with hCNT1, C(5) of the base moiety was not involved in binding to hCNT3 because introduction of either a fluoro or an iodo group at this position resulted in significantly higher affinities (t-test, $p < 0.05$, relative to the K_i value for Urd). The differences in binding energies for FUrd and IUrd ($\delta(\Delta G^0)$ = 4.3 and 1.7 kJ/mol, respectively, relative to that of Urd) may reflect interactions between the halogen and adjacent amino acid residues of the transporter protein. Methylation of N(3) resulted in a 3-fold decrease in affinity, relative to that of Urd. The observed $\delta(\Delta G^0)$ of less than 3 kJ/mol between 3MeUrd and Urd was probably due to steric effects.

hCNT3 tolerated modifications at C(2') well. The K_i value for 2'dUrd was similar to that for Urd. Further evidence for non-involvement of the 2'-hydroxyl group was that FdUrd and BrdUrd exhibited slightly lower K_i values than that of Urd. As observed with hCNT1, the inverted orientation of the 2'-hydroxyl group abolished binding of hCNT3 to

araU (K_i > 2 mM) and the substitution of the 2'-hydroxyl group by an azido or O-methyl group caused small changes in binding energy that might have been caused by steric effects.

In contrast to hCNT1, hCNT3 did not appear to have strong interaction with the 5'-hydroxyl group. The changes in ΔG^0 of 2 and 4.1 kJ/mol with 5'dUrd and 2',5'ddUrd, respectively, relative to that of Urd, did not match the energy contained in a hydrogen bond. As was observed with hCNT1, hCNT3 displayed higher apparent affinity for 5'CldUrd (K_i = 5.7 ± 0.6 μM) than for 5'dUrd (K_i = 15.2 ± 2.1 μM). hCNT3 exhibited high tolerance for this modification at the 5' position with a chloride, but lower tolerance for modification with other substituents. Replacement of the 5' hydroxyl group with an azido group or O-methyl group at C(5') yielded analogs with further reductions in binding energies ($\delta(\Delta G^0)$ = 4-6 kJ, relative to 5'dUrd).

hCNT3 had a low apparent binding affinity for 3'dUrd (K_i = 258 ± 41 μM) relative to that of Urd with a difference of 9 kJ/mol in binding energy, indicating the possible loss of hydrogen bonding. Of the three hydroxyl groups in the sugar moiety, the 3'-hydroxyl group below the plane of the sugar ring appeared to be most important for hydrogen bonding with hCNT3. Retention of this feature was a structural requirement for high-affinity interaction with hCNT3. Any further modifications at C(3') abolished the capacity of the Urd analogs to bind to hCNT3 in the present assay since modified nucleosides, including 2',3'ddUrd, 3',5'-ddUrd, AZT, 3'OMeUrd, iPUrd and 3'AzdUrd did not significantly inhibit Urd transport by recombinant hCNT3.

Discussion

Recombinant hCNTs have been functionally characterized in a number of model expression systems, including cultured cells (10,36,37) and *Xenopus laevis* oocytes (5,7,13). *S. cerevisiae* has been used previously to characterize human ENT1 and ENT2 (16,17,20,38). In the present study, hCNT1 and hCNT3 were successfully produced in yeast for the first time. The *fui1::TRP1* strain, which lacks the endogenous Urd transporter (FUI1) (15), enabled measurement of nucleoside uptake by recombinant hCNT1 or hCNT3 in the absence of endogenous transport activity. The ability of

recombinant hCNT1 and hCNT3 to transport different naturally occurring nucleosides was tested and found to match their reported selectivities. Kinetic studies of Urd uptake mediated by pYPhCNT1- or pYPhCNT3-containing yeast demonstrated that both recombinant transporters had high affinity for Urd. These results indicated that the production of recombinant hCNT1 and hCNT3 in yeast provided a good model system for structure-function studies.

The structural regions of the Urd molecule involved in binding to hCNT1 and hCNT3 were probed by analysis of inhibition profiles and binding energies as described elsewhere (39). Although hCNT1 and hCNT3 exhibited overall similarities, key differences in their ligand recognition profiles indicated differences in the permeant binding sites on the two concentrative transporters. hCNT1 and hCNT3 recognized Urd through distinguishable binding motifs. Since none of the hCNTs transport uracil or other nucleobases (5-7), indicating that the ribose moiety is essential for Urd binding, this study focused primarily on structural determinants in the sugar moiety for binding.

The regions of Urd most involved in interaction with hCNT1 were identified as C(3')-OH, C(5')-OH, and N(3)-H. The differences of 12.2, 10.5 and 7.9 kJ/mol in Gibbs free energy, respectively, when the 3'-hydroxyl, 5'-hydroxyl, and N(3)-H were modified, suggested that these groups are involved in hydrogen bonding with hCNT1. The total binding energy in the Urd-hCNT1 complex was calculated to be 31.5 kJ/mol, suggesting that the remaining structural features were less critical for hCNT1 binding of Urd. Neither C(5) in the base moiety nor C(2') in the sugar moiety appeared to be involved in direct binding of Urd to hCNT1 since modifications at these positions did not cause substantial losses in binding energy.

The most critical functional group of Urd for binding to hCNT3 was the 3'-hydroxyl, which might participate in hydrogen bonding, whereas the 5'-hydroxyl and 2'-hydroxyl groups and the N(3)-H of the base moiety, which were not required for binding, were evidently not involved in hydrogen bonding to hCNT3. Thus, most of the binding energy must come from interactions between the base ring and hCNT3. It is possible that the carbonyl groups at C(2) and/or C(4) form hydrogen bonds, and the base ring might

participate in hydrophobic interactions with amino acid residues in hCNT3. Urd analogs with modifications at C(2) and/or C(4) should be evaluated.

Almost any changes at the 3' position, including removal of the hydroxyl group or inversion of its configuration, modification, or substitution, dramatically altered the interaction of the nucleosides with hCNT proteins. In contrast, substitution of a variety of groups for the 2'- or 5'-hydroxyl group allows binding of Urd analogs. The importance of the 3'-hydroxyl group of nucleosides for interaction with hCNTs, as well as hENTs, which are structurally unrelated proteins, is well established (16,40). We thus hypothesize that the binding sites in the hCNTs recognize the 3'-hydroxyl group first and, through this binding, other parts of the nucleoside subsequently bind to the transporter proteins. The apparent stronger ability of hCNT1 than that of hCNT3 to bind AZT, a thymidine analog with a modification at C(3'), further indicates the differences in the binding sites of hCNT1 and hCNT3. Compared with Urd, the sugar moiety of AZT lacks both 2'- and 3'-hydroxyl groups and the hydroxyl group in the 3' position is substituted with an azido group; these modifications reduce the capacity of AZT to interact with hCNT1. Since hCNT1 was able to interact with thymidine with high affinity and would not be predicted to bind 3'-azido-2',3'-dideoxyuridine, the 5-methyl group of the base moiety might contribute to interaction of AZT with hCNT1. How hCNT1 interacts with the base moiety of thymidine needs further investigation.

Urd analogs with modifications at C(2') displayed similar inhibitory profiles for recombinant hCNT1 and hCNT3. Both transporters tolerated very well the removal of the 2'-hydroxyl group but less well the substitution of the hydroxyl group with an azido group and even less well the addition of an O-methyl group. Neither of the transporters tolerated inversion of configuration of the 2'-hydroxy group. Although binding of the transporter proteins at C(2') was not indicated, considerable cooperativity existed between C(2') and nearby Urd recognition motifs. Changes at these positions could possibly weaken the permeant-transporter interaction by steric interference and physical separation. A bulkier substituent at C(2') such as an azido or O-methyl group could make the 3'-hydroxyl function less accessible to residues at the binding sites of the transporters. C(5') of the sugar moiety might have similar influences on interactions of hCNT1 with Urd analogs. Another similarity between hCNT1 and hCNT3 was the tolerance for

modifications at C(5) of Urd with halogens. Substitution of a halogen at C(5) reduced K_i values, giving high-affinity analogs that were bound by both transporters.

Transmembrane domains 7-8 are thought to form part of the permeant translocation pore for CNT proteins and four critical residues (Ser^{319}, Gln^{320}, Ser^{353} and Leu^{354}) in this region of hCNT1 determine permeant selectivities (35). It is likely that certain amino acid residues within this region of hCNT1, which could serve as hydrogen-bond donors or acceptors within the postulated translocation pore, form part of the permeant binding sites and directly interact with functional group(s) of Urd. Currently, site-directed mutagenesis approaches are being applied to identify the amino acid residues that comprise the Urd binding sites of hCNT1 and hCNT3 proteins. Further understanding of Urd-hCNT interactions will depend on structural analysis of the purified hCNT proteins. With purified transporter proteins, the binding constants for interactions of permeants and/or inhibitors with the transporters might be predicted by computer simulation of their 3D structures.

In summary, the hCNT yeast expression system, which can be used to characterize the binding profiles of nucleoside transporters, will enable rapid screening of interactions of newly developed nucleoside-derived drugs with hCNT proteins. The present work established profiles for the interaction of Urd analogs with the hCNT1 and hCNT3 proteins. The differences in binding motifs for hCNT1 and hCNT3 reflect differences in nucleoside-binding domains of the two transporters. Since a high-affinity ligand may inhibit nucleoside transport without being transported, further studies, such as direct assay of time courses of uptake of radiolabeled ligand, are required to determine if the uridine compounds identified in this study are also permeants. Additional nucleosides with modifications in the base moiety should be assessed to generate more complete nucleoside-binding profiles to guide the rational design and use of nucleoside drugs in the treatment of human diseases. The interactions of nucleoside analogs or drugs with hCNT1 and hCNT3 might be predicted from the permeant-recognition models developed in the present study.

Table 2-1 K_i and Gibbs free energy values for inhibition of hCNT1- and hCNT3-mediated Urd uptake in *Saccharomyces cerevisiae* by Urd analogs

Urd compounds	hCNT1		hCNT3	
	K_i (μM)	ΔG^0(kJ/mol)	K_i (μM)	ΔG^0(kJ/mol)
Urd	3.1 ± 0.3	31.5	6.7 ± 1.0	29.5
Base modification				
5-fluorouridine (FUrd)	0.9 ± 0.2	34.5	1.2 ± 0.2	33.8
5-iodouridine (IUrd)	0.9 ± 0.1	34.5	3.4 ± 0.2	31.2
3-methyluridine (3MeUrd)	73.1 ± 16.8	23.6	22.0 ± 0.2	26.6
Sugar modification				
2'-deoxyuridine (2'dUrd)	7.0 ± 0.3	29.4	5.0 ± 1.3	30.3
5'-deoxyuridine (5'dUrd)	48.6 ± 7.9	24.6	15.2 ± 2.1	27.5
3'-deoxyuridine (3'dUrd)	420 ± 68	19.3	258 ± 41	20.5
1-(β-D-arabinofuranosyl)uracil (araU)	> 1000 +		> 2000 +	
1-(β-D-xylofuranosyl)uracil (xyloU)	> 1000 +		> 2000 +	
3',5'-dideoxyuridine (3',5'ddUrd)	> 2000 *		> 2000 +	
2',3'-dideoxyuridine (2',3'ddUrd)	> 2000 +		> 2000 *	
2',5'-dideoxyuridine (2',5'ddUrd)	94.2 ± 14.6	23.0	36.2 ± 3.2	25.4
2'-O-methyluridine (2'OMeUrd)	113 ± 22	22.5	143 ± 8.6	22
5'-O-methyluridine (5'OMeUrd)	210 ± 42	21.0	135 ± 11	22.1
3'-O-methyluridine (3'OMeUrd)	> 1000 +		> 1000 *	
5'-chloro-5'-deoxyuridine (5'CldUrd)	8.5 ± 1.1	28.9	5.7 ± 0.6	29.9
2'-azido-2'-deoxyuridine (2'AzdUrd)	11.5 ± 0.5	28.2	33.3 ± 2.0	25.6
3'-azido-3'-deoxyuridine (3'AzdUrd)	> 1000 *		> 1000 *	
5'-azido-5'-deoxyuridine (5'AzdUrd)	326 ± 31	19.9	82.2 ± 4.8	23.3
2',3'-O-isopropylideneuridine (iPUrd)	> 2000 +		> 2000 *	
Base & sugar modifications				
5-ethyl-2'-deoxyuridine (EtdUrd)	17.2 ± 2.4	27.2	26.2 ± 1.2	26.2
5-fluoro-2'-deoxyuridine (FdUrd)	2.0 ± 0.1	32.5	2.3 ± 1.4	32.2
5-bromo-2'-deoxyuridine (BrdUrd)	0.8 ± 0.3	34.8	3.9 ± 0.9	30.9
5-fluoro-5'-deoxyuridine	27.6 ± 4.9	26.0	22.0 ± 2.9	26.6
Thymidine (Thd)	2.6 ± 0.1	31.9	26.5 ± 0.8	26.1
3'-azido-3'-deoxythymidine (AZT)	293 ± 44	20.2	> 2000 +	

The transport of 1 μM [^{3}H]Urd into yeast (*fui1::TRP1*) expressing either pYPhCNT1 or pYPhCNT3 was measured over 30 min or 10 min, respectively, in the presence of graded concentrations of Urd or Urd analogs. Average IC_{50} values (mean ± S.E., n = 3-4) were determined using Graphpad Prism Version 3.0 Software and were converted to K_i values by the Cheng and Prusoff equation (21) using K_m values (mean ± S.E., n = 3) of 9.2 ± 3.8 μM and 8.7 ± 1.1 μM for recombinant hCNT1 and hCNT3, respectively. Free Gibbs energy (ΔG^0) was calculated from $\Delta G^0 = -RT\ln(K_i)$.

* No obvious inhibition was observed.

+ Inhibition of less than 50% was observed.

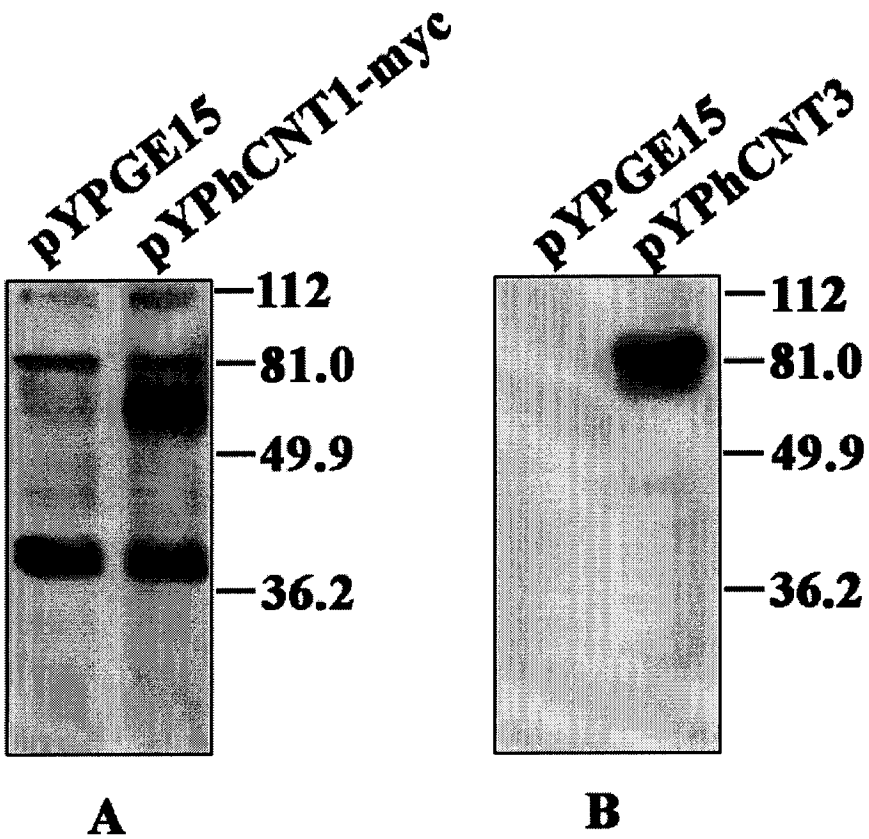

Figure 2-1 Immunoblotting to detect recombinant hCNT1-myc and hCNT3 in yeast.

Yeast cells (*fui1::TRP1*) were transformed with either pYPGE15, pYhCNT1-myc, or pYhCNT3 to form new yeast strains named *fui1::TRP1* + pYPGE15, *fui1::TRP1* + pYhCNT1-myc, and *fui1::TRP1* + pYhCNT3. Yeast membranes (20 μg in Panel A, 5 μg in Panel B) were subjected to SDS-polyacrylamide gel electrophoresis, after which proteins were transferred to polyvinylidene fluoride membranes that were subjected to immunoblotting with either 9E10 anti-myc monoclonal antibodies (Panel A) or anti-hCNT3 monoclonal antibodies (Panel B). The positions of the molecular mass markers are indicated in kDa at the right in each panel.

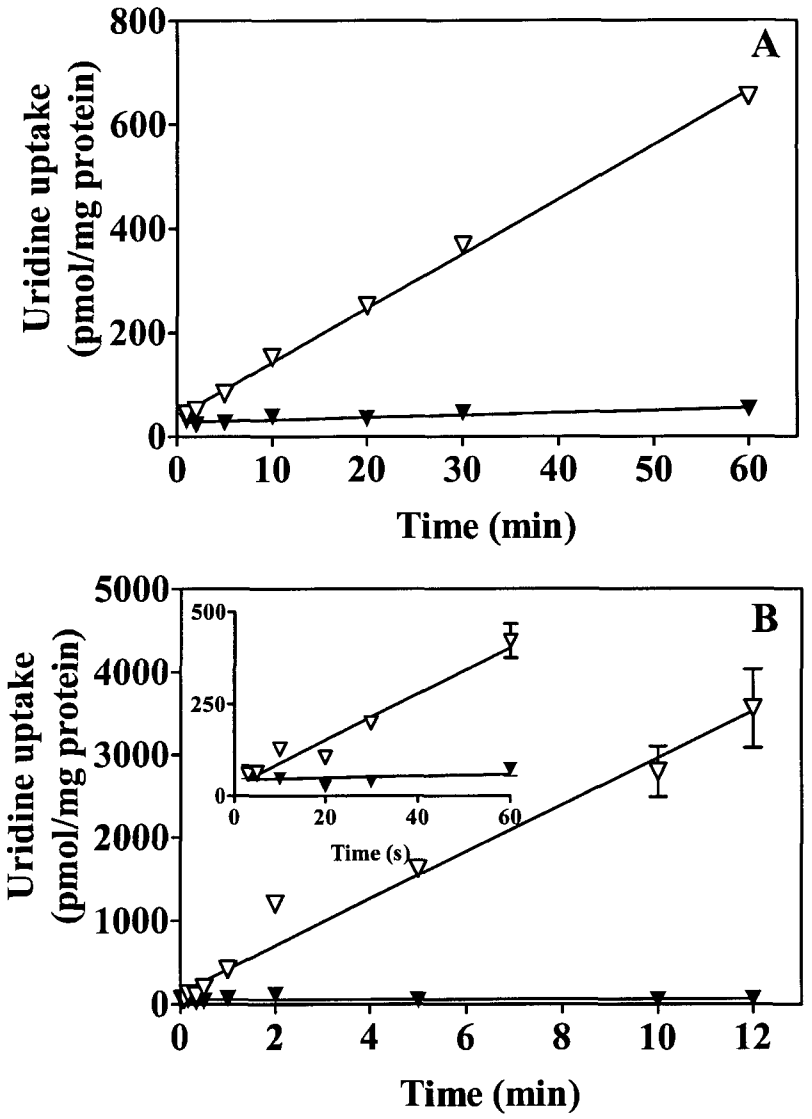

Figure 2-2 Time courses of [^{3}H]Urd uptake by recombinant hCNT1 (Panel A) and hCNT3 (Panel B) produced in yeast.

The uptake of 1 μM [^{3}H]Urd by yeast that were transformed with either pYhCNT1 or pYhCNT3 was measured in CMM/GLU (pH 7.0) in the presence of 100 mM NaCl, alone (open symbols) or with 10 mM non-radioactive Urd (closed symbols). Each point is the mean ± S.E. of triplicate determinations. S.E. values are not shown where they were smaller than the data points. Each graph represents one of three identical experiments that gave qualitatively similar results.

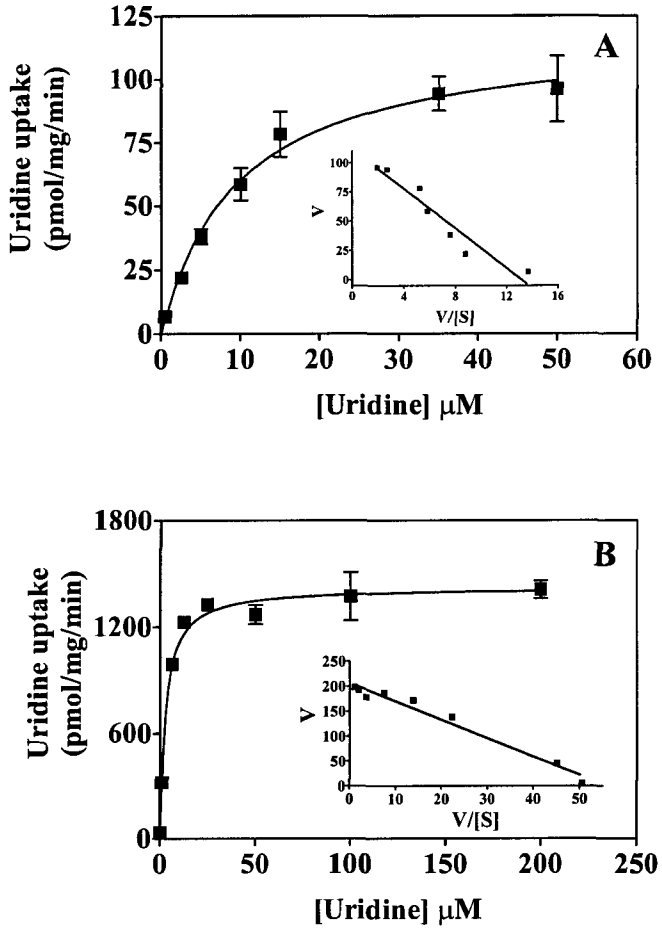

Figure 2-3 Kinetic properties of recombinant hCNT1 (Panel A) and hCNT3 (Panel B) produced in yeast.

Initial rates of Urd uptake in yeast transformed with pYhCNT1 or pYhCNT3 were measured in transport medium containing 100 mM NaCl. The mediated component of Urd transport (uptake of [^{3}H]Urd at a particular Urd concentration minus uptake at that concentration in the presence of 10 mM non-radioactive permeants) was plotted as a function of concentration and subsequently converted to V versus V/S plots (insets) to determine the kinetic properties of the transporters (PRISM, GraphPad Software). Each value is the mean ± S.E. of 6-9 determinations and S.E. values are not shown where they were smaller than the data points. Each kinetic curve represents one of three identical experiments that gave qualitatively similar results.

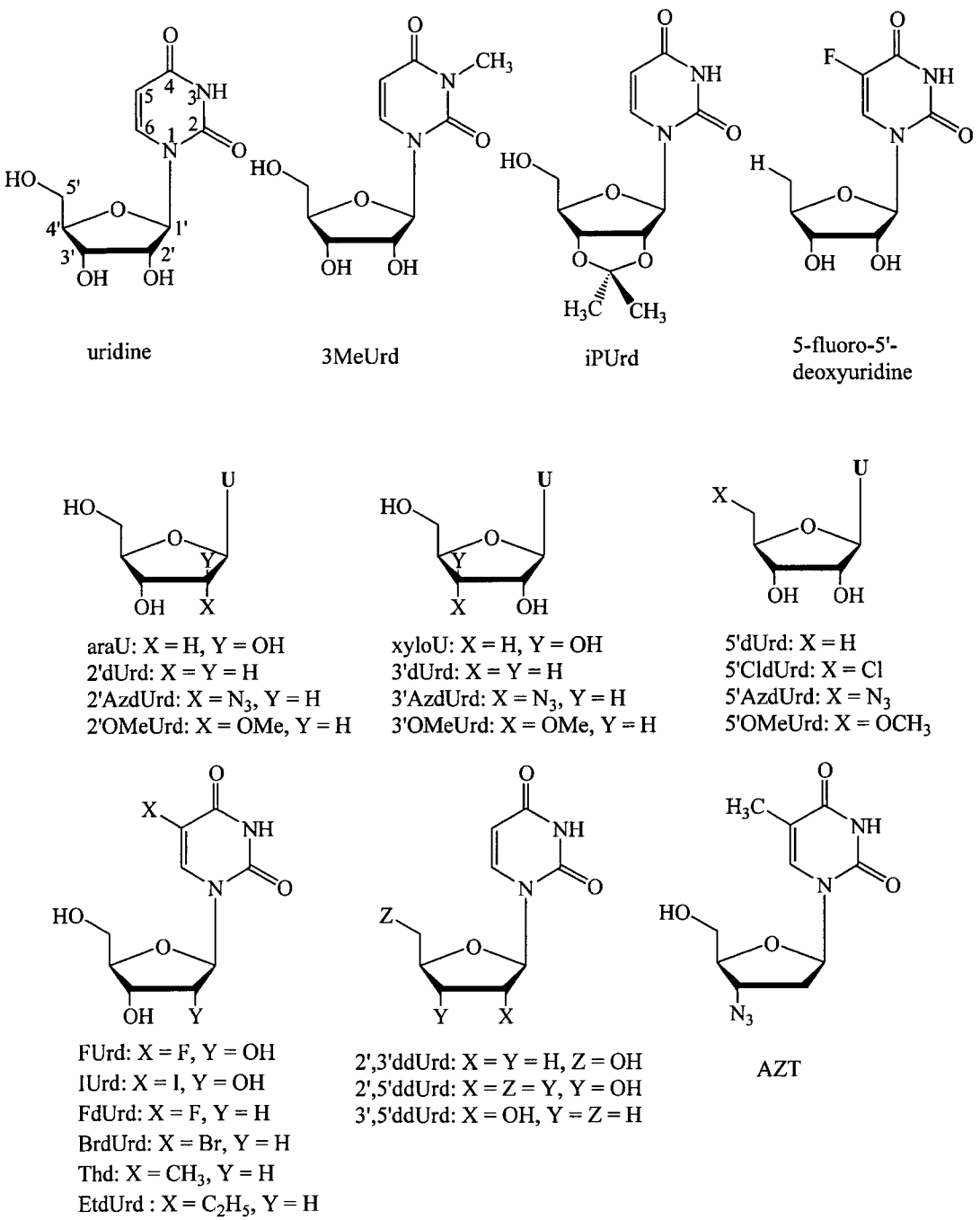

Figure 2-4 Structures of Urd and some Urd analogs.

Numbering for Urd is indicated.

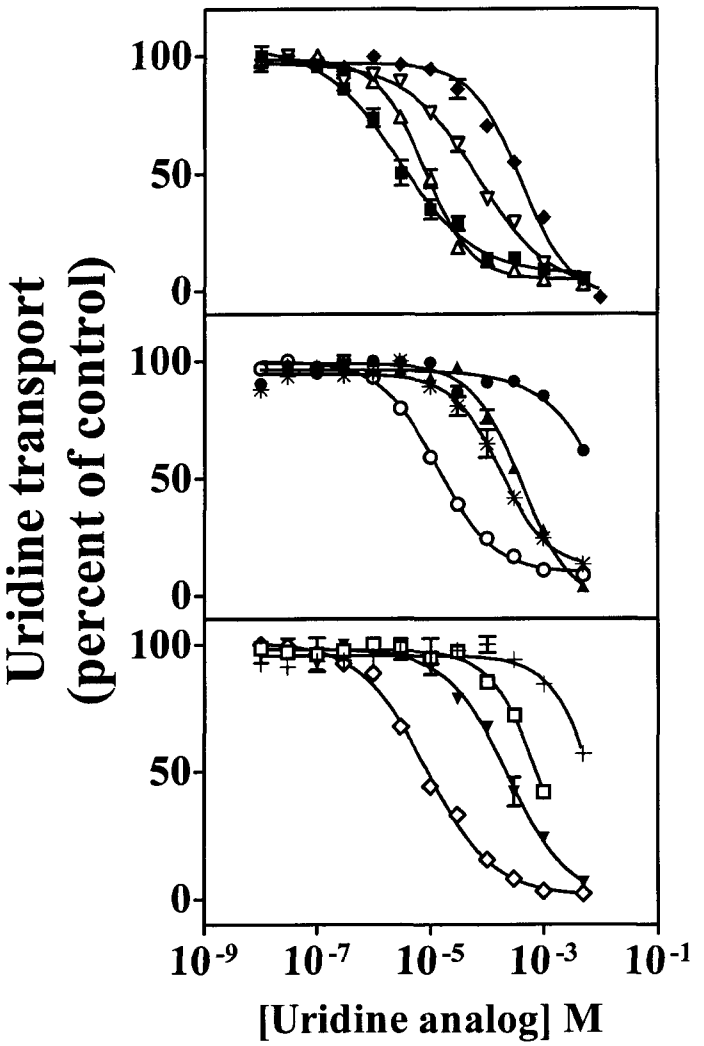

Figure 2-5 Inhibition of recombinant hCNT1-mediated Urd uptake by Urd analogs.

The uptake of 1 μM [^{3}H]Urd into *fui1::TRP1* yeast expressing pYPhCNT1 was measured over 30 min in the presence of graded concentrations of test compounds. The test compounds were: Urd (■), 2'dUrd (▽), 5'dUrd (△), 3'dUrd (◆), 5'OMedUrd (∗), 3'OMedUrd (●), 2'AzdUrd (○), 5'AzdUrd (▲), 5'CldUrd (◇), araU (□), iPUrd (+), and AZT (▼). Uptake values in the presence of Urd compounds are given as the percentage of uptake values in their absence. Each data point represents the means ± S.E. of quadruplicate determinations; error bars are not shown where they are smaller than the symbol. Three or four independent experiments gave similar results and results from representative experiments are shown.

References

1. Cass, C. E., Young, J. D., Baldwin, S. A., Cabrita, M. A., Graham, K. A., Griffiths, M., Jennings, L. L., Mackey, J. R., Ng, A. M. L., Ritzel, M. W. L., Vickers, M. F., and Yao, S. Y. M. (1999) in *Membrane Transporters as Drug Targets* (Amidon, G. L., and Sadee, W., eds) Vol. 12, 1 Ed., pp. 313-352, 12 vols., Kluwer Academic/Plenum Publishers
2. Baldwin, S. A., Mackey, J. R., Cass, C. E., and Young, J. D. (1999) *Mol Med Today* **5**, 216-224
3. Latini, S., and Pedata, F. (2001) *J Neurochem* **79**, 463-484
4. Burnstock, G. (2002) *Clin Med* **2**, 45-53
5. Ritzel, M. W., Yao, S. Y., Huang, M. Y., Elliott, J. F., Cass, C. E., and Young, J. D. (1997) *Am J Physiol* **272**, C707-714
6. Ritzel, M. W., Yao, S. Y., Ng, A. M., Mackey, J. R., Cass, C. E., and Young, J. D. (1998) *Mol Membr Biol* **15**, 203-211
7. Ritzel, M. W. L., Ng, A. M., Yao, S. Y. M., Graham, K., Loewen, S. K., Smith, K. M., Ritzel, R. G., Mowles, D. A., Carpenter, P., Chen, X., Karpinski, E., Hyde, R. J., Baldwin, S. A., Cass, C. E., and Young, J. D. (2001) *J Biol Chem* **276**, 2914-2927
8. Hamilton, S. R., Yao, S. Y., Ingram, J. C., Hadden, D. A., Ritzel, M. W., Gallagher, M. P., Henderson, P. J., Cass, C. E., Young, J. D., and Baldwin, S. A. (2001) *J Biol Chem* **276**, 27981-27988.
9. Ngo, L. Y., Patil, S. D., and Unadkat, J. D. (2001) *Am J Physiol Gastrointest Liver Physiol* **280**, G475-481.
10. Mackey, J. R., Mani, R. S., Selner, M., Mowles, D., Young, J. D., Belt, J. A., Crawford, C. R., and Cass, C. E. (1998) *Cancer Res* **58**, 4349-4357
11. Pennycooke, M., Chaudary, N., Shuralyova, I., Zhang, Y., and Coe, I. R. (2001) *Biochem Biophys Res Commun* **280**, 951-959.
12. Lu, X., Gong, S., Monks, A., Zaharevitz, D., and Moscow, J. A. (2002) *J Exp Ther Oncol* **2**, 200-212
13. Mackey, J. R., Yao, S. Y., Smith, K. M., Karpinski, E., Baldwin, S. A., Cass, C. E., and Young, J. D. (1999) *J Natl Cancer Inst* **91**, 1876-1881

14. Huang, Q. Q., Yao, S. Y., Ritzel, M. W., Paterson, A. R., Cass, C. E., and Young, J. D. (1994) *J Biol Chem* **269**, 17757-17760
15. Vickers, M. F., Yao, S. Y., Baldwin, S. A., Young, J. D., and Cass, C. E. (2000) *J Biol Chem* **275**, 25931-25938.
16. Vickers, M. F., Kumar, R., Visser, F., Zhang, J., Charania, J., Raborn, R. T., Baldwin, S. A., Young, J. D., and Cass, C. E. (2002) *Biochem Cell Biol* **80**, 639-644
17. Visser, F., Vickers, M. F., Ng, A. M., Baldwin, S. A., Young, J. D., and Cass, C. E. (2002) *J Biol Chem* **277**, 395-401.
18. Brunelli, J. P., Pall, M.L. (1993) *Yeast* **9**, 1309-1318
19. Ito, H., Fukuda, Y., Murata, K., and Kimura, A. (1983) *J Bacteriol* **153**, 163-168
20. Vickers, M. F., Mani, R. S., Sundaram, M., Hogue, D. L., Young, J. D., Baldwin, S. A., and Cass, C. E. (1999) *Biochem J* **339**, 21-32
21. Cheng, Y., and Prusoff, W. H. (1973) *Biochem Pharmacol* **22**, 3099-3108
22. de Koning, H. P., and Jarvis, S. M. (2001) *Acta Trop* **80**, 245-250.
23. Codington, J. F., Fecher, R., and Fox, J. J. (1960) *J Am Chem Soc* **82**, 2794-2803
24. Hampton, A., and Nichol, A. W. (1966) *Biochemistry* **5**, 2076-2082
25. Verheyden, J. P. H., Wagner, D., and Moffatt, J. G. (1971) *J Org Chem* **36**, 250-254
26. Robins, M. J., Naik, S. R., and Lee, A. S. K. (1974) *J Org Chem* **39**, 1891-1899
27. Yung, N. C., and Fox, J. J. (1961) *J Am Chem Soc* **83**, 3060-3066
28. Rhie, S.-Y., and Pfleiderer, W. (1994) *Nucleosides and Nucleotides* **13**, 1425-1452
29. Matray, T. J., and Gryaznov, S. M. (1999) *Nucleic Acids Res* **27**, 3976-3985
30. Wang, Y., Hogenkamp, H. P. C., Long, R. A., Revankar, G. R., and Robins, R. K. (1977) *Carbohydr Res* **59**, 449-457
31. Robins, M. J., Hansske, F., Wnuk, S. F., and Kanai, T. (1991) *Can J Chem* **69**, 1468-1474.
32. Horwitz, J. P., Tomson, A. J., Urbanski, J. A., and Chua, J. (1962) *J Org Chem* **27**, 3045-3048
33. Hovinen, J. (1997) *Helv Chim Acta* **80**, 851-855
34. Bender, D. M., Hennings, D. D., and Williams, R. M. (2000) *Synthesis*, 399-402
35. Loewen, S. K., Ng, A. M., Yao, S. Y., Cass, C. E., Baldwin, S. A., and Young, J. D. (1999) *J Biol Chem* **274**, 24475-24484

36. Graham, K. A., Leithoff, J., Coe, I. R., Mowles, D., Mackey, J. R., Young, J. D., and Cass, C. E. (2000) *Nucleosides Nucleotides Nucleic Acids* **19**, 415-434
37. Lai, Y., Bakken, A. H., and Unadkat, J. D. (2002) *J Biol Chem* **277**, 37711-37717
38. Vickers, M. F., Young, J. D., Baldwin, S. A., Ellison, M. J., and Cass, C. E. (2001) *Mol Membr Biol* **18**, 73-79.
39. Wallace, L. J., Candlish, D., and De Koning, H. P. (2002) *J Biol Chem* **277**, 26149-26156
40. Patil, S. D., Ngo, L. Y., and Unadkat, J. D. (2000) *Cancer Chemother Pharmacol* **46**, 394-402

Chapter 3 Uridine Binding and Transportability Determinants of Human Concentrative Nucleoside Transporters

A version of this chapter has been published:

Zhang, J., Smith, K. M., Tackaberry, T., Visser, F., Robins, M. J., Nielsen, L. P., Nowak, I., Baldwin, S. A., Young, J. D., and Cass, C. E. *Mol Pharmacol*, 68(3), 2005.

Acknowledgements

Drs. Kyla M. Smith and Edward Karpinski conducted the *X. laevis* nucleoside transport experiments. Ms. Tracey Tackaberry conducted part of the yeast transport assays. Dr. Frank Visser contributed to this project by helping with manuscript preparation and intellectual guidance. Dr. Morris Robins, Mr. Lars Nielsen and Mr. Ireneusz Nowak are the chemists who developed the series of uridine analogs. Drs. Stephen Baldwin and James Young are collaborative principle investigators who helped obtain research funding for this project and aided in manuscript preparation.

Introduction

Mammalian nucleoside transporters are classified into two structurally and mechanistically unrelated protein families, the concentrative and equilibrative nucleoside transporters (CNTs and ENTs) (1,2). The ENTs transport a broad range of purine and pyrimidine nucleosides down their concentration gradients, whereas the CNTs couple uphill nucleoside transport to downhill sodium transport and, in the case of hCNT3, also proton transport. Three human (h) CNTs with different permeant selectivities have been identified by molecular cloning and functional expression in oocytes of *Xenopus laevis* (3-5). hCNT1 and hCNT2 prefer pyrimidine nucleosides and purine nucleosides, respectively, although hCNT1 also transports adenosine and hCNT2 also transports uridine (Urd). hCNT3 transports a broad range of pyrimidine and purine nucleosides (5,6). The ENTs appear to be expressed in most human cell types. In contrast, the CNTs are found primarily in specialized cell types, including renal and gastrointestinal epithelia (4,5,7-9), suggesting an important role in absorption, secretion, distribution and elimination of physiologic nucleosides and nucleoside drugs. hCNTs have also been observed in leukemic cells and a few cancer cell lines (5,10,11). Differences in tissue distribution and permeant selectivities of hCNTs suggest different nucleoside-transport capacities of various tissues and distinct physiological and pharmacological roles.

Nucleoside analogs are used clinically in the treatment of cancer and viral infections. Understanding the structural requirements for transporter binding and translocation of nucleosides should enable the design of more effective strategies for use of therapeutic nucleosides. In the absence of detailed structures for nucleoside transporter proteins, several experimental approaches have been used to define the structural requirements of nucleosides for interaction with the transporters (12-15). A study with human intestinal brush border membrane vesicles suggested that the binding sites of hCNT1 and hCNT2 differentially interacted with analogs of their common permeants, Urd and adenosine (15). Using three-dimensional quantitative structure-activity relationships that were based on inhibition data obtained previously, this same group generated pharmacophore models in which the predominant determinants for ligand interaction were hydrogen bonding for hCNT2 and electrostatic and steric features

for hCNT1 and hENT1 (14). In a study with stably transfected human cell lines, hCNT1 and hCNT2 exhibited different capacities for binding of Urd and adenosine analogs with substituents on the ribosyl and/or base moieties (12,13). A high-throughput inhibitor-sensitivity assay in which recombinant hCNT1, hCNT3, hENT1, and hENT2 were produced in yeast was used to quantify the inhibitory effects of Urd analogs with systematic sugar modifications (6,16). A common observation in all of these inhibition studies was the importance of the 3'-hydroxyl group for high affinity interaction of permeants and/or inhibitors with the transporters.

A deficiency of the approaches taken thus far to define the structural determinants for interaction of nucleoside analogs with the transporters is that they are based primarily on inhibition data. The current work was undertaken to extend our earlier inhibition studies of Urd binding motifs with hCNT1 and hCNT3 (6) to include hCNT2, which was not utilized previously because of its low expression levels in the yeast strain initially used in the inhibition assay, and to determine the extent to which the inhibitory Urd analogs were also permeants. The original difficulty of hCNT2 production was circumvented by introducing the hCNT2-containing plasmid into a double knockout yeast strain (*fui1::HIS3*) that lacked both Urd permease (FUI1) and uracil permease (FUR4). The binding motif of hCNT2 exhibited distinct features when compared with hCNT1 and hCNT3. Since a high-affinity ligand may inhibit nucleoside transport without also being transported, two-voltage clamp experiments were performed in *Xenopus laevis* oocytes to determine if the Urd analogs that inhibited Urd transport were also permeants, thus defining the transportability profiles of hCNT1, hCNT2 and hCNT3. Each hCNT exhibited a distinct Urd transportability profile that was closely related to its permeant binding profile.

Material and Methods

Strains and media

BY4742-YBR021W (MATα, his3, leu2, lys2, ura3, ΔFUR4), which contains a disruption in the gene encoding the endogenous uracil permease, FUR4, was purchased

from American Type Culture Collection (Manassas, VA) and used as the parental yeast strain to generate the double permease knockout strain *fui1::HIS3*. *fui1::HIS3* was generated by deleting the fui1 gene using the polymerase chain reaction (PCR)-mediated one-step gene disruption method (17). Other strains were generated by transformation of the yeast-Escherichia coli shuttle vector pYPGE15 (18) into *fui1::HIS3* using a standard lithium acetate method (19).

The gene locus for FUI1 was disrupted by integration of the HIS3 expression cassette, encoding imidazoleglycerolphosphate dehydratase (EC 4.2.1.19) into the coding region of the FUI1 gene to create *fui1::HIS3*. The *fui1*-disruption mutants were selected in a medium that lacked histidine but contained 500 μM FUrd. Since FUI1-mediated transport of FUrd leads to yeast death (20), survival in 500 μM FUrd indicated the successful targeted integration of the HIS3 cassette into the yeast genome with disruption of the *fui1* gene. Three of the surviving yeast colonies and BY4742-YBR021W were then tested for their abilities to transport [^{3}H]uracil or [^{3}H]Urd in the presence and absence of either 5 or 10 mM non-radioactive uracil or Urd, respectively.

Yeast strains were maintained in complete minimal medium (CMM) containing 0.67% yeast nitrogen base (Difco, Detroit MI), amino acids (as required to maintain auxotrophic selection), and 2% glucose (CMM/GLU). Agar plates contained CMM with various supplements and 2% agar (Difco). Plasmids were propagated in *E. coli* strain TOP10F' (Invitrogen, Carlsbad, CA) and maintained in Luria broth with ampicillin (100 μg/ml).

DNA manipulation and plasmid construction

To construct the deletion strain *fui1::HIS3*, two 71-mer oligonucleotide primers were synthesized (Invitrogen, Carlsbad, CA), each containing (3' to 5') 21 bases of homology to the HIS3 cassette, a unique 50-bp tag sequence that was complementary to the region (either upstream or downstream of the *fui1* open reading frame) being targeted (including the start or stop codon). The 71-mer primers were used to amplify the HIS3 gene cassette, which was contained in plasmid pJJ215 (a generous gift from Dr. B. Lemire, University of Alberta, Edmonton, AB). The amplified PCR products were transformed into BY4742-YBR021W using the lithium acetate method and the resulting

transformed yeast were selected by growing on agar plates that contained 500 μM FUrd but lacked histidine.

For *S. cerevisiae* expression, the hCNT2 open reading frames were amplified from vectors (pCDNA3-hCNT2) by PCR methodology using the following primers (restriction sites underlined): 5'-XbaI-hCNT2 (5'-CTG TCT AGA ATG GAG AAA GCA AGT GGA AG-3'), 3'-KpnI-hCNT2 (5'-CGA GGT ACC TCA GGC ACA GAC GGT ATT GTT GTA G -3'). The amplified open reading frames were inserted into pYPGE15 (a high copy-number episomal yeast vector that expresses the inserted DNA constitutively under the transcriptional control of the phosphoglycerate kinase promoter) to generate pYPhCNT2. The PCR reactions were performed using *Pwo* polymerase (Roche Molecular Biochemicals, Indianapolis, IN) and the resulting PCR products were verified by DNA sequencing using an ABI PRISM 310 sequence detection system (PerkinElmer Life Sciences, Norwalk, CT).

Immunostaining of yeast membranes

Yeast membranes were prepared by a previously described method (20) and subjected to SDS-polyacrylamide gel electrophoresis (21), after which proteins were transferred to polyvinylidene fluoride membranes (Immobilon-P, Millipore, Bedford, MA). The transfer membranes were blocked overnight at 4°C first in TTBS (0.2% Tween-20, Tris-buffered saline) containing 5% (w/v) skim milk powder and then in TTBS with antibodies against hCNT2 and 5% (w/v) skim milk powder. The membranes were then washed three times with TTBS, incubated with TTBS-containing species-specific horseradish-peroxidase secondary antibodies (Jackson ImmunoResearch Laboratories Inc., West Grove, PA) and 5% (w/v) skim milk powder, washed with TTBS, and visualized with enhanced chemiluminescence (ECL, Amersham Pharmacia Biotech) and autoradiography. Monoclonal antibodies against hCNT2 were raised by established methods (22) against an immunogenic epitope that corresponded to residues 30-51 of hCNT2, a region predicted to be located in a large intracellular loop close to the amino terminus. The conjugated and unconjugated synthetic peptides were obtained from the Alberta Peptide Institute (Edmonton, Canada).

Urd uptake in yeast producing recombinant hCNT2

The uptake of [^{3}H]Urd, [^{3}H]adenosine, [^{3}H]cytidine and [^{3}H]inosine (Moravek Biochemicals, Brea, CA) into logarithmically proliferating yeast was measured using a cell harvester as described previously (6,23). Briefly, yeast were grown in CMM/GLU to an OD_{600} of 0.8-1.2, washed three times with fresh CMM/GLU (pH 7.4), and re-suspended to an OD_{600} of 4 in CMM/GLU (pH 7.4). Fifty-µl portions of CMM/GLU (pH 7.4) with [^{3}H]Urd and a test compound (if present) at twice the desired concentration were preloaded into 96-well plates. The transport assays were initiated by adding equal volume of yeast suspension at OD_{600} = 4 to the individual wells of the preloaded 96-well plates, which were placed on the semi-automated cell harvester (Micro96^{TM} HARVESTER, Skatron Instruments, Norway). At graded time intervals, groups of transport reactions (usually 24) were terminated simultaneously by harvesting yeast on glass-fiber filters (Skatron Instruments) with continued washing with demineralized water to remove unincorporated permeant. The filter discs with yeast corresponding to a particular transport assay were placed into individual scintillation counting vials (one disc/vial) to which 5 ml of scintillation counting fluid (EcoLite, ICN Biomedical Inc., Aurora, OH) was added. Scintillation vials were allowed to sit at room temperature overnight with shaking before analysis.

The binding of Urd and its analogs to recombinant hCNT2 was assessed by measuring their abilities to inhibit the uptake of [^{3}H]Urd in the "inhibitor-sensitivity" assay as follows. Yeast were incubated with graded concentrations of a particular test compound and 1 µM [^{3}H]Urd in CMM/GLU (pH 7.4) for 20 min after which [^{3}H]Urd uptake was measured. All experiments were carried out in quadruplicate. The amount of [^{3}H]Urd associated with yeast in the presence of 10 mM non-radioactive Urd was also determined to quantify non-specifically associated radioactivity, which was subtracted from total radioactivity for each transport assay. Data were fitted to theoretical inhibition curves by nonlinear regression to obtain IC_{50} values (concentrations that inhibited reactions by 50%). K_i (inhibitory constant) values were determined from the equation (24) in which $K_i = IC_{50}/[1 + (L/K_m)]$ and L = [^{3}H]Urd concentration, which was always 1 µM. Gibbs free energy (ΔG^0) was calculated from $\Delta G^0 = -RT\ln(K_i)$, in which R is the gas constant and T is the absolute temperature. The thermodynamic stability of

transporter-inhibitor complexes was quantitatively estimated from ΔG^0 as described elsewhere (25).

Steady-state electrophysiological studies

hCNT1, hCNT2 or hCNT3 cDNA in pGEM-HE (3-5) was linearized with *Nhe*1 and transcribed with T3 or T7 polymerase using the mMESSAGE mMACHINE™ (Ambion, Austin, TX) transcription system. *In vitro* synthesized transcripts were injected into isolated mature stage VI oocytes from *X. laevis* as described previously (26). Mock-injected oocytes were injected with water alone.

Oocyte membrane currents were measured using a GeneClamp 500B oocyte clamp (Axon Instruments, Inc., Foster City, CA, USA) in the two-electrode, voltage-clamp mode as described previously (26). All experiments were performed at room temperature (20°C) and oocytes were discarded if membrane potentials were unstable or more positive than –30 mV. The membrane potential was clamped at a holding potential of –50 mV and Urd or Urd analogs were added at various concentrations. The sodium currents induced by 100 μM Urd were used as controls to compare the transportability of Urd analogs by recombinant hCNT1, hCNT2 and hCNT3. The concentrations of Urd analogs for electrophysiological studies were chosen based on their K_i values for inhibition of hCNT1 and hCNT3 (6) and hCNT2 (this study) as determined in the inhibitor-sensitivity assay. The transport medium contained (mM): NaCl, 100; KCl, 2; $CaCl_2$, 1; $MgCl_2$, 1; Hepes, 10 (pH 7.5). Current values are presented as means ± S.E of three or more oocytes.

Urd analogs

The structures of Urd and its analogs were given previously (6,16). The abbreviations of Urd analogs are given in Table 1. The Urd analogs used in this study were either obtained from R. I. Chemical, Inc. (Orange, CA) or were synthesized as described elsewhere (6).

Stock solutions of test compounds were either prepared in water or dimethyl sulfoxide (DMSO) (Sigma-Aldrich Canada Ltd., Oakville, ON) and the final concentration of DMSO in transport reactions was 0.1% if DMSO was used as a solvent.

Results

Detection of recombinant hCNT2 in yeast membranes

The production of recombinant hCNT2 in *S. cerevisiae* was verified by immunoblotting using anti-hCNT2 antibodies (Fig. 3-1, Panel A). A 75-kDa immunoreactive species was detected in membranes of pYPhCNT2-containing yeast and was not detected in membranes of pYPGE15-containing yeast (Fig. 3-1, Panel A). The electrophoretic mobilities of the detected proteins were consistent with the predicted molecular mass of hCNT2.

Urd transport by recombinant hCNT2 produced in yeast

The FUI1, FUR4 double knockout strain (*fui1::HIS3*) was confirmed by demonstrating that it was unable to transport either [^{3}H]Urd or [^{3}H]uracil. The parental strain (BY4742-YBR021W) exhibited Urd, but not uracil, transport activity (data not shown).

The time course for uptake of 1 μM [^{3}H]Urd into *fui1::HIS3* that contained pYPGE15 was linear over extended periods (> 30 min) and exhibited rates of 0.05 ± 0.01 and 0.04 ± 0.01 pmol/mg protein/min in the presence and absence of 10 mM nonradioactive Urd, respectively (data not shown). When time courses for influx of 1 μM [^{3}H]Urd were measured in the presence and absence of 10 mM non-radioactive Urd into *fui1::HIS3* yeast that contained pYPhCNT2 (Fig. 3-1, Panel B), the time courses were linear for up to 30 min with mean rates (± S.E.) of 4.1 ± 0.09 and 0.05 ± 0.02 pmol/mg protein/min, respectively, indicating the presence of functional hCNT2 in yeast plasma membranes. Urd transport rates were determined for all subsequent experiments using incubation times of 20 min for recombinant hCNT2 produced in yeast, thereby providing large signal-to-noise ratios and maintaining initial rates of uptake. Results from similar experiments with other ^{3}H-labeled nucleosides demonstrated that recombinant hCNT2 also transported adenosine, inosine and guanosine, but not cytidine and Thd (data not shown), confirming that the permeant selectivity of recombinant hCNT2 produced in yeast was similar to that reported previously in cultured cells and *X.*

laevis oocytes (4,12,13), thus providing a good model system for structure-function studies.

The experiments of Fig. 3-1, Panel C showed that recombinant hCNT2 had a moderate apparent affinity and capacity for Urd uptake (K_m = 29 ± 7 μM, V_{max} = 146 ± 11 pmol/mg protein/min; mean ± S.E., n = 3). The K_m value of recombinant hCNT2 was slightly lower than those obtained with *X. laevis* oocytes (40 ± 6 μM, (4) and cultured mammalian cells (4,12); these differences are believed to be due to variations in post-translational modifications in the different expression systems and/or differences in membrane lipid environment (27).

Interaction of Urd analogs with recombinant hCNT2: inhibitor-sensitivity assays

To gain an understanding of the structural regions of Urd that interact with hCNT2, Urd analogs with modifications of the base and/or sugar moieties were tested systematically by assessing the concentration dependence of inhibition of transport of 1 μM Urd mediated by hCNT2. The inhibition of Urd uptake was assumed to be competitive since (i) the inhibitors tested were close structural analogs of Urd, and (ii) the transporter under study was most likely to be the sole source of interaction with the potential inhibitor. Representative concentration-effect curves of some of the analogs for inhibition of hCNT2-mediated Urd transport are shown in Fig. 3-2. In all cases, the Hill coefficients were close to –1 (mean ± S.E. = –0.9 ± 0.2), indicating a single class of inhibitor binding sites. The mean K_i values (± S.E.) and the corresponding Gibbs free energy values are listed in Table 1.

Base modifications. There were apparent weak interactions between hCNT2 and C(5) of Urd since the addition of larger substituents at the C(5) position resulted in decreases of 2-6 kJ/mol in ΔG° with 2-15 fold increases in K_i values. The K_i values increased dramatically with the increase in volume of the substituent (e.g., fluoro < bromo < iodo) at C(5); FUrd exhibited a K_i value of 61 ± 13 μM, twice that of Urd (28 ± 3 μM), and IUrd exhibited a K_i value of 359 ± 50 μM, with a loss of 5.7 kJ/mol in ΔG^0, suggesting that the interactions between hCNT2 and C(5) were steric. Although these interactions were not tight, high concentrations of FUrd, IUrd, and BrdUrd were capable

of completely inhibiting hCNT2-mediated transport of Urd. Thd was a weak inhibitor of Urd uptake with a K_i value of 566 ± 20 μM. The lower affinities for FdUrd, BrdUrd, IdUrd and EtdUrd, with ΔG^0 values of 8-20 kJ/mol, as compared to 2'dUrd, suggested that the ethyl and iodo substituents, with larger sizes than the fluoro and bromo substituents, may have sterically reduced the ability of the analog to efficiently contact the transporter protein.

The 3 position of the base moiety (N(3)-H) contributed a recognition determinant for binding to hCNT2. The low affinity of 3MeUrd, with a 20-fold increase in K_i value compared to that of Urd, indicated the importance of the N(3) position as part of the binding motif, with a difference of 7 kJ/mol binding energy, suggesting loss of a weak hydrogen bond.

Sugar modifications. hCNT2 displayed a reduced affinity for 2'dUrd relative to Urd (Fig. 3-3) with a small loss of free energy ($\delta(\Delta G^0)$ = 2.1 kJ/mol). However, C(2') was an important determinant for high-affinity binding of Urd by hCNT2 since other modifications at this position reduced interactions with hCNT2. The inverted orientation of the hydroxyl group produced an analog that could no longer interact with hCNT2 since AraU, an epimer of Urd with the 2'-hydroxyl group above the plane of the sugar ring, exhibited a pronounced reduction in its interaction with the transporter (K_i > 3 mM). Compounds with substitution of an O-methyl or azido group for the 2'-hydroxyl group failed to inhibit hCNT2-mediated Urd transport at high concentrations (K_i > 3 mM), most likely because of the bulkier size of the C(2')-O-CH_3 and C(2')-N3 substituents.

Strong interactions existed between hCNT2 and C(5')- and C(3')-OH moieties since the removal of either the 5'- or 3'-hydroxyl groups yielded K_i values > 3 mM, with losses of >10.5 kJ/mol in ΔG^0, suggesting that hydrogen bonding was important. Although 2'dUrd was a moderate-affinity inhibitor of hCNT2-mediated Urd transport, additional removal of the 3'- or 5'-hydroxyl groups diminished its inhibitory effects. The possible involvement of the 3'- and 5'-hydroxyl groups was also apparent from the effects of substitution of an azido or O-methyl group at these positions; hCNT2-mediated Urd transport remained unchanged in the presence of high concentrations of 3'AzdUrd, 3'OMeUrd, 5'AzdUrd or 5'OMeUrd. AZT, which is 3'-azido-3'-deoxyothymidine, failed to inhibited hCNT2-mediated Urd uptake. The loss of more than 8 kJ/mol in ΔG^0 value

upon substitution of a chloro group at the C(5') of 5'dUrd suggested the loss of hydrogen bonding between Urd and hCNT2. Although hCNT2 strongly bound Urd with the 3'-hydroxyl group below the sugar ring plane, its affinity for xyloU, with the 3'-hydroxyl group oriented upwards, was greatly reduced (K_i > 3 mM). Similarly, iPUrd failed to inhibit Urd transport, presumably due to the presence at the 3' position of the isopropylidene group.

Permeant selectivities of hCNT1, hCNT2 and hCNT3 for Urd analogs: transport assays

To determine if the Urd analogs that bound to either hCNT1 (6), hCNT3 (6) or hCNT2 (this study) were also permeants, two-electrode voltage clamp studies were used to measure their abilities to induce inward sodium currents in oocytes of *X. laevis* producing each of the transporters. Currents produced by Urd, 2'dUrd, 3'dUrd and 5'dUrd in a sodium-containing medium are shown in Fig. 3-3. Average current values for Urd analogs with base modifications observed in oocytes injected with transcripts are shown in Fig. 3-4. To compare the transportability of Urd and Urd analogs, the mean values of Urd analog-induced currents were normalized to the mean values of Urd-produced currents and summarized as I_{Analog}/I_{Urd} in Table 2 for hCNT1, hCNT2 and hCNT3. hCNT1 and hCNT2 generated similar inward currents (I_{Na} = 140 nA) while hCNT3 induced higher currents (I_{Na} = 330 nA) in the presence of 100 μM Urd. In all cases, the inward-directed sodium currents were reversible and abolished in a sodium-free medium and no steady-state currents were observed in control water-injected oocytes (data not shown).

Base modifications. Moderate currents (I_{Analog}/I_{Urd} = 20-60%) were elicited by hCNT1 and hCNT3 upon application of various concentrations of FUrd, IUrd, MeUrd and BrUrd whereas hCNT2 exhibited greatly reduced ability to transport Urd analogs with modifications at C(5), following a trend of diminished transportability with bulkier substituents [i.e., Urd (100 μM) > FUrd (50 and 100 μM) > MeUrd (500 μM) > IUrd and BrUrd (500 μM)]. Unlike hCNT1 and hCNT2, hCNT3 transported 3MeUrd well at higher concentrations (I_{analog}/I_{Urd} = 48%, 500 μM of 3MeUrd).

Sugar modifications. Moderate to large inward currents were elicited by hCNT1 with application of 2'dUrd or 5'dUrd (Fig. 2-3). The slightly higher currents of hCNT1 (I_{analog}/I_{Urd} = 112%) observed with 2'5'ddU (100 μM) compared with that of Urd (100 μM) indicated that the 2'- and 5'-hydroxyl groups were not obligatory for transportability by hCNT1. Addition of an O-methyl group at the 2' position resulted in a substantial decrease of sodium current; with a concentration of 1 mM, only 41% of I_{Urd} induced by 100 μM Urd was observed with 2'OMeUrd. Although hCNT1 was able to transport Urd analogs with different modifications at C(2'), including substitution of the hydroxyl group with an azido group (2'AzdUrd), it barely transported AraU (I_{analog}/I_{Urd} = 4.5%). hCNT1 exhibited high tolerance for substitution of the 5'-hydroxyl with chloro but lower tolerance for other substitutions (e.g., replacement with an azido or O-methyl group yielded poor permeants with I_{analog}/I_{Urd} values of less than 10% of that observed with Urd). 3'dUrd initiated moderate to high inward currents at high concentrations (I_{analog}/I_{Urd} = 91%, 3 mM of 3'dUrd, Fig. 3-3) and small but significant currents were induced by 3 mM of 2',3'ddUrd, 3',5'ddUrd, 3'AzdUrd, 3'MedUrdU and xyloU. No currents were observed in the presence of iPUrd.

hCNT2 transported Urd analogs with modifications at the C(2') position whereas those with modification at the C(5') and C(3') positions were poorly transported, if at all. Moderate currents were produced by 100 μM 2'dUrd while only small currents were induced by 3 mM 5'dUrd (I_{analog}/I_{Urd} = 14.7%). Surprisingly, 2',5'ddUrd, a poor permeant for hCNT2 at 100 μM (3.1% of I_{Urd}), induced a higher current at a concentration of 3 mM that was than that of 5'dUrd. Similarly, although poor permeants at low concentrations, compounds with C(2') modifications initiated significant inward currents at higher concentration (3mM), with 2'AzdUrd > 2'OMeUrd > araU. C(5') modifications significantly reduced transportability. hCNT2 transported 5'CldUrd and 5'AzdUrd poorly at high concentrations and was unable to transport 5'OMeUrd. Small and moderate currents were induced with 500 μM and 3 mM 3'dUrd, respectively (I_{analog}/I_{Urd} = 4.2% at 500 μM vs 30.4% at 3 mM). Although weak currents were detected with 3 mM 2'3'ddUrd, no currents were initiated by hCNT2 with xyloU, 3'5'ddUrd, 3'AzdUrd, 3'OMeUrd or iPUrd.

hCNT3 transported a broad range of Urd analogs. The absence of the 2'- and/or 5'-hydroxyl groups had no effect on transportability by hCNT3 since the sodium currents produced by 100 μM 2'Urd, 5'Urd and 2',5'ddUrd were similar to that of Urd (Fig. 3-3). At 50 μM, the 2'AzdUrd-induced current was similar to that induced by 100 μM Urd. However, hCNT3 showed reduced transportability of 2'OMeUrd (I_{analog}/I_{Urd} = 33.6% at 100 μM and 64.5% at 1 mM). Moderate inward currents were induced by 3 mM araU, suggesting that the translocation pore of hCNT3 is more flexible than those of hCNT1 and hCNT2. Urd analogs containing 5' modifications, including 5'CldUrd, 5'AzdUrd and 5'OMeUrd, were good permeants with I_{analog}/I_{Urd} of 29.0% for 10 μM 5'CldUrd and about 70% for 5'AzdUrd and 5'OMeUrd. hCNT3 handled Urd analogs with 3' modifications much better than hCNT1 and hCNT2. Large currents were induced by 3'dUrd at 500 μM (I_{analog}/I_{Urd} = 77. 5%). At high concentrations (3 mM), 3'dUrd (Fig. 3-3), 2',3'ddUrd and xyloU produced moderate to large inward currents whereas 3'AzdUrd, 3'OMeUrd and iPUrd induced low currents and thus were poor permeants of hCNT3.

Base and Sugar modifications. The hCNT1-mediated currents induced by FdUrd, BrdUrd, IdUrd and EtdUrd (I_{analog}/I_{Urd} = 50-70%) were similar to those induced by FUrd, BrUrd and IUrd. The hCNT2-mediated current induced by FdUrd was reduced compared to that induced by 2'dUrd (I_{analog}/I_{Urd} = 32.8% for 100 μM FdUrd vs 75.5% for 100 μM 2'dUrd); current was also induced by BrdUrd whereas IdUrd and EtdUrd had almost no effect. FdUrd, BrdUrd and IdUrd all induced moderate currents in hCNT3-producing oocytes. Lack of the 5'-hydroxyl group in 5-fluoro-5'dUrd compared to 5FUrd had no effect on current induction in either hCNT1- or hCNT3-producing oocytes, but resulted in dramatically decreased currents in hCNT2-producing oocytes. Thd and AZT induced large and moderate currents, respectively, for hCNT1 and hCNT3 but very small or no currents for hCNT2.

Discussion

The present work used an improved yeast expression system to characterize the Urd-binding motif of hCNT2. Among the three hCNT proteins, hCNT2 showed the lowest affinity for Urd and was most sensitive to modifications of its structure. The

regions of the sugar moiety most critical for interaction with hCNT2 were the C(3')- and C(5')-OH groups. Retention of these two hydroxyl groups was required for high-affinity interactions with hCNT2 since all modifications at C(3') and C(5') reduced the capacity of hCNT2 to bind Urd analogs. The critical region of the base moiety of Urd for binding was identified as N(3)-H. The loss of more than 10.5 and 6.7 kJ/mol in Gibbs free energy, respectively, when the 3'- or 5'-hydroxyl groups and the N(3)-H were removed or modified suggested that these groups were involved in hydrogen bonding with hCNT2. These findings were consistent with the predictions of a recent computer-based pharmacophore model for nucleoside-hCNT2 binding, which suggested that hydrogen-bonding was a dominant determinate of interaction between hCNT2 and nucleosides (14).

The C(2') and C(5) positions were important regions for hCNT2 binding. hCNT2 tolerated the removal of the 2'-hydroxyl group but not its inversion of configuration or substitution with an azido or an O-methyl group. Considerable steric interference and physical separation introduced by modifications evidently weakened permeant-transporter interactions. Weak interactions, probably through Van der Waals forces, existed between hCNT2 and the C(5) position of the base moiety. Addition of halogen, methyl or ethyl groups to the C(5) regions of Urd and 2'dUrd resulted in similar affinity losses, roughly corresponding to the volume size of the modifications.

Although the structural regions of Urd that were involved in binding to hCNT2 shared similarities with those of hCNT1 and hCNT3, distinguishable features of hCNT2-Urd interactions were observed. We established previously that the 3'-hydroxyl is the single most critical functional group of Urd for high-affinity binding by hCNT1 and hCNT3 (6); in this study we have found that both the 5'- and 3'-hydroxyl moieties were critical for hCNT2 binding. The C(2') and C(5) positions, which were relatively unimportant for hCNT1 or hCNT3 binding of Urd, were the second most important regions for hCNT2-Urd interactions. Multiple regions are required for direct or indirect hCNT2 interaction with Urd, suggesting that the amino acid residues composing the nucleoside-binding pocket of hCNT2 have limited selectivity for pyrimidine nucleosides.

Since the structural determinants of Urd that were identified by the inhibitor-sensitivity assay might not be equivalent to those required for physical translocation

across the membrane by the hCNT proteins, the two-voltage clamp assay was used to determine the regions of Urd that were important for hCNT transportability in the *X. laevis* oocyte expression system. The regions of Urd required for hCNT1-mediated transport were identified as C(5), N(3) and C(3'). The transportability of Urd analogs depended on both the structural region(s) and the nature of the modifications. Urd analogs with C(5) modifications, which were high-affinity inhibitors of hCNT1 (6), were also good permeants. Interestingly, a Urd analog with equal or even higher affinity than Urd did not necessarily produce higher currents than Urd. For example, hCNT1 exhibited significantly higher affinities for binding and transport of FUrd and FdUrd, since the apparent K_i and K_m values of FUrd and FdUrd were smaller than those of Urd (6,26), however, the currents induced by these two permeants were smaller than those induced by Urd. Methylation of N(3) reduced interactions with hCNT1 since the latter exhibited decreased affinity and greatly reduced transportability of 3MeUrd. C(2')-OH was not a determinant for hCNT1-Urd interactions since Urd analogs with modifications at this position were both good inhibitors (6) and permeants of hCNT1. The 5'-hydroxyl group, which was previously identified as a potential H-bond donor for high affinity hCNT1-Urd interactions (6), was not important for transport by hCNT1 because 5'dUrd and 5'CldUrd remained good permeants. However, 5'AzdUrd and 5'OMeUrd were not transported well by hCNT1, indicating that the 5' region of the sugar moiety contributes to permeant selectivity. Modifications at C(3') dramatically decreased the transportability of Urd analogs. hCNT1 was able to transport 3'dUrd and 2'3'ddUrd at very high concentrations but was unable to transport Urd analogs with bulkier C(3') substituents.

The transportability profile of hCNT2 corresponded well to its binding motif. Changes in almost all regions of Urd affected hCNT2 permeant selectivity. The most critical functional groups for binding to hCNT2 (i.e., the 3'- and 5'-hydroxyl groups) were also required for transportability. Almost any changes at the 3' or 5' positions, including removal of the hydroxyl group or inversion of configuration (at the 3' position), modification, or substitution, yielded Urd analogs that were poor permeants or not permeants at all. hCNT2 showed moderate affinity for 2'dUrd and also accepted 2'dUrd as a good permeant. Substitution of a variety of groups for the 2'-hydroxyl group yielded

Urd analogs with poor binding in hCNT2-producing yeast and poor transport in hCNT2-producing oocytes. The N(3) region of Urd was also a determinant of transportability. The small volume of the C(5) region was evidently needed for tight binding and efficient transport since substitution of H with bulkier groups resulted in a similarly large loss of both binding and transport.

The C(3'), C(5) and N(3) regions of Urd affected hCNT3 to different degrees. A potential hydrogen-bond interaction at C(3') of Urd was important for high-affinity binding and transport since removal or modification of the 3'-hydroxyl group significantly reduced analog binding and weakened transport. However, most poor inhibitors of hCNT3 protein appeared to be transported at high concentrations. The C(2') and C(5') regions of Urd, which were shown previously to be unimportant for Urd binding, were not important for transport since the C(2') and C(5') Urd analogs were also good permeants of hCNT3. Although modifications of C(5) and N(3) did not cause substantial changes in binding to hCNT3 (6), the corresponding Urd analogs were transported less well than either Urd or 2'dUrd, suggesting that these two regions were minor determinants for hCNT3 transportability.

The transportability of Urd analogs by hCNT1, hCNT2 and hCNT3 reflected well the results obtained in the inhibitor-sensitivity assays. Most, if not all, of the Urd analogs that inhibited hCNT1, 2, or 3-mediated Urd transport were also permeants. hCNT2, which showed the least tolerance for modifications of Urd in the inhibitor-sensitivity assay, also exhibited limited transport of Urd analogs in the sodium flux assay. In contrast, hCNT3, with the 3'-hydroxyl group being the only important structural determinant for binding, showed good tolerance to various modifications of Urd with respect to transportability.

In summary, an improved yeast expression system was developed and used to determine the Urd binding motif of hCNT2, after which Urd analogs were applied to evaluate the transportability profiles of inhibitors of hCNT1, hCNT2 and hCNT3 with the two-electrode voltage clamp assay in oocytes of *X. laevis*. The transporters displayed key differences in their ligand recognition and permeant selectivities, indicating differences in permeant binding and translocation sites. Although poor inhibitors, 3'dUrd, 2',3'ddUrd 3',5'ddUrd, araU, xyloU and AZT were permeants for hCNT1 and

hCNT3 at high concentrations, indicating the important roles of these transporters for delivery and distribution of nucleoside analogs. The results of this work may guide the rational design of nucleoside drugs for use in the treatment of human diseases.

Table 3-1 K_i and Gibbs free energy values for inhibition of hCNT2-mediated Urd uptake in *Saccharomyces cerevisiae* by Urd analogs

Urd compounds	IC_{50} (μM)	K_i (μM)	ΔG^0	$(\delta(\Delta G^0)$
Urd	29 ± 3	28 ± 3	23.8	0
Base modification				
5-fluorouridine (FUrd)	63 ± 13	61 ± 13	22.1	1.7
5-iodouridine (IUrd)	371 ± 51	358 ± 50	18.1	5.7
5-bromouridine (BrUrd)	238 ± 4	230 ± 4	19.1	4.7
5-methyluridine (MeUrd)	165 ± 0.3	160 ± 1	19.9	3.9
3-methyluridine (3MeUrd)	581 ± 151	562 ± 146	17.1	6.7
Sugar modification				
2'-deoxyuridine (2'dUrd)	76 ± 8	73 ± 8	21.7	2.1
5'-deoxyuridine (5'dUrd)	> 3000*	> 3000*	< 13.3	> 10.5
3'-deoxyuridine (3'dUrd)	> 3000$^+$	> 3000$^+$		
1-(β-D-arabinofuranosyl)uracil (araU)	> 3000*	> 3000*		
1-(β-D-xylofuranosyl)uracil (xyloU)	> 3000*	> 3000*		
2',5'-dideoxyuridine (2',5'ddUrd)	> 3000*	> 3000*		
3',5'-dideoxyuridine (3',5'ddUrd)	> 3000*	> 3000*		
2',3'-dideoxyuridine (2',3'ddUrd)	> 3000$^+$	> 3000$^+$		
2'-*O*-methyluridine (2'OMeUrd)	> 1000*	> 1000*	< 15.8	> 8.0
5'-*O*-methyluridine (5'OMeUrd)	> 3000*	> 3000*		
3'-*O*-methyluridine (3'OMeUrd)	> 3000*	> 3000*		
2'-azido-2'-deoxyuridine (2'AzdUrd)	> 3000$^+$	> 3000$^+$		
3'-azido-3'-deoxyuridine (3'AzdUrd)	> 3000*	> 3000*		
5'-azido-5'-deoxyuridine (5'AzdUrd)	> 3000*	> 3000*		
5'-chloro-5'-deoxyuridine (5'CldUrd)	> 1000*	> 1000*		
2',3'-*O*-isopropylideneuridine (iPUrd)	> 3000*	> 3000*		
Base & sugar modifications				
5-fluoro-2'-deoxyuridine (FdUrd)	156 ± 7	151 ± 7	20.0	3.8
5-bromo-2'-deoxyuridine (BrdUrd)	272 ± 75	263 ± 72	18.8	5.0
5-iodo-2'-deoxyuridine (IdUrd)	303 ± 20	293 ± 11	18.5	5.3
5-ethyl-2'-deoxyuridine (EtdUrd)	353 ± 40	341 ± 39	18.2	5.6
5-fluoro-5'-deoxyuridine	> 3000$^+$	> 3000$^+$		
Thymidine (Thd)	586 ± 20	566 ± 20	17.0	6.8
3'-azido-3'-deoxythymidine (AZT)	> 3000$^+$	> 3000$^+$		

* No obvious inhibition was observed.

+ Inhibition of less than 50% was observed.

The uptake of 1 μM [^{3}H]Urd into yeast (*fui1::HIS3*) expressing pYPhCNT2 was measured over 20 min in the presence of graded concentrations of non-radioactive Urd or Urd analogs. IC_{50} values (mean ± S.E., n = 3-4) were determined using Graphpad Prism Version 3.0 Software and were converted to K_i values (24) using K_m values (mean ± S.E., n = 3) of 29 ± 7 μM for recombinant hCNT2. Gibbs free energy (ΔG^0) was calculated from $\Delta G^0 = -RT\ln(K_i)$.

.

Table 3-2 The transportability of uridine analogs by hCNT1, hCNT2 and hCNT3 as measured by induction of sodium currents.

Uridine analogs	Concentration (μM)	I_{Analog}/I_{Urd} (% of value observed with 100 μM Urd)		
		hCNT1	hCNT2	hCNT3
Urd	100	100 ± 8.0	100 ± 9.2	100 ± 14.4
Base modifications				
IUrd	10	21.5 ± 2.6	1.2 ± 0.6	25.6 ± 1.2
IUrd	500	60.6 ± 3.1	12.4 ± 2.1	54.9 ± 3.4
MeUrd	100	66.6 ± 11.5	8.5 ± 0.7	55.5 ± 4.8
MeUrd	500	72.5 ± 5.7	24.9 ± 3.2	59.3 ± 8.8
FUrd	50	50.2 4.7	30.0 ± 4.0	45.6 ± 4.7
FUrd	100	66.3 ± 4.6	43.9 ± 3.0	44.2 ± 4.6
BrUrd	100	59.9 ± 5.6	4.3 ± 0.7	60.3 ± 6.9
BrUrd	500	61.6 ± 4.7	11.4 ± 1.6	71.8 ± 9.9
3MeUrd	100	0.5 ± 0.3	2.4 ± 0.6	4.6 ± 0.9
3MeUrd	500	3.8 ± 1.2	10.2 ± 0.2	48.4 ± 4.4
Sugar modifications				
2'dUrd	10	18 ± 3.6	16.8 ± 2.1	30.5 ± 2.5
2'dUrd	100	62.1 ± 9.0	75.5 ± 10.4	99.9 ± 7.8
5'dUrd	50	39.6 ± 6.3	1.0 ± 0.7	85.4 ± 3.5
5'dUrd	3000	218.9 ± 18.9	14.7 ± 2.1	150.9 ± 6.0
3'dUrd	500	39.6 ± 4.5	4.2 ± 2.0	75.4 ± 4.6
3'dUrd	3000	91 ± 9.9	30.4 ± 6.3	107.3 ± 6.4
araU	3000	4.5 ± 1.8	13.6 ± 1.5	52.1 ± 2.5
xyloU	3000	9.9 ± 1.8	0	62.3 ± 3.9
2',5'ddU	100	111.7 ± 7.2	3.1 ± 1.2	100.9 ± 4.6
2',5'ddU	3000	166.6 ± 12.6	46.2 ± 7.3	117.6 ± 14.6
3',5'ddU	3000	11.7 ± 2.7	0	29.8 ± 3.2
2',3'ddU	3000	54.9 ± 12.6	2.1 ± 1.0	87.8 ± 6.0
2'OMeUrd	100	23.4 ± 3.6	5.2 ± 1.2	33.6 ± 3.9
2'OMeUrd	1000	41.4 ± 5.4	29.4 ± 5.3	64.5 ± 5.7
5'OMeUrd	100	8.1 ± 2.7	0	63.0 ± 8.1
5'OMeUrd	3000	46.8 ± 5.4	0	79.0 ± 10.2
3'OMeUrd	3000	4.5 ± 1.8	0	12.0 ± 1.1
2'AzdUrd	50	28.8 ± 7.2	8.4 ± 2.0	75.8 ± 3.9
2'AzdUrd	3000	N.D.	39.9 ± 4.2	N.D.
3'AzdUrd	1000	0	N.D.	6.4 ± 1.4
3'AzdUrd	3000	3.6 ± 1.8	0	16.3 ± 2.5
5'AzdUrd	100	9.0 ± 2.7	N.D.	78.6 ± 4.3
5'AzdUrd	3000	N.D.	25.2 ± 3.1	N.D.
5'CldUrd	10	18.9 ± 1.8	0	29.0 ± 1.8
5'CldUrd	1000	149.5 ± 11.7	31.5 ± 8.4	147.7 ± 10.6
iPUrd	3000	0	0	2.5 ± 0.7
Base and sugar modifications				
FdUrd	10	22.2 ± 1.4	4.4 ± 0.5	31.8 ± 5.5
FdUrd	100	72.3 ± 5.0	32.8 ± 4.7	81.3 ± 18.8
BrdUrd	10	20.3 ± 2.4	2.1 ± 0.6	23.4 ± 3.2
BrdUrd	500	56.3 ± 9.0	32.6 ± 7.0	N.D.
IdUrd	100	72.1 ± 3.8	1.0 ± 0.3	54.9 ± 6.2
EtdUrd	50	51.4 ± 4.1	0.3 ± 0.3	51.5 ± 3.1
EtdUrd	500	113.5 ± 11.8	2.3 ± 0.1	70.6 ± 2.5
5-fluoro-5'dUrd	50	33.4 ± 0.8	0.0	37.7 ± 2.0
5-fluoro-5'dUrd	3000	N.D.	12.4 ± 2.1	N.D.
Thd	100	83.2 ± 2.8	4.1 ± 1.4	63.1 ± 10.6
AZT	100	19.2 ± 1.7	0.0	8.5 ± 1.3
AZT	1000	59.9 ± 6.5	0.0	28.1 ± 3.2

Oocytes producing hCNT1, 2 or 3 were voltage-clamped at -50 mV in a sodium-containing medium and currents were measured in the presence of Urd analogs at different concentrations (3-4 different oocytes per assay). The mean values of Urd analog-induced currents were normalized to the mean value of Urd-produced currents (100 μM of Urd) and summarized as I_{Analog}/I_{Urd}. None of the Urd analogs induced currents in water-injected control oocytes (data not shown). The expression vector was pGEM-T. N.D., not determined.

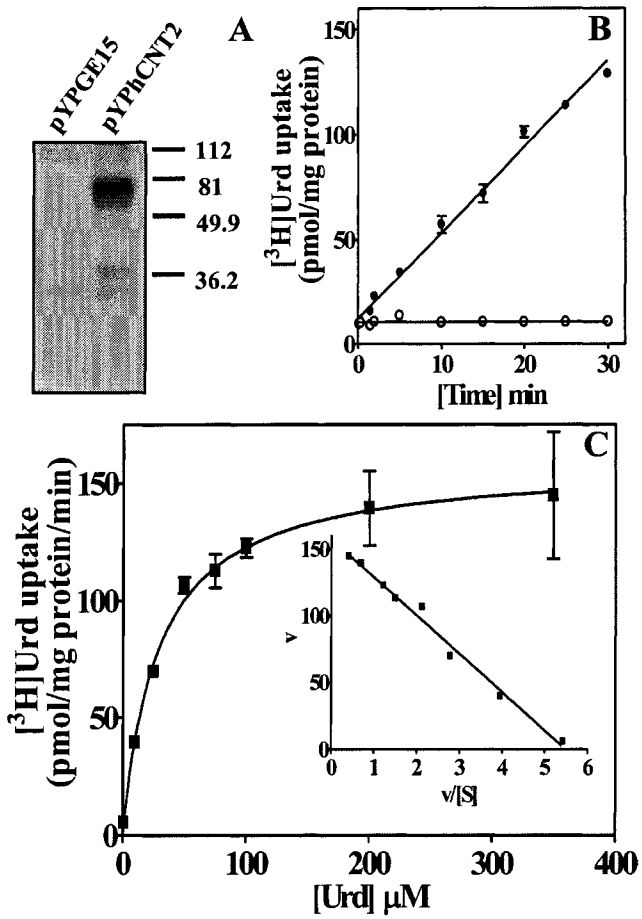

Figure 3-1 Immunoblotting detection and functional characterization of recombinant hCNT2 in yeast.

A. Immunoblotting. Yeast (*fui1::HIS3*) were transformed with either pYPGE15 or pYPhCNT2 to form new yeast strains named *fui1::HIS3* + pYPGE15 and *fui1::HIS3* + pYPhCNT2. Yeast membranes (20 μg protein) were subjected to immunoblotting with anti-hCNT2 monoclonal antibodies. **B. Time courses of [^{3}H]Urd uptake.** The uptake of 1 μM [^{3}H]Urd by yeast that were transformed with pYPhCNT2 was measured in CMM/GLU (pH 7.4) in the presence of 100 mM NaCl, either alone (close symbols) or with 10 mM non-radioactive Urd (open symbols). **C. Kinetic properties.** The mediated component of Urd transport (uptake rates of [^{3}H]Urd at a particular Urd concentration minus uptake rates at that concentration in the presence of 10 mM non-radioactive permeants) was plotted as a function of concentration and subsequently converted to *V versus V/S* plots (insets) to determine the kinetic constants for the hCNT2.

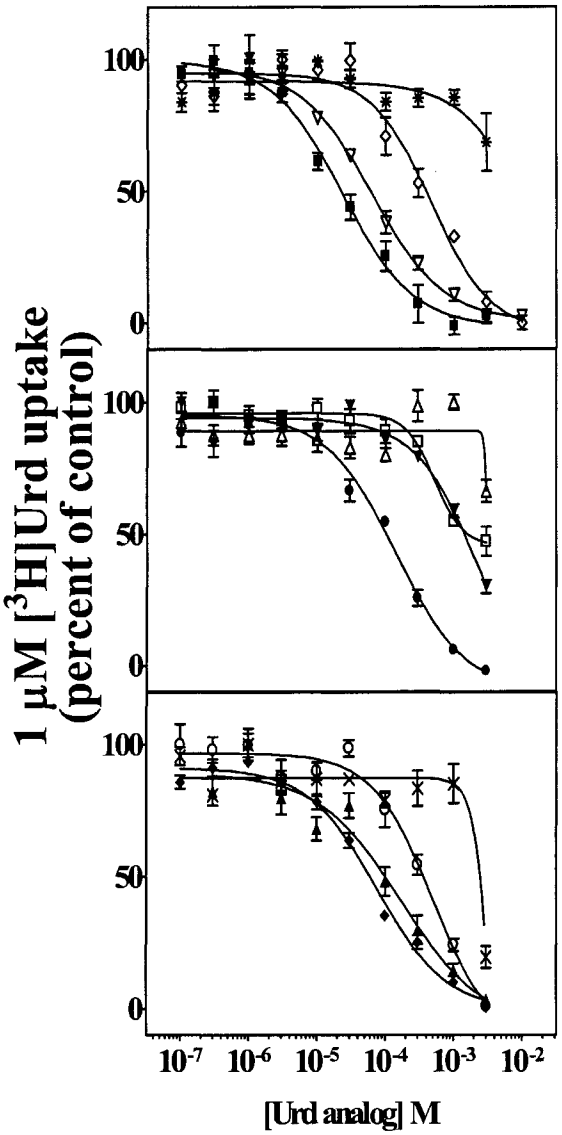

Figure 3-2 Inhibition of recombinant hCNT2-mediated Urd uptake by some Urd analogs.

The uptake of 1 μM [^{3}H]Urd into *fui1::HIS3* yeast producing hCNT2 was measured over 20 min in the presence of graded concentrations of test compounds. The test compounds were: Urd (■), 2'dUrd (▽), 3'dUrd (△), 5FUrd (◆), 3'AzdUrd (∗), FdUrd (●), EtdUrd (○), MeUrd (▲), IUrd (◇), 2'AzdUrd (□), 2'OMeUrd (+), and 5'CldUrd (▼). Uptake values in the presence of Urd compounds are given as the percentage of uptake values in their absence. Each data point represents the means ± S.E. of quadruplicate determinations; error bars are not shown where they are smaller than the symbol.

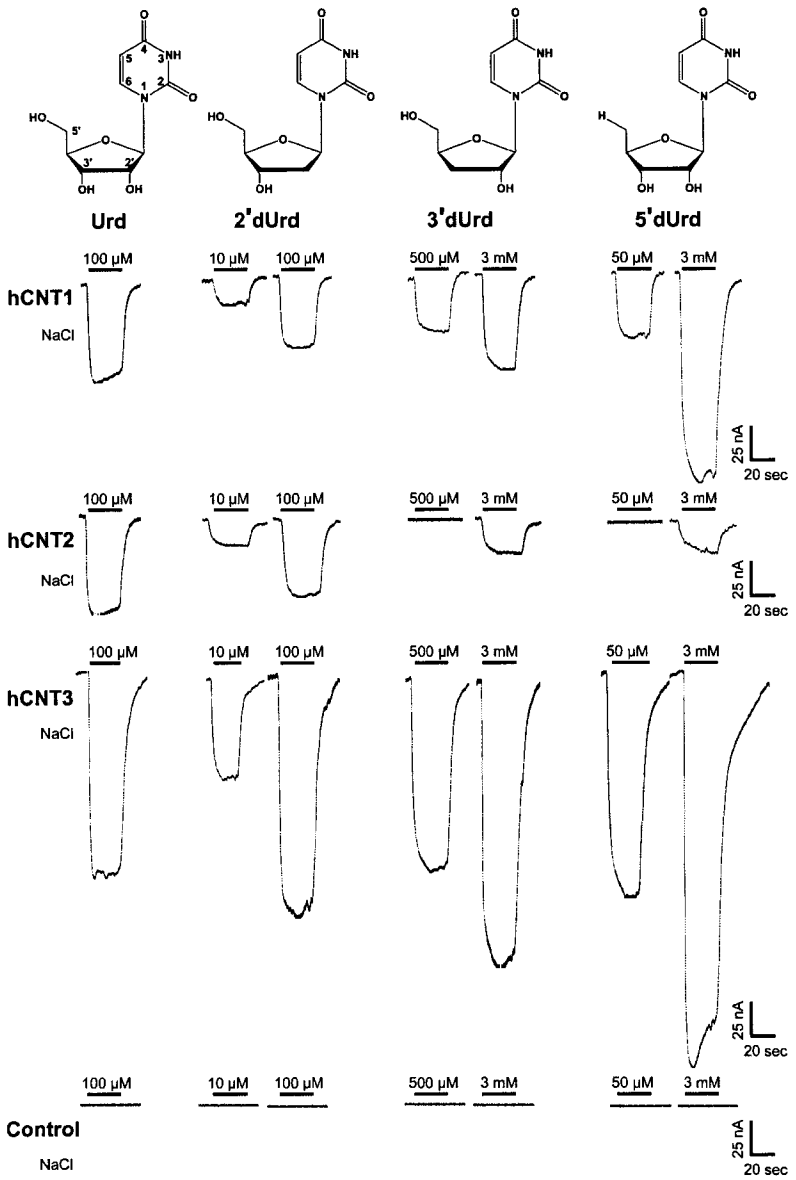

Figure 3-3 Representative sodium currents in the presence of Urd, 2'dUrd, 3'dUrd or 5'dUrd.

Oocytes were injected with 10 nl of water without (control) or with 10 ng of hCNT1, hCNT2 or hCNT3 transcripts. Current responses were generated by perfusing individual hCNT1, 2 or 3-producing oocytes with either Urd, 2'dUrd, 3'dUrd or 5'dUrd with the concentrations as indicated in a sodium-containing transport medium (top three panels). The same experiment was performed in a control water-injected oocyte (bottom panel).

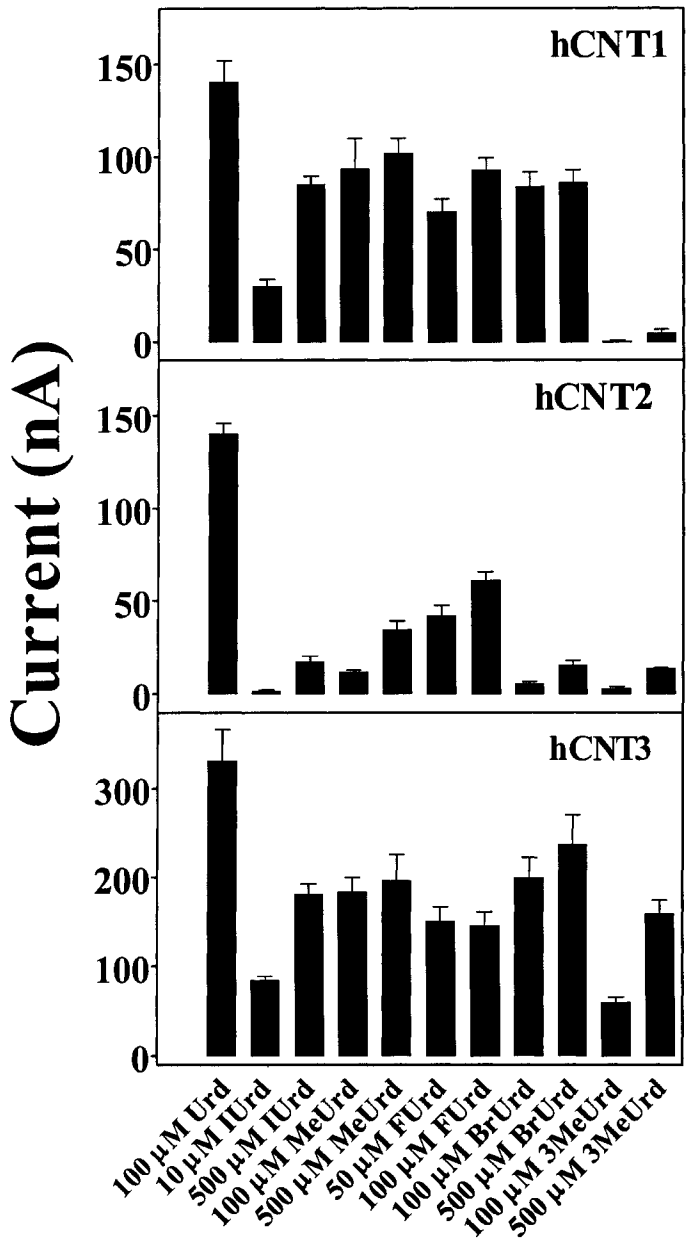

Figure 3-4 Transport of Urd and Urd analogs by hCNT1, hCNT2 and hCNT3.

Currents were generated by perfusing hCNT1, 2 or 3-producing oocytes with Urd or various Urd analogs with base modifications (concentrations as indicated) in a sodium-containing medium. Values are means ± S.E. for 3 different oocytes. The same experiment was also performed in control water-injected oocytes (data not shown); no inward currents were generated. The expression vector was pGEM-HE.

References

1. Cass, C. E., Young, J. D., Baldwin, S. A., Cabrita, M. A., Graham, K. A., Griffiths, M., Jennings, L. L., Mackey, J. R., Ng, A. M. L., Ritzel, M. W. L., Vickers, M. F., and Yao, S. Y. M. (1999) in *Membrane Transporters as Drug Targets* (Amidon, G. L., and Sadee, W., eds) Vol. 12, 1 Ed., pp. 313-352, 12 vols., Kluwer Academic/Plenum Publishers
2. Baldwin, S. A., Mackey, J. R., Cass, C. E., and Young, J. D. (1999) *Mol Med Today* **5**, 216-224
3. Ritzel, M. W., Yao, S. Y., Huang, M. Y., Elliott, J. F., Cass, C. E., and Young, J. D. (1997) *Am J Physiol* **272**, C707-714
4. Ritzel, M. W., Yao, S. Y., Ng, A. M., Mackey, J. R., Cass, C. E., and Young, J. D. (1998) *Mol Membr Biol* **15**, 203-211
5. Ritzel, M. W. L., Ng, A. M., Yao, S. Y. M., Graham, K., Loewen, S. K., Smith, K. M., Ritzel, R. G., Mowles, D. A., Carpenter, P., Chen, X., Karpinski, E., Hyde, R. J., Baldwin, S. A., Cass, C. E., and Young, J. D. (2001) *J Biol Chem* **276**, 2914-2927
6. Zhang, J., Visser, F., Vickers, M. F., Lang, T., Robins, M. J., Nielsen, L. P., Nowak, I., Baldwin, S. A., Young, J. D., and Cass, C. E. (2003) *Mol Pharmacol* **64**, 1512-1520
7. Ngo, L. Y., Patil, S. D., and Unadkat, J. D. (2001) *Am J Physiol Gastrointest Liver Physiol* **280**, G475-481.
8. del Santo, B., Tarafa, G., Felipe, A., Casado, F. J., and Pastor-Anglada, M. (2001) *J Hepatol* **34**, 873-880.
9. Li, J. Y., Boado, R. J., and Pardridge, W. M. (2001) *J Pharmacol Exp Ther* **299**, 735-740
10. Mackey, J. R., Mani, R. S., Selner, M., Mowles, D., Young, J. D., Belt, J. A., Crawford, C. R., and Cass, C. E. (1998) *Cancer Res* **58**, 4349-4357
11. Garcia-Manteiga, J., Molina-Arcas, M., Casado, F. J., Mazo, A., and Pastor-Anglada, M. (2003) *Clin Cancer Res* **9**, 5000-5008
12. Lang, T. T., Selner, M., Young, J. D., and Cass, C. E. (2001) *Mol Pharmacol* **60**, 1143-1152
13. Lang, T. T., Young, J. D., and Cass, C. E. (2004) *Mol Pharmacol* **65**, 925-933

14. Chang, C., Swaan, P. W., Ngo, L. Y., Lum, P. Y., Patil, S. D., and Unadkat, J. D. (2004) *Mol Pharmacol* **65**, 558-570
15. Patil, S. D., Ngo, L. Y., and Unadkat, J. D. (2000) *Cancer Chemother Pharmacol* **46**, 394-402
16. Vickers, M. F., Zhang, J., Visser, F., Tackaberry, T., Robins, M. J., Nielsen, L. P., Nowak, I., Baldwin, S. A., Young, J. D., and Cass, C. E. (2004) *Nucleosides Nucleotides Nucleic Acids* **23**, 361-373
17. Winzeler, E. A., Shoemaker, D. D., Astromoff, A., Liang, H., Anderson, K., Andre, B., Bangham, R., Benito, R., Boeke, J. D., Bussey, H., Chu, A. M., Connelly, C., Davis, K., Dietrich, F., Dow, S. W., El Bakkoury, M., Foury, F., Friend, S. H., Gentalen, E., Giaever, G., Hegemann, J. H., Jones, T., Laub, M., Liao, H., Davis, R. W., and et al. (1999) *Science* **285**, 901-906
18. Brunelli, J. P., Pall, M.L. (1993) *Yeast* **9**, 1309-1318
19. Ito, H., Fukuda, Y., Murata, K., and Kimura, A. (1983) *J Bacteriol* **153**, 163-168
20. Vickers, M. F., Yao, S. Y., Baldwin, S. A., Young, J. D., and Cass, C. E. (2000) *J Biol Chem* **275**, 25931-25938.
21. Vickers, M. F., Mani, R. S., Sundaram, M., Hogue, D. L., Young, J. D., Baldwin, S. A., and Cass, C. E. (1999) *Biochem J* **339**, 21-32
22. Jennings, L. L., Hao, C., Cabrita, M. A., Vickers, M. F., Baldwin, S. A., Young, J. D., and Cass, C. E. (2001) *Neuropharmacology* **40**, 722-731
23. Vickers, M. F., Kumar, R., Visser, F., Zhang, J., Charania, J., Raborn, R. T., Baldwin, S. A., Young, J. D., and Cass, C. E. (2002) *Biochem Cell Biol* **80**, 639-644
24. Cheng, Y., and Prusoff, W. H. (1973) *Biochem Pharmacol* **22**, 3099-3108
25. de Koning, H. P., and Jarvis, S. M. (2001) *Acta Trop* **80**, 245-250.
26. Smith, K. M., Ng, A. M., Yao, S. Y., Labedz, K. A., Knaus, E. E., Wiebe, L. I., Cass, C. E., Baldwin, S. A., Chen, X. Z., Karpinski, E., and Young, J. D. (2004) *J Physiol* **558**, 807-823
27. Visser, F., Zhang, J., Raborn, R. T., Baldwin, S. A., Young, J. D., and Cass, C. E. (2005) *Mol Pharmacol* **67**, 1291-1298

Chapter 4 Cysteine Accessibility Analysis of Transmembrane Domains 11, 12 and 13 of Human Concentrative Nucleoside Transporter

Acknowledgements

Ms. Tracey Tackaberry and Mr. Taylor Raborn constructed part of the mutants and conducted part of the yeast transport assays. Mrs. Mabel W. L. Ritzel gave some technical support. Ms. Gerry Barron helped with part of the confocal microscopy experiments. Drs. Stephen Baldwin and James Young are collaborative principle investigators who helped obtained research funding for this project and aided in manuscript preparation.

Introduction

Nucleosides are central metabolites in all life forms and as precursors of nucleotides, play an essential role in intermediary metabolism, biosynthesis of macromolecules and cell signaling through interaction with purinergic receptors. Since most nucleosides are hydrophilic molecules and do not cross cell membranes readily by diffusion, their cellular uptake is dependent on the activity of specialized membrane transporter proteins. Two distinct nucleoside transporter families, the equilibrative nucleoside transporters (ENTs) and the concentrative nucleoside transporters (CNTs) have been identified by molecular cloning and functional expression of cDNAs encoding transporter proteins from a variety of species, including mammals, protozoan parasites and bacteria. In humans (h), hENT1 and 2 mediate facilitated diffusion of nucleosides down their concentration gradients whereas hCNT1, 2 and 3 couple uphill nucleoside transport to downhill sodium transport and, in the case of hCNT3, also to downhill proton transport. hENT1 and 2 are functionally distinguished by different sensitivities (hENT1 >> hENT2) to nitrobenzylmercaptopurine ribonucleoside (NBMPR) and have therefore been assigned the functional designations equilibrative sensitive (*es*) and equilibrative insensitive (*ei*), respectively (1,2). hENT3, which is proton-dependent and like hENT1, broadly selective, is believed to be a transporter of intracellular membranes (3-5). hENT4, which mediates equilibrative transport of adenosine (3,6), also transports monoamine neurotransmitters (7). Three major CNT subtypes differ functionally with respect to their permeant selectivities. In humans as in other mammals, hCNT1 prefers pyrimidine nucleosides but also transports adenosine, whereas hCNT2, which is 72% identical to hCNT1, prefers purine nucleosides but also transports uridine (8,9). hCNT3, which is 48% identical to either hCNT1 or hCNT2, transports both pyrimidine and purine nucleosides (10). The ENTs appear to be expressed ubiquitously in human cells. In contrast, the CNTs are found primarily in specialized cell types (9-13), suggesting an important role in absorption, secretion, distribution and elimination of nucleoside and nucleoside analog drugs.

Interest in nucleoside transporters has increased because of their potential and proven therapeutic applications in cancer and stroke as well as cardiovascular, parasitic

and viral diseases. Nucleoside transporter proteins are critical in controlling extracellular concentrations of adenosine, a physiological ligand for purinergic receptors involved in coronary vasodilation, neuromodulation and platelet aggregation (14,15). The presence of nucleoside transporters in plasma membranes is required for effective cellular uptake of many anti-cancer nucleoside drugs (e.g., gemcitabine, capecitabine and fludarabine) and is linked mechanistically with drug sensitivities and toxicities (16-18). Data from an oligonucleotide array study revealed that expression of mRNA encoding hENTs and hCNTs positively correlated with chemosensitivity to nucleoside anti-cancer drugs (19). For example, a positive correlation existed between the expression level of hCNT3 mRNA and cytotoxicity of cytorabine and gemcitabine.

While considerable progress has been made in elucidating the structural basis of ENT proteins (20-24), studies on the structurally and functionally important residues of the CNT family are still at an early stage. Mammalian CNT proteins (~650 amino acid residues) of human, mouse, rat, rabbit and pig share high amino acid sequence identities (> 50%). The presence of 13 transmembrane domains (TMs) in mammalian CNTs predicted from sequence alignment has been experimentally verified using glycosylation-scanning mutagenesis (25). However, the three-dimensional packing of the TMs is still largely unknown, as are the molecular mechanisms by which CNTs bind and translocate their permeants. The first three TMs of mammalian CNTs, which are absent from prokaryote CNTs, are not essential for transport since both rat CNT1 (rCNT1) and hCNT1 that lack TMs 1-3 retained wild-type transporter properties (25). TMs 7-9 are thought to form part of the substrate translocation pore for CNT proteins and four critical residues (S319, Q320, S353 and L354) in this region of hCNT1 determine permeant selectivities (26,27). Furthermore, conserved residues F316 (putative TM 7) and G476 (putative TM 11) were identified as determinants for guanosine sensitivity and membrane expression of hCNT1, respectively (28). Chimeric proteins comprised of hCNT3 (TMs 1-6) and hCNT1 (TMs 7-13) and of hfCNT (TM 1-6) and hCNT1 (TM 7-13) produced in *X. laevis* oocytes exhibited hCNT1-like cation interactions as well as hCNT1-like permeant selectivities (29,30), establishing that the structural determinants of cation stoichiometry and binding affinity are located within the C-terminal half of the protein. The loss of proton-dependence of the hCNT3-hCNT1 chimera indicated that the proton-

binding site resides in the C-terminal half of the protein (29). Studies of transporters and their interactions with uridine analogs showed that the three hCNTs exhibit distinct permeant selectivities and nucleoside-binding motifs (31,32).

Several of the 13 putative TMs possess the potential to form amphipathic α-helices, which led to the hypothesis that these helices cluster together in the membrane to form the walls of a water-filled tunnel through which nucleosides translocate. It was further suggested that the hydroxyl- and amide-containing amino acid side chains within these helices form the nucleoside-binding pocket of hCNT3 via the formation of hydrogen bonds with the hydroxyl groups of nucleosides (31). In the present study, we used the substituted-cysteine accessibility method (SCAM) in conjunction with three sulfhydryl-specific methanethiosulfonate (MTS) reagents to systematically address the roles of TMs 11, 12 and 13 in the formation of the nucleoside translocation pathway. A fully functional cysteine-less hCNT3 mutant was constructed by substitution of the endogenous cysteine residues with serine. The single-cysteine mutants were constructed using cysteine-less hCNT3 as the starting point, and their expression patterns, transport activities, and sensitivities to MTS reagents were determined in *S. cerevisiae*. Our results suggest that portions of TMs 11 and 12 face the water-accessible uridine permeation pathway.

Experimental Procedures

Strains and Media

fui1::TRP1 (MATα, gal, ura3-52, trp1, lys2, ade2, hisd2000, *and Δfui1::TRP1*), which contains a disruption in the gene encoding the endogenous uridine permease (FUI1) (33), was the parental yeast strain used to produce the recombinant human nucleoside transporters (31,34). Other strains were generated by transformation of the yeast-*Escherichia coli* shuttle vector pYPGE15 (containing the constitutive PGK promoter) (35) into *fui1::TRP1* with a standard lithium acetate method (36). Yeast strains were maintained in complete minimal medium (CMM) containing 0.67% yeast nitrogen base (Difco, Detroit MI), amino acids (as required to maintain auxotrophic

selection), and 2% glucose (CMM/GLU). Agar plates contained CMM with various supplements and 2% agar (Difco, Detroit, MI). Plasmids were propagated in *E. coli* strain DH5α (Invitrogen, Carlsbad, CA) and maintained in Luria broth with 100 μg/ml ampicillin.

Construction of cysteine-scanning mutants

The hCNT3 open reading frame (GenBank™ accession number AF305210) was subcloned into the yeast expression vector pYPGE15 to generate pYPhCNT3 as previously described (31). pYPhCNT3 served as the template to generate plasmid containing cDNAs encoding cysteine-less hCNT3 (pYPhCNT3-cysteine-less) and the pYPhCNT3-cysteine-less served as the template to generate single cysteine mutants using the QuickChange Site-directed Mutagenesis Kit (Stratagene, La Jolla, CA) according to the manufacturer's instructions. The sequences of all the constructs were confirmed by DNA sequencing using an ABI PRISM 310 sequence detection system (PerkinElmer Life and Analytical Sciences, Boston, MA).

Immunofluorescence and confocal microscopy of yeast

Logarithmically growing yeast (10 OD units, A_{600} = 0.7-1.0) were fixed using 3.7% formaldehyde for 30 min with occasional mixing, after which cells were centrifuged (5 min, 3,000 × g) and washed with 4 ml of double distilled H_2O. The resulting pellets were resuspended in 1 ml of 700 μg /ml Zymolyase-100 T (MP Biomedicals, Irvine, CA) in solution B (1.2 M sorbitol, 100 mM potassium phosphate, pH 7.5) for 30-40 min at 30 °C. The yeast suspensions (300 μl) were applied onto poly L-lysine coated coverslips, permeabilized using chilled 1:1 acetone/methanol and incubated first with blocking buffer [2% goat serum in PBS (phosphate-buffered saline, pH 7.2)] for 30 min and then with anti-hCNT3 monoclonal antibodies (37) in PBST (PBS with 1 % Triton X-100) for 30 min. After extensive washing with PBST, the yeast were stained with the secondary antibodies [Alexa Fluor 488 goat-anti mouse IgG (1:250 dilution in PBS, Molecular Probes, ON)] for 30 min, followed by extensive washing with PBS. The coverslips were mounted and dried overnight. Confocal images were collected using a Zeiss LSM510 confocal laser scanning microscope with a 60 X 1.4

objective (F-Fluar) using a frame size of 512 × 512 pixels with a pixel resolution of 0.08 μM and a pixel depth of 8 bits.

Transport assay in S. cerevisiae

Yeast cells producing recombinant hCNT3 mutant proteins were grown in CMM/GLU medium to A_{600} of 0.7-1.2, washed twice in sodium-containing transport buffer (5 mM D-glucose, 20 mM Tris-HCl, 3 mM K_2HPO_4, 1 mM $MgCl_2$, 2 mM $CaCl_2$, and 130 mM NaCl, pH 7.4) and resuspended to A_{600} = 4.0 in sodium-containing transport buffer, pH 7.4. All transport assays were performed at room temperature and pH 7.4 using a cell-harvester based method as described previously (31,38). Transport reactions were initiated by rapid mixing of 50 μl of yeast suspension with 50 μl of sodium-containing buffer, pH 7.4, containing 2X [^{3}H]nucleoside in each of the individual wells of 96-well microtiter plates. Nucleoside uptake into yeast cells producing recombinant hCNT3 mutants was linear for up to 10-15 min and kinetic studies were therefore performed using rates obtained from 5-min exposures to ^{3}H-labeled nucleosides. At the end of 5-min incubations, the yeast cells were collected on glass-fiber filtermats (Skatron Instruments, Lier, Norway) using the semi-automated cell harvester (Micro96 HARVESTER; Skatron Instruments, Lier, Norway) with continuous washing with demineralized water. The individual filter portions, which corresponded to individual wells of the microtiter plates were excised and transferred to scintillation vials for liquid scintillation counting. Uptake rates are presented as pmol/mg of yeast protein. The quantification of yeast protein was determined using a Bio-Rad protein assay kit (Bio-Rad, Hercules, CA). K_m and V_{max} values for transport of nucleosides by yeast producing cysteine-less hCNT3 or single cysteine-mutant were calculated through rate vs concentration plots using PRISM GraphPad version 3.0 software (GraphPad Software Inc., San Diego, CA). Statistical significance of the reported data sets was evaluated using t-tests.

MTS modification experiments

Yeast containing pYPhCNT3-cysteine-less or one of the single-cysteine mutant plasmids were grown in CMM to A_{600} of 0.7 to 1.2, washed twice in sodium-containing

transport buffer, pH 7.4, and resuspended to A_{600} of 2.2. All MTS reagents were dissolved in ice-cold ddH_2O and kept on ice until use. Portions (0.9 ml) of the yeast suspension were distributed to microcentrifuge tubes to which had been added 100 µl of 25 mM MTSEA (MTS-ethylammonium), 100 mM MTSES (MTS-ethylsulfonate) or 10 mM MTSET (MTS-ethyltrimethylammonium) (Toronto Research Chemicals, Toronto, ON, Canada) alone or together with 100 mM uridine as protection permeant. After a 5-min incubation period, the cells were centrifuged and washed three times with ice-cold PBS to remove unreacted MTS reagent and uridine. The cells were resuspended to A_{600} of 4.0 in sodium-containing transport buffer, pH 7.4, and distributed to 96-well microtiter plates for uridine transport assays. For each individual mutant, the accessibility to MTS reagents was normalized by computing the percentages of uridine uptake in the presence of the MTS relative to that in its absence.

Results

Generation and characterization of cysteine-less hCNT3

Most endogenous cysteine residues are clustered in the carboxyl part of hCNT3 (Fig 1). To test the role of endogenous cysteine residues in hCNT3, 14 mutants in which a single cysteine residues changed to serine were constructed and the kinetic properties of uridine and adenosine transport were compared with those of wild-type hCNT3 (data not shown). No obvious differences were observed between the mutants and wild type hCNT3, indicating that none of the individual endogenous cysteine residues was important for function of activity of hCNT3. Therefore, a cysteine-less hCNT3 mutant, in which all 14 endogenous cysteine residues were replaced with serine residues were generated by site-directed mutagenesis. The resulting cysteine-less hCNT3 protein was produced in yeast and characterized for its ability to transport several naturally occurring nucleosides (uridine, cytidine, adenosine, inosine) and nucleoside analogs (gemcitabine and clofarabine). Compared with wild type hCNT3, the cysteine-less transporter exhibited similar affinities and a four-fold increase in transport activities (Table 1). The

global increase in V_{max} values for various nucleosides may have been due to increased production of cysteine-less hCNT3 in yeast cells.

Indirect immunostaining was used to compare the localization of hCNT3 and cysteine-less hCNT3 proteins in yeast. As shown in Fig. 4-2, yeast producing recombinant cysteine-less hCNT3 exhibited staining patterns similar to those of wild-type hCNT3, in which staining was predominantly localized to the plasma membrane. No significant fluorescence was observed for yeast transformed with the insert-free vector (pYPGE15) or for yeast producing recombinant hCNT3 or cysteine-less hCNT3 that were treated with either IgM isotype antibodies or secondary antibodies only (data not shown).

Recombinant hCNT3 produced in *X. laevis* oocytes exhibits a sodium/nucleoside coupling ratio of 2:1 (10). Using a radioisotope assay, the sodium-dependence of uridine influx mediated by recombinant hCNT3 was compared to that of cysteine-less hCNT3 produced in yeast. When uridine uptake was measured as a function of sodium concentration, K_{50} values for sodium activation of 4.5 ± 0.6 mM was observed cysteine-less hCNT3. Fitting the data to the Hill equation, $v = V_{max} \cdot [Na^+]/(K_{50}^n + [Na^+]^n)$, gave Hill coefficients (n) of 2.1 ± 0.2 (wild-type hCNT3) and 2.0 ± 0.1 (cysteine-less hCNT3), indicating that a sodium/nucleoside coupling ratio of 2:1 remained unchanged for cysteine-less hCNT3. These results demonstrated that the cysteine-less transporter, which maintained wild-type properties, is an appropriate substituent of hCNT3 for SCAM studies.

Functional expression of single-cysteine mutants in yeast

The cysteine-less hCNT3 was used as the template to construct 63 site-directed mutants in which single-cysteine mutations were systematically introduced at positions 479-499, 554-574 and 592-612, encompassing all of predicted TMs 11, 12 and 13 of hCNT3. The kinetic properties of each single-cysteine mutant were assessed by measurements of the concentration dependence of transport of [^{3}H]uridine and [^{3}H]adenosine (Table 2-4). Although the V_{max} values varied, most of the cysteine-substituted mutants were functional, exhibiting micromolar K_m values for uridine and adenosine similar to those of wild-type and cysteine-less hCNT3 (Table 2-4). Among the

functional mutants, only three, A564C, I571C and F603C exhibited large increases in K_m values for uridine and adenosine relative to those of cysteine-less hCNT3. I608C displayed higher affinity and capacity for uridine than for adenosine: K_m values, respectively, of 6.0 ± 1.2 and 18 ± 3.2 μM; V_{max} values, respectively, of 1250 ± 90 and 250 ± 50 pmol/mg/min. Six mutants (I485C, S568C, R593C, L595C, F603C and G610C) showed very low transport capacity with V_{max} values ≤ 200 pmol/mg/min for both uridine and adenosine. While the activities of these mutants were low, they were high enough above background to measure the effects of MTS reagents and thus were included in subsequent analyses. However, no significant transport activity was detected for six other mutants (M496C, G498C, F563C, A594C, G598C and A606C). Multiple sequence alignments across the mammalian CNT family (Fig. 4-3) revealed that most of the mutants that exhibited compromised transport affinity and/or capacity were highly conserved residues, indicating that these residues are structurally and/or functionally important for hCNT3 transport activity. Substitution of M496, G498, F563 and G598 with alanine resulted in two functional mutants. M496A exhibited K_m values of 2.7 ± 0.3 and 3.1 ± 0.6 μM and V_{max} values of 950 ± 30 and 990 ± 50 pmol/mg protein/min for uridine and adenosine, respectively, and G598A exhibited K_m values of 3.1 ± 0.6 and 2.7 ± 0.6 μM and V_{max} values of 320 ± 30 and 300 ± 50 pmol/mg/min for uridine and adenosine, respectively. However, mutants G498A and F563A remained nonfunctional, indicating that something other than the hydrophobic property of glycine or phenylalanine may be required at these positions.

Expression of the single-cysteine mutants in yeast was assessed visually by indirect immunofluorescence laser confocal microscopy using monoclonal anti-hCNT3 antibodies (Fig. 4-2). All recombinant single-cysteine hCNT3 mutants except G498C and L595C exhibited staining patterns similar to those of wild type and cysteine-less hCNT3, in which staining was predominantly localized to the plasma membrane (Fig. 4-2). Strong intracellular staining was observed in yeast producing G498C and weak staining was observed in yeast producing L595C, results that were consistent with the absence of detectable transport for mutant G498C and extremely low transport activity for mutant L595C (Table 2 and 4). The lack of nucleoside transport activity observed in other substitution mutants was not the result of reduced protein expression since strong

plasma membrane staining was observed for yeast that produced either of these mutants. No significant fluorescent signal was observed for yeast transformed with the insert-free vector (pYPGE15) or yeast producing recombinant hCNT3 that were treated with either IgM isotype antibodies or secondary antibodies only (data not shown).

SCAM of TMs 11, 12 and 13

The function of cysteine-less hCNT3 was not affected by the sulfhydryl-specific reagents, *p*-chloromercuribenzenesulfonate (data not shown) and MTS reagents (Fig. 4-4). The goal of SCAM was to determine if any portions of TMs 11, 12 and 13 contribute to the structure of the water-filled pore through which the permeant (uridine) is translocated into the cell. Three MTS reagents (MTSEA, MTSES and MTSET) with different sizes, charges and membrane permeabilities were used. Any time a cysteine residue has replaced an amino acid residue that is normally exposed to aqueous pore, MTSES, MTSET or MTESA should have access to the cysteine thiol group, resulting in formation of cysteine-MTS adduct, thus blocking permeant translocation.

Fig. 4-4 presents the normalized uridine transport activities of 57 single-cysteine mutants after treatment with either 2.5 mM MTSEA, 10 mM MTSES or 1 mM MTSET (100% was set as the activity of individual mutants without being incubated with MTS reagents). In every series of SCAM experiments, the cysteine-less hCNT3 served as a negative control and displayed no sensitivity towards the MTS reagents. Most of the mutants in TM 11 and TM 12 and all mutants of TM 13 were not affected by the MTS reagents, suggesting that either modification of these cysteine residues did not affect uridine translocation or, most likely, these residues were not accessible to MTS reagents. The uridine transport activities of single-cysteine mutants L480C, S487C in TM 11 and T557C in TM 12 were markedly reduced (<60% of control values) by all three reagents, indicating that these residues were accessible to hydrophilic reagents and probably faced the permeant translocation channel. Although positively charged, MTSEA is small and can cross plasma membranes by diffusion and react with cysteine side chains from both the extracellular and cytoplasmic side of the membrane (39). The transport activities of N565C, G567C and I571C in TM 12 were inhibited only by MTSEA (< 60% of control values) but not by MTSES and MTSET, which are membrane-impermeable and have

larger sizes than MTSEA. Several mutants (E483C, L484C and C486C in TM 11, I555C in TM 12 and R593C in TM 13) showed higher uridine transportability when treated with MTS reagents; the reason for the increased activities is not known.

Uridine protection of MTS modifications

To test the hypothesis that the mutants that showed high sensitivity to modifications by the MTS reagents were exposed to the aqueous translocation pore, permeant protection analysis was undertaken. It is assumed that occupying the translocation pathway with permeant before and during exposure to MTS reagents blocks access of the reagents to the pore-lining cysteine residues, thus protecting the residues from sulfhydryl modifications. Uridine at high concentration (10 mM) protected all six of the MTS-sensitive mutants from inhibition by MTS modification, although the extent of protection varied among mutants and MTS reagent applied (Fig. 4-5). These results provided evidence that L480, S487, T557, N565, G567 and I571 in TMs 11 and 12 formed part of the nucleoside permeation pathway. For MTSEA, application of 10 mM uridine completely protected N565C from inhibition whereas the other mutants were partially protected. For MTSES, uridine completly protected T557C but only partially protected L480C and S487C. For MTSET, L480C and T557C were completely protected by 10 mM uridine whereas S487C was only partially protected.

Discussion

The role of putative TMs 11, 12 and 13 in the current topology model of hCNT3 (Fig. 4-1) was investigated using cysteine-scanning mutagenesis in conjunction with the sulfhydryl-specific reagents, MTS. Sixty-three single-cysteine hCNT3 mutants were created from fully functional, cysteine-less hCNT3 by individually changing each residue along TMs 11, 12 and 13 to a cysteine. Immunofluorescence staining and transport assays were used to assess the membrane abundance, kinetic properties and sensitivities of the mutant proteins to MTS modifications. Cysteine substitutions at M496, G498, F563, A594, G598 and A606 abolished uridine and adenosine transport activities and substitutions at I485, A564, I571, R593, L595, F603, I608 and G610 resulted in

markedly decreased V_{max} values and/or increased K_m values, whereas substitutions at other positions resulted in either little or no effect on transport properties. Most of the residues, the mutation of which resulted in large functional changes are highly conserved across the CNT family (Fig. 4-2), consistent with their importance in transporter structure and/or function.

Immunostaining demonstrated that nonfunctional single-cysteine mutants, except G498C, were produced and localized to cell surfaces at levels similar to those of wild type and cysteine-less hCNT3, indicating that the impaired transport activity of the mutants was not due to defective trafficking. Cysteine substitution might have caused changes in transporter folding that resulted in compromised transportability. Future studies using a screen for second site suppressor residue(s) could be used to further assess the potential roles of these residues in protein processing. The decreased transport capacities of mutant L595C may have been due to its low abundance in yeast. Mutant G498C was detected mainly in intracellular regions, consistent with the observation that the GFP-tagged corresponding mutants of hCNT1 (G476A-GFP and G476L-GFP) were nonfunctional and could not be detected on plasma membranes in undifferentiated or differentiated Madin-Darby canine kidney cells (28). No transport activity was detected when G498 or F563 was converted to hydrophilic, small side chain residue alanine, suggesting that these two residues are essential and can not be substituted.

To determine the structural locations of the residues identified in this study, helical wheel projections of TMs 11, 12 and 13 were generated (Fig. 4-6). Both TM 11 and TM 12 are moderately amphipathic, suggesting that these two domains could line the permeant translocation pore. All of the MTS-accessible residues (L480, S487, T557, N565, G567 and I571) except G567 are highly conserved across the CNT family. Although the extent of uridine protection varied among the mutants and with different MTS reagents, all six MTS-sensitive residues were protected by uridine, supplying further evidence that these residues face the pore-lining pathway. Generally, uridine protection was higher for modifications by MTSES and MTSET than by MTSEA, probably because MTSEA was able to diffuse across the plasma membrane, affecting uridine binding from both sides of the membrane. S487C and L480C were accessible to three MTS reagents and are located close to each other on the hydrophilic face of TM 11

(Fig. 4-6). Residues M496 and I485, which were sensitive to cysteine substitution, are buried on the hydrophilic face of TM 11, suggesting that these two residues might be involved in stabilizing the structure of the transporter. Only two residues of TM 11 were MTS sensitive, suggesting that TM 11 is partially buried in the lipid membrane and contributes only a small portion of the nucleoside translocation pathway. TM 11 also contains a proline residue, which could induce a kink in its structure bringing residues M496 and I485 close to the water-filling pore. It is possible that TM 11 has a high degree of conformational flexibility and is involved in helical movements during the transport cycle, allowing the pore-lining side of the α-helix to be solvent accessible during nucleoside flux.

Four MTS-sensitive residues and most of the cysteine substitution-sensitive residues in TM 12 are clustered close to each other on the hydrophilic face of the putative TM segment (Fig. 4-6), suggesting that TM 12 forms part of the nucleoside translocation pore. I571 is the second residue of a highly conserved GXXXG helix-helix interaction motif involving G570 and G574. Given the accessibility of MTSEA to residue I571C and the effect of I571C on permeant binding affinity changes (20-fold decrease in affinities for both uridine and adenosine compared to cysteine-less hCNT3), I571 might be a pore-lining residue that is also involved in permeant interactions. It could also play a role in stabilizing the helix-helix packing interface involving G570 and G574. G567C, N565C and I571C mutants were only sensitive to the membrane-permeable sulfhydryl reagent MTSEA, indicating that these residues may be accessible from the cytoplasmic side of the membrane, providing evidence in support of the predicted orientation of TM 12 in the current putative topology model of hCNT3 in which these three residues are located in the cytoplasmic side of the plasma membrane (Fig. 4-1).

Putative TM 13 mainly contained hydrophobic residues and displayed no accessibility to any MTS reagents, suggesting that it is not in the permeabilization pathway. However, several of the cysteine substitution mutants in TM 13 displayed altered kinetic properties for nucleoside transport. Mutation of the highly conserved hydrophobic residues in TM 13 to hydrophilic cysteine residues was poorly tolerated. It is possible that these mutations created a conformational distortion that resulted in a nonfunctional transporter. TM 13 might be one of the outer helices that surround the

inner helical bundle that comprises the aqueous permeant-binding cavity. The compromised transportability observed in nearly half of the TM 13 mutants suggests an important structural role for this TM segment and the possibility that some of these unsubstitutable residues serve as direct determinants for permeant interactions cannot be excluded. The differential binding affinities and transport capacities that mutant I608C displayed for uridine and adenosine suggest a possible role of TM 13 in the recognition of pyrimidine and purine nucleosides.

Knowing the structure and mechanism of a transporter protein is crucial for understanding its biological function and designing drugs to interact with it. The lack of a crystal structure for any CNT family member is an impediment to interpreting the significance of the residues with functional roles within the TM regions. Although labor intensive, SCAM is a powerful tool in the elucidation and estimation of the tertiary structures of various membrane proteins. Mutagenesis approaches have identified several highly conserved residues that may be potential determinants for permeant interaction and/or structural stability and are worth further investigation. Direct evidence from SCAM studies suggested that part of the hydrophilic faces of TM 11 and TM 12 contribute to the nucleoside translocation pathway and TM 13 is not involved in permeation but may play crucial role in maintaining proper protein functions. Extension of the current study to the remaining TM segments will provide further insight into the mechanism and structure of concentrative nucleoside transporters.

Table 4-1 Kinetic properties of wild-type and cysteine-less hCNT3 produced in *S. cerevisiae*

	hCNT3		cysteine-less hCNT3	
	K_m (μM)	V_{max} (pmol/mg/min)	K_m (μM)	V_{max} (pmol/mg/min)
Uridine	1.7 ± 0.3	1402 ± 286	2.5 ± 0.4	5800 ± 142
Cytidine	3.6 ± 1.3	1310 ± 113	2.3 ± 0.4	5448 ± 112
Adenosine	2.2 ± 0.7	1020 ± 44	2.1 ± 0.5	5020 ± 110
Inosine	2.1 ± 0.6	1740 ± 114	3.1 ± 0.5	6420 ± 180
Gemcitabine	3.8 ± 1.0	390 ± 50	4.1 ± 1.1	1600 ± 50
Clofarabine	4.1 ± 1.3	410 ± 40	4.6 ± 1.5	1800 ± 120

The K_m, and V_{max} values shown are the means ± S.E. of three to four separate experiments.

Table 4-2 Kinetic properties of single-cysteine mutants of putative TM 11 of hCNT3

TM 11 Mutant	Uridine		Adenosine	
	K_m (μM)	V_{max} (pmol/mg/min)	K_m (μM)	V_{max} (pmol/mg/min)
Q479C	2.6 ± 0.3	2800 ± 60	2.1 ± 0.3	2300 ± 120
L480C	2.3 ± 0.3	930 ± 20	2.1 ± 0.8	770 ± 50
S481C	1.4 ± 0.2	3600 ± 20	1.6 ± 0.2	3820 ± 50
F482C	2.1 ± 0.3	730 ± 20	2.6 ± 0.4	870 ± 60
E483C	3.0 ± 0.8	620 ± 40	3.5 ± 0.7	760 ± 30
L484C	1.5 ± 0.2	2390 ± 120	2.1 ± 0.5	2500 ± 110
I 485C	4.1 ± 0.4	200 ± 10	3.1 ± 0.5	180 ± 20
C486C	2.7 ± 0.4	6460 ± 250	3.5 ± 0.9	7600 ± 260
S487C	1.5 ± 0.3	1890 ± 50	2.2 ± 0.5	2100 ± 120
Y488C	3.4 ± 0.6	2200 ± 80	3.8 ± 0.8	2400 ± 40
I489C	1.2 ± 0.2	2030 ± 40	1.8 ± 0.4	3300 ± 110
F490C	2.0 ± 0.4	4000 ± 140	2.2 ± 0.4	3900 ± 110
M491C	3.4 ± 0.3	3640 ± 70	3.9 ± 0.4	3890 ± 180
P492C	3.8 ± 0.5	3300 ± 120	3.7 ± 0.9	3540 ± 110
F493C	2.0 ± 0.3	3200 ± 90	2.4 ± 0.3	3500 ± 160
S494C	5.1 ± 0.5	2450 ± 60	6.8 ± 1.0	2600 ± 130
F495C	3.5 ± 0.8	660 ± 30	4.1 ± 0.5	680 ± 50
M496C	N.F.	-	-	-
M497C	2.9 ± 0.3	1800 ± 60	3.2 ± 0.8	1950 ± 40
G498C	N.F.	-	-	-
V499C	2.8 ± 0.2	4700 ± 80	3.5 ± 0.2	5100 ± 120

The K_m, and V_{max} values shown are the means ± S.E. of three separate experiments. N.F., not functional.

Table 4-3 Kinetic properties of single-cysteine mutants of putative TM 12 of hCNT3

TM 12 Mutant	Uridine		Adenosine	
	K_m (μM)	V_{max} (pmol/mg/min)	K_m (μM)	V_{max} (pmol/mg/min)
I554C	3.3 ± 0.3	2040± 50	2.8 ± 0.3	2100 ± 60
I555C	3.2 ± 0.5	500 ± 20	3.3 ± 0.8	480 ± 40
A556C	3.2 ± 0.5	2360 ± 70	3.8 ± 0.6	2550 ± 80
T557C	3.0 ± 0.5	3170 ± 130	3.5 ± 0.4	3670 ± 70
Y558C	4.5 ± 0.8	1350 ± 110	5.5 ± 0.9	1500 ± 140
A559C	6.2 ± 0.8	2620 ± 110	8.1 ± 1.4	2450 ± 120
L560C	7.2 ± 0.6	3130 ± 80	7.4 ± 1.0	3300 ± 130
C561C	1.3 ± 0.2	1200 ± 40	2.0 ± 0.4	1350 ± 50
G562C	6.0 ± 0.8	1100 ± 40	4.9 ± 0.5	1030 ± 50
F563C	NF	-	-	-
A564C	22 ± 1.1	2800 ± 100	21 ± 1.3	2900 ± 130
N565C	2.2 ± 0.4	1060 ± 30	1.9 ± 0.4	1100 ± 50
I566C	3.8 ± 0.6	2860 ± 120	3.4 ± 0.4	2340 ± 80
G567C	3.9 ± 0.3	4100 ± 120	3.8 ± 0.6	3960 ± 140
S568C	3.9 ± 0.5	160 ± 6	3.9 ± 0.2	140 ± 10
L569C	1.1 ± 0.2	1380 ± 30	1.3 ± 0.3	1540 ± 50
G570C	5.2 ± 1.4	1100 ± 100	4.6 ± 0.9	1180 ± 90
I571C	50 ± 8.0	2200 ± 150	48 ± 8.2	2280 ± 110
V572C	3.6 ± 0.8	5680 ± 380	2.8 ± 0.2	4980 ± 330
I573C	2.1 ± 0.4	1920 ± 40	1.8 ± 0.3	1930 ± 130
G574C	1.8 ± 0.3	2000 ± 50	1.5 ±0.3	1930 ± 70

The K_m, and V_{max} values shown are the means ± S.E. of three separate experiments.
N.F., not functional.

Table 4-4 Kinetic properties of single-cysteine mutants of putative TM 13 of hCNT3

TM 13	Uridine		Adenosine	
Mutant	K_m (μM)	V_{max} (pmol/mg/min)	K_m (μM)	V_{max} (pmol/mg/min)
V592C	2.3 ± 0.3	4020 ± 120	2.4 ± 0.2	4100 ± 90
R593C	2.5 ± 0.2	70 ± 10	2.1 ± 0.3	65 ± 5
A594C	NF	-	-	-
L595C	1.5 ± 0.2	110 ± 15	1.3 ± 0.3	200 ± 20
I596C	4.3 ± 0.8	4220 ± 140	3.8 ± 0.4	4000 ± 100
A597C	4.8 ± 0.6	3600 ± 100	4.2 ± 0.2	3660 ± 80
G598C	NF	-	-	-
T599C	2.0 ± 0.3	4070 ± 150	2.8 ± 0.3	4900 ± 180
V600C	1.7 ± 0.4	5180 ± 210	1.8 ± 0.3	4890 ± 170
A601C	7.4 ± 0.8	2800 ± 100	12.8 ± 2.0	2100 ± 90
C602C	1.8 ± 0.4	2800 ± 60	1.4 ± 0.3	2350 ± 120
F603C	17.2 ± 3.9	160 ± 50	20.0 ± 4.0	140 ± 30
M604C	3.7 ± 0.4	1100 ± 40	3.4 ± 0.8	1300 ± 100
T605C	2.0 ± 0.4	3300 ± 150	2.9 ± 0.4	4500 ± 230
A606C	NF	-	-	-
C607C	2.8 ± 0.7	6950 ± 230	3.0 ± 0.6	6980 ± 330
I608C	6.0 ± 1.2	1250 ± 90	18 ± 3.2	250 ± 50
A609C	2.4 ± 0.4	600 ± 70	2.5 ± 0.7	580 ± 40
G610C	5.4 ± 1.1	80 ± 9	4.9 ± 0.8	70 ± 10
I611C	2.2 ± 0.4	3070 ± 110	2.7 ± 0.4	3100 ± 90
L612C	3.1 ± 0.2	3040 ± 40	2.7 ± 0.2	2900 ± 80

The K_m, and V_{max} values shown are the means ± S.E. of three separate experiments.
N.F., not functional.

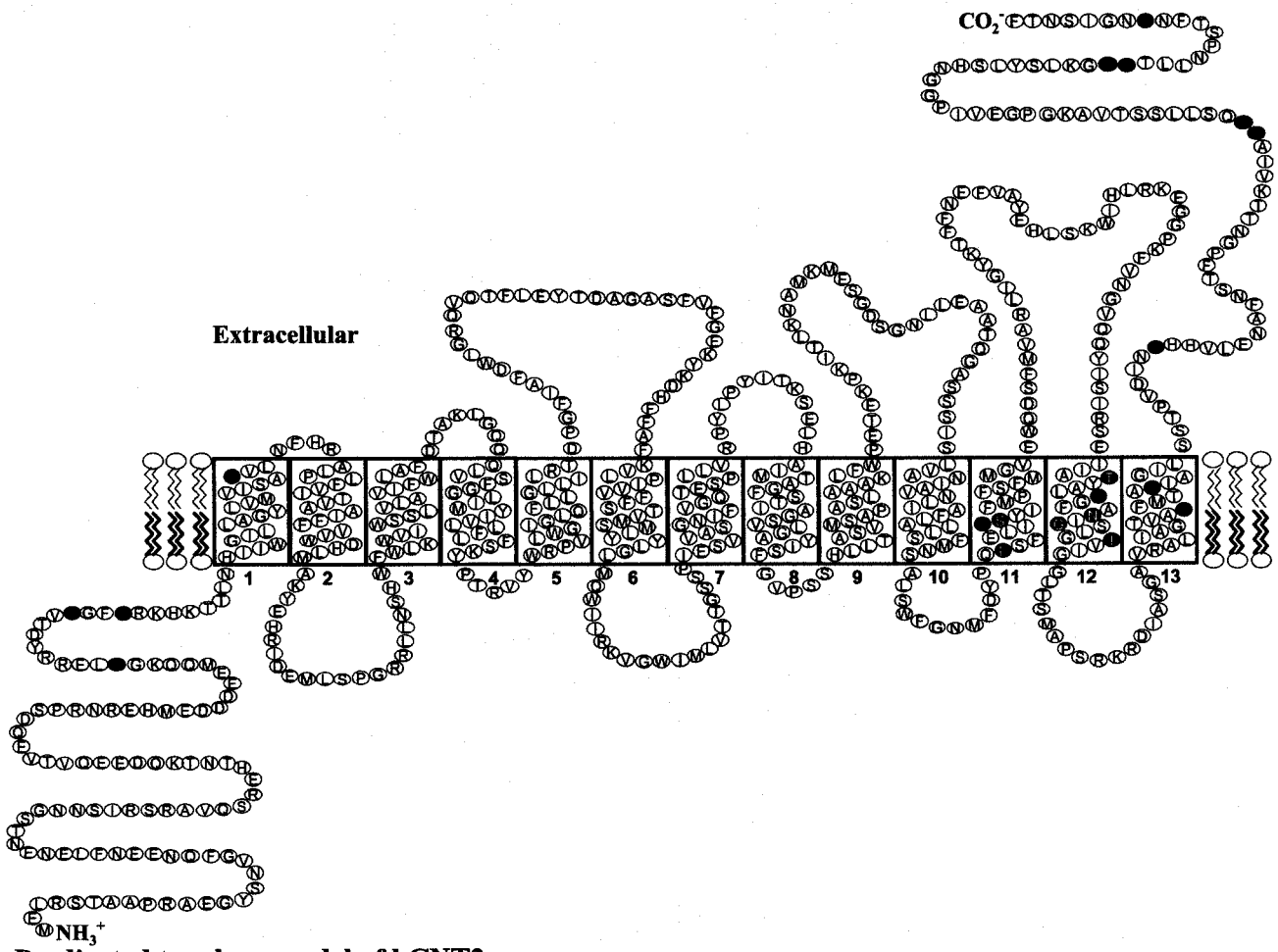

Figure 4-1 Predicated topology model of hCNT3.

Residues shaded in gray are endogenous cysteine residues and in black are MTS-sensitive residues.

Figure 4-2 Immunostaining of yeast producing cysteine-less hCNT3 or some single-cysteine hCNT3 mutants.

Yeast cells producing wild type hCNT3, cysteine-less hCNT3 or one of the 63 single-cysteine hCNT3 mutants were treated with anti-hCNT3 IgM as primary antibodies followed by Alexa Fluor 488 goat-anti mouse IgG as secondary antibodies. The images were captured by confocal microscopy as described in Materials and Methods using a 60X objective; and the scale bar represents a distance of 10 μm. Negative control cells containing empty vector (EV, pYPGE15) with no insert were stained with both the anti-hCNT3 IgM and Alexa Fluor 488 IgG antibodies. Other controls included yeast producing cysteine-less hCNT3 stained with IgM isotype primary antibodies in place of the anti-hCNT3 IgM or only with the secondary antibodies. No significant fluorescence signals were detected in these control conditions (data not shown). Images presented are representatives of 10-20 similar images recorded for cysteine-less hCNT3 and some of the single-cysteine hCNT3 mutants.

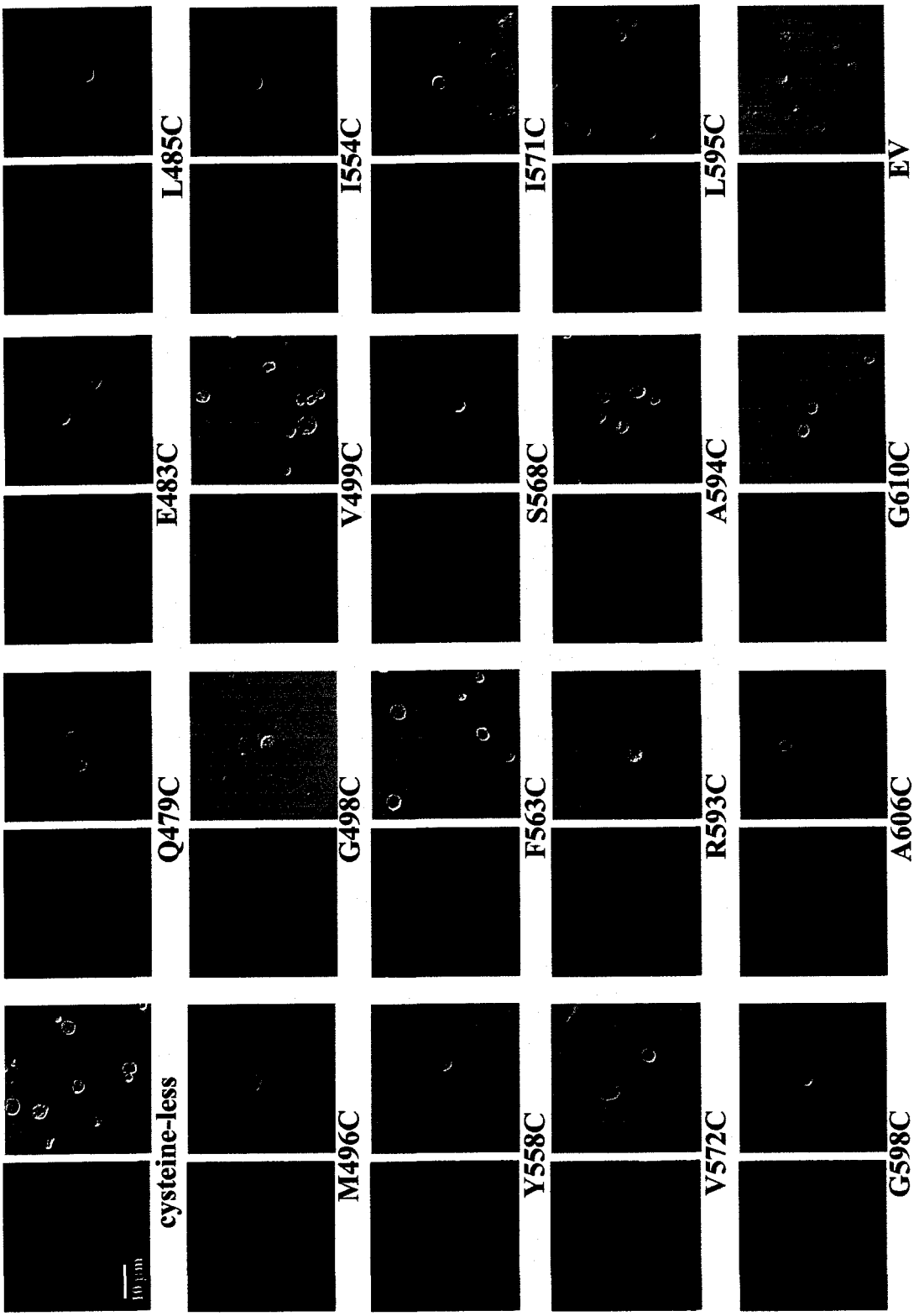

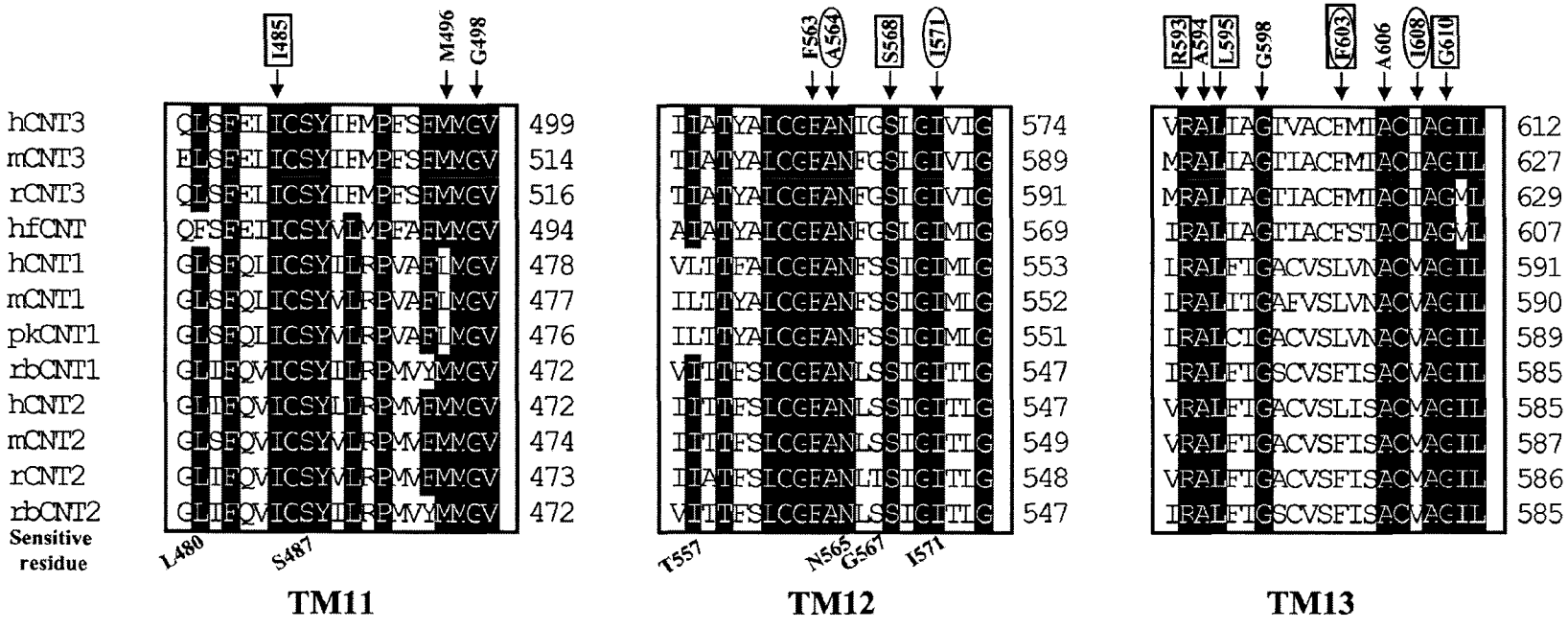

Figure 4-3 Protein sequence alignment of the TM 11, 12 and 13 of CNT transporter family.

Single-cysteine mutants that were inactivated by cysteine substitution are indicated. Single-cysteine mutants that showed large decreases in V_{max} values or increase in K_m values are boxed or circled, respectively. Abbreviations: h, human; r, rat; m, mouse; pk, pig; and rb, rabbit.

Figure 4-4 Reactivity of cysteine residues within TM 11 (top panel), TM 12 (middle panel) and TM 13 (bottom panel) with three MTS reagents.

Mutants are designated by the single-letter amino acid abbreviation for the targeted residue, followed by the sequence position number in hCNT3 and a second letter indicating the cysteine replacement. These three panels show the effects of MTSEA, MTSES and MTSET on the ability of single-cysteine substituted mutants to transport 1 μM [^{3}H]uridine. Activity is expressed as the mean percent of control value (no MTS reagent) for each individual mutant with standard deviations of quadruplicate values from a representative experiment. Black bars, 2.5 mM MTSEA; white bars, 10 mM MTSES; shaded bars, 1 mM MTSET. Three independent experiments were carried out and similar results were obtained.

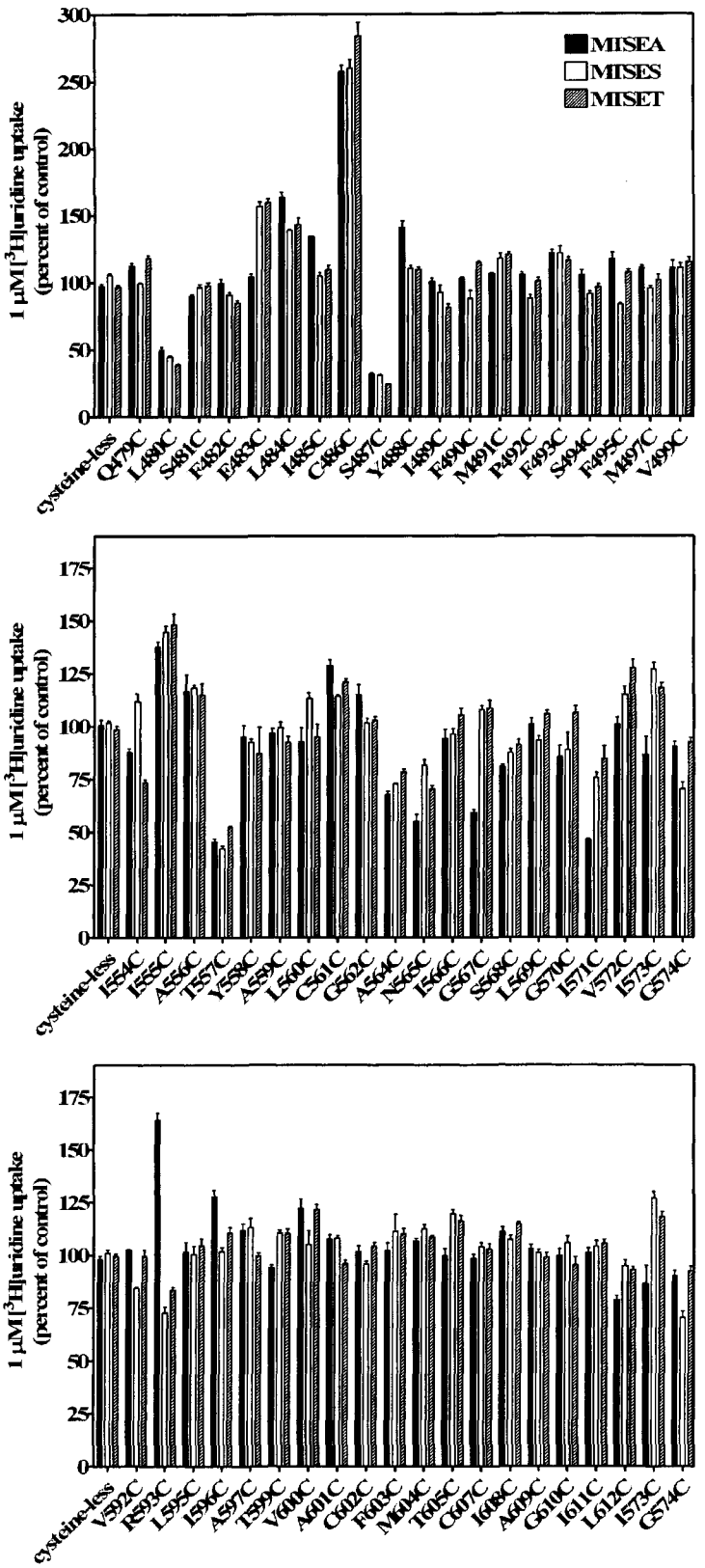

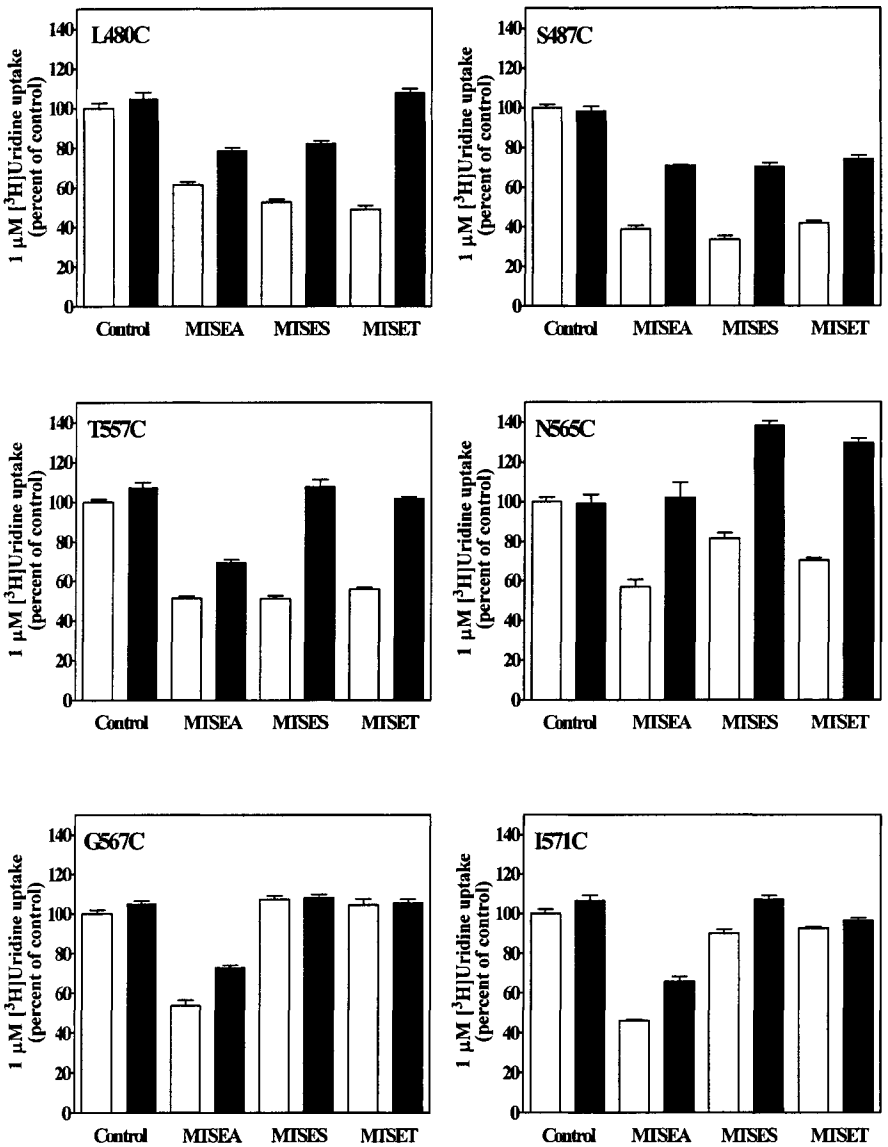

Figure 4-5 Protection from MTS reagent inhibition by uridine.

Yeast producing recombinant hCNT3 mutants were incubated with MTS reagents as indicated in the presence (black bar) or absence (control, white bars) of 10 mM uridine for 5 min, washed three times with PBS and assayed for their ability to transport 1 μM [^{3}H]uridine. Activity is expressed as the mean percent of control value (no MTS reagent, no 10 mM uridine) for each individual mutant with standard deviations of quadruplicate values from a representative experiment. Three independent experiments were carried out and similar results were obtained.

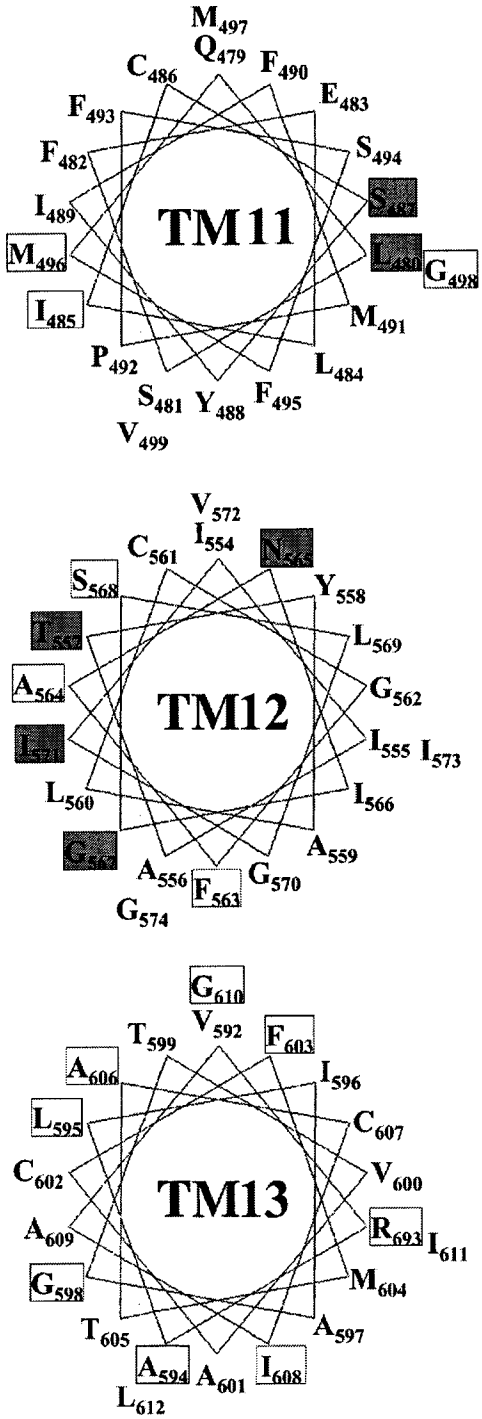

Figure 4-6 Helix wheel projection of putative TM 11, TM 12 and TM 13 of hCNT3.

Mutants that were sensitive to MTS reagents are in black box. Mutants that showed no assayable activity or significantly changed kinetic properties are labeled in white box.

References

1. Edwards, A. M., Arrowsmith, C. H., Christendat, D., Dharamsi, A., Friesen, J. D., Greenblatt, J. F., and Vedadi, M. (2000) *Nat Struct Biol* **7 Suppl**, 970-972.
2. Coe, I. R., Griffiths, M., Young, J. D., Baldwin, S. A., and Cass, C. E. (1997) *Genomics* **45**, 459-460
3. Acimovic, Y., and Coe, I. R. (2002) *Mol Biol Evol* **19**, 2199-2210
4. Baldwin, S. A., Yao, S. Y., Hyde, R. J., Ng, A. M., Foppolo, S., Barnes, K., Ritzel, M. W., Cass, C. E., and Young, J. D. (2005) *J Biol Chem* **280**, 15880-15887
5. Hyde, R. J., Abidi, F., Griffiths, M., Yao, S. Y. M., Sundaram, M., Phillips, S. E. V., Cass, C. E., Young, J. D. (2000) *Drug Dev Res* **50**, 38
6. Baldwin, S. A., Beal, P. R., Yao, S. Y., King, A. E., Cass, C. E., and Young, J. D. (2004) *Pflugers Arch* **447**, 735-743
7. Engel, K., Zhou, M., and Wang, J. (2004) *J Biol Chem* **279**, 50042-50049
8. Ritzel, M. W., Yao, S. Y., Huang, M. Y., Elliott, J. F., Cass, C. E., and Young, J. D. (1997) *Am J Physiol* **272**, C707-714
9. Ritzel, M. W., Yao, S. Y., Ng, A. M., Mackey, J. R., Cass, C. E., and Young, J. D. (1998) *Mol Membr Biol* **15**, 203-211
10. Ritzel, M. W. L., Ng, A. M., Yao, S. Y. M., Graham, K., Loewen, S. K., Smith, K. M., Ritzel, R. G., Mowles, D. A., Carpenter, P., Chen, X., Karpinski, E., Hyde, R. J., Baldwin, S. A., Cass, C. E., and Young, J. D. (2001) *J Biol Chem* **276**, 2914-2927
11. Ngo, L. Y., Patil, S. D., and Unadkat, J. D. (2001) *Am J Physiol Gastrointest Liver Physiol* **280**, G475-481.
12. del Santo, B., Tarafa, G., Felipe, A., Casado, F. J., and Pastor-Anglada, M. (2001) *J Hepatol* **34**, 873-880.
13. Li, J. Y., Boado, R. J., and Pardridge, W. M. (2001) *J Pharmacol Exp Ther* **299**, 735-740
14. Van Belle, H. (1993) *Cardiovasc Res* **27**, 68-76
15. Baldwin, S. A., Mackey, J. R., Cass, C. E., and Young, J. D. (1999) *Mol Med Today* **5**, 216-224

16. Mackey, J. R., Jennings, L. L., Clarke, M. L., Santos, C. L., Dabbagh, L., Vsianska, M., Koski, S. L., Coupland, R. W., Baldwin, S. A., Young, J. D., and Cass, C. E. (2002) *Clin Cancer Res* **8**, 110-116.

17. Mackey, J. R., Galmarini, C. M., Graham, K. A., Joy, A. A., Delmer, A., Dabbagh, L., Glubrecht, D., Jewell, L. D., Lai, R., Lang, T., Hanson, J., Young, J. D., Merle-Beral, H., Binet, J. L., Cass, C. E., and Dumontet, C. (2005) *Blood* **105**, 767-774

18. Mackey, J. R., Baldwin, S. A., Young, J. D., and Cass, C. E. (1998) *Drug Resistance Updates* **1**, 310-324

19. Huang, Y., Anderle, P., Bussey, K. J., Barbacioru, C., Shankavaram, U., Dai, Z., Reinhold, W. C., Papp, A., Weinstein, J. N., and Sadee, W. (2004) *Cancer Res* **64**, 4294-4301

20. Vickers, M. F., Mani, R. S., Sundaram, M., Hogue, D. L., Young, J. D., Baldwin, S. A., and Cass, C. E. (1999) *Biochem J* **339**, 21-32

21. Visser, F., Vickers, M. F., Ng, A. M., Baldwin, S. A., Young, J. D., and Cass, C. E. (2002) *J Biol Chem* **277**, 395-401.

22. Visser, F., Zhang, J., Raborn, R. T., Baldwin, S. A., Young, J. D., and Cass, C. E. (2005) *Mol Pharmacol* **67**, 1291-1298

23. Damaraju, S., Zhang, J., Visser, F., Tackaberry, T., Dufour, J., Smith, K. M., Slugoski, M., Ritzel, M. W., Baldwin, S. A., Young, J. D., and Cass, C. E. (2005) *Pharmacogenet Genomics* **15**, 173-182

24. Sundaram, M., Yao, S. Y. M., Ng, A. M. L., Griffiths, M., Cass, C. E., Baldwin, S. A., and Young, J. D. (1998) *J Biol Chem* **273**, 21519-21525

25. Hamilton, S. R., Yao, S. Y., Ingram, J. C., Hadden, D. A., Ritzel, M. W., Gallagher, M. P., Henderson, P. J., Cass, C. E., Young, J. D., and Baldwin, S. A. (2001) *J Biol Chem* **276**, 27981-27988

26. Loewen, S. K., Ng, A. M., Yao, S. Y., Cass, C. E., Baldwin, S. A., and Young, J. D. (1999) *J Biol Chem* **274**, 24475-24484

27. Wang, J., and Giacomini, K. M. (1997) *J Biol Chem* **272**, 28845-28848

28. Lai, Y., Lee, E. W., Ton, C. C., Vijay, S., Zhang, H., and Unadkat, J. D. (2005) *Am J Physiol Cell Physiol* **288**, C39-45

29. Smith, K. M., Slugoski, M. D., Loewen, S. K., Ng, A. M., Yao, S. Y., Chen, X. Z., Karpinski, E., Cass, C. E., Baldwin, S. A., and Young, J. D. (2005) *J Biol Chem*
30. Yao, S. Y., Ng, A. M., Vickers, M. F., Sundaram, M., Cass, C. E., Baldwin, S. A., and Young, J. D. (2002) *J Biol Chem* **277**, 24938-24948
31. Zhang, J., Visser, F., Vickers, M. F., Lang, T., Robins, M. J., Nielsen, L. P., Nowak, I., Baldwin, S. A., Young, J. D., and Cass, C. E. (2003) *Mol Pharmacol* **64**, 1512-1520
32. Zhang, J., Smith, K. M., Tackaberry, T., Visser, F., Robins, M. J., Nielsen, L. P., Nowak, I., Baldwin, S. A., Young, J. D., and Cass, C. E. (2005) *Mol Pharmacol* **68**
33. Vickers, M. F., Yao, S. Y., Baldwin, S. A., Young, J. D., and Cass, C. E. (2000) *J Biol Chem* **275**, 25931-25938
34. Vickers, M. F., Kumar, R., Visser, F., Zhang, J., Charania, J., Raborn, R. T., Baldwin, S. A., Young, J. D., and Cass, C. E. (2002) *Biochem Cell Biol* **80**, 639-644
35. Brunelli, J. P., Pall, M.L. (1993) *Yeast* **9**, 1309-1318
36. Crawford, C. R., Ng, C. Y., Ullman, B., and Belt, J. A. (1990) *Biochim Biophys Acta* **1024**, 289-297
37. Lang, T. (2003) in *Oncology*, pp. 420, University of Alberta, Edmonton, Canada
38. Vickers, M. F., Zhang, J., Visser, F., Tackaberry, T., Robins, M. J., Nielsen, L. P., Nowak, I., Baldwin, S. A., Young, J. D., and Cass, C. E. (2004) *Nucleosides Nucleotides Nucleic Acids* **23**, 361-373
39. Frillingos, S., Sahin-Toth, M., Wu, J., and Kaback, H. R. (1998) *Faseb J* **12**, 1281-1299

Chapter 5 Studies of Nucleoside Transporters Using Autofluorescent Nucleoside Analogs

A version of this chapter has been submitted to *Biochemistry*.

Acknowledgements

Dr. Xuejun Sun contributed to this project by developing the protocols for real time analysis of transport of autofluorescence compounds in live cells and providing intellectual guidance. Mrs. Pat Carpenter and Ms. Geraldine Barron conducted cell culture and part of the imaging experiments. Dr. Kyla M. Smith conducted the *X. laevis* nucleoside transport experiments. Dr. Morris J. Robins and Mr. Yunshan Peng are chemists who synthesized the autofluorescence nucleoside analogs. Drs. Frank Visser, Stephen Baldwin and James Young aided in manuscript preparation.

Introduction

Integral membrane proteins mediate the passage of nucleosides, including anticancer and antiviral nucleoside analogs, across biological membranes (1,2). Two distinct nucleoside transporter families, the equilibrative nucleoside transporters (ENTs) and the concentrative nucleoside transporters (CNTs), have been identified by molecular cloning and functional expression of cDNAs from a variety of sources, including mammals, protozoan parasites and bacteria. In human (h) cells and tissues, hENT1 and 2 mediate facilitated diffusion of nucleosides down their concentration gradients and hCNT1, 2 and 3 couple uphill transport of nucleosides to downhill transport of sodium ions and, in the case of hCNT3, also to downhill transport of protons. hENT1 and 2 are functionally distinguished by different sensitivities (hENT1 >> hENT2) to nitrobenzylmercaptopurine ribonucleoside (NBMPR) and have therefore been assigned the functional designations equilibrative sensitive (*es*) and equilibrative insensitive (*ei*), respectively (3,4). hENT3, which is proton-dependent and, like hENT1, broadly selective, transports nucleosides across lysosomal membranes (5-7) and hENT4, which mediates equilibrative transport of adenosine (5,8), also transports monoamine neurotransmitters (9). The three hCNTs differ functionally in their permeant selectivities (10-12). hCNT1 and 2 prefer pyrimidine nucleosides and purine nucleosides, respectively, although hCNT1 also transports adenosine and hCNT2 also transports uridine (Urd) whereas hCNT3 transports both pyrimidine and purine nucleosides.

Interest in nucleoside transporters has increased because of their potential and proven therapeutic applications in cancer, stroke and cardiovascular, parasitic and viral diseases. Nucleoside transporter proteins are critical in controlling extracellular concentrations of adenosine, the ligand for cell-surface purinergic P1 receptors, which are involved in a variety of physiological responses, including coronary vasodilation, neuromodulation and platelet aggregation (13,14). The presence of nucleoside transporters in plasma membranes is required for efficient delivery of many anti-cancer nucleoside drugs (e.g., gemcitabine, capecitabine and fludarabine) and has been linked mechanistically with drug sensitivities and toxicities (15-17). The presence of *es* and *ei* activities has been demonstrated in preparations containing nuclear envelop and

endoplasmic reticulum membranes, suggesting that hENT1 and hENT2 may mediate translocation of nucleosides between intracellular compartments (18). hENT1 has been detected in mitochondrial membranes and may be involved in mitochondrial toxicity caused by some antiviral nucleosides (19). The newly identified hENT3 was found to be partially localized in lysosomal membranes (18), and may play a role in lysosomal release of nucleosides derived from degradation of nuclear nucleic acids. However, knowledge of intracellular trafficking and distribution of nucleosides and nucleoside metabolites is limited.

We describe here the development of a novel strategy for visualizing and measuring transport processes in living cells. FuPmR [3-(β-D-ribofuranosyl)furo[2,3-*d*]pyrimidin-2(3*H*)-one] and dFuPmR [3-(2-deoxy-β-D-*erythro*-pentofuranosyl)furo[2,3-*d*]pyrimidin-2(3*H*)-one] were assessed as prototypic fluorescent nucleoside probes (see Fig. 5-1, Panel A for chemical structures). The apparent affinities of human nucleoside transporters for FuPmR and dFuPmR were determined by measuring their relative abilities to inhibit transport of [^{3}H]Urd in yeast producing a particular recombinant transporter using a high-throughput assay described previously (20,21). The transportabilities of FuPmR and dFuPmR by members of the hCNT family, which are sodium-nucleoside symporters, were assessed directly by measuring induction of sodium/proton currents in *Xenopus laevis* oocytes producing recombinant hCNT1, hCNT2 or hCNT3 as described previously (22). For both compounds, the apparent binding affinities were high (hCNT3), moderate (hENT1) and low (hCNT1 and 2, hENT2) and the transportabilities were high (hCNT3), low (hCNT1) and not detectable (hCNT2). The transportabilities of FuPmR and dFuPmR by hENT1 and 2 were assessed by live cell imaging in a cultured human cell line (BeWo choriocarcinoma) previously shown (23) to possess high levels of *es* activity (i.e., hENT1), low levels of *ei* activity (i.e., hENT2) and no concentrative activity (i.e., hCNT1, 2 and/or 3). The initial rates of uptake of FuPmR into the cytoplasm, mitochondria and nuclei of living BeWo cells were measured by real time confocal microscopy. Inhibition of cellular uptake by potent and specific inhibitors of hENT1-mediated transport demonstrated involvement of hENT1 in passage across plasma membranes. The movements of FuPmR across various membranes were further confirmed by fluorescence recovery after photobleaching

(FRAP). The measurement of cellular and organellar uptake of fluorescent nucleoside analogs by fluorescence microscopy with digital processing of data to extract rates provides a new approach to quantitatively study nucleoside transport activities and to evaluate the intracellular distribution of nucleosides and their metabolites in living cells.

Materials and Methods

Synthesis of FuPmR and dFuPmR

The fluorescent furopyrimidine analogs were synthesized by the methods of Robins and Barr (38,39). Briefly, 2',3',5'-tri-*O*-acetyluridine (for FuPmR) and 3',5'-di-*O*-acetyl-2'-deoxyuridine (for dFuPmR) were iodinated (38), and the 5-iodo compounds were coupled with trimethylsilylacetylene (39). Fluoride-promoted removal of the trimethylsilyl group followed by copper(I) iodide-catalyzed cyclization gave the furopyrimidine derivatives (39), which were deacylated with methanolic ammonia to provide 3-(β-D-ribofuranosyl)furo[2,3-*d*]pyrimidin-2(3*H*)-one (FuPmR) and 3-(2-deoxy-β-D-*erythro*-pentofuranosyl)furo[2,3-*d*]pyrimidin-2(3*H*)-one (40) (dFuPmR). The structures of FuPmR and dFuPmR are shown in Fig. 5-1, Panel A.

Cell culture and cytotoxicity assays

The origins and maintenance of human choriocarcinoma (BeWo) cells were described previously (41). Cells were grown as adherent monolayers in Roswell Park Memorial Institute 1640 medium supplemented with 10% fetal bovine serum (v/v) at 37°C in 5% CO_2/95% air and were subcultured by trypinization every two to three days to maintain exponential growth. One day before imaging experiments, cells were seeded into a six-well plate, each well of which contained a glass coverslip (5,000 cells/well in 2 ml growth medium).

Cytotoxicity assays were conducted with the CellTiter 96 proliferation assay kit (Promega, Madison, WI, USA). Cells were seeded into 96-well plates at densities of 5,000 (72-h exposures) or 20,000 cells (4 h exposures) per well and incubated at 37°C for 24 h before exposure to test compounds. Cells were exposed to graded concentrations of

FuPmR or dFuPmR (0–1000 μM) for 4 or 72 h and then treated with 3-(4,5-dimethylthiazol-2-yl)-5-(3-carboxymethoxyphenyl)-2-(4-sulfophenyl)-2H-tetrazolium (MTT) reagent for assessment of cytotoxicity as described by the manufacturer. The concentrations that reduced MTT-dependent absorbance by 50% (IC_{50} values) were calculated from nonlinear regression analysis of data plotted as percentages of control values against the logarithm of the fluorescent analogue concentrations.

Measurement of [^{3}H]Urd uptake mediated by recombinant NTs produced in S. cerevisiae

Construction of the yeast expression systems for hENT1 and 2 and hCNT1, 2 and 3 was performed as described (20,21,24). Yeast producing individual recombinant hENT or hCNT proteins were maintained in logarithmic growth phase in complete minimal medium (pH 7.4) with 2% glucose. Transport experiments were conducted with a high-throughput assay described previously (20) that used 96-well plates and a semi-automated cell harvester (Micro96 Harvester; Skatron Instruments, Lier, Norway). The relative affinities of the transporters for FuPmR and dFuPmR were assessed by measuring the concentration dependence of their inhibition of uptake of [^{3}H]Urd as follows. Yeast producing recombinant hENT1, hENT2, hCNT1, hCNT2 or hCNT3 were incubated with graded concentrations of FuPmR and dFuPmR in the presence of 1 μM [^{3}H]Urd for 10 min (hENT1, hENT2, hCNT1, hCNT2) or 5 min (hCNT3). Each experiment was repeated at least three times. Nonspecifically associated radioactivity was determined in the presence of 10 mM nonradioactive Urd, and the resulting values were subtracted from total uptake values. Data were subjected to nonlinear regression analysis using GraphPad Prism Software version 3.0 (GraphPad Software Inc., San Diego, CA) to obtain IC_{50} values for FuPmR and dFuPmR; K_i values were determined using the Cheng-Prusoff equation(42) and the K_m values for transport of Urd obtained for each of the recombinant transporters produced in yeast (20,21,43).

Production of recombinant hCNTs and measurement of hCNT-induced sodium and proton currents in oocytes of Xenopus laevis

The cDNAs of hCNT1, hCNT2 and hCNT3 were individually subcloned into vector pGEM-HE. Plasmids were linearized with *Nhe*I (pGEM-HE) and transcribed with T7 polymerase mMESSAGE mMACHINE^{TM} (Ambion Inc., Austin, TX, USA). Stage VI oocytes of *X. laevis* were microinjected with 20 nl of water or 20 nl of water containing RNA transcripts (20 ng) for the appropriate transporter and incubated in modified Barth's medium (changed daily) at 18°C for 72 h as described (22) prior to the assay of transport activity.

Oocyte membrane currents were measured using a GeneClamp 500B oocyte clamp (Axon Instruments, Inc., Foster City, CA, USA) in the two-electrode, voltage-clamp mode as described(22). All experiments were performed at room temperature (20°C) and oocytes were discarded if the membrane potential was unstable or more positive than –30 mV. Membrane potentials were clamped at a holding potential (V_h) of –50 mV. Oocytes were perfused with transport medium containing 100 mM NaCl, 2 mM KCl, 1 mM $CaCl_2$, 1 mM $MgCl_2$, and 10 mM HEPES, pH 7.5 or 8.5., and cation/nucleoside cotransport was initiated by changing the permeant-free solution to one containing 100 μM Urd, dFUPMR or FUPMR. For experiments that were conducted in the absence of sodium, choline replaced sodium, and proton-dependent uptake of Urd, dFUPMR or FUPMR was measured in choline-containing transport medium acidified to pH 5.5 (buffered with 10 mM MES) (22).

Time-lapse confocal microscopy and fluorescence recovery after photobleaching

Time-lapse microscopy was performed using a Zeiss LSM510 Confocal Laser Scanning Microscope (Carl Zeiss, Jena, Germany) mounted on an Axiovert 100M inverted microscope. A coverslip with adherent BeWo cells was washed three times with phosphate buffered saline (PBS, pH 7.4) and glued onto the edge of an open hole located in the middle of a two-μm thick metal slide to form a well. Five hundred μl of PBS alone or PBS containing the appropriate transport inhibitor at the desired concentration were added to the well, which was held at room temperature for 5 min before confocal studies.

The solution in the well was maximally removed by gentle suction and time-lapse image capturing was started a few sec before adding 500 μl PBS containing the appropriate autofluorescent nucleoside analogue into the well. The live cell imaging lasted 10-70 min. To visualize mitochondria, cells growing on glass coverslips were incubated with 0.1 μM MitoTracker Orange (Molecular Probes Inc. Eugene, OR) in cell culture medium for 30 min at 37°C in the dark in an atmosphere of 5% CO_2, washed three times with PBS and subjected to confocal imaging. Timelapse images were collected with 40X(NA1.3) F-fluar lenses and digitized at 12 bits with an interval of 1-3 sec during the first 5 min and 60 sec after 5 min. The zoom and frame sizes were set according to the Nyquist digitization criteria. Minimum laser intensities were used to collect the images in order to reduce the photobleaching and phototoxicity to the cells. For FuPmR and dFuPmR, a 351-nm laser line was used as the excitation source and the emission signal was collected with a Longpass filter of 385 nm. For Mitotracker Orange, an excitation of 543 nm laser line was used and the emission signal was collected with a Longpass filter of 560 nm.

Fluorescence recovery after photobleaching (FRAP) analyses was performed using the same microscope. Photobleaching of the fluorescent signal at the focal plane of interest was performed using wavelengths of 351 and 364 nm at maximum power for 10 iterations. Time-lapse images were collected immediately before and after photobleaching. Differential interference contrast (DIC) images of cells were taken before and after FRAP in case there were changes in cell shape and position; none were observed. Average $t_{1/2}$, the time for fluorescence to recover to 50% of its original value, was determined from fluorescence recovery curves which were generated by plotting change in fluorescence intensity as a function of time.

Fluorescence intensities were measured by placing a circle around the stored digital image of a targeted cell or intracellular part. The integrated intensities were exported to a linked Microsoft Excel worksheet. Background fluorescence, which was defined as the fluorescent intensity of the same measurement circle in a nearby extracellular region, was determined and subtracted from each cellular measurement.

Results

Cytotoxicity of FuPmR and dFuPmR to BeWo cells

Previous studies showed that BeWo cells possess *es*- and *ei*-mediated nucleoside transport activities and extraordinarily high NBMPR-binding sites (23) and express hENT1 and hENT2 mRNAs (18). Before using FuPmR and DFuPmR in live cell imaging studies, their toxicities to BeWo cells during short (4 h) and prolonged (72 h) exposure periods were assessed using the MTT cytotoxicity assay. The 4-hour exposures to either compound had no effect (data not shown) whereas the 72 h exposures revealed differences in cytotoxicity at high concentrations. At 1 mM, <5% of the cells survived FuPmR exposures whereas >90% of the cells survived dFuPmR exposures; FuPmR had an IC_{50} (inhibitory concentration 50%) value of 146 ± 10 μM (Fig. 5-1, Panel B). All subsequent experiments involved exposures of <1.1 h.

Interaction of FuPmR and dFuPmR with recombinant nucleoside transporters produced in yeast

The inhibitory effects of FuPmR and dFuPmR on transporter-mediated uptake of [^{3}H]Urd was examined using a yeast expression system as previously described (20,21,24). Representative concentration-effect curves for FuPmR and dFuPmR inhibition of hENT1-, hENT2-, hCNT1-, hCNT2- and hCNT3-mediated Urd transport are shown in Fig. 5-2. The IC_{50} values obtained from the data of Fig. 5-2 and previously reported kinetic constants for Urd (20,21,25) were used to calculate apparent K_i values, which provided a measure of the relative affinities of FuPmR and dFuPmR for the various transporters. hCNT3 displayed relatively high affinities for FuPmR and dFuPmR, with apparent K_i values (mean ± S.E., n = 3) of 4.2 ± 0.8 and 15 ± 2 μM, respectively. FuPmR and dFuPmR were moderate inhibitors of hENT1-mediated Urd transport, with apparent K_i values (mean ± S.E., n = 3) of 380 ± 20 and 170 ± 11 μM, respectively. Although hCNT1-mediated transport of Urd was sensitive to inhibition by both compounds, high concentrations did not completely inhibit transport and apparent K_i values could not be calculated. FuPmR and dFuPmR were poor inhibitors of Urd

uptake mediated by either hENT2 or hCNT2, with maximum inhibitory effects (50-70%) observed at concentrations of 3 mM.

Transportability of FuPmR and dFuPmR by hCNT1, hCNT2 and hCNT3 produced in X. laevis oocytes

The transportability of FuPmR and dFuPmR by members of the hCNT protein family was examined by comparing the currents they induced in *X. laevis* oocyte producing recombinant hCNT1, hCNT2 or hCNT3. Fig. 5-3, Panel A shows representative total current recordings in hCNT-producing oocytes bathed in 100 mM Na^+-containing transport medium at pH 8.5 (to minimize proton-coupled transport) or 100 mM Na^+-free medium at pH values of 7.5 and 5.5. Urd, which was included at 100 μM as a control permeant, elicited large currents in Na^+-containing media for all three transporters and in choline-containing medium at pH 5.5 for hCNT3. No currents were detected in control oocytes that had been injected with water without transporter transcripts.

For hCNT1-producing oocytes, small inward currents were elicited by application of 100 μM FuPmR or dFuPmR with slightly higher currents (mean ± S.E., n = 3) observed with FuPmR (I_{Na} = 11 ± 0.9 nA) than with dFuPmR (I_{Na} = 6.5 ± 0.3 nA). For hCNT2-producing oocytes, no currents were elicited by either 100 μM FuPmR or dFuPmR. No currents were observed with 100 μM Urd, FuPmR or dFuPmR when oocytes producing recombinant hCNT1 or hCNT2 were perfused with sodium-free ChCl medium at pH 7.5 or pH 5.5 (Fig. 3B).

hCNT3 has a greater ability to transport permeants against their concentration gradients than either hCNT1 or 2, because its sodium:nucleoside coupling ratio is 2:1 whereas that of hCNT1 and 2 is 1:1 (26). Additionally, hCNT3 differs from hCNT1 and hCNT2 in that it is also proton-dependent (26). Both sodium and proton currents were observed in oocytes producing hCNT3 (Fig. 5-3). Large sodium-dependent currents (mean ± S.E., n = 3) were induced by 100 μM Urd (140 ± 15 nA), FuPmR (77 ± 8 nA) and dFuPmR (89 ± 11 nA) at pH 8.5. Using choline as the sodium substitute, a small current was observed with 100 μM Urd at pH 7.5 whereas no current was observed with either 100 μM FuPmR or dFuPmR. In acidified choline-containing media (pH 5.5),

small but reproducible proton currents (mean ± S.E., n = 3) were produced by application of 100 μM FuPmR (13 ± 2 nA) or dFuPmR (3.5 ± 1.5 nA).

Live cell imaging of FuPmR uptake into BeWo cells

The uptake of FuPmR into BeWo cells was evaluated using confocal microscopy and an excitation wavelength of 351 nm. Autofluorescence of BeWo cells was observed (Fig. 5-4, Panel A, time 0 sec). The extracellular medium emitted fluorescence (color coded as green) instantly upon addition of 500 μM FuPmR to the well whose bottom was the coverslip with BeWo cells attached (Fig. 5-4, Panel A, time 0 sec) and the fluorescent intensity of the medium barely changed during the observational period (Fig. 5-4, Panel B). As shown in the time-lapse images of Fig. 5-4, Panel A, the cytoplasm and the nucleus became fluorescent after exposure to FuPmR and a significant intracellular accumulation of fluorescent signals was observed by 15 min. The fluorescence intensities continued to increase over a period of 60 min (data not shown). The time course of intracellular fluorescence accumulation exhibited two phases of uptake (Fig. 5-4, Panel B). The first phase lasted about 40 sec with a steep slope, indicating a rapid initial rate of uptake. The second phase was slower and the increase of intracellular fluorescence intensity was linear for about 1 hour (data not shown), suggesting continuous trapping of FuPmR and/or its metabolites. No uptake of FuPmR was observed in the presence of 5 μM NBMPR (data not shown), indicating that FuPmR uptake was mediated primarily by hENT1.

Mitotracker orange was introduced as a control of the fluorescent signal as well as a probe for monitoring accumulation of FuPmR (and/or its metabolites) in mitochondria (Fig. 5-4). The fluorescence intensities of Mitotracker orange maintained stable levels in intracellular compartments in the presence of 500 μM FuPmR (Fig. 5-4, Panel B). Accumulation of FuPmR (and/or its metabolites) in mitochondria was evident since the green fluorescent signals of the mitochondrial compartment kept increasing (Fig. 5-4, Panel A, combined channels) as shown by the gradual change of the fluorescent color from orange to yellow. A three-fold increase of green fluorescent intensities was observed in mitochondrial regions in the presence of 500 μM FuPmR over 15 min (data not shown).

Experiments similar to those shown in Fig. 5-4 were conducted in BeWo cells with the 2'-deoxy analogue dFuPmR (data not shown) and demonstrated uptake via an NBMPR-sensitive process (i.e., hENT1), albeit at slower rates than for FuPmR. Subsequent investigations were carried out exclusively with the riboside FuPmR.

Measuring initial rates of FuPmR uptake

To calculate initial rates of FuPmR uptake during the first stage of cellular accumulation, which lasted for approximately 40 sec, time zero was set at the moment of addition of FuPmR and fluorescence intensity (after background subtraction) was normalized as the percentage of the highest uptake value (100%) during the initial 40-sec exposure. The slopes of the uptake time courses were linear during the first few sec and yielded initial rates with mean values (± S.E., n = 5 cells) of 9.3 ± 0.3 and 4.8 ± 0.2 relative fluorescence intensity/cell/sec for 500 and 250 μM FuPmR, respectively (Fig. 5-5, Panel B). Initial rates were greater at higher FuPmR concentrations (Fig. 5-5, Panel B and C, n = 5-8), indicating the concentration-dependence of uptake. The K_m value for FuPmR uptake could not be estimated because of the low sensitivity of detection of FuPmR at low concentrations.

As shown in Fig. 5-5, Panel A, a significant increase in fluorescence was observed in BeWo cells after a 5-min exposure to FuPmR whereas little, if any, increase was observed in the presence of 5 μM NBMPR, indicating that permeation of FuPmR was mediated primarily by hENT1. Inhibition of FuPmR transport by NBMPR was concentration-dependent with an IC_{50} value of 1 nM (Fig. 5-5, Panel C), which was close to values obtained with other nucleosides in radioisotope-flux experiments(23). The majority of FuPmR uptake was blocked by 10 or 100 nM NBMPR and the remaining uptake was totally inhibited by 1 μM NBMPR. The NBMPR inhibitory experiment was also performed in sodium-free buffer and similar results were observed, indicating that the uptake of FuPmR was mediated mostly by hENT1 and partially by hENT2, and no concentrative transport process of the fluorescent compound was involved in undifferentiated BeWo cells (data not shown). Two potent inhibitors of both hENT1 and 2, dipyridamole and dilazep, also inhibited FuPmR transport into BeWo cells (Fig. 5-5, Panel C).

The rates of accumulation of FuPmR (500 μM) into different intracellular compartments were measured by placing circles of similar size on different parts of the digital time-lapsed images of the same cells. The initial rates of uptake (mean ± S.E., n = 4) into cytoplasmic regions (9.7 ± 2.2 relative fluorescence intensity/cell/sec) were slightly faster than those in mitochondrial and nuclear regions (8.0 ± 1.2 relative fluorescence intensity/cell/sec) (Student's t-test, $p < 0.05$) (Fig. 5-5, Panel D), suggesting that the passage of FuPmR across intracellular membranes also occurred by mediated processes.

FRAP analysis of the movement of the fluorescent compound

By photobleaching regions of whole cells that had been incubated with 500 μM FuPmR for 30 min, FRAP was used to determine the extent of recovery of fluorescence signals. Results from a representative experiment are shown in Figs. 5-6, Panel A (whole cell images) and 5-6, Panel B (recovery curves). In the absence of 5 μM NBMPR, the bleached cell (Fig. 5-6, Panel B, left panel) showed >50% recovery with a half-recovery time ($t_{1/2}$) of 80 sec whereas the nearby unbleached (control) cell exhibited continuous slow accumulation of fluorescence. The incomplete fluorescence recovery was partially due to the bleaching of autofluorescence since the autofluorescence observed in cells without FuPmR treatment exhibited no recovery during the period of measurement (data not shown). In the presence of 5 μM NBMPR, recovery of fluorescence by bleached cells reached about 5% after 200 sec, further evidence that the movement of FuPmR across plasma membranes was mediated by hENTs.

Discussion

The most commonly used method to measure nucleoside transporter activities is analysis of radioisotope fluxes. Additionally, measurements of current can be used to assess activities of sodium and/or proton-coupled transporters. Approaches that could be used to visualize nucleoside transport activities *in situ* have not previously been available. Fluorescent inhibitors of ENT1 (e.g., SAENTA-χ_2-Fluorescein (27,28)) have enabled ligand-cell interactions to be analyzed by flow cytometry (29,30). We describe

here a novel methodology for real-time visualization of nucleoside transport processes in living cells.

FuPmR and dFuPmR are autofluorescent nucleoside analogs that differ from each other by the presence of a hydroxyl group at the C(2') position in FuPmR; they share high structural similarities with the naturally-occurring pyrimidine nucleosides. An inhibitor sensitivity assay with yeast producing recombinant human nucleoside transporters revealed that both compounds were high-affinity inhibitors of hCNT3, moderate-affinity inhibitors of hENT1 and low-affinity inhibitors of hENT2, hCNT1 and hCNT2. Because hCNTs are cation/nucleoside co-transporters, the transportability of FuPmR and dFuPmR was tested by the voltage clamp technique, which showed that they were good and poor permeants for hCNT3 and hCNT1, respectively, and neither was transported by hCNT2. The different affinity and transportability profiles for the nucleoside transporter subtypes raised the possibility that FuPmR and dFuPmR could be used as probes to differentially detect nucleoside transport activities mediated by certain types of nucleoside transporters.

We used laser scanning confocal microscopy and the FRAP technique to demonstrate that transport processes could be directly visualized and quantified *in situ* with FuPmR. The fluorescent properties of FuPmR permitted assessment of hENT1 activity in BeWo cells which exhibit large numbers ($>10^7$/cell) of NBMPR-binding sites and an unusually large capacity for NBMPR-sensitive nucleoside transport relative to other cell types (23). The uptake of FuPmR by BeWo cells was concentration-dependent with high sensitivity to nanomolar concentrations of NBMPR, indicating that its uptake was predominantly mediated by hENT1. Real-time imaging combined with fluorescence intensity digitalization revealed a two-stage uptake process. The first stage, which represented the true initial rate of the transport process, was short-lived. Previously, oil-stop and dilazep-stop methods (31), as well as a quenched-flow method (32), have been used to measure initial rates of nucleoside influx into mammalian cells. The second stage showed continued accumulation of fluorescent signals at much slower rates in a linear manner that lasted for at least an hour. The extended linear time courses may have resulted from intracellular metabolism of FuPmR (e.g., by phosphorylation), thereby maintaining the apparent concentration gradient of FuPmR between the extracellular and intracellular compartments.

Although *es* and/or *ei* transport activities have been observed in nuclear membranes, endoplasmic reticulum and mitochondria (18,19) and endogenous hENT3 has been observed in the intracellular compartments of cells (6), the functional analyses of nucleoside transport processes across intracellular membranes has previously been conducted in isolated membrane preparations. The development of autofluorescent permeants offers the possibility of visualizing the intracellular distribution of nucleosides and/or their metabolites. Live cell imaging clearly showed accumulation of fluorescence into nuclei, which was further confirmed by FRAP experiments. The increased fluorescence intensities of mitochondrial regions after the application of FuPmR supplied the first *in situ* demonstration of movement of a nucleoside (or its metabolite) from cytosol to mitochondria. The initial rates of increase in fluorescence intensities in nuclear and mitochondrial regions were slower than those of a randomly selected cytoplasmic region of the same cell, suggesting that movement of FuPmR (or its metabolites) across nuclear and mitochondrial membranes was also mediated. It is known that nucleotides, the phosphorylated metabolites of nucleosides, must be transported across the highly impermeable inner mitochondrial membrane by specific transporters or translocators (33,34).

The properties of FuPmR raise the possibility that it could be used for other research purposes. For example, the availability of specific fluorescent permeants for nucleoside transporters would enable measurements of intracellular accumulation by flow cytometry, a technique that can differentiate subpopulations of cells on the basis of differences in fluorescence, allowing collection of high- or low-transport activity cells. Different nucleoside transporter subtypes have been localized on the apical and basolateral membranes of some polarized epithelia (35-37) and use of fluorescent nucleosides of which FuPmR is the prototype might enable visualization of trans-epithelial nucleoside transport in a cultured epithelium.

In conclusion, we have demonstrated that an autofluorescent nucleoside analogue can be used as a tool to visualize and quantify the transport process mediated by nucleoside transporters in living cells. FuPmR enabled visualization of the intracellular fate of a nucleoside (and/or its metabolite) in living cells for the first time. However, this analogue has limitations and must be regarded as a complement to existing tools for

nucleoside transporter studies. The excitation peaks of both analogs are at 280 nm. UV excitation is not widely available for confocal laser scanning microscopy. Most optics for light microscopy have poor transmission in the UV range. More importantly, UV excitation is highly phototoxic to living cells and excitation around 351 nm generates considerable auto-fluorescence from excitation of many biomolecules (e.g., NADH, NADHP, Lipofuscin and nucleic acids, etc.). Ongoing efforts are focused on the design of highly sensitive fluorescent nucleoside probes with different excitation/emission spectra and unique permeant/inhibitor properties that will allow real-time, multicolor analysis of different nucleoside transporter subtypes in living cells.

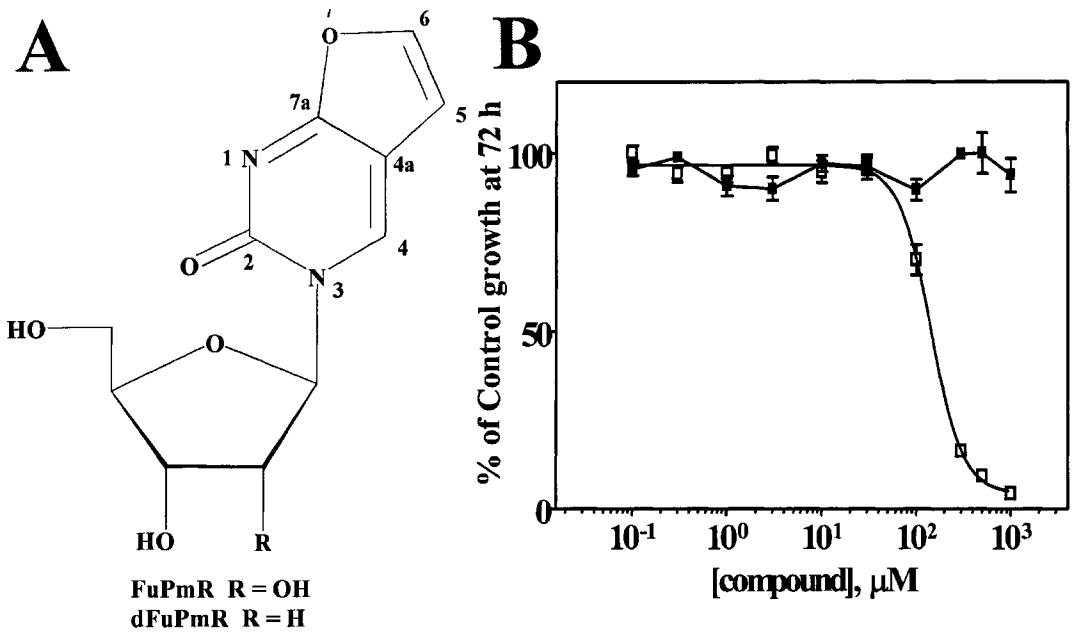

Figure 5-1 Structures and cytotoxicities of FuPmR and dFuPmR.

A. Chemical structures of 3-(β-D-ribofuranosyl)furo[2,3-*d*]pyrimidin-2(3*H*)-one (FuPmR) and 3-(2-deoxy-β-D-*erythro*-pentofuranosyl)furo[2,3-*d*]pyrimidin-2(3*H*)-one (dFuPmR). B. Growth-inhibitory effects of FuPmR and dFuPmR on BeWo cells. Actively proliferating cells were incubated at 37°C with graded concentrations of FuPmR (open squares) or dFuPmR (closed squares) for 72 h after which the MTT assay was conducted as described in *Materials and Methods*. Representative cytotoxicity relationships are shown; each data point represents the mean ± S.E. of six determinations and error bars are not shown where they are smaller than the symbol. IC_{50} values (given in the text) were obtained from the MTS-cytotoxicity relationships (means of at least three independent experiments).

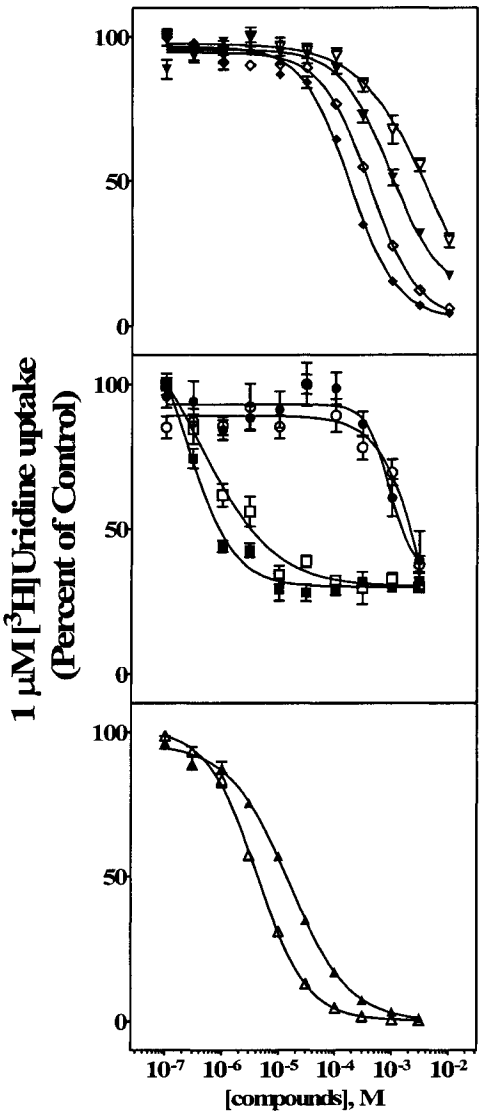

Figure 5-2 Inhibition of Urd uptake in yeast producing recombinant human nucleoside transporters by FuPmR or dFuPmR.

The uptake of 1 μM [^{3}H]Urd into yeast producing the appropriate recombinant human nucleoside transporter was measured at room temperature over 20 min (hENT1/2 and hCNT1/2) or 5 min (hCNT3) in the presence or absence of graded concentrations of FuPmR (open symbols) or dFuPmR (closed symbols) as described in *Material and Methods*. The nucleoside transporters were hENT1 (◆,◇), hENT2 (▼,▽), hCNT1 (■,□), hCNT2 (●,○) and hCNT3 (▲,△). Uptake values in the presence of FuPmR or dFuPmR are given as the percentage of uptake values in their absence.

Figure 5-3 Analysis of transport of FuPmR and dFuPmR by hCNT1, hCNT2 and hCNT3.

A. Representative sodium and proton currents in the presence of FuPmR or dFuPmR. Oocytes were injected with 10 nl of water alone (control) or that contained 10 ng of hCNT1, hCNT2 or hCNT3 transcripts as described in *Materials and Methods*. Currents were generated by perfusing individual oocytes producing either hCNT1, 2 or 3 with either 100 μM FuPmR or 100 μM dFuPmR in the appropriate transport media. The currents produced by 100 μM Urd in sodium-containing medium are shown for comparison. The same experiment was performed in a control water-injected oocyte (bottom panel). **B. Mean sodium and proton currents induced by Urd, FuPmR and dFuPmR.** Currents were generated as described for Panel A in sodium-containing (pH 8.5) or sodium-free (pH 7.5 or pH 5.5) media. Values are means ± S.E. for three different oocytes. The same experiment was also performed in control water-injected oocytes (data not shown); no inward currents were generated.

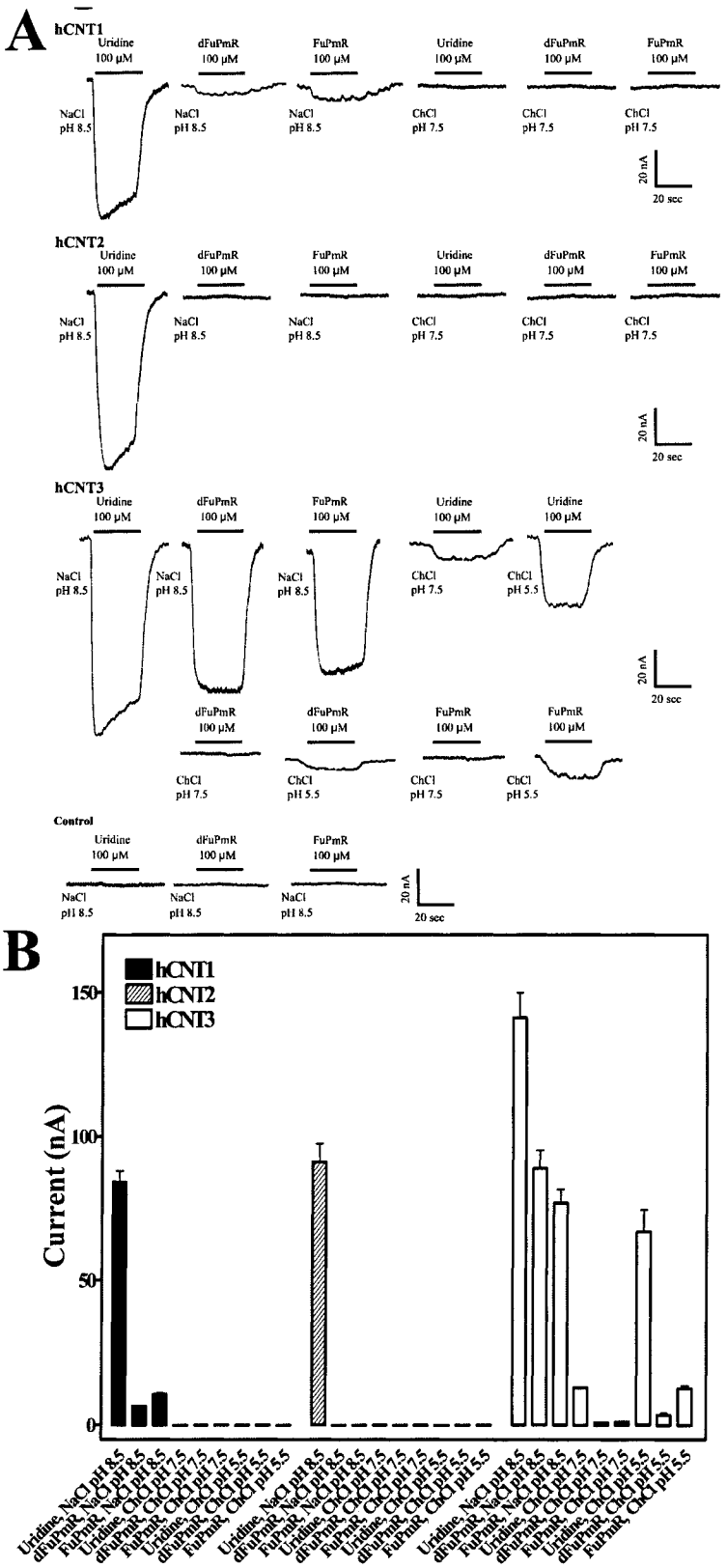

Figure 5-4 Live cell imaging of FuPmR uptake into BeWo cells.

A. Time-lapse series of images before and after the addition of FuPmR. BeWo cells were labeled with 0.1 μM MitoTracker orange (shown in red channel) at 37°C for 30 min, washed three times with PBS and then incubated with 500 μM FuPmR (shown in green channel) for 1 h. Images were taken before adding FuPmR (first column) and every three sec for the first 300 sec and every 60 sec until 1 h after the addition of FuPmR. Time in sec is shown in the upper left corner. **B. Representative time courses of FuPmR uptake.** The whole-cell fluorescence intensities of FuPmR (green line) and MitoTracker orange (red line) and the extracellular fluorescence intensities of FuPmR (blue line) at different time points were measured from eight cells and one extracellular region (similar in size as a cell), respectively, and the resulting mean values (± S.E.) were plotted against time. Each value for whole-cell fluorescence intensity is the mean ± S.E. of eight determinations and S.E. values are not shown where they were smaller than the data points. The left graph shows the time courses for the first 120 sec of the right graph.

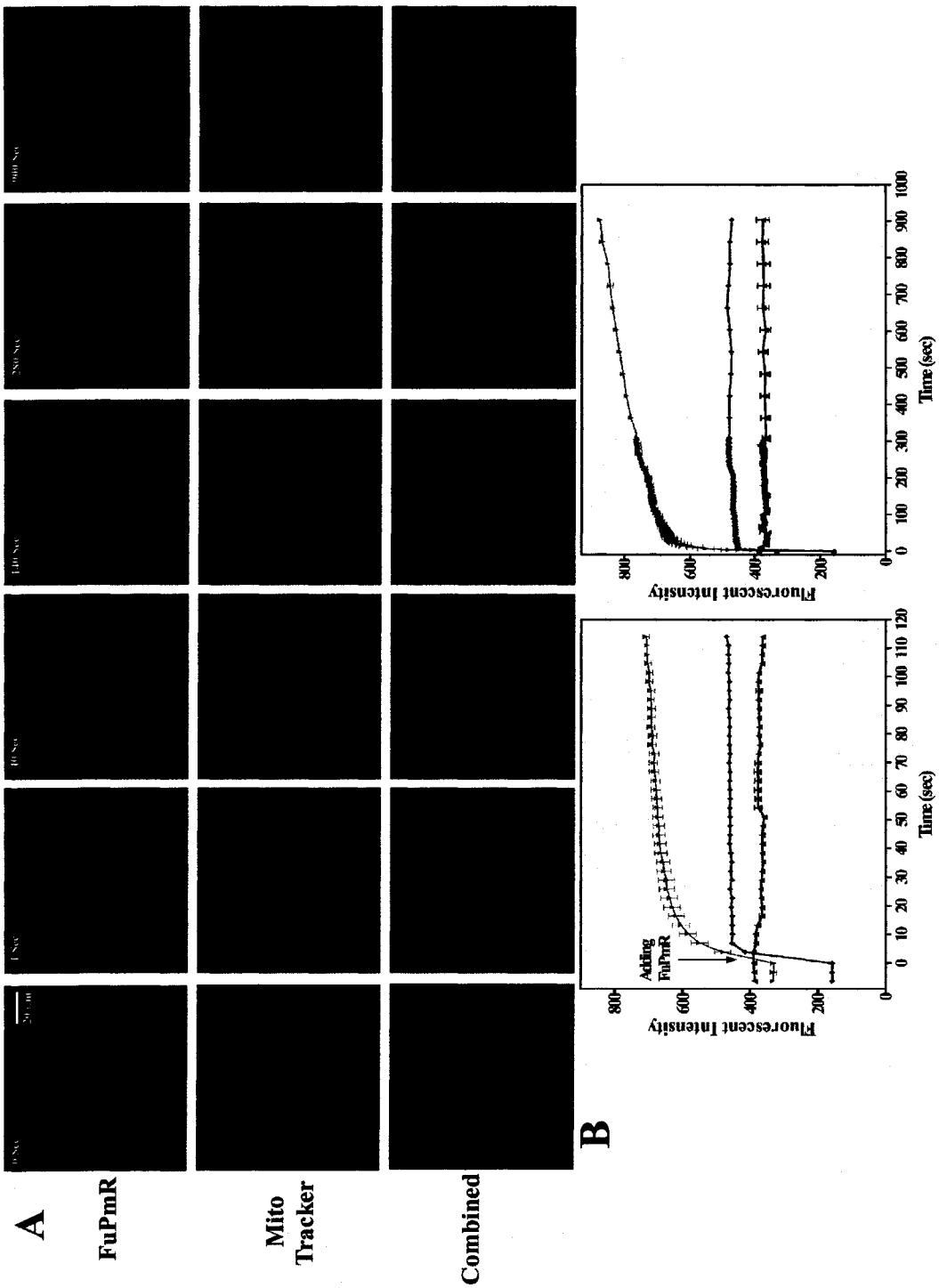

Figure 5-5 Use of live cell imaging to quantify rates of FuPmR transport into BeWo cells.

A. FuPmR accumulation into BeWo cells in the presence or absence of 5 μM NBMPR. Images were taken before and 180 sec after the addition of 500 μM FuPmR to BeWo cells as described in *Materials and Methods*. **B. Representative time courses used to calculate initial rates of FuPmR uptake.** To calculate the initial rates of FuPmR uptake, time zero was set at the point of adding 500 μl of either 250 or 500 μM FuPmR to the well, the bottom of which was a coverslip with adhered BeWo cells. Fluorescent intensities were measured and expressed as the percent of the highest uptake value (100%) during the first uptake stage. Values are means for four different determinations; S.E. are not shown. **C. Effects of ENT inhibitors on initial rates of FuPmR uptake.** The initial rates were calculated from time courses of uptake of various concentrations of FuPmR (closed bars) or 500 μM FuPmR together with either dipyridamole, dilazep or NBMPR at the concentrations indicated (open bars). **D. Initial rates of fluorescent intensity changes in cytoplasmic, mitochondrial and nuclear regions.** Fluorescence intensities were measured in different regions of the same cell during exposure to 500 μM FuPmR and initial rates were obtained as described in panel B. Values are means for three or four different determinations; S.E. are not shown.

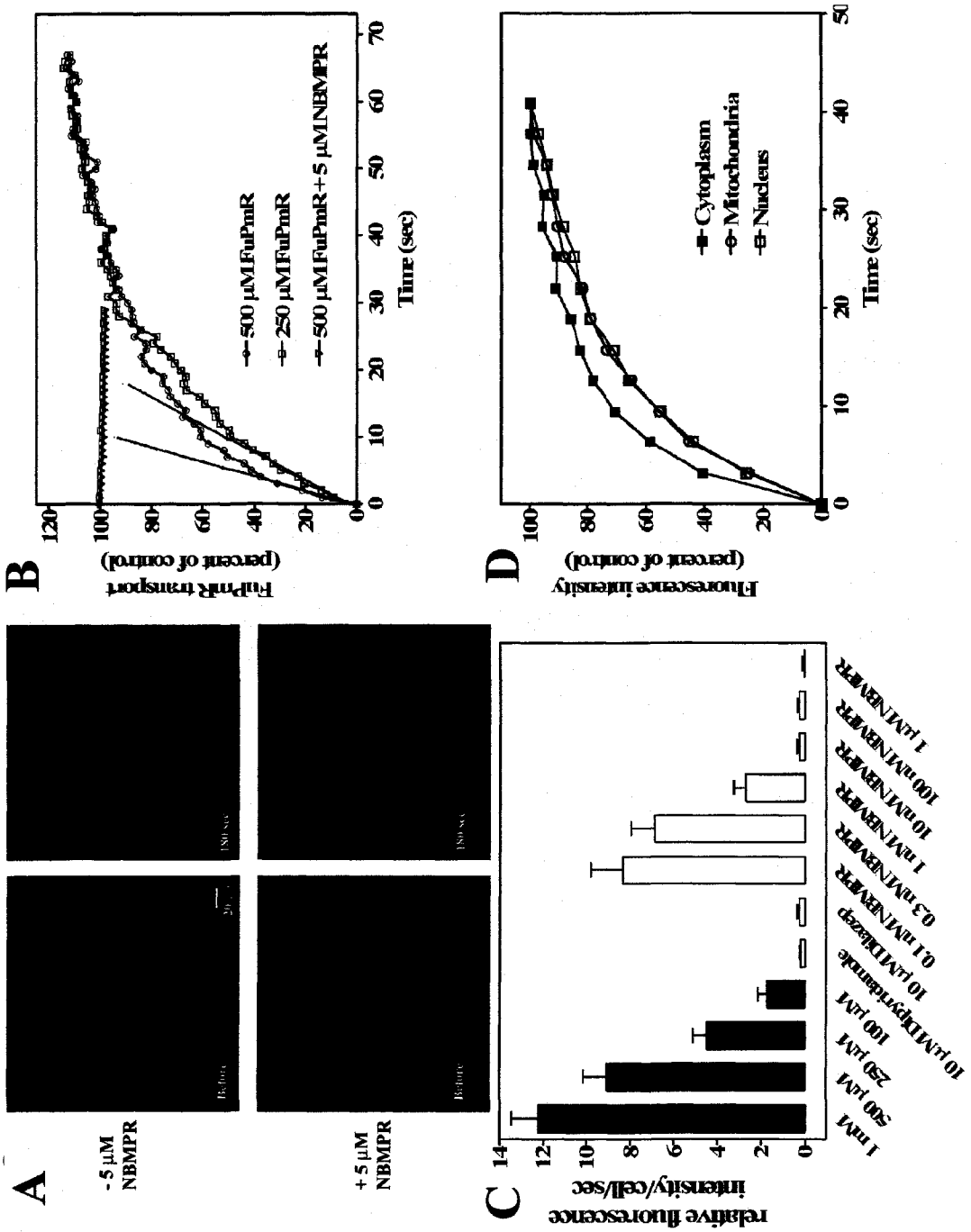

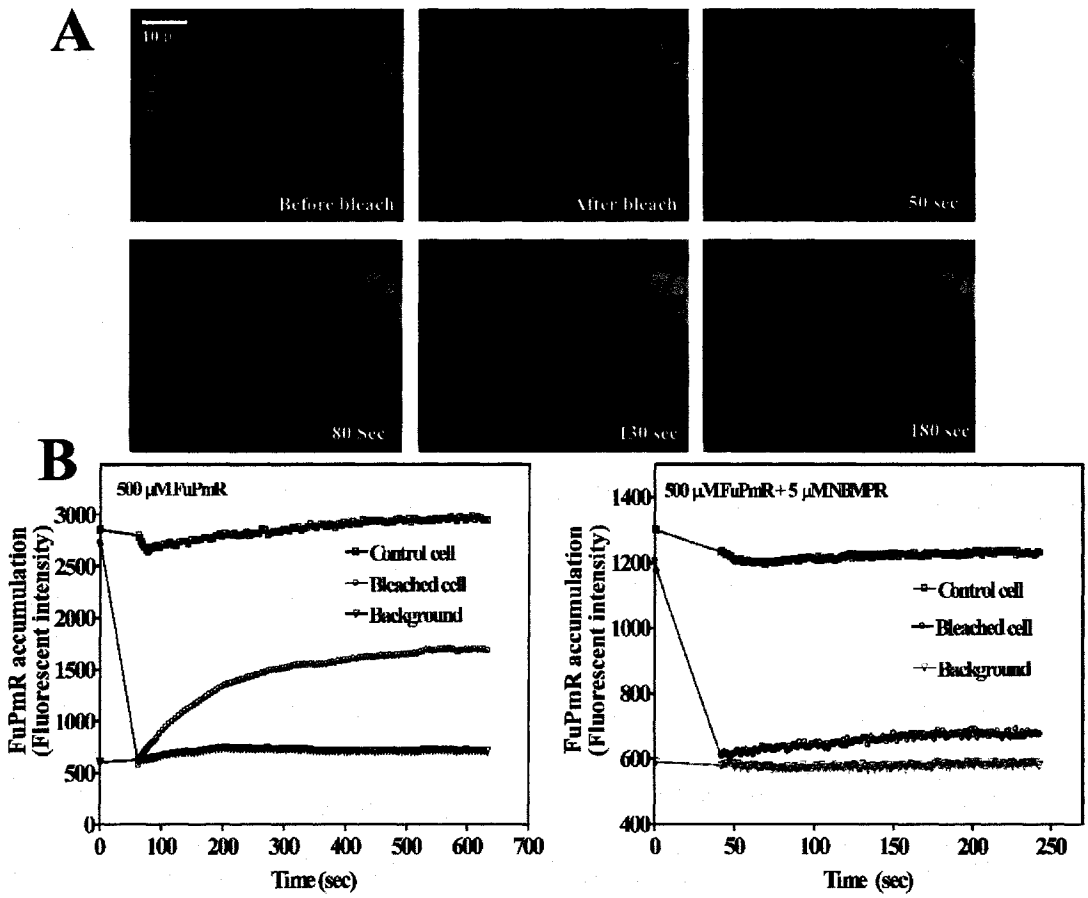

Figure 5-6 FRAP analysis of FuPmR movement into BeWo cells.

A. Time-lapse image capturing of BeWo cells before and after photobleaching. BeWo cells were incubated with 500 μM FuPmR for 30 min and two pre-bleach images were taken, after which the region of interest was bleached using full laser power at wavelengths of 350 and 360 nm for 10 iterations; the fluorescence recovery was monitored immediately after bleaching by time-lapse imaging with one sec/frame over 600 sec. **B. Quantitative analysis of FRAP experiments.** Fluorescence intensities before and after bleaching of the bleached cell and a nearby control cell were measured using Zeiss LSM software as described in *Materials and Methods*. FRAP curves were obtained from BeWo cells incubated with 500 μM FuPmR in the absence (left graph) and presence (right graph) of 5 μM NBMPR.

References

1. Cass, C. E. (1995) in *Drug Transport in Antimicrobial and Anticancer Chemotherapy* (Georgopapadakou, N. H., ed), pp. 403-451, Marcel Deker, New York, NY
2. Cass, C. E., Young, J. D., Baldwin, S. A., Cabrita, M. A., Graham, K. A., Griffiths, M., Jennings, L. L., Mackey, J. R., Ng, A. M. L., Ritzel, M. W. L., Vickers, M. F., and Yao, S. Y. M. (1999) in *Membrane Transporters as Drug Targets* (Amidon, G. L., and Sadee, W., eds) Vol. 12, 1 Ed., pp. 313-352, 12 vols., Kluwer Academic/Plenum Publishers
3. Edwards, A. M., Arrowsmith, C. H., Christendat, D., Dharamsi, A., Friesen, J. D., Greenblatt, J. F., and Vedadi, M. (2000) *Nat Struct Biol* **7 Suppl**, 970-972.
4. Coe, I. R., Griffiths, M., Young, J. D., Baldwin, S. A., and Cass, C. E. (1997) *Genomics* **45**, 459-460
5. Acimovic, Y., and Coe, I. R. (2002) *Mol Biol Evol* **19**, 2199-2210
6. Baldwin, S. A., Yao, S. Y., Hyde, R. J., Ng, A. M., Foppolo, S., Barnes, K., Ritzel, M. W., Cass, C. E., and Young, J. D. (2005) *J Biol Chem*
7. Hyde, R. J., Abidi, F., Griffiths, M., Yao, S. Y. M., Sundaram, M., Phillips, S. E. V., Cass, C. E., Young, J. D. (2000) *Drug Dev Res* **50**, 38
8. Baldwin, S. A., Beal, P. R., Yao, S. Y., King, A. E., Cass, C. E., and Young, J. D. (2004) *Pflugers Arch* **447**, 735-743
9. Engel, K., Zhou, M., and Wang, J. (2004) *J Biol Chem* **279**, 50042-50049
10. Ritzel, M. W., Yao, S. Y., Huang, M. Y., Elliott, J. F., Cass, C. E., and Young, J. D. (1997) *Am J Physiol* **272**, C707-714
11. Ritzel, M. W., Yao, S. Y., Ng, A. M., Mackey, J. R., Cass, C. E., and Young, J. D. (1998) *Mol Membr Biol* **15**, 203-211
12. Ritzel, M. W. L., Ng, A. M., Yao, S. Y. M., Graham, K., Loewen, S. K., Smith, K. M., Ritzel, R. G., Mowles, D. A., Carpenter, P., Chen, X., Karpinski, E., Hyde, R. J., Baldwin, S. A., Cass, C. E., and Young, J. D. (2001) *J Biol Chem* **276**, 2914-2927
13. Van Belle, H. (1993) *Cardiovasc Res* **27**, 68-76
14. Baldwin, S. A., Mackey, J. R., Cass, C. E., and Young, J. D. (1999) *Mol Med Today* **5**, 216-224

15. Mackey, J. R., Jennings, L. L., Clarke, M. L., Santos, C. L., Dabbagh, L., Vsianska, M., Koski, S. L., Coupland, R. W., Baldwin, S. A., Young, J. D., and Cass, C. E. (2002) *Clin Cancer Res* **8**, 110-116.
16. Mackey, J. R., Galmarini, C. M., Graham, K. A., Joy, A. A., Delmer, A., Dabbagh, L., Glubrecht, D., Jewell, L. D., Lai, R., Lang, T., Hanson, J., Young, J. D., Merle-Beral, H., Binet, J. L., Cass, C. E., and Dumontet, C. (2005) *Blood* **105**, 767-774
17. Mackey, J. R., Baldwin, S. A., Young, J. D., and Cass, C. E. (1998) *Drug Resistance Updates* **1**, 310-324
18. Mani, R. S., Hammond, J. R., Marjan, J. M., Graham, K. A., Young, J. D., Baldwin, S. A., and Cass, C. E. (1998) *J Biol Chem* **273**, 30818-30825
19. Lai, Y., Tse, C. M., and Unadkat, J. D. (2004) *J Biol Chem* **279**, 4490-4497
20. Zhang, J., Visser, F., Vickers, M. F., Lang, T., Robins, M. J., Nielsen, L. P., Nowak, I., Baldwin, S. A., Young, J. D., and Cass, C. E. (2003) *Mol Pharmacol* **64**, 1512-1520
21. Zhang, J., Smith, K. M., Tackaberry, T., Visser, F., Robins, M. J., Nielsen, L. P., Nowak, I., Baldwin, S. A., Young, J. D., and Cass, C. E. (2005) *Mol Pharmacol*
22. Smith, K. M., Ng, A. M., Yao, S. Y., Labedz, K. A., Knaus, E. E., Wiebe, L. I., Cass, C. E., Baldwin, S. A., Chen, X. Z., Karpinski, E., and Young, J. D. (2004) *J Physiol* **558**, 807-823
23. Boumah, C. E., Hogue, D. L., and Cass, C. E. (1992) *Biochem J* **288**, 987-996
24. Visser, F., Vickers, M. F., Ng, A. M., Baldwin, S. A., Young, J. D., and Cass, C. E. (2002) *J Biol Chem* **277**, 395-401.
25. Visser, F., Zhang, J., Raborn, R. T., Baldwin, S. A., Young, J. D., and Cass, C. E. (2005) *Mol Pharmacol* **67**, 1291-1298
26. Hamilton, S. R., Yao, S. Y., Ingram, J. C., Hadden, D. A., Ritzel, M. W., Gallagher, M. P., Henderson, P. J., Cass, C. E., Young, J. D., and Baldwin, S. A. (2001) *J Biol Chem* **276**, 27981-27988
27. Jamieson, G. P., Brocklebank, A. M., Snook, M. B., Sawyer, W. H., Buolamwini, J. K., Paterson, A. R., and Wiley, J. S. (1993) *Cytometry* **14**, 32-38

28. Wiley, J. S., Brocklebank, A. M., Snook, M. B., Jamieson, G. P., Sawyer, W. H., Craik, J. D., Cass, C. E., Robins, M. J., McAdam, D. P., and Paterson, A. R. (1991) *Biochem J* **273**, 667-672
29. Sen, R. P., Delicado, E. G., Alvarez, A., Brocklebank, A. M., Wiley, J. S., and Miras-Portugal, M. T. (1998) *FEBS Lett* **422**, 368-372
30. Gupte, A., and Buolamwini, J. K. (2004) *Bioorg Med Chem Lett* **14**, 2257-2260
31. Harley, E. R., Paterson, A. R., and Cass, C. E. (1982) *Cancer Res* **42**, 1289-1295
32. Paterson, A. R., Harley, E. R., and Cass, C. E. (1984) *Biochem J* **224**, 1001-1008
33. Barile, M., Valenti, D., Passarella, S., and Quagliariello, E. (1997) *Biochem Pharmacol* **53**, 913-920
34. Barile, M., Brizio, C., De Virgilio, C., Delfine, S., Quagliariello, E., and Passarella, S. (1997) *Eur J Biochem* **249**, 777-785
35. Lai, Y., Bakken, A. H., and Unadkat, J. D. (2002) *J Biol Chem* **277**, 37711-37717
36. Mangravite, L. M., Lipshutz, J. H., Mostov, K .E., Giacomini, K. M. (2001) *Am J Phisiol Renal Physiol* **280**, F879-885
37. Mangravite, L. M., Xiao, G., and Giacomini, K. M. (2003) *Am J Physiol Renal Physiol* **284**, F902-910
38. Robins, M. J., Barr, P. J., and Giziewicz, J. (1982) *Can. J. Chem.* **60**, 554-557
39. Robins, M. J., and Barr, P. J. (1983) *J. Org. Chem.* **48**, 1854-1862
40. Woo, J., Meyer, R. B., Jr., and Gamper, H. B. (1996) *Nucleic Acids Res.* **24**, 2470-2475
41. Pattillo, R. A., and Gey, G. O. (1968) *Cancer Res* **28**, 1231-1236
42. Cheng, Y., and Prusoff, W. H. (1973) *Biochem Pharmacol* **22**, 3099-3108
43. Visser, F., Baldwin, S. A., Isaac, R. E., Young, J. D., and Cass, C. E. (2005) *J Biol Chem* **280**, 11025-11034

Chapter 6 Characterization of Uridine Permease, FUI1, of *Saccharomyces cerevisiae:* the transport mechanism and permeant-binding motif

Acknowledgements

Dr. Kyla Smith and Ms. Melissa Slugoski conducted the *X. laevis* current measurement experiments. Ms. Tracey Tackaberry conducted part of the yeast transport assays. Dr. Xuejun Sun contributed to this project by helping confocal image analysis. Dr. Morris Robins, Mr. Lars Nielsen and Mr. Ireneusz Nowak are the chemists who developed the series of uridine analogs. Drs. Stephen Baldwin and James Young are collaborative principle investigators who helped obtain research funding for this project and aided in manuscript preparation.

Introduction

Nucleoside transporters are integral membrane proteins that mediate the uptake and release of naturally occurring nucleosides and cytotoxic nucleoside analogs (1-4). Mammalian nucleoside transporters are classified into two structurally unrelated protein families, the concentrative and equilibrative nucleoside transporters (CNTs and ENTs) (1,2,5). Nucleoside permeation into *Saccharomyces cerevisiae* is mediated by FUI1, a permease with high specificity for uridine (Urd), which has no sequence similarities with the mammalian transporters (6,7). Although *S. cerevisiae* cells also salvage nucleobases through FUR4 (uracil permease) and FCY2 (purine-cytosine permease), they appear to lack the capacity to transport thymidine and purine nucleosides across plasma membranes (8). Whereas considerable information is available for the nucleobase transporters, FUR4 and FCY2 of *S. cerevisiae* (9-17), relatively little is known about the FUI1 protein.

FUI1 belongs to the uracil/allantoin permease family (FUR family) of yeast, which also includes FUR4, THI10 (thiamine permease) and DAL4 (allantoin permease). FUI1 (629 amino acids, 72 KDa) shares high amino acid identity (50-60%) with the other family members. The predicated topology of FUR4 consists of ten transmembrane segments (TMs) with long N- and C-terminal tails, which have been shown to be intracellular (17). It is believed that the two-dimensional FUR4 structural model could be extended to all members of the yeast uracil/allantoin permease family (14). The similarity of amino acid sequences is greatest in the putative TM segments of the four proteins. Based on the high sequence identity of FUR4 and FUI1, we hypothesized that these two transporters might have similar transport mechanisms and that FUI1 also operates as an electrogenic proton/permeant symporter. Charged amino acid residues in the membrane-spanning regions of transporters are known to play important roles in permeant binding (18,19), proton coupling (20), transporter stability and activity (21) and plasma membrane targeting (22). One charged amino acid residue in TM 4 of FUR4, K272, which is highly conserved in the uracil/allantoin permease family, was identified as a critical residue involved in uracil binding and translocation (14). The functional importance of the corresponding lysine residue of FUI1 (K288) in TM 4, and of two other charged residues in TMs 3 and 7, was investigated in the current study.

In vivo labeling of DNA using nucleosides and nucleoside analogs, such as thymidine and 5-bromo-2'-deoxyuridine (BrdUrd), has long been a cornerstone of replication studies. *S. cerevisiae* has been used extensively as a model organism in defining the genetic elements required for DNA replication. In the absence of the introduction of heterogeneous nucleoside transporters (e.g., hENT1) (23), FUI1 is the dominant route that allows entry of nucleoside and nucleoside analogs into *S. cerevisiae*. Among the nucleoside transporters identified so far, from bacteria to higher eukaryotes, only *S. cerevisiae* FUI1 mediates transport of Urd but not that of other naturally occurring pyrimidine and purine nucleosides, implying a specialized function for Urd. The abundance of FUR4 is determined by extracellular uracil availability by regulation of the efficiency of its ubiquitylation. Similarly, FUI1 was shown to be sorted for early vacuolar degradation in cells exposed to toxic levels of Urd, which indicates that extracellular Urd controls FUI1 trafficking and prevents harmful Urd uptake that results in a decrease in growth rate (24). Knowledge of the transport mechanism and permeant selectivities of FUI1 will contribute to an understanding of its physiological significance in the budding yeast, *S. cerevisiae*, one of the most important model organisms.

FUI1 orthologs of *Candida albicans* and *Candida glabrata* with high sequence identities with FUI1 of *S. cerevisiae* (>70%) were revealed from contigs of the Stanford *C. albicans* genome sequence databank and the assembled open reading frame (ORF) databank of *C. glabrata* genome (Genebank number: 50287475) (25), respectively. *C. albicans* is one of the most commonly encountered human pathogens, which causes a wide variety of infections ranging from superficial disorders in generally healthy individuals to invasive, rapidly fatal systemic infections in individuals with impaired immunity. *C. glabrata* has emerged as the second causative agent of human candidiasis worldwide, and is more resistant to drug therapy than *C. albicans*. Few classes of drugs are effective against these fungal infections, and drug efficacy is limited by toxicity and side effects. Nucleoside antibiotics, such as the nikkomycins and neopolyoxins, have been considered as candidate inhibitors of opportunistic candidal infections in AIDS and organ-transplant patients (26). Efforts to develop more effective nucleoside analogs are underway (27). Because transportability is a potential determinant of the cytotoxic

efficacy of nucleoside analog drugs, characterization of the Urd-binding profile of FUI1 will prove useful in the development of antifungal therapies with nucleoside drugs.

We report here the characterization of FUI1 in a double-permease knockout yeast strain (*fui1::HIS3*) that enabled analysis of Urd transport in a nucleoside transport-free background. FUI1 transported Urd into yeast with high affinity and high capacity in a proton-dependent manner. The roles of three charged amino acid residues (E259, K288, D474) in putative TMs 3, 4 and 7, as well as the cellular location of the mutant transporters, were investigated using site-directed mutagenesis and green fluorescent protein (GFP) tags. Of the three charged residues, only the lysine at position 288 was important for the transport capacity of FUI1. A quantitative inhibitor-sensitivity assay was used to gain an understanding of the structural regions of Urd that interact with FUI1. Knowledge of the Urd-binding motif of FUI1 will guide the design of novel antifungal nucleoside analogs that may selectively target FUI1 orthologs in pathogenic fungi.

Material and Methods

Strains and media

BY4742-YBR021W (MATα, his3, leu2, lys2, ura3, *Δfur4*), which contains a disruption in the gene encoding the endogenous uracil permease, FUR4, was purchased from the American Type Culture Collection (Manassas, VA) and used as the parental yeast strain to generate the double permease knockout strain *fui1::HIS3*, by deleting the *fui1* gene using the polymerase chain reaction (PCR)-mediated one-step gene disruption method as described previously (28). Other strains were generated by transformation of the yeast-*Escherichia coli* shuttle vector pYPGE15 (29) into *fui1::HIS3* using a standard lithium acetate method (30).

Yeast strains were maintained in complete minimal medium (CMM) containing 0.67% yeast nitrogen base (Difco, Detroit MI), amino acids (as required to maintain auxotrophic selection), and 2% glucose (CMM/GLU). Agar plates contained CMM with various supplements and 2% agar (Difco). Plasmids were propagated in *E. coli* strain

TOP10F' (Invitrogen, Carlsbad, CA) and maintained in Luria broth with ampicillin (100 μg/ml).

Plasmid construction

All oligonucleotide primers were synthesized by Invitrogen (Carlsbad, CA). For *S. cerevisiae* expression, the FUI1 open reading frames (ORFs) were amplified from vectors (pYSE2-FUI1) (6) by PCR methodology using the following primers (restriction sites underlined): 5'-XbaI-FUI1 (5'-CTG TCT AGA ATG CCG GTA TCT GAT TCT GGA TTC-3'), 3'-XhoI-FUI1 (5'-CGA CTC GAG TTA GAT ATA TCG TAT CTT TTC ATA GC-3'). For *Xenopus* oocyte expression, the following primers were used: 5'-BamHI-FUI1 (5'-GTC GGA TCC ATG CCG GTA TCT GAT TCT GGA TTC-3') and 3'-XbaI-FUI1 (5'-CGA TCT AGA TTA GAT ATA TCG TAT CTT TTC ATA G-3'). To construct GFP-tagged FUI1, the ORF of FUI1 without a stop codon was first amplified using the forward primer 5'-XbaI-FUI1 and a reverse primer which contained (3' to 5') 21 bases of homology to *fui1* and a unique tag sequence that was complementary to the first 50 nucleotides of the ORF of GFP. The C-terminal tagged FUI1-GFP was obtained by overlapping PCR using the product of the first run PCR and pGFPuv vector (Promega, Madison, WI) as templates and 5'-XbaI-FUI1 and 3'-KpnI-GFP (5'-CTG GGT ACC CTA TTT GTA GAG CTC ATC CAT GCC) as primers. GFP-ORF was also amplified by PCR using the forward and reverse primers: 5'-XbaI-GFP (5'-CGT TCT AGA ATG GCC AGC AAA GGA GAA CTT-3') and 3'-EcoRI-GFP (5'-CGT GAA TTC CTA TTT GTA GAG CTC ATC CAT GCC). The amplified ORFs were inserted into pYPGE15 (a high copy-number episomal yeast vector that expresses the inserted DNA constitutively under the transcriptional control of the phosphoglycerate kinase promoter) to generate pYPFUI1, pYPFUI1-GFP and pYPGFP or into the *Xenopus* expression vector, pGEM-HE, to generate pGEFUI1. pYPFUI1-K288A, pYPFUI1- K288E, pYPFUI1-K288R, pYPFUI1-E259A, pYPFUI1-D474A and the corresponding GFP versions were generated using the Quikchange XL Site-directed Mutagenesis Kit (Stratagene, La Jolla, CA).

The PCR reactions were performed using *Pwo* polymerase (Roche Molecular Biochemicals, Indianapolis, IN) and all constructs were verified by DNA sequencing

using an ABI PRISM 310 sequence detection system (Perkin Elmer Life Sciences, Norwalk, CT).

Nucleoside Transport in S. cerevisiae

The uptake of [^{3}H]Urd or [^{3}H]5-fluorouridine (FUrd) (Moravek Biochemicals, Brea, CA) into logarithmically proliferating yeast was measured using a cell harvester as described previously (31,32). Yeast cells containing pYPFUI1, pYPFUI1-GFP or individual mutant transporters were grown in CMM/GLU medium to A_{600} of 0.7-0.9, washed twice in fresh medium and resuspended to OD_{600} of 4.0. Transport assays were performed at room temperature at pH 4.5 unless otherwise specified by adding 50-µl portions of yeast suspensions to 50-µl portions of 2x concentrated [^{3}H]nucleoside in CMM/GLU medium in 96-well microtiter plates. Yeast cells were collected on filter mats using a Micro96 Cell Harvester (Skatron Instruments, Lier, Norway) and rapidly washed with deionized water. The individual filter circles corresponding to wells of the microtiter plates were removed from filter mats and transferred to vials for scintillation counting.

The binding of Urd and its analogs to recombinant FUI1 was assessed by measuring their abilities to inhibit inward transport of 1 µM [^{3}H]Urd in the "inhibitor-sensitivity" assay as follows. Yeast producing FUI1 were incubated with graded concentrations of Urd or Urd analogs in the presence of 1 µM [^{3}H]Urd for 30 s. Each experiment was repeated at least three times. Nonspecific radioactivity was determined in the presence of 10 mM nonradioactive Urd, and these values were subtracted from total uptake values. Data were subjected to nonlinear regression analysis using GraphPad Prism Software version 3.0 (GraphPad Software Inc., San Diego, CA) to obtain IC_{50} values (concentrations that inhibited reactions by 50%) for Urd and Urd analogs; K_i (inhibitory constant) values were determined from the Cheng-Prusoff equation (33) and the K_m values for Urd. Gibbs free energy (ΔG^0) was calculated from $\Delta G^0 = -RT\ln(K_i)$, in which R is the gas constant and T is the absolute temperature. The thermodynamic stability of transporter-inhibitor complexes was quantitatively estimated from ΔG^0 as described elsewhere (34).

Measurements of FUI1-induced H^+ currents and H^+:Urd coupling ratios

pGEFUI1 was linearized with *Nhe*1 and transcribed with T7 polymerase using the mMESSAGE mMACHINE™ (Ambion, Austin, TX) transcription system. *In vitro* synthesized transcripts were injected into isolated mature stage VI oocytes from *X. laevis* as described previously (35). Mock-injected oocytes were injected with water alone. Electrophysiology studies used transport medium composed of 100 mM ChCl, 2 mM KCl, 1 mM $CaCl_2$, 1 mM $MgCl_2$ and 10 mM Hepes (for pH values > 6.5) or 10 mM MES (for pH values ≤ 6.5). Proton-dependence was tested in ChCl-containing transport medium at pH values ranging from 4.5 to 8.5.

Urd-evoked membrane currents were measured in FUI1-producing oocytes at room temperature (20°C) using a GeneClamp 500B oocyte clamp (Axon Instruments Inc., Foster City, CA) in the two-electrode, voltage-clamp mode as described previously (35) and interfaced to an IBM-compatible PC *via* a Digidata 1200A/D converter and controlled by pCLAMP software (Version 8.0, Axon Instruments Inc.). The microelectrodes were filled with 3 M KCl and had resistances that ranged from 0.5 - 2.5 MΩ (megaohms). Oocytes were penetrated with the microelectrodes and their membrane potentials were monitored for periods of 10 - 15 min. Oocytes were discarded when membrane potentials were unstable, or more positive than -30 mV. The oocyte membrane potential was clamped at a holding potential (V_h) of -50 mV and Urd was added in the appropriate transport medium. Current signals were filtered at 20 Hz (four-pole Bessel filter) and sampled at intervals of 20 ms. For data presentation, the signals were further filtered at 0.5 Hz by the pCLAMP program suite.

The H^+/Urd coupling ratio for FUI1 was determined by simultaneously measuring H^+ currents and [^{14}C]Urd (200 μM, 1 μCi/ml, Amersham Pharmacia Biotech, NJ) uptake under voltage-clamp conditions. Individual FUI1-producing oocytes were placed in a perfusion chamber and voltage-clamped at V_h of -50 mV in choline-containing (100 mM ChCl) nucleoside-free medium (pH 5.5) for a 10-min period to monitor baseline currents. When the baseline was stable, the nucleoside-free medium was exchanged with medium of the same composition containing radiolabelled Urd. Current was measured for two min, and uptake was terminated by washing the oocyte with nucleoside-free medium until the current returned to baseline. The oocyte was then transferred to a scintillation

vial and solubilized with 1% (w/v) SDS (sodium dodecyl sulfate) for quantitation of oocyte-associated radioactivity. Urd-induced current was calculated as the difference between baseline current and total inward current. The total charge translocated into the oocyte during the uptake period was calculated from the current-time integral and correlated with the measured radiolabelled flux for each oocyte to determine the charge/uptake ratio. Basal [^{14}C]Urd uptake was determined in control water-injected oocytes (from the same donor frog) under equivalent conditions and used to correct for endogenous non-mediated nucleoside uptake over the same incubation period. Coupling ratios (± S.E.) were calculated from slopes of least-squares fits of Urd-dependent charge *versus* Urd accumulation in oocytes.

Confocal microscopy of yeast

Logarithmically growing yeast transformed with GFP-tagged vector (10 μM, A_{600} = 0 .7-0.9) were mixed with 30 μl anti-fading mounting media, smeared on a glass slide and checked for green fluorescence using the excitation wavelength of 488 nm. Confocal images were collected using a Zeiss LSM510 confocal laser scanning microscope with a 63 × 1.4 objective (plan-Apochromat) using a frame size of 512 × 512 pixels with a pixel resolution of 0.08 μm and a pixel depth of 8 bits. For qualitative fluorescence measurements, confocal images were taken using a 40 × 1.3 objective (F-Fluar) with a frame size of 1024 × 1024 pixels (pixel resolution, 0.11 μm; pixel depth, 12 bits).

Metamorph version 6.1 software (Universal Imaging Corp, Downingtown, PA) was used to measure pixel intensities of fluorescent yeast over the defined regions. The average green fluorescence intensity (defined as total intensity divided by defined region) of each yeast cell was digitalized after background subtraction. To estimate and compare the plasma membrane abundance of FUI1-GFP and the mutants, the average green fluorescence intensities of plasma membrane regions of variously transformed yeast were obtained by subtracting intracellular fluorescence intensities from the total intensities. About 100 to 150 cells per yeast strain were measured and the data were exported to GraphPad Prism version 4.0 for comparison of the relative plasma membrane abundance of FUI1-GFP and the mutants (Student's t-test).

Urd analogs

The structures of Urd and its analogs were given previously (31). The abbreviations of Urd analogs are given in Table 6-2. The Urd analogs used in this study were either obtained from R. I. Chemical, Inc. (Orange, CA) or were synthesized as described elsewhere (31). Stock solutions of test compounds were prepared in water or dimethyl sulfoxide (DMSO) (Sigma-Aldrich Canada Ltd., Oakville, ON) and the final concentration of DMSO in transport reactions was 0.1% when DMSO was used as a solvent.

Results

Transport characteristics of FUI1

At pH 4.5, transport of 1 μM [^{3}H]Urd into *fui1::HIS3* yeast that contained pYPFUI1 was rapid and linear over 90 s with a mean rate (± S.E.) of 285 ± 5 pmol/mg protein/s (Fig. 6-1, Panel A). This rate was reduced to 0.3 ± 0.1 pmol/mg protein/s in the presence of 10 mM nonradioactive Urd, indicating the presence of functional FUI1 in yeast plasma membranes. Urd transport rates were determined for all subsequent experiments using incubation periods of 30 s for recombinant FUI1 produced in yeast, thereby providing large signal-to-noise ratios while maintaining initial rates of uptake. FUrd is cytotoxic to *S. cerevisiae* (6,7)} and the evidence that the transport of FUrd into yeast is mediated by FUI1 is indirect, based on the association of resistance to FUrd with a mutation in the *fui1* gene. The time course for uptake of 1 μM [^{3}H]FUrd into *fui1::HIS3* that contained pYPFUI1 was linear for at least 10 min and exhibited an initial uptake rate of 4.0 ± 0.2 pmol/mg protein/s, 1.5% of that of Urd, indicating that FUrd is a poor permeant for FUI1. Consistent with results of a previous study (6), similar experiments with other ^{3}H-labeled nucleosides demonstrated that adenosine, inosine, guanosine, cytidine and Thd were not transported by FUI1 (data not shown).

FUI1 activity was strictly pH dependent with an optimum at pH 4-5, and the protonophore carbonyl cyanide *m*-chlorophenylhydrazone (CCCP, 400 μM) strongly inhibited Urd transport at every pH condition tested (Fig. 6-2, Panel A). FUI1-mediated

Urd transport (pH 5.0) was sensitive to CCCP in a concentration-dependent manner with a mean IC_{50} value (± S.E.) of 50 ± 4 μM (Fig. 6-2, Panel B), indicating that a proton gradient was required for FUI1 function. The transport mechanism of FUI1 was also studied in *Xenopus* oocytes producing FUI1. Fig. 6-2, Panel C illustrates the effect of an imposed H^+ gradient on Urd-evoked proton currents mediated by FUI1. Perfusion of FUI1-produing oocytes with medium containing 100 μM Urd induced net inward currents, the magnitude of which increased as the extracellular pH was lowered. Inward currents were not detected at pH 8.5, strongly supporting the notion that protons were cotransported with Urd. No currents were observed in control water-injected oocytes for any of the conditions tested.

The H^+/nucleoside stoichiometry of FUI1 was directly determined by simultaneously measuring Urd-evoked currents and [^{14}C]Urd uptake under voltage-clamp conditions. The H^+/nucleoside coupling ratio was determined in sodium-free medium (pH 5.5) at a membrane potential of -50 mV. Each data point in Fig. 6-2, panel D represents a single oocyte, and the H^+/nucleoside coupling ratio, given by the slope of the linear fit of charge (pmol) *versus* uptake (pmol) was 0.86 ± 0.09, indicating a proton to Urd stoichiometry of 1:1.

Mutational analysis of charged amino acid residues in putative TMs 3, 4 and 7

There are only three charged residues in the TM segments of the topology model of FUI1 (36). The hydrophobic locations of these charged residues suggest that they could be important in transporter structure and function. To determine the effects of mutations at the three charged amino acids in TMs 3, 4 and 7, site-directed mutagenesis was undertaken at E259, K288 and D474. All of the resulting mutants (FUI1-K288A, -K288E, -K288R, -E259A and -D474A) and their GFP fusion proteins remained functional, and some exhibited substantial changes in kinetic properties. To assess the effects of mutations on permeant transport characteristics, the apparent K_m and V_{max} values of Urd transport by yeast producing wild-type or mutant FUI1 were determined by measuring uptake rates at increasing concentrations of [^{3}H]Urd (Fig. 6-3). In all cases, Urd uptake conformed to simple Michaelis-Menten kinetics (Fig. 6-3, panel A). Wild-

type FUI1 showed a high apparent affinity and capacity for Urd uptake (K_m = 10.8 ± 0.9 μM, V_{max} = 2500 ± 60 pmol/mg protein/s; mean ± S.E., n = 3). The apparent K_m value for FUI1 reported here was lower than that reported previously (20 μM) (6), probably because the contribution to Urd uptake by uracil permease, FUR4, was avoided in the current study by using the double permease knockout strain *fui1::HIS3*.

Replacement of the acidic glutamate and aspartate residues at positions 259 and 474, respectively, with a neutral alanine residue did not change the kinetic parameters (Table 6-1), indicating that these residues in TMs 3 and 7, respectively, were not critical for Urd uptake. By contrast, the replacement of lysine at position 288 with alanine produced a mutant (FUI1-K288A) with a similar apparent K_m value and a significantly reduced V_{max} value compared to that of wild-type FUI1. The resulting transport efficiency (V_{max}/K_m) value was only 12% of that of wild-type FUI1. To determine if replacement of the positive charge of the lysine residue was responsible for the reduced transportability, further site-directed mutagenesis was carried out to analyse the function of K288. Replacement of this residue with positively charged arginine or negatively charged aspartate produced FUI1-K288R and FUI1-K288E, which displayed kinetic properties similar to those of FUI1-K288A (Fig. 6-3 and Table 6-1). This indicates that K288 is critical for maintaining the high transport efficiency of FUI1, but probably is not involved in proton binding and/or translocation, a conclusion that is supported by studies in which Urd transport was tested in buffers at different pH values (data not shown). None of the mutants showed altered pH-dependence of transport.

Detection and quantitation of GFP-tagged FUI1 and FUI1 mutants

Because some of the FUI1 mutants exhibited reduced V_{max} values for Urd in comparison with those of wild-type FUI1, the GFP tag was used to determine if impaired transporter capacity was due to changes in localization and/or abundance. FUI1-GFP and mutant FUI-GFP fusion proteins displayed similar kinetic parameters as the corresponding non-tagged proteins (data not shown), indicating that addition of a GFP tag at the C-terminal end of the transporter did not change the transport properties of FUI1 or the FUI1-mutants. As shown in Fig. 6-4, panel A, yeast producing FUI1 mutants exhibited fluorescence patterns similar to those of wild-type FUI1, which

showed plasma membrane localization and intracellular accumulations. The intracellular patterns varied from bright fluorescence areas, which might have been due to retention of over-expressed proteins in vacuoles for degradation (24), to fluorescence circles, which might have been due to the presence of the proteins in intracellular membranes. Diffuse green fluorescence was observed in yeast transformed with pYPGFP, and no fluorescence was observed in yeast transformed with the insert-free vector (pYPGE15) (Fig. 6-4, panel A).

To measure the protein abundance of recombinant FUI1 and the mutants, the fluorescence intensities of 100-150 cells per yeast strain were obtained and averaged to calculate mean fluorescence intensities (illustrated in Fig. 6-4, Panel B). The mean fluorescence intensities for either whole cells (data not shown) or for plasma-membrane regions (Fig.6-4, Panel C) were not significantly different (Student's t test, FUI1-GFP *vs* FUI1-GFP mutant, $p > 0.05$) between FUI1-GFP and each of the five mutants, indicating that replacement of the charged amino acids at the putative TM regions had little effect on either production or localization of the resulting proteins.

Interaction of Urd analogs with FUI1

To gain an understanding of the structural regions of Urd that interact with FUI1, inhibitor-sensitivity assays using Urd analogs with modifications of the base and/or sugar moieties were used as described previously in studies of recombinant human transporters produced in yeast (28,31,37). The inhibition of initial rates of Urd uptake (i.e., the transport step in the uptake process) was assumed to be competitive since (i) the inhibitors tested were close structural analogs of Urd, and (ii) FUI1 was most likely to be the only plasma-membrane protein that interacted with the potential inhibitors. Representative concentration-effect curves of some of the analogs for inhibition of FUI1-mediated Urd transport are shown in Fig. 6-5. In all cases, the Hill coefficients of the concentration-effect curves were close to −1 (mean ± S.E. = −0.9 ± 0.2), indicating a single binding site for the inhibitors. The mean K_i values (± S.E.) and the corresponding Gibbs free energy values are listed in Table 6-2.

Base modifications. There were apparent strong interactions between FUI1 and C(5) of Urd since the addition of a substituent with different sizes at the C(5) position

resulted in K_i values of over 3 mM and decreases of >12.9 kJ/mol in $\Delta G°$ values. Since 2'dUrd was a low affinity inhibitor of Urd uptake, the inability of FdUrd, BrdUrd, IdUrd, EtdUrd and Thd to inhibit Urd was likely due primarily to modifications at the C(5) position. The 3 position of the base moiety (N(3)-H) also contributed a recognition determinant for FUI1-Urd interactions since 3MeUrd did not inhibit Urd transport (K_i > 3 mM). There was a difference of over 12.9 kJ/mol binding energy relative to ΔG^0 of Urd, suggesting loss of hydrogen bonding.

Sugar modifications. The 2'-hydroxyl group appeared to be a critical determinant for high-affinity binding of Urd by FUI1 since its removal (2'dUrd) produced a difference of 8.9 kJ/mol in ΔG^0 with a 51-fold increase in K_i value, suggesting that hydrogen bonding could be important. Any further modifications at the C(2') position, *e.g.*, substitution of an azido group for a hydrogen atom at the C(2') of 2'dUrd (2'AzdUrd), addition of a methyl group (2'OMedUrd) or inversion of the orientation of the hydroxyl group (araU), dramatically reduced interactions with FUI1 (apparent affinities for 2'AzdUrd, 2'OMeUrd and araU: K_i > 3 mM).

Very strong interactions between FUI1 and the C(3')-OH moiety are apparent because removal of the 3'-hydroxyl group (3'dUrd) yielded K_i values > 3 mM, with losses of > 12.9 kJ/mol in ΔG^0, suggesting strong hydrogen bonding. Although 2'dUrd inhibited FUI1-mediated Urd transport, additional removal of the 3'-hydroxyl group (2',3'ddUrd) abolished the inhibitory effects. The contribution of the 3'-hydroxyl group as a recognition determinant for binding to FUI1 was also apparent from the effects of substitution of an azido or O-methyl group at these positions; FUI1-mediated Urd uptake remained unchanged in the presence of high concentrations of 3'AzdUrd or 3'OMeUrd. AZT, which is 3'-azido-3'-deoxythymidine, failed to inhibit FUI1-mediated Urd uptake. Although FUI1 strongly bound Urd with the 3'-hydroxyl group below the sugar ring plane, its affinity for xyloU, an epimer of Urd with the 3'-hydroxyl group oriented above the plane of the sugar ring, was markedly reduced (K_i > 3 mM). The inverted orientation of the hydroxyl group evidently produced an analog that could no longer interact with FUI1. Similarly, iPUrd failed to inhibit Urd transport as also observed with 2',3'ddUrd.

The C(5') of Urd is not part of a stringent binding motif because 5'dUrd and 5'CldUrd were both potent inhibitors with somewhat lower K_i values than Urd itself (*t*-

test, $P < 0.05$). FUI1 displayed relatively high affinities for 5'AzdUrd and 5'OMedUrd (Fig. 6-4), supplying further evidence that the 5'-hydroxyl group was not essential for FUI1-Urd interactions. Although FUI1 exhibited low apparent affinity for 2'dUrd (K_i = 520 ± 57 μM), additional removal of the 5'-hydroxyl group partially restored affinity for FUI1 (2'5'ddUrd, K_i = 144 ± 36 μM). The slightly higher binding energy of 2'5'ddUrd than 2'dUrd ($\delta(\Delta G^0)$ = -2.9 kJ/mol relative to ΔG^0 of 2'dUrd) is evidently due to energy gained by removal of the hydroxyl group at the 5' position, resulting in an analog that has a better fit in the binding pocket of FUI1. Also, inhibition of FUI1-mediated Urd transport with FUrd was barely detectable, whereas relatively high concentrations of 5-fluoro-5'dUrd (K_i = 438 ± 47 μM) did inhibit Urd transport.

Discussion

FUI1 is the primary permease involved in uptake of nucleosides into the yeast *S. cerevisiae* (37). Uracil permease, FUR4, exhibits weak transportability for Urd (Zhang J. and Cass C.E., unpublished data). Compared with other nucleoside transporters identified so far, FUI1 exhibits highly specific permeant selectivity. As a high-affinity, high-capacity transporter for Urd, FUI1 has also been suggested to mediate the uptake of the cytotoxic nucleoside analog, FUrd, and was initially discovered because a mutant selected for resistance to FUrd had lost the capacity to import FUrd and Urd (7). The current study was undertaken to characterize the transport mechanism and to identify structural determinants and Urd binding motifs of the FUI1 protein.

Results from experiments with both yeast and oocytes producing wild-type FUI1 suggested a simple proton:Urd cotransport mechanism. The optimal Urd transportability under acidic conditions and the sensitivity to proton uncoupling by CCCP suggested that FUI1 functions through a secondary active transport process. Two-electrode voltage-clamp analysis of oocytes producing recombinant FUI1 showed that proton currents induced by Urd were stimulated and inhibited by externally acidic and alkaline pH environments, respectively, and the H^+/Urd coupling ratio was 1:1. In yeast and plants, protons are likely to be the preferred coupling ions for nutrient transport, and the proton electrochemical gradient is maintained by plasma membrane H^+/ATPase (38,39).

Utilization of the transmembrane proton gradient to energize active transport has been demonstrated for other members of the FUR family of transporters (15,40), as well as ENTs of parasitic protozoa (3) and CNTs of *C. albicans and C. elegans* (41,42). In contrast, mammalian CNTs function predominantly as Na^+/nucleoside symporters, although hCNT3 is also able to utilize protons (43).

Highly conserved charged residues within TM regions of transporter proteins are likely candidates for involvement in binding and translocation of ions. According to the topology model for the FUR4 family (17), the predicted membrane segments of FUR4 contain three charged amino acid residues (E243, K272 and E539 in putative TM 3, 4 and 11, respectively) that are highly conserved in other family members of which only the lysine residue was important for activity (14). In this study, the kinetic properties of the three conserved charged amino acid residues in putative TM 3, TM 4 and TM 7 of FUI1 were characterized through mutagenesis and transport assays. The two negatively charged residues, E259 in TM 3 and D474 in TM 7, were not essential for FUI1 function since mutation to alanine had no effect on transport activity. In contrast to results obtained by mutation of the conserved lysine (K272) in TM 4 of FUR4 (*i.e.*, changes in both binding and translocation of uracil (14)), mutation of the corresponding lysine (K288) in TM 4 of FUI1 to either positively charged, negatively charged or neutral residues had no effect on the affinities but greatly decreased the V_{max} values for Urd.

The results of the GFP-tagging study established that the decreases in transport capacity of the FUI1-K288 mutants were not due to decreased abundance of the mutant proteins, relative to that of the wild-type, in yeast plasma membrane. The GFP-tagged mutant proteins also had similar cellular distribution patterns. Residue K288 *per se* is important for Urd transport capacity. K_{cat}/K_m is a measure of catalytic efficiency and $K_{cat} = V_{max}/[E]_T$, where $[E]_T$ is the amount of transporter. $[E]_T$ was similar for wild-type FUI1 and the FUI1-K288 mutants. Replacement of lysine at position 288 by arginine, glutamate or alanine affected Urd transport efficiency in a parallel manner, which suggests that this lysine plays a key role in Urd translocation.

Structural regions of the Urd molecule involved in binding to FUI1 were probed by analysis of inhibition profiles and binding energies as described previously (31,44). These regions were identified as C(3')-OH, C(5) and N(3)-H. The loss of more than 12.9

kJ/mol of Gibbs free energy when the 3'-hydroxyl and N(3)-H were modified suggested that these groups were involved in hydrogen bonding with FUI1. FUI1 also exhibited low affinities for Urd analogs with C(5) modifications. Removal of the 2'-hydroxyl group resulted in a loss of 8.9 kJ/mol of binding energy. The C(5') region in the sugar moiety did not appear to be required for Urd binding because modifications at this position did not cause substantial losses in binding energy. The unchanged (or even increased with both 2' and 5' modifications) affinities for Urd analogs with C(5') substituents indicates that this position could be modified without seriously affecting binding to FUI1.

The Urd binding motif of FUI1 exhibited both similarities and distinct differences when compared with the human members of the ENT and CNT families of nucleoside transporters. The importance of the 3'-hydroxyl group for binding interactions with the hCNTs and hENTs, which are structurally unrelated proteins, is well established (31,37,45,46). In this work, the 3'-hydroxyl was also identified as a critical functional group for nucleoside binding to FUI1. Any changes at the 3' position, including removal of the hydroxyl group or inversion of its configuration, dramatically altered the FUI1-Urd analog interactions. The C(2') position, which plays a minor or moderate role in Urd interactions with hCNT and hENT proteins, was involved in strong interactions with FUI1. Interestingly, FUI1 had no major interactions with C(5')-OH, whereas the hCNTs and hENTs interact with C(5')-OH to various degrees (28,31,37). These results suggest that new Urd analogs might be designed to specifically target fungal nucleoside transporters.

In summary, FUI1 of *S. cerevisiae* was demonstrated to be an electrogenic transporter with a H^+:Urd coupling stoichiometry of 1 :1. FUI1 mediates high-affinity transport of Urd and low, but significant, transport of the cytotoxic nucleoside analog FUrd. Structure-function studies of FUI1 revealed its Urd recognition motif, which was substantially different from those of the human nucleoside transporters (hCNTs, hENTs). This raises possibilities for the design and application of Urd analog drugs with cytotoxic substituent(s) that would be transported differentially by fungal and human nucleoside transporters. Of the three charged residues in the membrane-spanning regions of FUI1, only the lysine at position 288 was found to be important for transport of Urd. Because

all of the K288 mutants were found to be targeted to yeast plasma membranes with similar abundances, the severe impairment of transport capacity likely results from defects in the translocation process. Further studies are needed to fully elucidate the structural features of FUI1 that are critical for permeant binding and translocation.

Table 6-1 Kinetic properties of Urd transport for wild-type and mutant FUI1

FUI1	Apparent K_m	Apparent V_{max}	V_{max}/K_m
	μM	pmol/mg/s	μM/ pmol/mg/s
Wild-type	10.8 ± 0.9	2500 ± 60	232
E259A	9.2 ± 1.5	2100 ± 94	228
K288A	7.8 ± 1.1	210 ± 28	27
K288R	12.2 ± 1.5	380 ± 41	31
K288E	13.5 ± 2.0	390 ± 37	29
D474A	9.1 ± 1.3	2200 ± 88	241

The K_m and V_{max} values were determined using GraphPad Prism version 4.0 software by nonlinear regression analysis. Representative plots for Urd transport by FUI1, FUI1-K288A, FUI1- K288E, FUI1-K288R, FUI1-E259A and FUI1-D474A are shown in Fig. 6-3. The K_m, and V_{max} values shown are the means ± S.E. of three separate experiments.

Table 6-2 K_i and Gibbs free energy values for inhibition of FUI1-mediated Urd uptake in *Saccharomyces cerevisiae* by Urd analogs

Urd compounds	K_i (μM)	ΔG^0	$\delta(\Delta G^0)$
Urd	10.2 ± 0.4	26.1	0
Base modifications			
5-bromouridine (BrUrd)	> 3000$^+$		
5-fluorouridine (FUrd)	> 3000$^+$		
5-iodouridine (IUrd)	> 3000$^+$		
5-methyluridine (MeUrd)	> 3000$^+$		
3-methyluridine (3MeUrd)	> 3000*		
Sugar modifications			
2'-deoxyuridine (2'dUrd)	520 ± 57	17.2	8.9
3'-deoxyuridine (3'dUrd)	> 3000$^+$	< 13.2	> 12.9
5'-deoxyuridine (5'dUrd)	2.7 ± 0.7	29.1	-3.0
1-(β-D-arabinofuranosyl)uracil (araU)	> 3000*		
1-(β-D-xylofuranosyl)uracil (xyloU)	> 3000$^+$		
2',3'-dideoxyuridine (2',3'ddUrd)	> 3000$^+$		
2',5'-dideoxyuridine (2',5'ddUrd)	144 ± 36	20.1	6.0
3',5'-dideoxyuridine (3',5'ddUrd)	> 3000$^+$		
2'-*O*-methyluridine (2'OMeUrd)	> 3000$^+$	< 15.8	> 8.0
3'-*O*-methyluridine (3'OMeUrd)	> 3000*		
5'-*O*-methyluridine (5'OMeUrd)	13.6 ± 3.5	25.4	0.7
2'-azido-2'-deoxyuridine (2'AzdUrd)	> 2000$^+$	< 14.1	> 12
3'-azido-3'-deoxyuridine (3'AzdUrd)	> 2000*		
5'-azido-5'-deoxyuridine (5'AzdUrd)	14.4 ± 1.9	25.3	0.8
5'-chloro-5'-deoxyuridine (5'CldUrd)	2.3 ± 0.3	29.4	-3.3
2',3'-*O*-isopropylideneuridine (iPUrd)	> 3000*		
Base & sugar modifications			
3'-azido-3'-deoxythymidine (AZT)	> 3000*		
5-bromo-2'-deoxyuridine (BrdUrd)	> 3000$^+$		
5-ethyl-2'-deoxyuridine (EtdUrd)	> 3000$^+$		
5-fluoro-2'-deoxyuridine (FdUrd)	> 3000$^+$		
5-iodo-2'-deoxyuridine (IdUrd)	> 3000$^+$		
Thymidine (Thd)	> 3000$^+$		
5-fluoro-5'-deoxyuridine	438 ± 47	17.6	8.5

[+] Inhibition of less than 50% was observed.

[*] No inhibition was observed.

The uptake of 1 μM [^{3}H]Urd into yeast (*fui1::HIS3*) expressing pYPFUI1 was measured over 30 s in the presence of graded concentrations of non-radioactive Urd or Urd analogs. IC_{50} values (mean ± S.E., n = 3-4) were determined using Graphpad Prism Version 3.0 Software and were converted to K_i values (33) using K_m values (mean ± S.E., n = 3) of 10.8 ± 0.9 μM for recombinant FUI1. Gibbs free energy (ΔG^0) was calculated from $\Delta G^0 = -RT\ln(K_i)$.

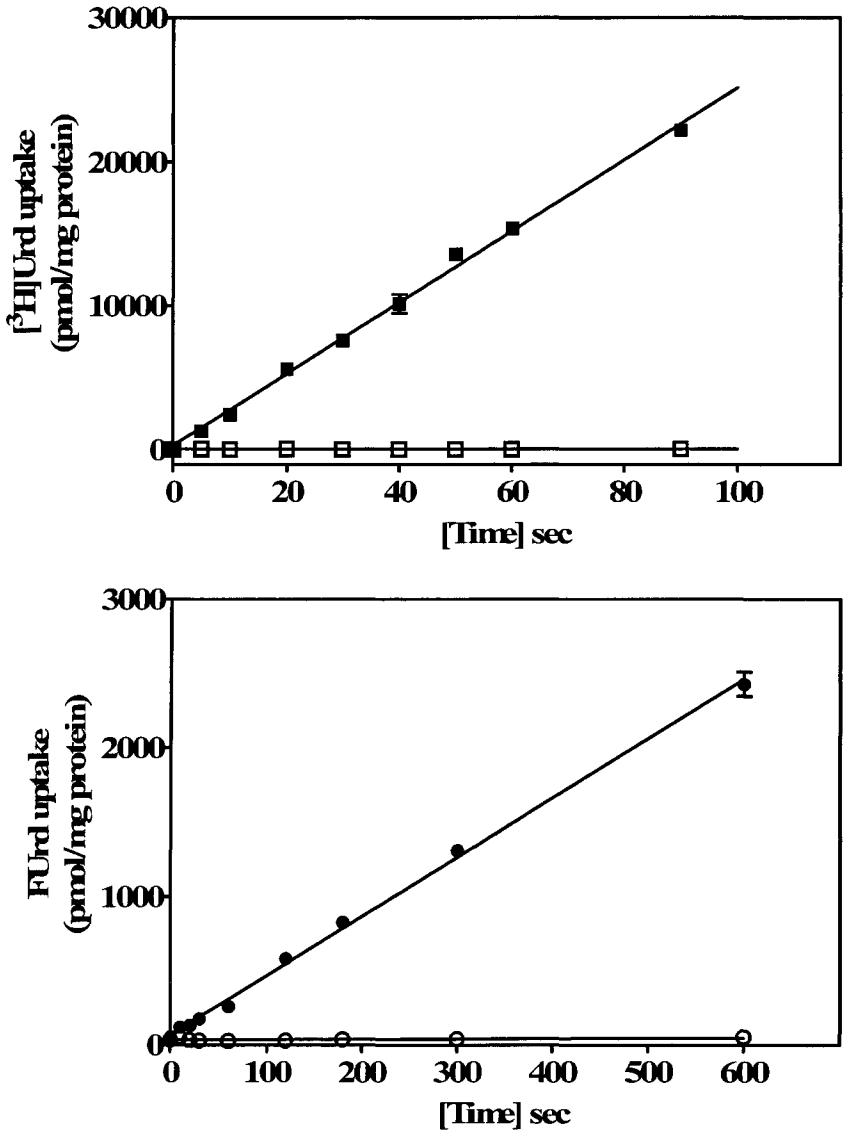

Figure 6-1 Time courses of Urd and FUrd transport into *S. cerevisiae.*

The uptake of 1 μM [^{3}H]Urd (top panel) or [^{3}H]FUrd (bottom panel) by yeast that were transformed with pYPFUI1 was measured in CMM/GLU (pH 4.5), either alone (close symbols) or with 10 mM non-radioactive Urd (open symbols). Each data point represents the means ± S.E. of eight determinations; error bars are not shown where they are smaller than the symbol. Each curve represents one of three identical experiments that gave qualitatively similar uptake rates.

Figure 6-2 The pH and proton-dependency of Urd uptake mediated by FUI1.

A. The effects of pH and CCCP on Urd transport in yeast. Uptake of [^{3}H]Urd into *fui1::HIS3* yeast producing FUI1 was measured over 30 s in transport media with different pH values in the presence (open squares) and absence (close squares) of 400 μM CCCP. Each data point represents the mean ± S.E. of eight determinations; error bars are not shown where they are smaller than the symbol. **B. Inhibitory effects of CCCP on Urd transport mediated in yeast by FUI1.** Yeast transformed with pYPFUI1 were incubated with CCCP at graded concentrations for 5 min before initiating the transport assay. The uptake of 1 μM [^{3}H]Urd into yeast was measured over a 30-s incubation period in the presence and absence of CCCP. Uptake values in the presence of CCCP are given as the percentage of uptake values in the absence of CCCP. Each data point represents the mean ± S.E. of quadruplicate determinations; error bars are not shown where they are smaller than the symbol. Three or four independent experiments gave similar results and results from representative experiments are shown. **C. Proton currents induced in oocytes by exposure of recombinant FUI1 to uridine.** Averaged inward currents in FUI1-producing oocytes perfused with 100 μM Urd in choline-containing (100 mM ChCl) transport medium (pH 8.5 - 4.5) at a membrane potential of -50 mV. Currents are means ± S.E. of five different oocytes from the same batch of cells used on the same day. No currents were observed in control water-injected oocytes. **D. Stoichiometry of H+:Urd symport by recombinant FUI1.** A plot of charge versus [14C]Urd uptake was generated with ten different FUI1-producing oocytes in transport media containing choline (100 mM ChCl) and acidified to pH 5.5 at a membrane holding potential of V_h= -50 mV. Integration of the Urd-evoked current was used to calculate the net cation influx (charge) and was correlated to the net [^{14}C]Urd influx (flux). Each closed circle represents a single oocyte. Linear regression analysis of the data is indicated by the *solid line*. The *dashed line* indicates a theoretical 1:1 charge:uptake ratio. Linear fits passed through the origin.

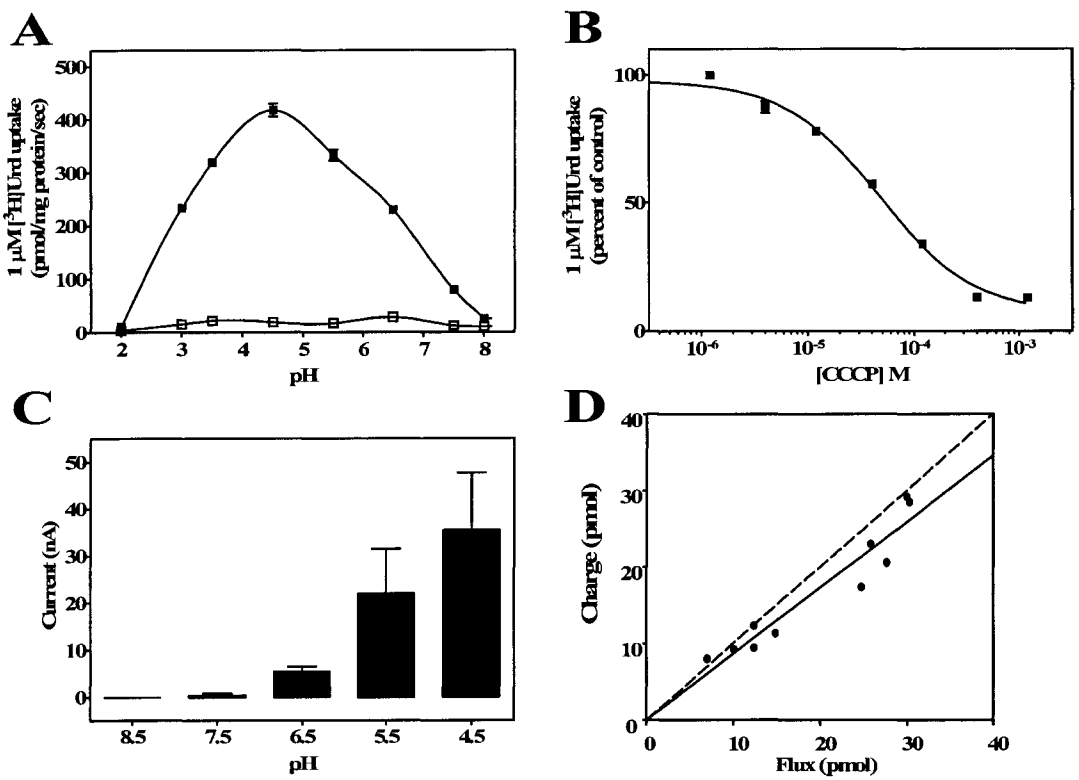

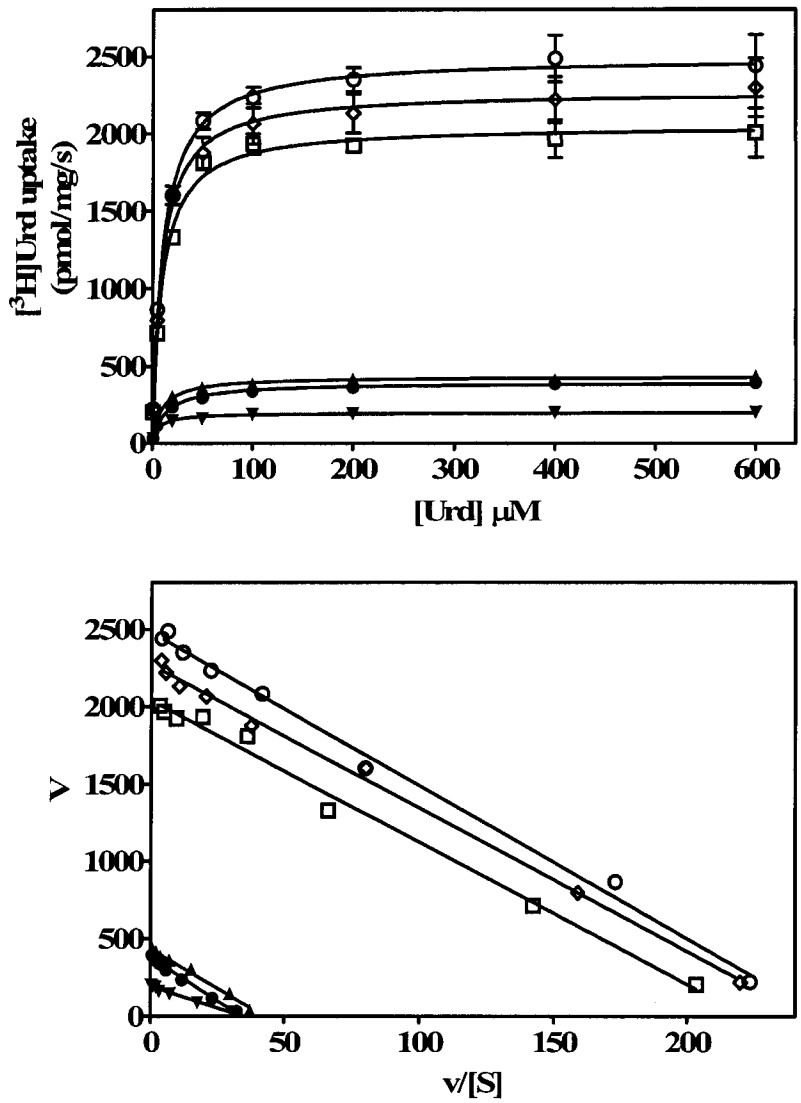

Figure 6-3 Kinetic properties of FUI1 and FUI1 mutants.

The mediated component of Urd transport (uptake rates of [^{3}H]Urd at a particular Urd concentration minus uptake rates at that concentration in the presence of 10 mM non-radioactive permeants) was plotted as a function of concentration (top panel) and subsequently converted to *V versus V/S* plots (bottom panel) to determine the kinetic constants for wild-type FUI1 (○) and the mutants, FUI1-E259A (□), FUI1-K288A (▼), FUI1-K288E (▲), FUI1-K288R (●), FUI1-D474A (◇) (PRISM, GraphPad Software). Each value is the mean ± S.E. of nine determinations and S.E. values are not shown where they were smaller than the data points.

Figure 6-4 Localization and protein abundance of wild-type FUI1-GFP and its mutants produced in *S. cerevisiae.*

A. Plasma membrane and intracellular locations of GFP-tagged FUI1 and FUI1 Mutant protein. Representative cells producing GFP alone (control) or GFP fused FUI1, FUI1-E259A, FUI1-K288A, FUI1-K288R, FUI1-K288E or FUI1-D474A were immobilized onto glass slides using polylysine and viewed under the confocal microscope. EV, empty vector, pYPGE15. **B. Method for measuring plasma membrane abundance of FUI1-GFP fusion proteins.** Metamorph version 6.1 software was used to define the plasma membrane regions and measure pixel intensities of fluorescent yeast over the defined areas. After background subtraction, the green fluorescence intensity of plasma membrane region (region between two circles) was obtained by subtracting the intracellular fluorescence intensity (region within the inner circle) from the total cellular intensity (region within the outer circle); and the average green fluorescence intensity that represented the plasma membrane abundance of each yeast cell was calculated as the resulting intensity divided by the defined region. **C. Average fluorescence intensities of yeast producing wild-type FUI1-GFP and its mutants.** The fluorescence signals for plasma membranes of 100-150 yeast cells were quantified using Metamorph version 6.1 software as described in *Materials and Methods* and the mean ± S.E. values of average fluorescence intensities were analyzed with GraphPad Prism version 4.0 software.

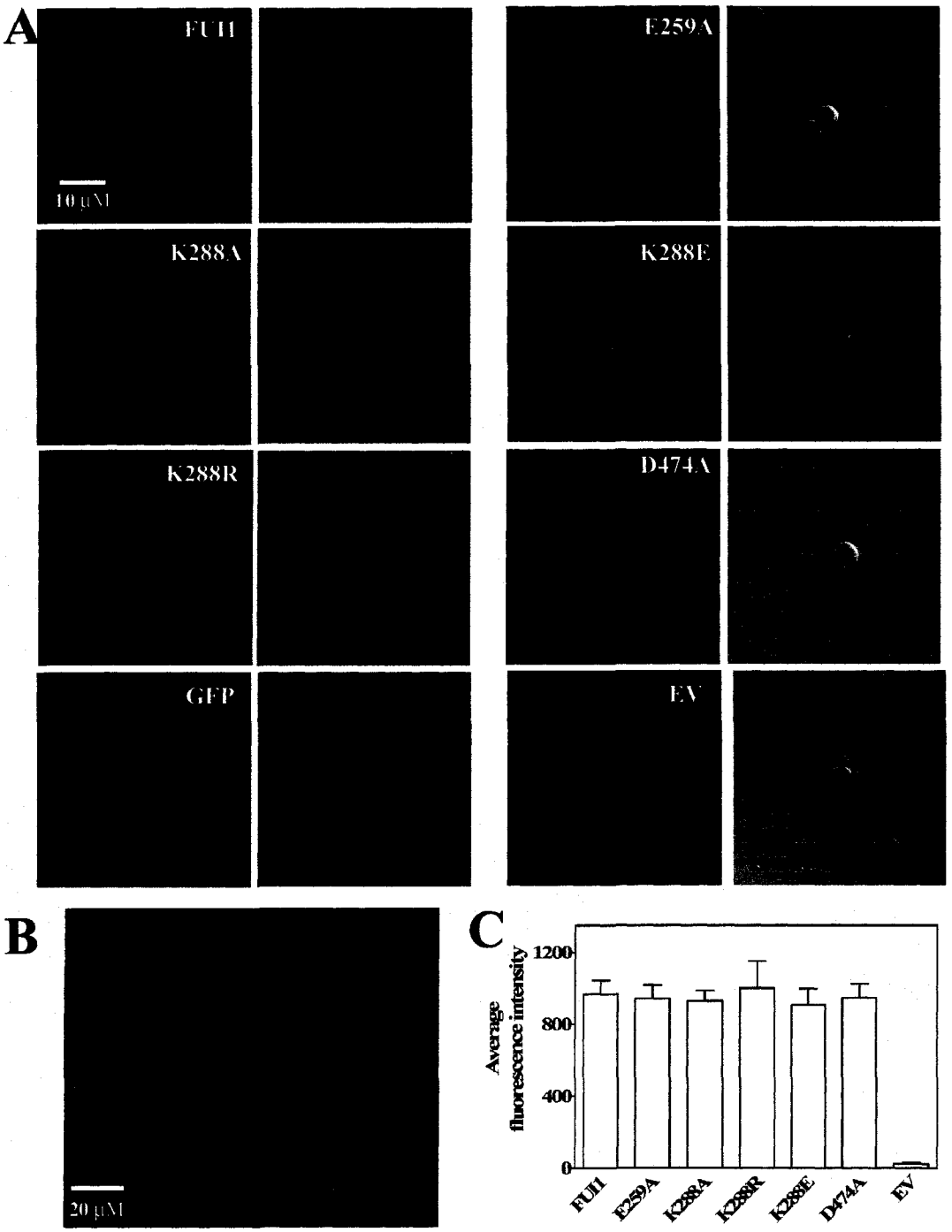

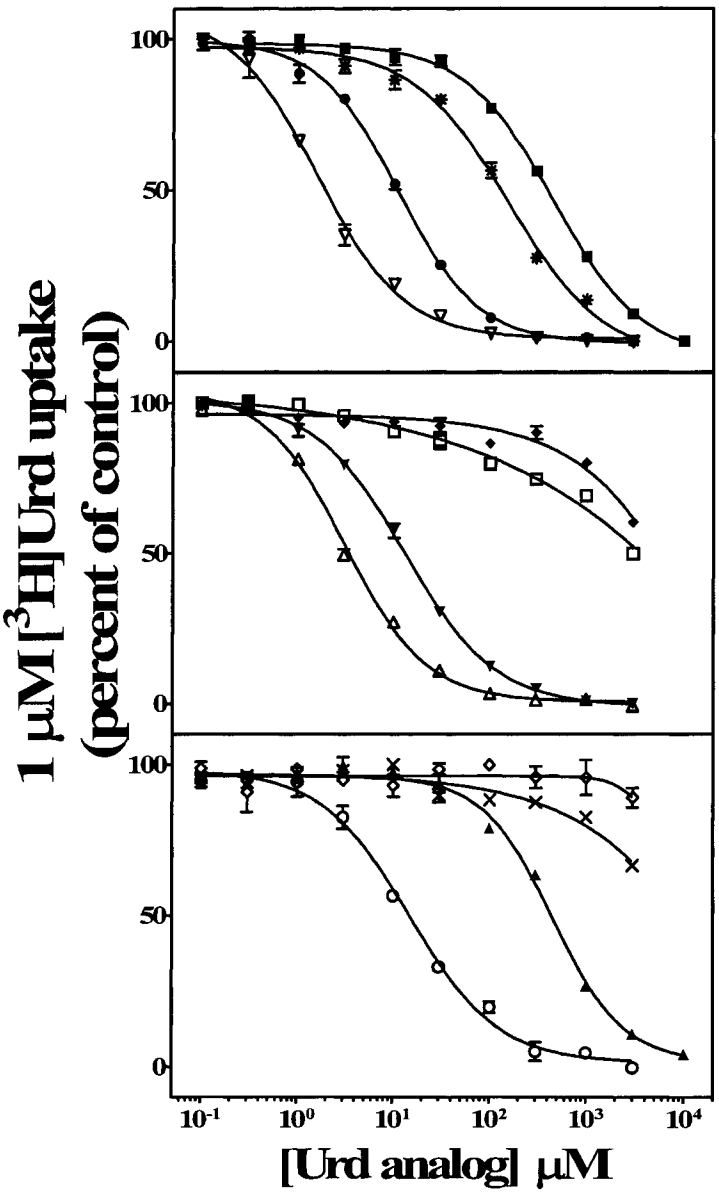

Figure 6-5 Inhibition of recombinant FUI1-mediated Urd uptake by some Urd analogs.

The uptake of 1 μM [^{3}H]Urd into *fui1::HIS3* yeast producing FUI1 was measured over a period of 30 s in the presence of graded concentrations of test compounds. The test compounds were: Urd (●), 2'dUrd (■), 5'dUrd (▽), 2'5'ddUrd (❋), 3'dUrd (□), 5'OMeUrd (▼), xyloU (◆), 5'CldUrd (△), 5'AzdUrd (○), 5-fluoro-5'dUrd (▲), 3MeUrd (◇) and FUrd (×). Uptake values in the presence of Urd compounds are given as the percentage of uptake values in their absence.

References

1. Baldwin, S. A., Mackey, J. R., Cass, C. E., and Young, J. D. (1999) *Mol Med Today* **5**, 216-224
2. Cass, C. E., Young, J. D., Baldwin, S. A., Cabrita, M. A., Graham, K. A., Griffiths, M., Jennings, L. L., Mackey, J. R., Ng, A. M. L., Ritzel, M. W. L., Vickers, M. F., and Yao, S. Y. M. (1999) in *Membrane Transporters as Drug Targets* (Amidon, G. L., and Sadee, W., eds) Vol. 12, 1 Ed., pp. 313-352, 12 vols., Kluwer Academic/Plenum Publishers
3. Landfear, S. M., Ullman, B., Carter, N. S., and Sanchez, M. A. (2004) *Eukaryot Cell* **3**, 245-254
4. Pastor-Anglada, M., Molina-Arcas, M., Casado, F. J., Bellosillo, B., Colomer, D., and Gil, J. (2004) *Leukemia* **18**, 385-393
5. Vickers, M. F., Young, J. D., Baldwin, S. A., and Cass, C. E. (2000) *Emerging Therapeutic Targets* **4**, 515-539
6. Vickers, M. F., Yao, S. Y., Baldwin, S. A., Young, J. D., and Cass, C. E. (2000) *J Biol Chem* **275**, 25931-25938
7. Wagner, R., de Montigny, J., de Wergifosse, P., Souciet, J. L., and Potier, S. (1998) *FEMS Microbiol Lett* **159**, 69-75
8. Visser, F., Zhang, J., Raborn, R. T., Baldwin, S. A., Young, J. D., and Cass, C. E. (2005) *Mol Pharmacol* **67**, 1291-1298
9. Volland, C., Garnier, C., and Haguenauer-Tsapis, R. (1992) *J Biol Chem* **267**, 23767-23771
10. Seron, K., Blondel, M. O., Haguenauer-Tsapis, R., and Volland, C. (1999) *J Bacteriol* **181**, 1793-1800
11. Volland, C., Urban-Grimal, D., Geraud, G., and Haguenauer-Tsapis, R. (1994) *J Biol Chem* **269**, 9833-9841
12. Pinson, B., Pillois, X., Brethes, D., Chevallier, J., and Napias, C. (1996) *Eur J Biochem* **239**, 439-444
13. Pinson, B., Napias, C., Chevallier, J., Van den Broek, P. J., and Brethes, D. (1997) *J Biol Chem* **272**, 28918-28924
14. Pinson, B., Chevallier, J., and Urban-Grimal, D. (1999) *Biochem J* **339**, 37-42

15. Eddy, A. A., and Hopkins, P. (1998) *Biochem J* **336**, 125-130
16. Marchal, C., Haguenauer-Tsapis, R., and Urban-Grimal, D. (2000) *J Biol Chem* **275**, 23608-23614
17. Garnier, C., Blondel, M. O., and Haguenauer-Tsapis, R. (1996) *Mol Microbiol* **21**, 1061-1073
18. Unkles, S. E., Rouch, D. A., Wang, Y., Siddiqi, M. Y., Glass, A. D., and Kinghorn, J. R. (2004) *Proc Natl Acad Sci U S A* **101**, 17549-17554
19. Muth, T. R., and Schuldiner, S. (2000) *Embo J* **19**, 234-240
20. Grewer, C., Watzke, N., Rauen, T., and Bicho, A. (2003) *J Biol Chem* **278**, 2585-2592
21. Kaback, H. R. (1997) *Proc Natl Acad Sci U S A* **94**, 5539-5543
22. Arastu-Kapur, S., Ford, E., Ullman, B., and Carter, N. S. (2003) *J Biol Chem* **278**, 33327-33333
23. Vernis, L., Piskur, J., and Diffley, J. F. (2003) *Nucleic Acids Res* **31**, e120
24. Blondel, M. O., Morvan, J., Dupre, S., Urban-Grimal, D., Haguenauer-Tsapis, R., and Volland, C. (2004) *Mol Biol Cell* **15**, 883-895
25. Dujon, B., Sherman, D., Fischer, G., Durrens, P., Casaregola, S., Lafontaine, I., De Montigny, J., Marck, C., Neuveglise, C., Talla, E., Goffard, N., Frangeul, L., Aigle, M., Anthouard, V., Babour, A., Barbe, V., Barnay, S., Blanchin, S., Beckerich, J. M., Beyne, E., Bleykasten, C., Boisrame, A., Boyer, J., Cattolico, L., Confanioleri, F., De Daruvar, A., Despons, L., Fabre, E., Fairhead, C., Ferry-Dumazet, H., Groppi, A., Hantraye, F., Hennequin, C., Jauniaux, N., Joyet, P., Kachouri, R., Kerrest, A., Koszul, R., Lemaire, M., Lesur, I., Ma, L., Muller, H., Nicaud, J. M., Nikolski, M., Oztas, S., Ozier-Kalogeropoulos, O., Pellenz, S., Potier, S., Richard, G. F., Straub, M. L., Suleau, A., Swennen, D., Tekaia, F., Wesolowski-Louvel, M., Westhof, E., Wirth, B., Zeniou-Meyer, M., Zivanovic, I., Bolotin-Fukuhara, M., Thierry, A., Bouchier, C., Caudron, B., Scarpelli, C., Gaillardin, C., Weissenbach, J., Wincker, P., and Souciet, J. L. (2004) *Nature* **430**, 35-44
26. Kimura, K., and Bugg, T. D. (2003) *Nat Prod Rep* **20**, 252-273
27. Rapp, R. P. (2004) *Pharmacotherapy* **24**, 4S-28S; quiz 29S-32S

28. Zhang, J., Smith, K. M., Tackaberry, T., Visser, F., Robins, M. J., Nielsen, L. P., Nowak, I., Karpinski, E., Baldwin, S. A., Young, J. D., and Cass, C. E. (2005) *Mol Pharmacol* **68**, 830-839
29. Brunelli, J. P., Pall, M.L. (1993) *Yeast* **9**, 1309-1318
30. Ito, H., Fukuda, Y., Murata, K., and Kimura, A. (1983) *J Bacteriol* **153**, 163-168
31. Zhang, J., Visser, F., Vickers, M. F., Lang, T., Robins, M. J., Nielsen, L. P., Nowak, I., Baldwin, S. A., Young, J. D., and Cass, C. E. (2003) *Mol Pharmacol* **64**, 1512-1520
32. Visser, F., Baldwin, S. A., Isaac, R. E., Young, J. D., and Cass, C. E. (2005) *J Biol Chem* **280**, 11025-11034
33. Cheng, Y., and Prusoff, W. H. (1973) *Biochem Pharmacol* **22**, 3099-3108
34. de Koning, H. P., and Jarvis, S. M. (2001) *Acta Trop* **80**, 245-250.
35. Smith, K. M., Ng, A. M., Yao, S. Y., Labedz, K. A., Knaus, E. E., Wiebe, L. I., Cass, C. E., Baldwin, S. A., Chen, X. Z., Karpinski, E., and Young, J. D. (2004) *J Physiol* **558**, 807-823
36. de Montigny, J., Straub, M. L., Wagner, R., Bach, M. L., and Chevallier, M. R. (1998) *Yeast* **14**, 1051-1059
37. Vickers, M. F., Zhang, J., Visser, F., Tackaberry, T., Robins, M. J., Nielsen, L. P., Nowak, I., Baldwin, S. A., Young, J. D., and Cass, C. E. (2004) *Nucleosides Nucleotides Nucleic Acids* **23**, 361-373
38. Serrano, R. (1984) *Curr Top Cell Regul* **23**, 87-126
39. Serrano, R., Kielland-Brandt, M. C., and Fink, G. R. (1986) *Nature* **319**, 689-693
40. Hopkins, P., Chevallier, C., Jund, R., and Eddy, A. A. (1988) *FEMS Microbiol. Lett.* **49**, 173-177
41. Slugoski, M. D., Loewen, S. K., Ng, A. M., Baldwin, S. A., Cass, C. E., and Young, J. D. (2004) *Yeast* **21**, 1269-1277
42. Xiao, G., Wang, J., Tangen, T., and Giacomini, K. M. (2001) *Mol Pharmacol* **59**, 339-348
43. Ritzel, M. W., Ng, A. M., Yao, S. Y., Graham, K., Loewen, S. K., Smith, K. M., Hyde, R. J., Karpinski, E., Cass, C. E., Baldwin, S. A., and Young, J. D. (2001) *Mol Membr Biol* **18**, 65-72

44. Wallace, L. J., Candlish, D., and De Koning, H. P. (2002) *J Biol Chem* **277**, 26149-26156
45. Vickers, M. F., Kumar, R., Visser, F., Zhang, J., Charania, J., Raborn, R. T., Baldwin, S. A., Young, J. D., and Cass, C. E. (2002) *Biochem Cell Biol* **80**, 639-644
46. Patil, S. D., Ngo, L. Y., and Unadkat, J. D. (2000) *Cancer Chemother Pharmacol* **46**, 394-402

Chapter 7 General Discussion

Uridine binding motifs

Many studies have shown that the presence of nucleoside transporter proteins in cell membranes is essential for cellular uptake of most nucleosides and that cells that lack functional nucleoside transporters are resistant to many cytotoxic nucleoside drugs. A major applied goal of my research was to use knowledge of mechanisms of nucleoside transport process to improve the utilization of nucleosides as anticancer and antiviral drugs. In this thesis, I used recombinant-protein expression systems in yeast to assess the ability of nucleoside analogs as either permeants or inhibitors to develop "transportability guidelines" for use in the development of nucleoside-based therapies.

Uridine (Urd) analogs were specifically prepared by Dr. M. J. Robins (Brigham Young University) to enable systematic analysis of structural determinants in the sugar moiety for interaction with the individual nucleoside transporters. hCNT1, hCNT2 and hCNT3 exhibit different functional characteristics and a better understanding of their permeant selectivities is critical for development of nucleoside analog drugs with optimal pharmacokinetic properties. The modeling of the transporter recognition motifs (Fig. 7-1) of the transporters reported in this thesis enabled predictions of transporter affinities that will guide the design of novel nucleoside compounds for drugs that may selectively target specific nucleoside transporter isoforms.

hCNT1, hCNT2 and hCNT3 recognized Urd through distinguishable binding motifs. hCNT1 was sensitive to modifications at C(3'), less sensitive at C(5') or N(3), and much less sensitive at C(2'). hCNT2 was sensitive to modifications at C(3') and C(5') and less sensitive at N(3), C(2') and C(5). hCNT3 was sensitive to modifications at C(3'), but much less sensitive at N(3), C(5') or C(2'). The changes of binding energy between transporter proteins and different Urd analogs suggested that hCNT1 and hCNT2 formed H-bonds with C(3')-OH, C(5')-OH or N(3)-H of Urd, but not with C(2')-OH, whereas hCNT3 formed H-bonds to C(3')-OH, but not to N(3)-H, C(5')-OH and C(2')-OH. The C(2') and C(5) regions of Urd played minor but significant roles for Urd-hCNT2 binding, possibly through Van der Waals interactions. All transporters barely tolerated modifications at C(3') or inversion of configurations at C(2') or C(3'). The binding profiles identified in this study can be used to predict the potential transportability of

nucleoside analogs, including anti-cancer or antiviral nucleoside drugs, by hCNT1, hCNT2 and hCNT3.

Because hCNT1, 2 and 3 share high protein sequence identities yet appear to bind Urd via different mechanisms, it should be informative to exploit the difference in Urd binding among these three proteins via chimera approaches. Instead of substituting large regions between any two transporters that may nonspecifically alter the tertiary structure of the protein to produce "artificial" effects, substituting of individual TMs might better define their involvement, leading to identification of individual residues responsible for the binding differences.

Although the structural regions of Urd involved in binding to yeast Urd permease FUI1 share similarities with those of human nucleoside transporters, distinguishable features of FUI1-Urd interactions were observed. Analysis of the binding energies between FUI1 and different Urd analogs suggested that FUI1 interacts with C(3')-OH, C(2')-OH, C(5)-H and N(3)-H of Urd. FUI1 barely tolerated modifications at C(3'), C(5) and N(3) or inversion of configurations at C(2') or C(3'). FUI1 was sensitive to modifications at C(3'), C(5) and N(3), less sensitive at C(2'), and not sensitive at C(5'). The possible H-bond interaction of FUI1-Urd at C(2') is a unique feature of FUI1 since the C(2') position was relatively unimportant for most human nucleoside transporters (1) (chapter 2 and 3). The 3'-hydroxyl group, however, remains as the only important determinant for high-affinity binding for all transporters tested. The requirement for the 3'-hydroxyl group suggests a strong evolutionary pressure to maintain a permeant binding site for C(3')-OH. Multiple regions are required for direct or indirect FUI1 interactions with Urd, suggesting that the Urd-binding pocket of FUI1 is highly specific and has limited selectivity for Urd analogs. The different Urd binding motifs observed between yeast and human nucleoside transporters should allow selective uptake of Urd analogs by either transporter. The binding profiles identified for FUI1 can be used to predict the potential transportability of nucleoside analogs and direct the design and application of nucleoside analogs for anti-fungal therapy.

Uridine transportability determinants

The therapeutic index of antimetabolite nucleoside analogs is in large part determined by the extent to which they are selectively accumulated by the target cell. Although several pharmacological studies involving various nucleoside analog drugs have been undertaken, no systematic studies of the nucleoside analog translocation abilities of individual hCNT protein have been published. The studies of Chapter 3 provided insight into the molecular determinants of Urd transportability of the hCNT family proteins.

Since the yeast assay only provided information about potential transportability, the permeant selectivities of recombinant hCNT1, 2 and 3 produced in oocytes of *Xenopus laevis* were investigated using a two-electrode voltage clamp assay. hCNT1-mediated transport was sensitive to modifications of the N(3), C(3') and C(5') positions of Urd. hCNT2 showed some tolerance for transporting Urd analogs with C(2') or C(5) modifications, little tolerance for N(3) modifications and no tolerance for any modifications at C(3') or C(5') of Urd. Although hCNT3 was sensitive to C(3') modifications, it transported a broad range of variously substituted Urd analogs. The transportability profiles identified in this study, which reflected well the binding profiles, should prove useful in the development of anti-cancer and antiviral therapies with nucleoside drugs that are permeants of members of the hCNT protein family.

hCNT1, hCNT2 and hCNT3 displayed key differences in their permeant recognition and selectivities, indicating differences in permeant binding and translocation sites. The models for the permeant recognition and translocation motifs for hCNT1, 2 and 3 presented in this thesis demonstrated that there is ample scope for selective uptake of Urd analogs and possibly pyrimidine nucleoside analogs by either transporter. Although the current study did not aim to identify novel nucleoside drugs, several of the compounds used in the main structural study, notably analogs with modifications at the C(3') or C(5) positions, are proven or potential anticancer and antiviral nucleoside drugs. However, most of these compounds were not high affinity permeants for human concentrative nucleoside transporters. Future studies need to extend the current approach to a large number of potential inhibitors of hCNT proteins family with the aims of

identifying the interactions between permeant and transporter binding pockets that determine permeant specificity and establishing a complete pyrimidine and purine nucleoside recognition profile for hCNT proteins.

Mutagenesis studies of hCNT3 and FUI1

An emphasis of this thesis was to identify structural determinants of human and yeast nucleoside transporters to improve the design and application of chemotherapeutic nucleoside analog drugs used in the treatment of cancer and viral diseases as well as fungal infections. The different mechanisms by which the CNT proteins interact with their permeants indicate that the geometry of their binding domains is likely to be different. Continued mutagenesis studies using chimeras, the substituted-cysteine accessibility method (SCAM) and site-directed mutagenesis should reveal the molecular basis of permeant recognition and translocation mediated by the concentrative nucleoside transporters.

To understand its Urd binding and translocation mechanisms, a cysteine-less version of hCNT3 was constructed and used for cysteine-accessibility and permeant-protection assays. Cysteine-less hCNT3, with 14 endogenous cysteine residues changed to serine, displayed wild-type properties in yeast expression system, indicating that endogenous cysteine residues are not essential for hCNT3-mediated nucleoside transport. A series of 63 cysteine-substitution mutants spanning predicted transmembrane domains (TMs) 11, 12 and 13 located in the C-terminal part of the protein were constructed and tested for accessibility to sulfhydryl-specific reagents. Mutants M496C, G498C, F563C, A594C, G598C and A606C had no detectable transport activity, indicating that a cysteine substitution at each of these positions was not tolerated. It is currently unclear whether the intolerance to cysteine substitutions at these highly conserved positions was due to effects on the permeant translocation channel.

Single cysteine mutants of hCNT3 have been assessed for their intrinsic kinetic properties and for the ability of membrane-permeant and membrane-impermeant thiol reagents to inhibit the transport of Urd. By this means we have identified a number of residues located in putative TMs 11, 12 and 13 that appear to play key roles in the

transport mechanism or lie on the pathway taken by permeants through the protein. Two functional mutants in putative TM 11 (L480C and S487C) and four in putative TM 12 (N565C, T557C, G567C and I571C) were partially inhibited by methanethiosulfonate reagent and high concentrations of Urd protected against inhibition, indicating that TMs 11 and 12 may form part of the nucleoside translocation pathway. The lack of accessibility of methanethiosulfonate reagents to the thiol groups in TM 13 mutants suggests that TM 13 is not exposed to the nucleoside translocation pathway. Furthermore, G567C, N565C and I571C mutants were only sensitive to methanethiosulfonate ethylammonium, a membrane-permeable sulfhydryl reagent, indicating that these residues were accessible from the cytoplasmic side of the membrane, providing evidence in support of the predicted orientation of TM 12 in the current putative topology model of hCNT3.

The uptake of Urd into the yeast *Saccharomyces cerevisiae* is mediated by FUI1, a Urd-specific nucleoside transporter encoded by the *fui1* gene and a member of the FUR family of permeases of yeast, which includes the uracil, allantoin and thiamine permeases. When FUI1 was produced in Urd transport-defective yeast, Urd transport was stimulated at acidic pH and sensitive to the protonophore carbonyl cyanide *m*-chlorophenylhydrazone. Electrophysiological analysis of recombinant FUI1 produced in *Xenopus* oocytes demonstrated that FUI1-mediated Urd uptake was dependent on proton cotransport with a stoichiometry of 1:1, indicating that FUI1 is a Urd/proton sympoter.

Mutagenesis analysis of three charged amino acids (E259, K288 and D474) in putative TMs 3, 4 and 7, respectively, revealed that K288 was a key residue for maintaining high transport efficiency of FUI1. No evidence was found indicating the existence of ionic interactions such as formation of salt bridges between oppositely charged residues in membrane spanning regions of FUI1 and none of the negatively charged residues appeared to be involved in any major change in the active structure because the replacement of either E259 or D474 by a neutral residue (E259A and D474A) had no effect on transport affinity and capacity. All mutations corresponding to substitutions of K288 led to severe defects in Urd uptake rates without affecting affinities, indicating that K288 was a key residue for maintaining high transport efficiency of FUI1. The severe decrease in Urd uptake capacity observed when K288

was replaced by other amino acids was not due to a failure in permease targeting to the plasma membrane, since the protein abundance and distribution patterns observed between wild type FUI1-GFP and the mutants were similar. K288 as well as TM 4 may form part of the active site of the permease, being involved in controlling of permeant turnover rate. It would be of interest to systematically investigate the role of TM 4 in Urd translocation using the SCAM approach.

Live cell imaging of FuPmR transport

To better understand nucleoside transport processes and intracellular fates of nucleosides, we have developed a pair of fluorescent nucleoside analogs, FuPmR [3-(β-D-ribofuranosyl)furo[2,3-*d*]pyrimidin-2(3*H*)-one] and dFuPmR [3-(2-deoxy-β-D-*erythro*-pentofuranosyl)furo[2,3-*d*]pyrimidin-2(3*H*)-one], that differ only in the sugar moiety (ribofuranosyl versus 2'-deoxy, respectively), for real-time analysis of nucleoside transport into living cells by confocal microscopy. The binding and transportability of the two compounds were assessed for five recombinant human nucleoside transporters (hENT1/2, hCNT1/2/3) produced in *Saccharomyces cerevisiae* and/or oocytes of *Xenopus laevis*. The ribosyl derivative (FuPmR) was used to demonstrate proof of principle in live cell imaging studies in an adherent cultured cell line (BeWo choriocarinoma) that possesses high hENT1 activity. The autofluorescence emitted from FuPmR enabled direct visualization of its movement from the extracellular medium into the intracellular compartment of live BeWo cells and this process was blocked by inhibitors of hENT1 (nitrobenzylmercaptopurine ribonucleoside, dipyridamole and dilazep). Quantitative analysis of fluorescence signals revealed two stages of FuPmR uptake: a fast first stage that represented the initial uptake rate (i.e., transport rate) followed by a slow long-lasting second stage. The accumulation of FuPmR and/or its metabolites in nuclei and mitochondria was also visualized by live cell imaging. Measurements of fluorescence intensity increases in nuclei and mitochondria revealed rate-limited processes of permeant translocation across intracellular membranes, demonstrating for the first time the intracellular distribution of nucleosides and/or nucleoside metabolites in living cells. The use of autofluorescent nucleosides in time-

lapse confocal microscopy is a novel strategy to quantitatively study membrane transport of nucleosides and their metabolites that will provide new knowledge of nucleoside biology.

The novel method presented in Chapter 6 represents a landmark study on fluorescent approaches to nucleoside, nucleic acid and transporter research that will be of interest to a large number of investigators. More sensitive compounds are being developed by Dr. Robins. We anticipate that there will be a large demand for using these autofluorescence compounds to study real-time nucleoside/nucleotide trafficking and metabolism. Similar approaches could be extended to study other types of transporters.

Future directions

The results of the studies described in this thesis led to the identification of binding and/or transportability determinants of hCNT1, hCNT2, hCNT3 and yeast Urd permease FUI1 that are critical for Urd-transporter interactions, suggesting that the different transporter proteins bind and translocate Urd differently. The finding that proton-coupled hCNT3 and sodium-coupled hCNT3 exhibited different transportability towards antiviral dideoxynucleoside analogs (2) suggested that coupling of different cations induces conformation changes of hCNT3 that have different permeant selectivities. The yeast inhibitory sensitivity assay, combined with the series of Urd analogs used in my research and mutagenesis analysis, should be applied to define the transportability of hCNT3 under different cation binding conditions. Such studies may lead to the identification of amino acid residues that are responsible for the differential permeant selectivities of sodium- or proton-coupled hCNT3 (2). Furthermore, exploitation of the different ion dependencies and differing permeant selectivities of hCNT family members should allow the identification of regions of the transporters involved in permeant/ion recognition.

Alternatively, the amino acid(s) specific for permeant binding and/or translocation in hCNT3 could be identified by screening of hCNT3 random mutants using a phenotypic complementation approach (3,4). Some nucleoside drugs, e.g., 5-fluorouridine (5FUrd), are toxic to yeast and disruption of the *fui*1 gene abolishes their cytotoxicities (5). hCNT3 has recently been shown to mediate uptake of 5FUrd into

yeast (Zhang J., and Cass C.E., unpublished data), resulting in death of hCNT3-positive yeast exposed to this drug. Expression of hCNT3 in a yeast strain deficient in adenine biosynthesis (ade2) allowed yeast growth on plates lacking adenine but containing adenosine. Cytotoxicity assays were undertaken to determine the minimal lethal dose of 5FUrd against yeast (ade2 deficiency strain) producing hCNT3 (Zhang J. and Cass C.E., unpublished data). The transportability of 5FUrd by recombinant hCNT3 was directly determined by radioisotope flux assays in the experiments of Chapter 3. 5FUrd could be used to screen a randomly mutated hCNT3 cDNA library by phenotypic selection. Only yeast that produce mutated hCNT3 proteins that are unable to transport cytotoxic 5FUrd would be expected to survive; these yeast would be duplicated to the plates containing adenosine but not adenine. Yeast cells that survive the double selection would be expected to produce hCNT3 mutants that are unable to transport 5FUrd but maintain the ability to transport adenosine. This strategy should allow the identification of amino acid residues of hCNT3 that are critical for interaction with Urd and Urd analogs but not for adenosine. The identified mutants would then be introduced into the cysteine-less hCNT3 and subjected to methanethiosulfonate reagents for detailed structure-function studies.

Another direction for research on concentrative nucleoside transporters is searching for high-affinity CNT inhibitors. The development of the high throughput yeast expression system and inhibitory-sensitivity assay should enable the screening of a library of chemicals to identify CNT inhibitor molecules. Novel inhibitors identified could be subjected to the yeast-based phenotype complementation assay developed in the Cass laboratory (6,7) to define the structural determinants of CNT proteins that are responsible for high-affinity inhibitor-transporter interactions.

More sensitive autofluorescent nucleoside analogs are being developed by Dr. Robins. We are currently measuring the uptake rates of FuPmR using the live cell imaging technique presented in Chapter 5 in ten different cancer cell lines with different abundance of nucleoside transporters in order to demonstrate the application of this fluorescent compound in other cell types. The transport processes of FuPmR and newly developed compounds, as well as their intracellular fates, could also be investigated by real-time confocal microscopy in recombinant expression systems (e.g., *X. laevis*

oocytes) that produce individual nucleoside transporter subtypes to explore the roles of a specific nucleoside transporter on transport of these compounds.

In summary, the research on structure-activity relationships of nucleosides and nucleoside transporters and the proposed future studies presented in this thesis should improve our understanding of the structural determinants for nucleoside-transporter interactions and of nucleoside translocation mechanisms. The ultimate goal is to use this knowledge about nucleoside transporters to guide nucleoside-based chemotherapy.

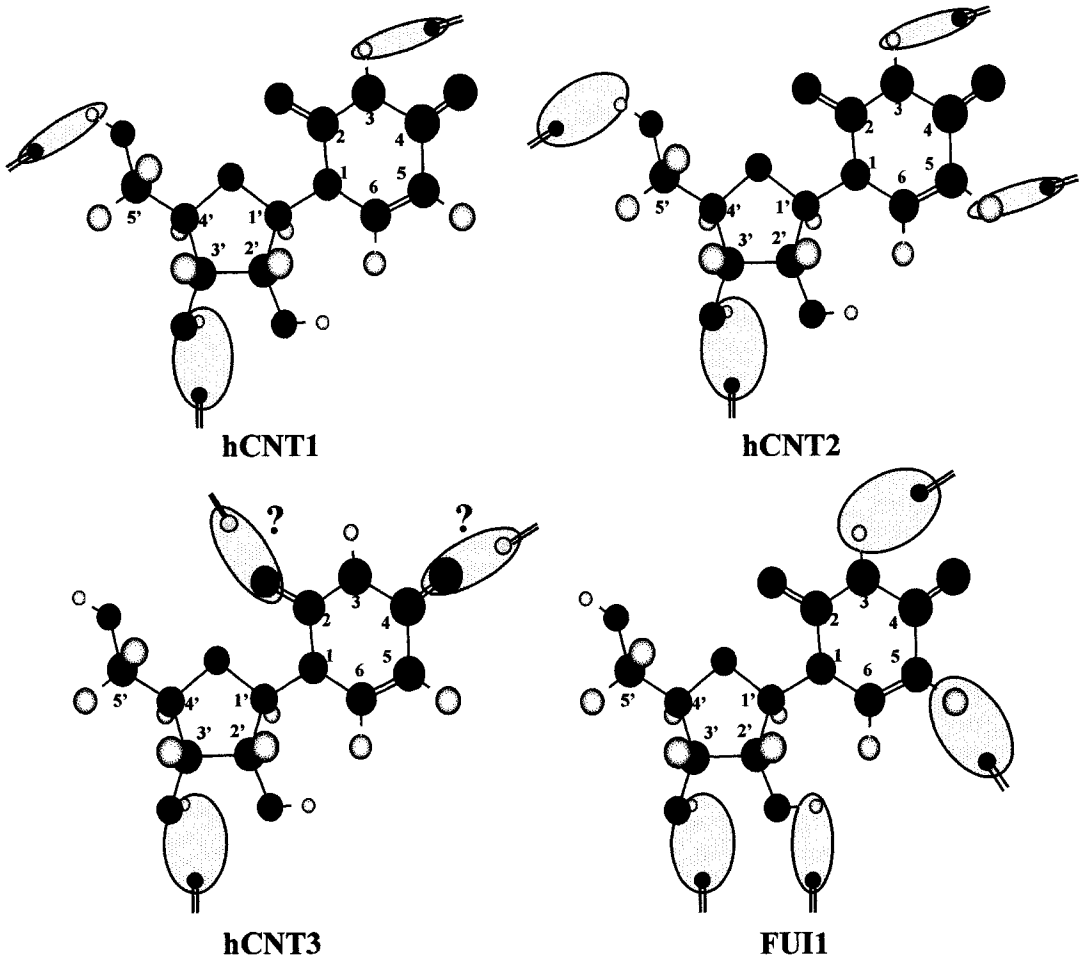

Figure 7-1 Models of the interactions between uridine and the hCNT1, hCNT2, hCNT3 or FUI1.

Structural determinants of uridine that are proposed to interact with amino acid residues in the transporter binding pocket and their interactions are indicated as *shaded areas*, the sizes of which correspond to the values of binding energy. Numbering of Urd is indicated. Functional groups of the transporter are speculative and for presentation purpose only. The 3D structure of uridine was generated using ChemDraw Chem3D software.

References

1. Vickers, M. F., Zhang, J., Visser, F., Tackaberry, T., Robins, M. J., Nielsen, L. P., Nowak, I., Baldwin, S. A., Young, J. D., and Cass, C. E. (2004) *Nucleosides Nucleotides Nucleic Acids* **23**, 361-373
2. Smith, K. M., Slugoski, M. D., Loewen, S. K., Ng, A. M., Yao, S. Y., Chen, X. Z., Karpinski, E., Cass, C. E., Baldwin, S. A., and Young, J. D. (2005) *J Biol Chem* **280**, 25436-25449
3. Maser, P., Sutterlin, C., Kralli, A., and Kaminsky, R. (1999) *Science* **285**, 242-244
4. Endres, C. J., Sengupta, D. J., and Unadkat, J. D. (2004) *Biochem J* **380**, 131-137
5. Vickers, M. F., Yao, S. Y., Baldwin, S. A., Young, J. D., and Cass, C. E. (2000) *J Biol Chem* **275**, 25931-25938.
6. Visser, F., Vickers, M. F., Ng, A. M., Baldwin, S. A., Young, J. D., and Cass, C. E. (2002) *J Biol Chem* **277**, 395-401.
7. Visser, F., Baldwin, S. A., Isaac, R. E., Young, J. D., and Cass, C. E. (2005) *J Biol Chem* **280**, 11025-11034